Short title (56 characters max.):

FINITE ELEMENTS FOR VECTOR FIELDS IN ELECTROMAGNETICS

# TRIANGULAR FINITE ELEMENTS / FOR

VECTOR FIELDS IN ELECTROMAGNETICS

bу

Adalbert Konrad, B. Eng., M. Eng.

A thesis submitted to

the Faculty of Graduate Studies and Research

in partial fulfillment of the requirements for the degree of

Doctor of Philosophy

Department of Electrical Engineering,

McGill University,

Montreal, Québec.

- September, 1974

C Adalbert Konrad 1976

# ABUTRACT

This thesis presents a variational finite element formulation for bounded, loss-free electromagnetic field problems. The treatment is general, encompassing any timeharmonic field in an infinite wavéguide structure filled with source free media. A stationary energy functional is constructed for either of the three components of the electric or of the magnetic field vector. In Cartesian coordinates this functional is specialized to linearly polarized travelling waves while in cylindrical coordinates it is specialized to circularly polarized circulating waves. Solution of the functional is accomplished by the high-order polynomial triangular finite element method which reduces the functional to a matrix form. Two finite element computer programs are presented, one for the solution of linearly polarized travelling waves in anisotropic waveguides and another for the analysis of linear accelerator davities. Very fast matrix assembly is obtained by using /pre-calculated, universally constant finite element matrices for up to and including 6th-order polynomial approximation. Various examples are given and the program results are analyzed in detail.

#### RESUME

L'objet de cette thèse est la formulation variationelle des problèmes de champs electromagnetiques non dissipatifs dans des domains bornés, en vue d'utiliser la méthode des éléments finis. Cette approche générale permet de traiter tous les problèmes relatifs à des champs stationnaires dans des guides d'ondes constitués par un milieu sans sources. Une fonctionelle énergétique stationnaire est construite pour chacune des trois composantes des vecteurs représentant les champs électriques ou magnétiques. En coordonnées cartésiennes cette fonctionelle est appliquée à la propagation des ondes à polarisation linéaire, tandis qu'en coordonnées cylindriques on étudie les ondes à polarisation circulaire. La résolution de cette fonctionelle est effectuée par une méthôde des éléments finis triangulaires d'ordre supérieure qui permet de mettre le problème sous forme matricielle. Deux programmes de calculs utilisant les éléments finis sont annexés; l'un pour la propagation des ondes à polarisation linéaire dans des guides d'ondes anisotropes, l'autre pour l'analyse des cavités d'un accélérateur linéaire. L'assemblage matriciel est obtenu très rapidement grâce à l'emploi de matrices universelle calculées à l'avance pour des éléments finis allant jusqu'à l'ordre (6). Les résultats de divers éxemples présentés dans la thèse sont analysés en détail.

# <u>ACKNOWLEDGEMENTS</u>

Above all, the author would like to express his gratitude towards his thesis advisor, Dr. P. Silvester, who skillfully guided the research work contained in this thesis. His numerous invaluable comments and ability to generate enthusiasm are responsible for channeling the author's efforts in the positive direction.

The author is indebted to Dr. Z. Csendes for the time spent on carefully reading and constructively criticising the thesis manuscript.

Special thanks are due to all of the author's former and present colleagues for providing a pleasant and cheerful atmosphere to work in.

Financial support by the National Research Council of Canada is greatfully acknowledged.

# TABLE OF CONTENTS

ABSTRACT	ľ	J.	Page 1
RÉSUM <b>É</b>	-	·	ii
,			
VCKNOMIT	EDGEM1	ENTS	iii
"TABLE OF	F CON	CENTS	iv
CHAPTER	I	INTRODÚCTION	1
i	1.2 1.3	Nature of the Problem State of the Art The Original Contributions Outline of the Thesis	1 2 8 9
CHAPTER		THE CONSTRUCTION OF AN ENERGY FUNCTIONAL BASED ON MAXWELL'S EQUATIONS	12
1	2.2 2.3 2.4	Summary Derivation of the Curlcurl Equation Functional Formulation Boundary Conditions Uniqueness = Explicit Forms of the Functional	12 18 22 28 31
CHAPTER	III	DISCRETIZATION OF THE FUNCTIONAL BY APPROXIMATION OF VECTOR FIELDS WITH HIGH-ORDER POLYNOMIAL TRIANGULAR FINITE ELEMENTS	׳36
		Summery	`₩36 36
		Types of Waves and Their Mathematical 'Representations	37
'e *	,	Explicit Forms of the Functional for Travelling and Circulating Waves Discretization. The Element Matrices	41 · 45 58
,	3.5°	Minimization of the Discretized Functionals over a Compound Triangular Region	<sup>°</sup> 68
CHAPTER	Ϋ́	COMPUTER PROGRAM, RESULTS AND APPLICATIONS	75
	4.1	Summary The Three Component Magnetic Field Vector	75
i .		The Three-Component Magnetic Field Vector Program	75
	4.2	Solution to a Homogeneous, Isotropic Waveguide Problem	78
	4.4	An Inhomogeneous, Isotropic Waveguide Problem A Microstrip Problem	92 100
	4.5	The Origin of the Spurious Modes .	105

	4.6		Page
	4.7	Waveguide Problem Homogeneous, Electrically	115
	•	Anisotropic Waveguide Problems	129
CHAPTER	٧	LACC: A LINEAR ACCELERATOR CAVITY CODE BASED ON THE FINITE ELEMENT METHOD	144
4	5.1	Summary Introduction	144 144
	5.2	The Linac Cavity Electromagnetic Field Problem	145
	5.3	Finite Element Method for the Computation of the Magnetic Field Intensity	151
	5.4	Special Quantities Related to Linac Cavity Design	155
	5.5	Numerical Methods Used in the LACC Computer Program	160
	5.6	Input/Output Features of the LACC Computer Program	170
· · · · · · · · · · · · · · · · · · ·	5.7	Accuracy, Speed, Convergence and a Comparison with the LALA Program	191
	5.8	Field Computation for Other Types of Cavities by the LACC Program	206
CHAPTER	<del>1</del> 7- <del>-14</del>	1	21.7
OTATIER	i		
	6.1 6.2 6.3	Summary Advantages and Disadvantages of the Method Recommendations for Further Research	217 218 223
REFÉREN	CES		225
APPENDI (fiche		Formac Programs (QSYM, USYM, YSYM, QANT, UANT) for the Computation of the Element Matrices	238
APPENDI (fiche		Block Data Generator Program (V3BG)	238
APPENDI (fiche		Block Data Generator Program (V3XY)	238
APPENDI (fiche (fiche	4)	Three-Component Magnetic Field Vector Program (XY3D)	239
APPENDI (fiche (fiche (fiche	6) 7)	Linear Accelerator Cavity Code (LACC) and Block Data Generator Program (V1BG)	239 240
APPENDI (fiche		LinacPLoT Program (LPLT)	240

#### CHAPTER I

#### INTRODUCTION

# 1.1 Nature of the Problem

Due to the broad variety of practical applications of waveguides, resonators and other microwave devices, the development of methods to solve the associated electromagnetic field problems has neceived a great deal of attention in the past two decades. At the beginning, attention was focused on analytical methods, but with the advent of electronic computers, numerical methods have gained prominence. Of these, finite difference methods were the first to gain acceptance among microwave engineers. In recent years however, finite clement methods have been recognized to be more readily suited to solve waveguide problems [1,16-18]. This thesis presents a general finite element method for such problems.

The electromagnetic boundary value problems treated in this thesis are those associated with:

- homogeneous, isotropic waveguides;
- inhomogeneous, isotropic waveguides;
- homogeneous, anisotropic waveguides;
- inhomogeneous, anisotropic waveguides;
- 'axisymmetric resonant cavities for linear accelerators. These problems, with the exception of homogeneous isotropic waveguides, require a formulation in which the electromagnetic fields are treated as vector quantities. With a few exceptions [2,3,13,19-21], the tendency in recent years has been to

terms of the longituanual electric and respectic field components which satisfy the helmholtz equation [4-10,14,15]. This thesistrontains a unified formulation of the above problems in terms of all three components of the magnetic or of the electric field vector. By employing the finite element method, the formulation allows the treatment of waveguide geometries with an arbitrary, cross-section. Furthermore, it allows general purpose computer programs to be written which can be used by a microwave engineer even if he is unfamiliar with the details of the method.

#### 1.2 State of the Art

In a review paper [1] which appeared in 1969, Wexler makes the following remark in connection with the variational solution of electromagnetic field problems:

"Although there are some indications of how to proceed, the author has not seen any teneral computer methods for fields with all six components of electric and magnetic field present. Such fields require both an electric and rametic vector potential function to generate them. Perhaps it would be just as well to solve the electric and rametic fields directly rather than through two potential functions."

In his concluding remarks he adds that

"In the immediate future, emphasis should perhaps be placed upon the development of finite difference and variational techniques for solving fields naving all compenents of electric and magnetic field present everywhere. To date, with a few exceptions (e.g., [59, pp.172-188]), most methods appear to permit solution only of fields derivable from a single scalar potential. It is not difficult to formulate and solve field problems in a multidielectric region, but it may not correspond to the actual electromagnetic problem. This is indicated by the continuing discussion of "quasi-TEM" microstrip waves."

The exception referred to by Mexler is Harrington's well known romegraph [2] which appeared in 1968 and contains a chapter on field solution in resonant cavities filled with inhomogeneous and/or anisotropic medium. In essence, this chapter contains the results presented in a doctoral dissertation by Gupta [3] in 1965. The moment method is applicable to cavities and waveguides of arbitrary cross-section and arbitrary linear media, provided that the empty cavity or waveguide modes are known. The field components in a cavity or waveguide filled with anisotropic material are expanded in terms of the field components of the empty cavity or waveguide modes to obtain'a matrix equation; the order of this matrix equation depends upon the number of empty cavity or waveguide modes used in the expansion. In principle, the accuracy of the solution can be of any degree but is in practice limited by the size of the computer. In the formulation used, the matrix equations are developed for a general anisotropic medium and them specialized for rectangular cavities containing plasmas and ferrites; the frequency dependence of the material property tensors is not included and hence the rodes obtained do not exist simultaneously.

In 1967, Hannaford [4] described a finite difference/variational method for homogeneous isotropic waveguides of arbitrary shape. His formulation is based upon the solution of the Helmholtz equation in terms of the longitudinal electric and magnetic field components and the derivation of a variational expression. A puzzling feature of his work is that he deals with complex functions for E<sub>z</sub> and H<sub>z</sub> even after the removal of the z-dependence from the expressions. The finite difference formulae used are obtained from a Taylor series expansion in which terms of

order 4 or higher are ignored. Although the body of the thesis deals with isotropic media, mannaford briefly discusses the extension of the method to plasma-loaded waveguide's and waveguides containing transversely magnetized ferrites. The proposed method for the solution of transversely magnetized ferriteloaded waveguide problems involves a finite difference matrix which is not symmetric. Consequently, according to Hannaford, the physical interpretation of the resulting complex eigenvalues is difficult. Further, the material property tensors used by a Hannaford are restricted in the sense that null elements are included and the frequency dependence of the material property tensors is not taken into consideration during computation. For inhomogeneous isotropic media, the resulting coefficient matrix in Hannaford's formulation becomes indefinite above the 45 degree 'air-line' on the dispersion diagram. Since 1967, this shortcoming of two-component formulations has reoccured in a number of other finite difference and finite element variational methods [5-12]. Referring to the vector variational integrals deduced by Berk [13], Hannaford dismisses three- and six-component vector formulations as being more complicated than the  $E_{z}$ - $H_{z}$  formulation.

Berk's variational expressions have been referred to many times since the publication of reference [13] in 1956. In this work, which is based on his doctoral dissertation at LIT in 1954, Berk derived three- and six-component vector variational expressions in the form of Rayleigh quotients for the resonance frequencies of a resonator filled with loss-free, anisotropic, homogeneous or inhomogeneous media. His expressions are either in terms of the electric field  $\overline{E}$  or of the magnetic field  $\overline{H}$  or both. However, only the magnetic field expressions have natural

boundary conditions at perfect electric conductors in a threecomponent vector formulation. Having worked prior to the
development of finite elements, one of Berk's principal concerns

"...one should make every effort to select-trial fields which satisfy as many of the known features of the solution as possible. In particular, one should attempt to devise trial fields which, at surfaces of discontinuity, not only have continuous tangential components, but continuous normal components of  $(\varepsilon.E)$  and  $(\mu.H)$  as well. This is because the last set of boundary conditions does not follow from the first set unless the trial fields satisfy Naxwell's equations."

An impressive effort on more or less the same theme is evident in the works of Thomas [14,15] in 1969. However, his work is basically a scalar formulation of the isotropic wave-guide problem based on the Rayleigh-Ritz approximation method using polynomials in polar coordinates as a trial set [15]. Since 1969 a variety of other methods for the solution of isotropic waveguide problems appeared in the literature; these have been reviewed in recent papers by Silvester and Csendes [16], by Mavies [17] and by Ng [18].

The only three-component vector variational method appearing in recent years is due to English and Young [19] in 1971.

In their paper the authors state [19]

"The rector variational formulations of the Maxwell. equations which have been presented in the literature are expressed in terms of all six electromagnetic field components [4]-[6]. This paper develops and applies a vector variational formulation of the Maxwell equations in terms of the electric field E vector (a three-component formulation) by expressing the magnetic field vector in the Maxwell equations in terms of the electric field vector. An alternative formulation in terms of the magnetic field H vector is also possible. However, the electric field formulation has more associated Dirichlet guide-wall boundary conditions than the magnetic field formulation and thus has a faster solution convergence rate."

Taus English and Young select the E Tield formulation on the tisis of the number of Dirichlet boundary conditions to be satisfied. They list the advantages of the three-component vector formulation as reduced matrix size and denser coefficient matrices in comparison to the six-component formulation given by English in his doctoral dissertation [20] in 1969 and in a paper by English [21] which appeared in 1971. However, they find that with this formulation the matrix elements are more complicated to calculate, the guide, -wall boundary conditions on the trial functions are more restrictive and the imposition of continuity constraints on the trial field components is less straightforward. English and Young apply their method to inhomogeneously filled isotropic parallel plate waveguides and to rectangular waveguides. Unfortunately, in their formulation the condition  $\overline{n} \times \overline{E} = 0$  must be satisfied exactly by the trial functions, so that waveguide shapes other than circular or rectangular cannot be treated. The authors enforce the continuity of the normal component of the electric flux density vector at dielectric interfaces. This means that the trial-function choice depends upon the mode under consideration and therefore each particular problem requires separate treatment. Finally, with regard to anisotropic media, English and Young conclude that the coefficient matrix will be Hermitian; that this statement is not true is evident from the present work.

Interesting enough, the six-component vector formulation, although criticized by many including English [19], still has new proponents. Very recently, a six-component formulation has been presented by Satomura, Matsuhara and Kumagai [22] in connection with the analysis of anisotropic slab waveguides.

They represent the field of waves propagating in the longitudinal direction in terms of a linear combination of elementary plane waves. In the course of the analysis they arrive at a dispersion relation from which they conclude that in order to obtain a solution, the tensor components must satisfy certain propagation conditions. This leads them to incorrectly state that only when these propagation conditions are satisfied are anisotropic materials capable of transmitting waves which propagate in the z-direction. In fact, the conditions they derive are only valid for linearly polarized travelling waves.

It is interesting to note that the formulation given in this thesis is more closely related to a paper presented by Stone [23] in 1973 for the solution of acoustic wave propagation, than to the methods listed above for electromagnetic wave propagation. Stone's formulation is based upon Silvester's high-order finite-element formulation of potential problems [24], as is the method in this thesis, although he considers acoustic wave propagation. In connection with the dielectric waveguide problem Stone says that "the variational principle must be modified to accommodate the required interface conditions", apparently not realizing that an analogous three-component formulation of electromagnetic wave problems is also possible. Remarkably, the finite element matrices used by Stone [23] are precisely the same as the ones computed in this thesis for the travelling wave problem. Two of these matrices have been given previously in Silvester's work [24], a third one has been computed independently by Csendes [7,12] and by Daly [9,25] and the remaining two have been computed by Stone [23,26]. However, in each of these cases, the matrices are given only

up to fourth order, not six as in this thesis. First- and second-order finite element solutions to elastic surface waves have also been given by others [27,28], but these formulations are less intimately related to the present method.

It is evident from the foregoing literature survey that the need for a unified three-component vector variational formulation of the loss-free bounded electromagnetic field problem has long been recognized. Although the necessary ingredients for a general formulation have existed, the  $E_2$ - $H_2$  approach has been favoured over three-component and six-component  $\overline{E}$ - $\overline{H}$  vector formulations. Furthermore, the finite element method [29-35] has been applied only to  $E_2$ - $H_2$  formulations [7-9,12]. It is hoped that the work presented in this thesis will both complement and provide an alternative to existing methods.

# 1.3 The Original Contributions

Briefly, the original contributions contained in this thesis can be summarized as follows:

- a) A unified, general, three-component vector variational formulation of electromagnetic field problems is presented using the high-order polynomial triangular finite element method;
- b) Specialized functionals are introduced for various wave types depending on the electromagnetic properties of the media, without recourse to complex arithmetic;

- c) Finite element matrices are derived and computed for three-component vector field problems in cylindrical coordinates for polynomial approximations of orders 1 to 6 inclusive;
- d) A three-component magnetic field vector solving computer program is presented which permits the analysis of linearly polarized travelling waves in waveguides of arbitrary cross-section and includes the anisotropy of the medium;
- e) The occurrence of non-physical (spurious) solutions in variational formulations is explained;
- f) A linear accelerator cavity field analysis computer program based on the high-order polynomial triangular finite element method is presented.

# 1.4 Outline of the Thesis

Starting in Chapter II, the curlcurl equation is derived from Maxwell's equations and an energy functional with stationary properties at the solution of this equation is constructed for non-conductive anisotropic media. This functional is then specialized to different wave types in Chapter III and special forms of the functional are discretized by using the finite element method.

The computer programming of the special functional forms is included in the Appendices. In these, Fortran programs are presented which return the components of the magnetic field intensity vector and the wave-number for a given value of the propagation constant. A description of the program for linearly

dedicated effort is made to prove that the computer program returns correct (and accurate) solutions. The examples presented in Chapter IV illustrate the generality of the method and of the computer program and indicate potential applications.

As is pointed out, the program returns not only the expected physically meaningful solutions but also eigenvectors and eigenvalues void of physical meaning. It is shown by an example in Chapter IV that these non-physical solutions are due to a larger than expected set of natural boundary conditions.

A corresponding computer program for the solution of circulating waves in cylindrical geometry has not been implemented in this thesis, although the corresponding finite element matrices have been computed and are made available. However, a computer program for a more restricted class of axisymmetric problems, namely those with only an azimuthal vector component present, has been written [36]. A very specialized version of this program for linear accelerator cavity applications is included in the Appendices and is described fully in Chapter V. This computer program illustrates the power of the present method if the programming is carried far enough. It may be noted that the program is now being used for accelerator cavity design at the Karlsruhe Nuclear Research Centre.

This thesis touches on variety of topics held together
by the generality of the finite element formulation given in
Chapters II and III. The programming done by the author is quite
extensive. However, because of the wealth of solution techniques
discovered, much of the programming can be regarded as a pilot

work for the development of even more efficient and more versatile computer programs in the future.

,

4

,

,

--'

•

;

-

1

#### CHAPTER II

# THE CONSTRUCTION OF AN ENERGY FUNCTIONAL BASED ON MAXWELL'S EQUATIONS

#### Summary

1

The behaviour of electromagnetic fields is governed by Maxwell's equations. The objective of this chapter is to cast these equations into a form which lends itself easily to variational treatment. The basic differential operator equation derived is referred to as the curlcurl equation; various forms of this equation are associated with a host of physical problems of practical importance. The derivation is kept as general as possible and it includes the treatment of anisotropic media. The boundary conditions associated with physical problems are also treated in detail and a discussion of the uniqueness of the solution appears as well. A functional related to energy is derived for the curlcurl equation in Cartesian and cylindrical coordinates.

# 2.1 Derivation of the Curlcurl Equation

- Consider Maxwell's equations for time-harmonic fields [37, 38]:

$$\operatorname{curl} \overline{E} = -j\omega \overline{B}$$
 (2.1)

$$\operatorname{curl} \overline{H} = +j\omega \overline{D} + \overline{J} \tag{2.2}$$

$$\operatorname{div} \overline{B} = 0 \tag{2.3}$$

$$\operatorname{div} \overline{D} = 9 \tag{2.4}$$

The vectors  $\overline{\Xi}$  and  $\overline{H}$  are known as the electric and magnetic

field intensities and the vectors  $\overline{D}$  and  $\overline{B}$  are referred to as electric and magnetic flux densities respectively.  $\overline{J}$  denotes current density and it analyses impressed currents  $(\overline{J}_1)$  as well as induced conduction currents  $(\overline{J}_c)$ . Charge density is represented by  $\boldsymbol{\varsigma}$ . The imaginary unit  $\boldsymbol{j}$  in equations (2.1) and (2.2) can be interpreted as a phase difference of  $\frac{\pi}{2}$  in time (or space) between the electric and magnetic field vectors. It originates from the assumption that the electromagnetic fields are time-harmonic with angular frequency  $\boldsymbol{\omega}$ .

Since the divergence of the curl of any vector is identically equal to zero, it is immediately obvious that equations (2.3) and (2.4) are implicit in equations (2.1) and (2.2) respectively. Equation (2.2) yields

$$\operatorname{div} \overline{D} = -\frac{1}{j\omega} \operatorname{div} \overline{J}$$
 (2.5)

where the right-hand side is equal to the charge density 5 by the principle of the conservation of charge. Consequently, attention will be focused on equation (2.1) and (2.2) in the following.

Let  $\hat{\mu}$ ,  $\hat{\epsilon}$  and  $\hat{\sigma}$  be the <u>tensor permeability</u>, <u>tensor</u> <u>permittivity</u> and <u>tensor conductivity</u> functions respectively. These tensors describe the medium and in general they are functions of the spatial coordinates, frequency, and the fields themselves. The constitutive relationships for anisotropic media can be written as follows

$$. \overline{B} = \hat{a} \underline{H}$$
 (2.6)

$$\overline{D} = \hat{\epsilon} \, \overline{E} \tag{2.7}$$

$$\overline{J}_{C} = \hat{\sigma} \, \overline{E} \tag{2.8}$$

۶.

(2.1) and (2.2) respectively and then taking curl of both sides, one obtains

$$\operatorname{curl}(\hat{\mu}^{-1}\operatorname{curl}\overline{E}) = -j\omega\operatorname{curl}\overline{H}$$

$$\operatorname{curl}(\hat{\epsilon}^{-1}\operatorname{curl}\overline{H}) = +j\omega\operatorname{curl}\overline{E} + \operatorname{curl}(\hat{\epsilon}^{-1}\hat{\sigma}\overline{E} + \hat{\epsilon}^{-1}\overline{J}_{i})$$
 (2.10)

Now, substituting for curl  $\overline{H}$  in equation (2.9) from equation (2.2) and for curl  $\overline{E}$  in equation (2.10) from equation (2.1) gives

$$\operatorname{curl}(\hat{\mu}^{-1}\operatorname{curl}\overline{E}) - \omega^2 \hat{\epsilon}\overline{E} + j\omega \hat{\sigma}\overline{E} = -j\omega\overline{J}_{\dot{1}}$$
 (2.11)

$$\operatorname{curl}(\hat{\boldsymbol{\epsilon}}^{-1}\operatorname{curl}\,\overline{\boldsymbol{H}}) - \boldsymbol{\omega}^2\hat{\boldsymbol{\mu}}\overline{\boldsymbol{H}} - \operatorname{curl}(\hat{\boldsymbol{\epsilon}}^{-1}\hat{\boldsymbol{\sigma}}\overline{\boldsymbol{E}}) = \operatorname{curl}(\hat{\boldsymbol{\epsilon}}^{-1}\overline{\boldsymbol{J}}_{\dot{1}}) \ (2.12)$$

Equations (2.11) and (2.12) are equivalent to Maxwell's equations (2.1) through (2.17). For any particular problem, both of these equations can be solved to give  $\overline{E}$  and  $\overline{H}$ . However, equation (2.11) depends only on  $\overline{E}$  whereas equation (2.12) involves both  $\overline{E}$  and  $\overline{H}$ . For nonconductive media, i.e. where  $\hat{\sigma}$  is identically zero, the equations reduce to the more attractive form

$$\operatorname{curl}(\hat{\boldsymbol{\mu}}^{-1}\operatorname{curl}\overline{E}) - \omega^2 \hat{\boldsymbol{\epsilon}}\overline{E} = -j\omega\overline{J}_i \qquad (2.13)$$

$$\operatorname{curl}(\hat{\epsilon}^{-1}\operatorname{curl}\overline{H}) - \omega^2 \hat{\mu}\overline{H} = \operatorname{curl}(\hat{\epsilon}^{-1}\overline{J}_i)$$
 (2.14)

For <u>conductive media</u> in which <u>displacement currents</u> can be <u>neglected</u>, equation (2.11) becomes

$$\operatorname{curl}(\hat{\boldsymbol{\mu}}^{-1}\operatorname{curl}_{E}^{-1}) + j\boldsymbol{\omega}\hat{\boldsymbol{\sigma}}E = -j\boldsymbol{\omega}J_{i}$$
 (2.15)

whereas equation (2.12) reduces to

$$\operatorname{curl} \overline{H} - \hat{\sigma} \overline{E} = \overline{J}_{i}$$
 (2.16)

Renegating the manipulations performed previously to arrive at equation (2.12), one can obtain from (2.10), (2.1) and (2.6) an equation similar to (2.15)

$$\operatorname{curl}(\hat{\sigma}^{-1}\operatorname{curl}\overline{H}) + j\omega\hat{\mu}\overline{H} = \operatorname{curl}(\hat{\sigma}^{-1}\overline{J}_{i}) \qquad (2.17)$$

The divergenceless character of the magnetic flux density  $\overline{B}$  can be exploited by inventing the concept of a magnetic vector potential  $\overline{A}$  and an electric scalar potential  $\phi$ . Thus, since div curl of any vector and curl grad of any scalar are identically zero.  $\overline{B}$  may be written as

$$\overline{B} = \operatorname{curl}(\overline{A} + \frac{1}{j\omega} \operatorname{grad} \emptyset)$$
 (2.18)

According to equation (2.1),  $\overline{E}$  can then be obtained by removing the curl operator

$$\overline{E} = -j\omega\overline{A} - \operatorname{grad} \emptyset$$
 (2.19)

Making use of equations (2.4), (2.7) and (2.19) one now obtains

$$\operatorname{div} \overline{D} = -j\omega \operatorname{div}(\hat{\epsilon} \overline{A}) - \operatorname{div}(\hat{\epsilon} \operatorname{grad} \phi) = \S \qquad (2.20)$$

It should be noted from equations (2.19) and (2.11) that when the frequency  $\omega$  is zero, i.e. in the case of static fields, equation (2.11) is satisfied identically and therefore it cannot be used to solve for  $\overline{E}$ . Instead, one must use equation (2.20) with  $\omega$  set to zero

$$\operatorname{div}(\hat{\boldsymbol{\epsilon}} \operatorname{grad} \boldsymbol{\phi}) = -\boldsymbol{\varsigma} \tag{2.21}$$

Thus one can solve for  $\phi$  and then obtain  $\overline{E}$  from equation (2.19); this solution will be valid both in conductive and in nonconductive media. In a conductive medium, the conduction

current  $\overline{J}_c = \widehat{\mathfrak{g}} \, \overline{E}$  will cause a morntic field  $\overline{H}$  to appear. If  $\overline{J}_c$  is the only current flowing, then equation (2.2) gives

$$\operatorname{curl} \overline{H} = \overline{J}_{\mathbf{c}} \tag{2.22}$$

This combined with equations (2.18) and (2.6) becomes

$$\operatorname{curl}(\hat{\mu}^{-1}\operatorname{curl}\overline{A}) = \overline{J}_{c} \tag{2.23}$$

A rore general form of this equation is obtained by substituting for  $\Xi$  in equation (2.11) from equation (2.19)

$$\operatorname{curl}(\hat{\mu}^{-1}\operatorname{curl}\overline{A}) - \omega^{2}\hat{\epsilon}\overline{A} + j\omega\hat{\sigma}\overline{A} = \overline{J}_{1} - (\hat{\sigma} + j\omega\hat{\epsilon})\operatorname{grad}\beta \quad (2.24)$$

$$\overline{a} \times (\overline{b} \times \overline{c}) = \overline{b}(\overline{a}.\overline{c}) - (\overline{a}.\overline{b})\overline{c}$$
 (2.25)

to the first term on the left-hand side of (2.24). This yields

$$\mu^{-1}\operatorname{grad}(\operatorname{div}\overline{A}) - (\operatorname{div}.\mu^{-1}\operatorname{grad})\overline{A} - \omega^{2}\widehat{\epsilon}\overline{A} + j\omega\widehat{\sigma}\overline{A} =$$

$$\overline{J}_{i} - (\widehat{\sigma} + j\omega\widehat{\epsilon})\operatorname{grad}\emptyset \quad (2.26)$$

Since the divergence of  $\overline{A}$  is unspecified up to this point, one can now choose div  $\overline{A}$  such that the following relationship is satisfied

$$\operatorname{grad}(\operatorname{div} \overline{A}) = -(\mu \hat{\sigma} + j\omega \mu \hat{\epsilon}) \operatorname{grad} \emptyset$$
 (2.27)

Equation (2.27) is a generalized Lorentz condition for electrically anisotropic media characterized by the tensors and of and the scalar permeability  $\mu$ . Hence equation (2.26)

$$(\operatorname{div}.\mu^{-1}\operatorname{grad})\,\overline{A} + \omega^2 \hat{\epsilon}\,\overline{A} - j\omega \hat{\sigma}\,\overline{A} = \overline{J}_{i_{\bar{\alpha}}} \tag{2.28}$$

Here the vector potential  $\overline{A}$  has both its curl and its divergence fixed. When the permeability is a tensor quantity, one must use equation (2.24) and must make other simplifying assumptions to eliminate the electric scalar potential  $\phi$  from the equation.

One should mention here in passing that Maxwell's equations may be extended if one accepts the mathematical concepts of electric vector potential  $\overline{F}$ , magnetic scalar potential  $\Psi$ , magnetic charge m and magnetic current density  $\overline{M}$ . Essentially, this amounts to the observation that equation (2.20) remains satisfied if one adds to the right-hand side of (2.10) the curl of the electric vector potential  $\overline{F}$ . Since  $\overline{A}$  and  $\overline{F}$ ,  $\emptyset$  and  $\Psi$ ,  $\S$  and m and  $\overline{J}$  and  $\overline{M}$  are dual quantities, it is quite easy to write analogous equations to the ones derived here for  $\overline{F}$  and  $\Psi$ .

The primary concern of this thesis is the solution of equations (2.13), (2.14) and (2.23) in bounded regions. The differential operators in these equations are self-adjoint and therefore lend themselves readily to a Rayleigh-Ritz type of finite element method. The operators in equations (2.15) and (2.17) are not self-adjoint due to the presence of the multiplier  $j\omega$  and are thus not amenable to the same treatment. Finite element matrices derived for the operators of equations (2.13), (2.14) and (2.23) can however be used without modification in a Galerkin type solution of equations (2.15) and (2.17) [39]. The operators in equations (2.21) and (2.28)

contain the Lablacian operator. This operator has been widely treated by the variational finite element method for the case of isotropic media [29-35]. Provided that the tensors are Hermitian, extension to anisotropic media is straightforward [44].

Equations (2.13), (2.14) and (2.23) are special cases of the following general equation depending on the interpretation of  $\hat{p}$ ,  $\bar{q}$ ,  $\bar{V}$  and  $\bar{g}$ 

$$\operatorname{curl}(\hat{p}\operatorname{curl}\overline{V}) - \omega^2 \hat{q}\overline{V} = -\overline{g} \qquad (2.29)$$

In the next section an energy related functional which is variationally stationary at the solution point will be given for the operator in equation (2.29). It will be shown that for lossless media p and q are Hermitian tensors and thus the self-adjoint property of the curlcurl operator is preserved.

# 2.2 Functional Formulation

An energy functional [40] associated with the operator of equation (2.29) is given by

$$F(\overline{v}) = \langle \text{curl}(\hat{p} \text{ curl } \overline{v}), \overline{v} \rangle - \omega^2 \langle \hat{q} \overline{v}, \overline{v} \rangle + \langle \overline{g}, \overline{v} \rangle^2 + \langle \overline{v}, \overline{g} \rangle$$
 (2.30)

In view of the fact that the electric and magnetic field intensities vary harmonically in time, and therefore have both magnitudes and phases, the following inner product should be used

$$\langle \overline{a}, \overline{b} \rangle = \iiint (\overline{b} \cdot \overline{a}) dU$$
 (2.31)

The asterisk here denotes complex conjugate. With this definition of inner product, the functional in (2.30) can be rewritten as

$$F(\overline{v}) = \iiint [\overline{v}^*.\text{curl}(\hat{p} \text{ curl } \overline{v})] dU - \omega^2 \iiint (\overline{v}^*.\hat{q}\overline{v}) dU$$

$$+ \iiint (\overline{v}^*.\overline{g}) dU + \iiint (\overline{g}^*.\overline{v}) dU \qquad (2.32)^2$$

Consider now the following vector identity:

$$\operatorname{div}(\overline{a} \times \overline{b}) = (\operatorname{curl} \overline{a}) \cdot \overline{b} - \overline{a} \cdot \operatorname{curl} \overline{b}$$
, (2.33)

Integrating both sides and then applying the divergence theorem to the left-hand side yields

With  $\overline{a}$  replaced by  $\overline{v}$ \* and  $\overline{b}$  replaced by  $(\hat{p} \text{ curl } \overline{v})$  one obtains

$$\iiint [\overline{\mathbf{v}}^*.\operatorname{curl}(\hat{\mathbf{p}} \operatorname{curl} \overline{\mathbf{v}})] d\mathbf{U} = \iiint [\operatorname{curl}(\overline{\mathbf{v}}^*).(\hat{\mathbf{p}} \operatorname{curl} \overline{\mathbf{v}})] d\mathbf{U}$$

$$- \oiint [\overline{\mathbf{v}}^* \times (\hat{\mathbf{p}} \operatorname{curl} \overline{\mathbf{v}})].\overline{\mathbf{n}} d\mathbf{S} \quad (2.35)$$

Note that (2.35) is merely the application of Green's first identity in vector form. Since the curl operator is linear, one can write

$$\operatorname{curl}(\overline{\mathbf{v}}^*) = (\operatorname{curl} \overline{\mathbf{v}})^* \tag{2.36}$$

Now, substituting (2.35) into (2.32) one obtains

$$F(\vec{v}) = \iint [(\operatorname{curl} \vec{v})^* \cdot (\hat{p} \operatorname{curl} \vec{v})] dU - \omega^2 \iint (\vec{v}^* \cdot \hat{q} \vec{v}) dU + \iint (\vec{v}^* \cdot \vec{g} + \vec{g}^* \cdot \vec{v}) dU - \oiint [\vec{v}^* \times (\hat{p} \operatorname{curl} \vec{v})] \cdot \vec{n} dS$$
 (2.37)

By denoting the components of the vectors  $\overline{g}$ ,  $\overline{v}$  and  $\overline{v}$  by  $g_i$ ,  $v_i$  and  $(\text{curl }\overline{v})_i$ , i=1,2,3, and the components of

the tensors  $\hat{p}$  and  $\hat{q}$  by  $p_{i,j}$  and  $q_{i,j}$ , i,j=1,2,3, respectively, one can rewrite the functional in the following form

$$\mathbb{T}(\overline{v}) = \sum_{i=1}^{3} \iiint [p_{i,i} | (\operatorname{curl} \overline{v})_{i}|^{2} + p_{i,i+1} (\operatorname{curl} \overline{v})_{i}^{*} (\operatorname{curl} \overline{v})_{i+1} \\
+ p_{i+1,i} (\operatorname{curl} \overline{v})_{i} (\operatorname{curl} \overline{v})_{i+1}^{*} - \omega^{2}(q_{i,i} | v_{i}|^{2} \\
+ q_{i,i+1} v_{i}^{*} v_{i+1}^{*} + q_{i+1,i} v_{i} v_{i+1}^{*}) + v_{i}^{*} g_{i}^{*} + g_{i}^{*} v_{i}^{*} ] dU \\
+ \sum_{i=1}^{3} \operatorname{ff}[\overline{1}_{i} \sum_{j=1}^{3} (p_{i+1,j} v_{i+2}^{*} - p_{i+2,j} v_{i+1}^{*}) (\operatorname{curl} \overline{v})_{j}].\overline{n} dS \\
i = 1 \Gamma$$
(2.38)

The subscripts in (2.38) are cyclic modulo 3. The unit vector in the i-th coordinate direction is denoted by  $\overline{1}_i$ . The volume integral is defined over some volume  $\alpha$  bounded by a surface.  $\Gamma$ . The surface integral is carried out over  $\Gamma$ . The unit vector  $\overline{n}$  is outward normal everywhere to the surface  $\Gamma$ .

The functional  $F(\overline{v})$  is an energy related quantity. This relationship arises from the fact that all the terms in the integrand of the volume integral are proportional to volume energy density. For instance, if  $\overline{v}$  represents the electric field intensity  $\overline{E}$  and  $\hat{p}$  represents the inverse of the permeability tensor  $\hat{\mu}_i$ , then the term  $(\text{curl }\overline{v})^*.(\hat{p}\,\text{curl }\overline{v})$  is equivalent to  $-\omega^2\overline{B}^*.\overline{H}$ ; the dot product  $\overline{B}^*.\overline{H}$  has the dimensionality of volume energy density.

If one assumes that the <u>medium is lossless</u>, then by its relation to energy, the functional  $F(\overline{v})$  must be a real number. Consequently, one can immediately establish that the diagonal elements of the tensors  $\hat{p}$  and  $\hat{q}$  must be real, i.e.  $p_{i,i}$  and  $q_{i,i}$  must be real. Now, if  $\hat{p}$  and  $\hat{q}$  have

complex of fields, and elements, then the only way in which  $f(\overline{v})$  can be real is if  $\hat{p}$  and  $\hat{q}$  are complex conjugate symmetric tensors (i.e. Hermitian tensors). To show this, consider for instance the following term in the functional (2.38):

$$q_{i,i+1}v_{i}^{*}v_{i+1} + q_{i+1,i}v_{i}v_{i+1}^{*} = \frac{1}{2}$$

$$(q_{i,i+1} + q_{i+1,i})[Re(v_{i}^{*})Re(v_{i+1}^{*}) - Im(v_{i})Im(v_{i+1}^{*})] + \frac{1}{2}$$

$$(\sqrt{-1})(q_{i+1,i} - q_{i,i+1})[Im(v_{i})Re(v_{i+1}^{*}) + Re(v_{i})Im(v_{i+1}^{*})]$$

$$(2.39)$$

Equation (2.39) can also be written in the following way

$$q_{i,i-1}v_{i}^{*}v_{i+1}^{+} + q_{i+1,i}v_{i}v_{i+1}^{*} = \\ \left[ \operatorname{Re}(q_{i,i+1}, q_{i+1,i}) + \sqrt{-1} \operatorname{Im}(q_{i,i+1}^{i} + q_{i+1,i}) \right] \left[ \operatorname{Re}(v_{i+1}^{*}v_{i}) \right] + \\ \left[ \operatorname{Im}(q_{i,i+1}, q_{i+1,i}) + \sqrt{-1} \operatorname{Re}(q_{i+1,i}, q_{i,i+1}) \right] \left[ \operatorname{Im}(v_{i+1}^{*}v_{i}) \right]$$

$$(2.40)$$

If q is Hermitian, then the following relations hold true:

$$Re(q_{i+1,i}) = Re(q_{i,i+1})$$

$$Im(q_{i+1,i}) = -Im(q_{i,i+1})$$

$$Using (2.41) and (2.42), equation (2.40) becomes$$
(2.41)

$$q_{i,i+1}v_{i}^{*}v_{i+1}^{*}+q_{i+1,i}v_{i}^{*}v_{i+1}^{*}=$$

$$2[Re(q_{i,i+1})Re(v_{i+1}^{*}v_{i}) + Im(q_{i,i+1})Im(v_{i+1}^{*}v_{i})] =$$

$$2Re(q_{i,i+1}^{*}v_{i+1}^{*}v_{i}) = 2Re(q_{i+1,i}v_{i+1}^{*}v_{i}) =$$

$$Re[(q_{i+1,i}^{*} c_{i,i+1}^{*})v_{i+1}^{*}v_{i}^{*}]$$

$$(2.43)$$

which is definitely real. An entirely analogous derivation yields

$$p_{i,i+1}(\text{curl } \overline{v})_{i}^{*}(\text{curl } \overline{v})_{i+1} + p_{i+1,i}(\text{curl } \overline{v})_{i}(\text{curl } \overline{v})_{i+1}^{*}$$

$$\text{Re}[(p_{i+1,i} + p_{i,i+1}^{*})(\text{curl } \overline{v})_{i+1}^{*}(\text{curl } \overline{v})_{i}] \qquad (2.44)$$

In view of these results the functional in (2.38) can be rewritten in the following way

$$F(\overline{v}) = \sum_{i=1}^{3} \iiint \{p_{i,i} | eurl \overline{v}\}_{i}^{2} + 2Re[p_{i+1}, \overline{v}(eurl \overline{v})_{i+1}^{*}(eurl \overline{v})_{i}]$$

$$-\omega^{2}[q_{i,i} | v_{i}|^{2} + 2Re(q_{i+1,i}v_{i}, v_{i})] + 2Re(g_{i}v_{i}^{*})\} dv$$

$$+ \sum_{i=1}^{3} \iiint \{p_{i,i} | v_{i}|^{2} + 2Re(q_{i+1,i}v_{i}, v_{i})] + 2Re(g_{i}v_{i}^{*})\} dv$$

$$+ \sum_{i=1}^{3} \iiint \{p_{i,i} | v_{i}|^{2} + 2Re(q_{i+1,i}v_{i}, v_{i})\} + 2Re(g_{i}v_{i}^{*})\} dv$$

$$(2.45)$$

# 2.3 Boundary Conditions

Up to this point, a functional associated with the curlcurl equation has been derived. According to the Minimum Theorem [40] the vector function  $\overline{V}$  which minimizes  $F(\overline{V})$  is a solution of the associated differential equation. There are infinitely many functions  $\overline{V}$  which satisfy a differential equation. Of these, only the one which satisfies certain boundary conditions is needed. It is therefore assumed that the region  $\Omega$  is bounded by a perfectly conducting surface  $\Gamma$  and that there is no net transfer of energy across it.

Let  $\overline{v}$  represent the electric field intensity  $\overline{E}$ . Then

$$\hat{\mathbf{p}} \text{ curl } \overline{\mathbf{v}} = \hat{\boldsymbol{\mu}}^{-1} \text{ curl } \overline{\mathbf{E}} = -\mathbf{j} \boldsymbol{\omega} \overline{\mathbf{H}}$$
 (2.46)

<u>ئ</u> ۽

and the surface integral term in the functional (2.37) can be written as

$$- \underset{\Gamma}{\text{ff}} [\overline{\mathbf{v}}^* \mathbf{x} (\hat{\mathbf{p}} \operatorname{curl} \overline{\mathbf{v}})] . \overline{\mathbf{n}} dS = \mathbf{j} \omega \underset{\Gamma}{\text{ff}} (\overline{\mathbf{E}}^* \mathbf{x} \overline{\mathbf{H}}) . \overline{\mathbf{n}} dS \qquad (2.47)$$

The cross product  $\overline{E}^*x$   $\overline{H}$  is the well known complex Poynting vector-representing the density of power flux. The surface integral in (2.47) therefore represents the net power flow across the boundary surface. If the boundary is a perfect conductor, then no energy is transferred and the Poynting vector is tangential everywhere to the surface. Mathematically this idea is expressed by the equation

$$[\overline{\mathbf{v}}^*\mathbf{x}(\hat{\mathbf{p}}\,\mathrm{curl}\,\overline{\mathbf{v}})].\overline{n} = 0 \qquad (2.48)$$

The boundary conditions that are implicitly enforced by leaving out the surface integral from the functional, i.e. that correspond to the choice given by equation (2.48), are called the natural boundary conditions of the functional [29-35]. It is a well known property of scalar triple products that they remain unchanged under a cyclic permutation of three vectors. Thus one can write the following equalities:

$$[\overline{\mathbf{v}}^* \mathbf{x} (\hat{\mathbf{p}} \operatorname{curl} \overline{\mathbf{v}})].\overline{\mathbf{n}} = [(\hat{\mathbf{p}} \operatorname{curl} \overline{\mathbf{v}}) \mathbf{x} \overline{\mathbf{n}}].\overline{\mathbf{v}}^*$$

$$= (\overline{\mathbf{n}} \mathbf{x} \overline{\mathbf{v}}^*).(\hat{\mathbf{p}} \operatorname{curl} \overline{\mathbf{v}})$$

$$= \begin{vmatrix} n_1 & n_2 & n_3 \\ v_1^* & v_2^* & v_3^* \\ (\hat{\mathbf{p}} \operatorname{curl} \overline{\mathbf{v}})_1 & (\hat{\mathbf{p}} \operatorname{curl} \overline{\mathbf{v}})_2 & (\hat{\mathbf{p}} \operatorname{curl} \overline{\mathbf{v}})_3 \end{vmatrix}$$

$$= (\widehat{\mathbf{n}} \mathbf{x} \overline{\mathbf{v}}^*).(\widehat{\mathbf{p}} \operatorname{curl} \overline{\mathbf{v}})_1 & (\widehat{\mathbf{p}} \operatorname{curl} \overline{\mathbf{v}})_2 & (\widehat{\mathbf{p}} \operatorname{curl} \overline{\mathbf{v}})_3 \end{vmatrix}$$

$$= (\widehat{\mathbf{n}} \mathbf{x} \overline{\mathbf{v}}^*).(\widehat{\mathbf{p}} \operatorname{curl} \overline{\mathbf{v}})_1 & (\widehat{\mathbf{p}} \operatorname{curl} \overline{\mathbf{v}})_2 & (\widehat{\mathbf{p}} \operatorname{curl} \overline{\mathbf{v}})_3 \end{vmatrix}$$

It will now be shown that the boundary conditions implicit in

y = \$1987 - 4mg

(2.48) are exactly the same as those commonly encountered in connection with electromagnetic problems.

Let  $\overline{v}$  represent the electric field  $\overline{E}$  again. Then by (2.49) it is obvious that equation (2.48) will be satisfied whenever

$$\overline{n} \times \overline{\Xi} = \overline{n} \times \hat{\epsilon}^{-1} \operatorname{curl} \overline{H} = 0$$
 on  $\Gamma$  (2.50)

Now, let  $\overline{v}$  represent the magnetic field  $\overline{H}$ . Then, again by virtue of (2.49) it can be seen that equation (2.48) will be satisfied whenever (2.50) is true. The boundary condition expressed in equation (2.50) is the one commonly used [37.38] on perfect electric conductors. It merely states that the electric field intensity vector  $\overline{E}$  must be normal everywhere at the boundary.

The boundary condition given by

$$\overline{n} \times \overline{H} = \overline{n} \times \hat{\mu}^{-1} \text{curl } \overline{E} = 0$$
 on  $\Gamma$  (2.51)

is equally correct and satisfies (2.48), but it is only meaningful if one accepts the idea of perfect magnetic conductor. This is defined as a raterial for which  $\overline{H}$  must be normal everywhere at its surface.

The boundary conditions (2.50) and (2.51) can also be obtained in terms of the magnetic vector potential  $\overline{A}$ . For perfect electric conductors, by virtue of equation (2.19), one can write

$$\overline{n} \times \overline{E} = \overline{n} \times \overline{A} = 0$$
 on  $\Gamma$  (2.52)

while for perfect magnetic conductors one obtains

$$\overline{n} \times \overline{H} = \overline{n} \times \hat{\mu}^{-1} \operatorname{curl} \overline{A} = 0$$
 on  $\Gamma$  (2.53)

The boundary condition for  $\overline{E}$  on a perfect electric conductor must be examined more closely. The cross product  $\overline{n}$  x  $\overline{E}$  produces a vector with three components. Each component must vanish individually. If the components of  $\overline{n}$  are  $n_1$ ,  $n_2$  and  $n_3$  and those of  $\overline{E}$  are  $E_1$ ,  $E_2$  and  $E_3$ , then the following three equations will result

$$n_i E_{i+1} - n_{i+1} E_i = 0$$
 i cyclic mod 3 (2.54)

The solution to the system of three equations given by (2,54) is

$$E_2 = (n_2/n_1)E_1 : n_1 \neq 0 : E_1 \text{ arbitrary}$$
 (2.55)

$$E_3 = (n_3/n_1)E_1 ; n_1 \neq 0 ; E_1 \text{ arbitrary}$$
 (2.56)

$$E_2 = (n_2/n_3)E_3 : n_3 \neq 0 : E_1 = 0 : n_1 = 0 : E_3 \text{ arbitrary (2.57)}$$

$$E_2 = \text{arbitrary} \; ; \; n_2 = 1 \; ; \; E_1 = E_3 = 0 \; ; \; n_1 = n_3 = 0$$
 (2.58)

Therefore  $\overline{n} \times \overline{E} = 0$  does not specify  $\overline{E}$  in magnitude, it only specifies its direction, i.e.  $\overline{E}$  has to be everywhere normal to the boundary surface.

A very similar reasoning can be carried out for the components of  $\hat{\epsilon}^{-1}$  curl  $\overline{H}$ . The solution of these equations result in three impedance type boundary conditions, one for each component of  $\overline{H}$ . These boundary conditions are given here in rectangular coordinates (x,y,z) and in cylindrical coordinates  $(r,\theta,z)$ . The symbols  $\overline{v}$  and  $\hat{p}$  are used instead of  $\overline{H}$  and  $\hat{\epsilon}^{-1}$  in order to preserve generality. In rectangular coordinates (x,y,z), the following is obtained by setting each component of the vector  $(\hat{p} \text{ curl } \overline{v}) \times \overline{n}$  to zero:

$$\frac{\partial v_{x}}{\partial n} = \frac{\partial v_{x}}{\partial x} \frac{dx}{dn}$$

$$+(p_{yy}+p_{zz})^{-1} \left[p_{yy} \frac{\partial v_{x}}{\partial y} + p_{zz} \frac{\partial v_{y}}{\partial x} + p_{zx} (\frac{\partial v_{z}}{\partial y} - \frac{\partial v_{y}}{\partial z}) + p_{zy} (\frac{\partial v_{x}}{\partial z} - \frac{\partial v_{z}}{\partial x})\right] \frac{dy}{dn}$$

$$+(p_{yy}+p_{zz})^{-1} \left[p_{yy} \frac{\partial v_{z}}{\partial x} + p_{zz} \frac{\partial v_{x}}{\partial z} - p_{yx} (\frac{\partial v_{z}}{\partial y} - \frac{\partial v_{y}}{\partial z}) - p_{yz} (\frac{\partial v_{y}}{\partial x} - \frac{\partial v_{x}}{\partial y})\right] \frac{dz}{dn}$$

$$(2.59)$$

$$\frac{\partial v_{y}}{\partial n} = \frac{\partial v_{y}}{\partial y} \frac{dy}{dn}$$

$$+ (p_{xx} + p_{zz})^{-1} \left[ p_{xx} \frac{\partial v_{y}}{\partial x} + p_{zz} \frac{\partial v_{x}}{\partial y} - p_{zx} (\frac{\partial v_{z}}{\partial y} - \frac{\partial v_{y}}{\partial z}) - p_{zy} (\frac{\partial v_{x}}{\partial z} - \frac{\partial v_{z}}{\partial x}) \right] \frac{dx}{dn}$$

$$+ (p_{xx} + p_{zz})^{-1} \left[ p_{xx} \frac{\partial v_{z}}{\partial y} + p_{zz} \frac{\partial v_{y}}{\partial z} + p_{xy} (\frac{\partial v_{x}}{\partial z} - \frac{\partial v_{z}}{\partial x}) + p_{xz} (\frac{\partial v_{y}}{\partial x} - \frac{\partial v_{x}}{\partial y}) \right] \frac{dz}{dn}$$

$$(2.60)$$

$$\frac{\partial \mathbf{v}_{z}}{\partial n} = \frac{\partial \mathbf{v}_{z}}{\partial z} \frac{dz}{dn} 
+ (\mathbf{p}_{xx} + \mathbf{p}_{yy})^{-1} \left[ \mathbf{p}_{xx} \frac{\partial \mathbf{v}_{z}}{\partial x} + \mathbf{p}_{yy} \frac{\partial \mathbf{v}_{x}}{\partial z} + \mathbf{p}_{yx} (\frac{\partial \mathbf{v}_{z}}{\partial y} - \frac{\partial \mathbf{v}_{y}}{\partial z}) + \mathbf{p}_{yz} (\frac{\partial \mathbf{v}_{y}}{\partial x} - \frac{\partial \mathbf{v}_{x}}{\partial y}) \right] \frac{dx}{dn} 
+ (\mathbf{p}_{xx} + \mathbf{p}_{yy})^{-1} \left[ \mathbf{p}_{xx} \frac{\partial \mathbf{v}_{y}}{\partial z} + \mathbf{p}_{yy} \frac{\partial \mathbf{v}_{z}}{\partial y} - \mathbf{p}_{xy} (\frac{\partial \mathbf{v}_{x}}{\partial z} - \frac{\partial \mathbf{v}_{z}}{\partial x}) - \mathbf{p}_{xz} (\frac{\partial \mathbf{v}_{y}}{\partial x} - \frac{\partial \mathbf{v}_{x}}{\partial y}) \right] \frac{dy}{dn}$$
(2.61)

These equations appear to be quite complicated. Note however, that for two-dimensional problems defined in the x-y plane, dz/dn is zero and the equations become somewhat simplified.

In cylindrical coordinates  $(r, \theta, z)$  the above equations take on a similar form:

$$\frac{\partial v_{r}}{\partial n} = \frac{\partial v_{r}}{\partial r} \frac{dr}{dn}$$

$$+ (p_{\theta\theta} + p_{zz})^{-1} \left[ p_{\theta\theta} \frac{\partial v_{r}}{\partial \theta} + p_{zz} \frac{\partial rv_{\theta}}{\partial r} + p_{zr} (\frac{\partial v_{z}}{\partial \theta} - r\frac{\partial v_{\theta}}{\partial z}) + p_{z\theta} r (\frac{\partial v_{r}}{\partial z} - \frac{\partial v_{z}}{\partial r}) \right] \frac{d\theta}{dn}$$

$$+ (p_{\theta\theta} + p_{zz})^{-1} \left[ p_{\theta\theta} \frac{\partial v_{z}}{\partial r} + p_{zz} \frac{\partial v_{r}}{\partial z} - p_{\theta r} (\frac{\partial v_{z}}{r\partial \theta} - \frac{\partial v_{\theta}}{\partial z}) - \frac{p_{\theta z}}{r} (\frac{\partial rv_{\theta}}{\partial r} - \frac{\partial v_{r}}{\partial \theta}) \right] \frac{dz}{dn}$$

$$(2.62)$$

$$\frac{\partial v_{\theta}}{\partial n} = \frac{\partial v_{\theta}}{\partial \theta} \frac{d\theta}{dn} + (p_{rr} + p_{zz})^{-1} \left[ p_{rr} \frac{\partial v_{\theta}}{\partial r} - p_{zz} \left( \frac{v_{\theta}}{r} - \frac{\partial v_{r}}{\partial \theta} \right) - p_{zr} \left( \frac{\partial v_{z}}{r \partial \theta} - \frac{\partial v_{\theta}}{\partial z} \right) - p_{z\theta} \left( \frac{\partial v_{r}}{\partial z} - \frac{\partial v_{z}}{\partial r} \right) \right] \frac{dr}{dn} + (p_{rr} + p_{zz})^{-1} \left[ p_{rr} \frac{\partial v_{z}}{\partial \theta} + p_{zz} \frac{\partial v_{\theta}}{\partial z} + p_{r\theta} \left( \frac{\partial v_{r}}{\partial z} - \frac{\partial v_{z}}{\partial r} \right) + \frac{p_{rz}}{kr} \left( \frac{\partial rv_{\theta}}{\partial r} - \frac{\partial v_{r}}{\partial \theta} \right) \right] \frac{dz}{dn}$$
(2.63)

$$\frac{\partial v_{z}}{\partial n} = \frac{\partial v_{z}}{\partial z} \cdot \frac{\partial z}{\partial n}$$

$$+ (p_{rr} + p_{\theta\theta})^{-1} \left[ p_{rr} \frac{\partial v_{z}}{\partial r} + p_{\theta\theta} \frac{\partial v_{r}}{\partial z} + p_{\theta r} (\frac{\partial v_{z}}{\partial \theta} - \frac{\partial v_{\theta}}{\partial z}) + \frac{p_{\theta z}}{r} (\frac{\partial rv_{\theta}}{\partial r} - \frac{\partial v_{r}}{\partial \theta}) \right] \frac{\partial r}{\partial n}$$

$$+ (p_{rr} + p_{\theta\theta})^{-1} \left[ p_{rr} \frac{\partial v_{\theta}}{\partial z} + p_{\theta\theta} \frac{\partial v_{z}}{\partial \theta} - p_{r\theta} r (\frac{\partial v_{r}}{\partial z} - \frac{\partial v_{z}}{\partial r}) - p_{rz} (\frac{\partial rv_{\theta}}{\partial r} - \frac{\partial v_{r}}{\partial \theta}) \right] \frac{\partial \theta}{\partial n}$$

$$(2.64)$$

Notice again that for axisymmetric problems defined in the r-z plane  $d\theta/dn=0$  and the expressions above become less complicated.

The boundary conditions (2.59) to (2.64) are valid for  $\overline{E}$ ,  $\overline{H}$  and  $\overline{A}$  at perfect electric and magnetic conductors. These boundary conditions are natural boundary conditions of the functional when the surface integral is set to zero and will be automatically satisfied by the function which

minimizes the functional. In other words one does not need to restrict the set from which the function  $\overline{v}$  his taken. Dirichlet boundary conditions such as the ones contained in equations (2.55) through (2.58) have, of course, to be taken care of explicitly. This is usually easy to accomplish.

One question in connection with boundary conditions remains unanswered: Are the boundary conditions derived here sufficient to guarantee a unique solution? The answer to this question is not at all obvious since one is dealing with vector quantities. Thus, if one is solving for  $\overline{E}$ , is it sufficient to specify  $\overline{n} \times \overline{E} = 0$  or does one also have to specify another condition? At least one well known textbook on electromagnetic theory states that two conditions must be specified in the case of a vector function [41].

# 2.4 Uniqueness

It will now be shown that the boundary conditions given in (2.50) through (2.53) for perfect electric or magnetic conductors do indeed guarantee unique solutions to the curlcurl equation (2.29). Suppose that two distinct solutions exist for the same boundary value problem and denote them by  $\overline{V}_1$  and  $\overline{V}_2$ . Electromagnetically,  $\overline{V}_1$  and  $\overline{V}_2$  could be either electric field intensity vectors or magnetic field vectors. It is required that the curls of the two solutions  $\overline{V}_1$  and  $\overline{V}_2$  be equal so that  $\overline{V}_1$  and  $\overline{V}_2$  both have the same volume sources. Due to the linear nature of the curl operator the difference solution  $\overline{V}_d = \overline{V}_1 - \overline{V}_2$  also satisfies the

differential equation (2.29), but with a vanishing source term. Moreover, the curl of  $\overline{V}_d$  is zero.

The energy norm of the vector field  $\overline{V}$  will be defined by the following integral

$$\|\overline{\mathbf{v}}\| = \left[ \int \int \overline{\mathbf{v}}^* \cdot \hat{\mathbf{q}} \overline{\mathbf{v}} \, d\mathbf{u} \right]^{\frac{1}{2}} \tag{2.65}$$

where the integration is over a volume  $\Omega$  bounded by a , surface  $\Gamma$ . The norm of  $\overline{V}$  as given by (2.65) is a number assigned to  $\overline{V}$  which is in the energy sense a measure of the magnitude of  $\overline{V}$ . The vector function  $\overline{V}$  belongs to a linear space S. The norm given in (2.65) is valid provided that the following conditions are met

- $(1) \quad ||\overline{a}|| \geqslant 0 \quad \overline{a} \in S$
- (2)  $\left\| c\overline{a} \right\| = \left| c \right| \left\| \overline{a} \right\|$  where c is any real number
- (3)  $\|\bar{a} + \bar{b}\| \le \|\bar{a}\| + \|\bar{b}\|$  (triangle inequality)  $\bar{b} \in S$
- (4)  $\|\overline{a}\| = 0$  implies  $\overline{a} \equiv 0$

If the 3 by 3 non-singular Aermitian matrix representing the material property tensor  $\hat{\mathbf{q}}$  is positive definite, then the Hermitian form  $[V]^*[q][V]$  is strictly positive for all non-trivial [V]. This is the only requirement needed to meet the four conditions above. Permittivity and permeability tensors of passive media are all positive definite 3 by 3 matrices.

One would like to find the conditions under which the square of the energy norm of  $\overline{V}_d$  vanishes. If the energy norm is zero then by property number (4) above  $\overline{V}_d$  itself will be zero 'almost everywhere'. By substituting for  $\hat{q}.\overline{V}_d$  from

 $<sup>^1</sup>$  'almost everywhere' implies everywhere except on a denumerable subset of  $\, \Omega \,$  such as the surface  $\Gamma .$ 

the curlcurl equation and then using Green's first identity in vector form (see equation (2.35)), the energy norm of  $\overline{V}_d$  can be transformed as follows

$$\iiint \overline{V}_{d}^{*}.(\hat{q} \, \overline{V}_{d}) dU = (1/\omega^{2}) \iiint \overline{V}_{d}^{*}.[\operatorname{curl}(\hat{p} \, \operatorname{curl} \, \overline{V}_{d})] dU$$

$$= (1/\omega^{2}) \iiint [\operatorname{curl}(\overline{V}_{d}^{*}).(\hat{p} \, \operatorname{curl} \, \overline{V}_{d})] dU$$

$$- (1/\omega^{2}) \oiint [\overline{V}_{d}^{*} \times (\hat{p} \, \operatorname{curl} \, \overline{V}_{d})].\overline{n} \, dS \qquad (2.66)$$

The volume integral over  ${\bf n}$  vanishes because the curl of  $\overline{V}_d$  is zero within the volume. In order to make the surface integral vanish one requires that the integrand be zero.

$$[\overline{V}_{d}^{*} \times (\hat{p} \operatorname{curl} \overline{V}_{d})].\overline{n} = 0$$
 (2.67)

This is true whenever either

$$\overline{n} \times \overline{V}_{d} = 0 \tag{2.68}$$

or

$$\bar{n} \times (\hat{p} \operatorname{curl} \overline{V}_{d}) = 0$$
 (2.69)

Obviously, if  $\overline{V}_1$  and  $\overline{V}_2$  both satisfy either of these conditions at the boundary surface, then  $\overline{V}_d$  also satisfies them and (2.66) is equal to zero. Therefore  $\overline{V}_1$  and  $\overline{V}_2$  are one and the same unique solution of the curlcurl equation. Note that the proof breaks down when the frequency  $\omega$  is zero.

The situation is quite different for the magnetic vector potential  $\overline{A}$ . The boundary conditions given in (2.52) and (2.53) in terms of  $\overline{A}$  for perfect electric and magnetic conductors, respectively, guarantee that the electric and

magnetic fields  $\widetilde{E}$  and  $\widetilde{H}$  derived from the solution of equation (2.23) will be unique. However, unless the divergence of  $\widetilde{A}$  is somehow fixed,  $\widetilde{A}$  itself is not unique. If the Coulomb convention is adopted, the divergence of  $\widetilde{A}$  will be zero and equation (2.23) will reduce to the vector Poisson equation. Even so, the solution is not unique if only the boundary condition  $\widetilde{n} \times \widehat{\mu}^{-1} \operatorname{curl} \widetilde{A} = 0$  is applied to all parts of the boundary.

# 2.5 Explicit Forms of the Functional

If a region of space is bounded by a perfect electric conductor with no magnetic currents flowing on its surface, i.e. if  $\overline{n} \times \overline{E}$  is zero, then equation (2.13) can be solved for the vector  $\overline{E}$  by using the boundary condition  $\overline{n} \times \overline{E} = 0$ . The corresponding vector  $\overline{H}$  can be obtained for the same problem by solving equation (2.14) with the boundary condition  $\overline{n} \times \hat{\epsilon}^{-1}$  curl  $\overline{H} = 0$ . The electric current induced on the surface of the perfect electric conductor can be obtained by evaluating  $\overline{n} \times \overline{H}$ . The induced electric curface charge density is given by  $\overline{n} \cdot (\hat{\epsilon} \cdot \overline{E})$ .

If the boundary of the region behaves like a perfect magnetic conductor with no electric currents flowing on its surface, i.e. if  $\overline{n} \times \overline{H}$  is zero, then equation (2.14) can be solved for the magnetic field vector  $\overline{H}$  by using the boundary condition  $\overline{n} \times \overline{H} = 0$ . The corresponding vector  $\overline{E}$  can be obtained for the same problem by solving equation (2.13) with the boundary condition  $\overline{n} \times \widehat{\mu}^{-1}$  curl  $\overline{E} = 0$ . The magnetic current induced on the surface of the perfect a gnetic conductor is

given by  $\overline{n}$   $\times \overline{\Xi}$ . The induced fictitious ragnetic surface charge density is given by  $\overline{n}$ . ( $\hat{\mu}$   $\overline{H}$ ). No electric charges are found on the magnetic conductor.

If the boundary consists partly of a perfect electric conductor and partly of a perfect magnetic conductor, then the vector  $\overline{E}$  can be obtained by solving equation (2.13) with the boundary condition  $\overline{n} \times \overline{E} = 0$  on the electric conductor and with the boundary condition  $\overline{n} \times \hat{\mu}^{-1}$  curl  $\overline{E} = 0$  on the magnetic conductor. The corresponding vector  $\overline{H}$  is obtained by solving equation (2.14) with the boundary condition  $\overline{n} \times \hat{\epsilon}^{-1}$  curl  $\overline{H} = 0$  where the electric conductor is located and with the boundary condition  $\overline{n} \times \overline{H} = 0$  where the magnetic conductor is found.

The solutions are unique in all of the above cases. The medium is of course localess, nonconductive and for many practical problems it can also be considered to be sourcefree (i.e.  $\overline{J}_i$  is zero). The sources most often met in practical problems are of the conduction current type in which case it is easier to solve equation (2.23) for the magnetic vector potential. It will be assumed from here on that the medium is linear and that the frequency dependence of the material property tensors can be neglected.

For an abrupt discontinuity in the permittivity  $\hat{\epsilon}$  in an inhomogeneous medium there is an abrupt change in the electric field  $\overline{E}$  as well. In such cases it is advantageous to solve for the magnetic field from equation (2.14). Similarly, for an inhomogeneous medium with discontinuities in the permeability  $\hat{\mu}$ ,  $\overline{H}$  displays discontinuities and it is easier to solve for  $\overline{E}$  from equation (2.13) than for  $\overline{H}$  from

reputtion (2.14). The simultaneous occurrence of both types of inhomogeneities is rare.

The solution of the curlcurl equation is achieved by minimizing the associated functional. The boundary conditions (2.59) through (2.64) are natural if the surface integral is neglected from the functional. For the boundary condition  $\overline{n} \times \overline{v} = 0$ , which must be taken care of explicitly, the surface integral still vanishes. Without the surface integral, the functional given in (2.45) takes on the following form in rectangular coordinates (x,y,z):

$$F(\overline{v}) = \int \int \Re \left[ p_{xx} \left( \frac{\partial v_{z}}{\partial y} \frac{\partial v_{z}^{*}}{\partial y} - \frac{\partial v_{z}}{\partial y} \frac{\partial v_{y}^{*}}{\partial z} - \frac{\partial v_{z}^{*}}{\partial y} \frac{\partial v_{y}}{\partial z} + \frac{\partial v_{y}}{\partial z} \frac{\partial v_{y}^{*}}{\partial z} \right) \right]$$

$$+ p_{yy} \left( \frac{\partial v_{x}}{\partial z} \frac{\partial v_{x}^{*}}{\partial z} - \frac{\partial v_{x}}{\partial z} \frac{\partial v_{x}^{*}}{\partial x} - \frac{\partial v_{x}^{*}}{\partial z} \frac{\partial v_{z}}{\partial x} + \frac{\partial v_{z}}{\partial z} \frac{\partial v_{z}^{*}}{\partial x} \right)$$

$$+ p_{zz} \left( \frac{\partial v_{y}}{\partial x} \frac{\partial v_{y}^{*}}{\partial x} - \frac{\partial v_{y}}{\partial x} \frac{\partial v_{x}^{*}}{\partial y} - \frac{\partial v_{y}^{*}}{\partial x} \frac{\partial v_{x}}{\partial y} + \frac{\partial v_{x}}{\partial y} \frac{\partial v_{x}^{*}}{\partial y} \right)$$

$$+ 2p_{yx} \left( \frac{\partial v_{z}^{*}}{\partial y} \frac{\partial v_{y}^{*}}{\partial z} - \frac{\partial v_{y}^{*}}{\partial z} \frac{\partial v_{y}^{*}}{\partial z} - \frac{\partial v_{z}^{*}}{\partial y} \frac{\partial v_{x}^{*}}{\partial y} + \frac{\partial v_{y}^{*}}{\partial z} \frac{\partial v_{x}^{*}}{\partial x} \right)$$

$$+ 2p_{zx} \left( \frac{\partial v_{z}^{*}}{\partial y} \frac{\partial v_{y}^{*}}{\partial x} - \frac{\partial v_{y}^{*}}{\partial z} \frac{\partial v_{y}^{*}}{\partial x} - \frac{\partial v_{z}^{*}}{\partial y} \frac{\partial v_{x}^{*}}{\partial y} + \frac{\partial v_{y}^{*}}{\partial z} \frac{\partial v_{x}^{*}}{\partial y} \right)$$

$$+ 2p_{zy} \left( \frac{\partial v_{z}^{*}}{\partial z} \frac{\partial v_{y}^{*}}{\partial x} - \frac{\partial v_{y}^{*}}{\partial z} \frac{\partial v_{y}^{*}}{\partial x} - \frac{\partial v_{z}^{*}}{\partial y} \frac{\partial v_{x}^{*}}{\partial y} + \frac{\partial v_{z}^{*}}{\partial z} \frac{\partial v_{x}^{*}}{\partial y} \right)$$

$$+ 2p_{zy} \left( \frac{\partial v_{z}^{*}}{\partial z} \frac{\partial v_{y}^{*}}{\partial x} - \frac{\partial v_{z}^{*}}{\partial z} \frac{\partial v_{y}^{*}}{\partial x} - \frac{\partial v_{z}^{*}}{\partial z} \frac{\partial v_{x}^{*}}{\partial y} + \frac{\partial v_{z}^{*}}{\partial z} \frac{\partial v_{x}^{*}}{\partial y} \right)$$

$$+ 2p_{zy} \left( \frac{\partial v_{z}^{*}}{\partial z} \frac{\partial v_{y}^{*}}{\partial x} - \frac{\partial v_{z}^{*}}{\partial z} \frac{\partial v_{y}^{*}}{\partial x} - \frac{\partial v_{z}^{*}}{\partial z} \frac{\partial v_{x}^{*}}{\partial y} - \frac{\partial v_{z}^{*}}{\partial z} \frac{\partial v_{x}^{*}}{\partial y} + \frac{\partial v_{z}^{*}}{\partial z} \frac{\partial v_{x}^{*}}{\partial y} \right)$$

$$+ 2p_{zy} \left( \frac{\partial v_{z}^{*}}{\partial z} \frac{\partial v_{y}^{*}}{\partial x} - \frac{\partial v_{z}^{*}}{\partial z} \frac{\partial v_{y}^{*}}{\partial x} - \frac{\partial v_{z}^{*}}{\partial z} \frac{\partial v_{z}^{*}}{\partial y} - \frac{\partial v_{z}^{*}}{\partial z} \frac{\partial v_{z}^{*}}{\partial y} + \frac{\partial v_{z}^{*}}{\partial z} \frac{\partial v_{z}^{*}}{\partial y} \right)$$

$$+ 2q_{zx}^{*} v_{z} v_{x}^{*} + 2q_{zy} v_{y} v_{y}^{*} + 2\left( g_{x}^{*} v_{x}^{*} + g_{y} v_{y}^{*} + g_{y} v_{y}^{*} + g_{z} v_{z}^{*} \right) \right] dx dy dz$$

For the two-dimensional, homogeneous, isotropic waveguide problem the above expression reduces to the familiar form [29]

$$F(\overline{v}) = \int \int (\operatorname{grad} v_z \cdot \operatorname{grad} v_z - \omega^2 \mu_0 \epsilon_0 v_z^2 + 2 g_z v_z) dx dy \qquad (2.71)$$

In cylindrical coordinates (r,0,z) the functional given in (2.45) takes on the following form:

$$F(\overline{v}) = \iiint \mathbb{R} e \left[ p_{rr} \left( \frac{\delta v_{z}}{r \delta \theta} \frac{\delta v_{z}^{*}}{\delta \theta} - \frac{\delta v_{z}}{\delta \theta} \frac{\delta v_{\theta}^{*}}{\delta z} - \frac{\delta v_{z}^{*}}{\delta \theta} \frac{\delta v_{\theta}}{\delta z} + r \frac{\delta v_{\theta}}{\delta z} \frac{\delta v_{\theta}^{*}}{\delta z} \right]$$

$$+ p_{\theta \theta} r \left( \frac{\delta v_{r}}{\delta z} \frac{\delta v_{r}^{*}}{\delta z} - \frac{\delta v_{r}}{\delta z} \frac{\delta v_{z}^{*}}{\delta z} - \frac{\delta v_{r}^{*}}{\delta z} \frac{\delta v_{z}}{\delta r} + \frac{\delta v_{\theta}}{\delta r} + \frac{\delta v_{\theta}}{\delta r} \right)$$

$$+ p_{zz} \left( r \frac{\delta v_{\theta}}{\delta r} \frac{\delta v_{\theta}^{*}}{\delta r} + v_{\theta}^{*} \frac{\delta v_{\theta}}{\delta r} + v_{\theta} \frac{\delta v_{\theta}^{*}}{\delta r} + \frac{v_{\theta}^{*} v_{\theta}}{r} - \frac{\delta v_{r}}{\delta \theta} \frac{\delta v_{\theta}^{*}}{\delta r} \right)$$

$$+ 2 p_{zz} \left( r \frac{\delta v_{\theta}}{\delta r} \frac{\delta v_{\theta}^{*}}{\delta r} - v_{\theta} \frac{\delta v_{r}^{*}}{\delta \theta} - \frac{v_{\theta}^{*}}{r} \frac{\delta v_{r}}{\delta \theta} + \frac{\delta v_{r}}{r} \frac{\delta v_{\theta}^{*}}{\delta \theta} \right)$$

$$+ 2 p_{\theta r} \left( \frac{\delta v_{z}}{\delta \theta} \frac{\delta v_{r}^{*}}{\delta z} - r \frac{\delta v_{\theta}}{\delta z} \frac{\delta v_{r}^{*}}{\delta z} - \frac{\delta v_{\theta}^{*}}{\delta \theta} \frac{\delta v_{r}^{*}}{\delta r} + r \frac{\delta v_{\theta}}{\delta z} \frac{\delta v_{r}^{*}}{\delta r} \right)$$

$$+ 2 p_{zr} \left( \frac{\delta v_{z}^{*}}{\delta \theta} \frac{\delta v_{\theta}}{\delta r} + v_{\theta}^{*} \frac{\delta v_{z}^{*}}{\delta \theta} - r \frac{\delta v_{\theta}^{*}}{\delta z} \frac{\delta v_{\theta}}{\delta r} - v_{\theta} \frac{\delta v_{\theta}^{*}}{\delta z} \right)$$

$$+ 2 p_{zr} \left( \frac{\delta v_{z}^{*}}{\delta \theta} \frac{\delta v_{\theta}}{\delta r} + v_{\theta}^{*} \frac{\delta v_{r}^{*}}{\delta z} - r \frac{\delta v_{\theta}^{*}}{\delta z} \frac{\delta v_{\theta}}{\delta r} - v_{\theta} \frac{\delta v_{\theta}^{*}}{\delta z} \right)$$

$$+ 2 p_{z} \left( r \frac{\delta v_{r}^{*}}{\delta z} \frac{\delta v_{\theta}^{*}}{\delta r} + v_{\theta}^{*} \frac{\delta v_{r}^{*}}{\delta z} - r \frac{\delta v_{\theta}^{*}}{\delta z} \frac{\delta v_{\theta}}{\delta r} - v_{\theta} \frac{\delta v_{\theta}^{*}}{\delta z} \right)$$

$$+ 2 p_{z} \left( r \frac{\delta v_{r}^{*}}{\delta z} \frac{\delta v_{\theta}^{*}}{\delta r} + v_{\theta}^{*} \frac{\delta v_{r}^{*}}{\delta z} - v_{\theta}^{*} \frac{\delta v_{\theta}^{*}}{\delta r} - r \frac{\delta v_{z}^{*}}{\delta r} \frac{\delta v_{\theta}^{*}}{\delta r} \right)$$

$$+ 2 p_{z} \left( r \frac{\delta v_{r}^{*}}{\delta z} \frac{\delta v_{\theta}^{*}}{\delta r} + v_{\theta}^{*} \frac{\delta v_{r}^{*}}{\delta z} - v_{\theta}^{*} \frac{\delta v_{\theta}^{*}}{\delta r} - r \frac{\delta v_{z}^{*}}{\delta r} \frac{\delta v_{\theta}^{*}}{\delta r} \right)$$

$$- \frac{\delta v_{r}^{*}}{\delta z} \frac{\delta v_{r}^{*}}{\delta \theta} - \frac{\delta v_{z}^{*}}{\delta r} \frac{\delta v_{\theta}^{*}}{\delta \theta} \right)$$

$$- \omega^{z} r \left( q_{rr} v_{r}^{*} v_{r}^{*} + r q_{\theta}^{*} v_{\theta}^{*} v_{\theta}^{*} + r q_{z}^{*} v_{\theta}^{*} + r q_{\theta}^{*} v_{\theta}^{*} \right)$$

$$+ 2 q_{z}^{*} r v_{z}^{*} + r q_{\theta}^{*} v_{\theta}^{*} v_{\theta}^{*} + r q_{z}^{*} v_{\theta}^{*} v_{\theta}^{*} + r q_{\theta}^{*} v_{\theta}^{*} + r q_{\theta}^{*} v_{\theta}^{*} \right)$$

Notice the factor 1/r in some of the terms in the integrand. The r arises from the Jacobian of the conformal transformation from rectangular to cylindrical coordinates. The singularity at r=0 is potentially troublesome as far as the integration is concerned. Although one cannot make the assertion from examining the above expression, one can state from an understanding of the physics of the problem that the singularity is integrable [37,38,42]. The limit of the terms with the 1/r

singularity as r tends to zero is indeterminate; this suggests that l'Horpital's rule can be applied. In such analysis the limits of these quantities are finite instead of blowing up, suggesting that the singularity can be removed. This point will be discussed in more detail in a later chapter.

At this point one could easily ask: How does one know if the functionals (2.45), (2.70) and (2.72) are correct? There is a way of checking the functional, and this has been done. If the integrand of the volume integral part of the functional  $F(\overline{v})$  is denoted by L, then according to the calculus of variations, the first variation of F will be zero provided that the following equations are satisfied:

$$\sum_{j=1}^{3} \frac{\partial^{2}L}{\partial a_{j} \partial (\frac{\partial v_{i}}{\partial a_{j}})} = \frac{\partial L}{\partial v_{i}} \qquad i = 1, 2, 3 \qquad (2.73)$$

These equations are referred to as the Euler equations associated with the Lagrangian L [43]. The  $a_j$  represent spatial coordinates. It has, been verified that (2.73) reduces (2.45), (2.70) and (2.72) to the curlcurl equation.

#### CHAPTER III

# DISCRETIZATION OF THE FUNCTIONAL BY APPROXIMATION OF VECTOR FIELDS WITH HIGH-ORDER POLYNOMIAL TRIANGULAR FINITE ELEMENTS

### Summary

This chapter discusses the solution of electromagnetic vector field problems in cases where travelling, circulating or evanescent waves occur in a bounded environment. Variationally stationary functionals are derived for specific wave types in planar and axisymmetric two-dimensional geometries. The singularities encountered in the functional for axisymmetric geometries are eliminated by a transformation of the field components. The transformed fields are expressed as a linear combination of local high-order, interpolation polynomials over triangular regions in the x-y and r-z coordinate planes. The coefficients of the expansion are equivalent to the numerical values of the fields at the interpolation nodes over the triangle. By substituting the polynomial approximations of the fields into the functional, a matrix expression is obtained which is the discretized equivalent of the original functional. The matrix expression is assembled from universally constant element matrices and geometric factors relating to triangle shape, sizé and position. The necessary element matrices have been computed and tabulated with the aid of a PL/I FORMAC preprocessor. Additional element matrices are obtained from these by simple row and column permutations. The procedure for assembling a global problem is stated. Finally, a matrix.

equation is generated by minimizing the discretized functional. Solutions of the matrix equation yield approximate solutions of the original field equations.

## 3.1 Types of Maves and Their Mathematical Representations

In this section, the types of guided waves which may exist in bounded, lossless media will be discussed. In the (x,y,z) coordinate system, it will be assumed that the behaviour of the function which describes the waves in the z-direction is known. In the  $(r,\theta,z)$  system, the same condition is assumed with respect to the  $\theta$ -direction. These assumptions are necessary in order to reduce the equations to two dimensional spaces.

Although waves may exist over the entire frequency spectrum, they will propagate only if the frequency is above the cutoff frequency. At and above cutoff, a guided wave in the rectangular coordinate system (x,y,z) is characterized by the relative phases of its field vector components and by a propagation constant  $\beta$ . Below the cutoff frequency the propagation constant & is replaced by an attenuation constant a characterizing an evanescent wave decaying in the z-direction. The functions describing the field components in the x-y plane and the frequency  $\omega$  at which the wave occurs in a medium described by the material property tensors  $\hat{\boldsymbol{\epsilon}}$ , and  $\hat{\boldsymbol{\mu}}$ , are in general unknown. Similarly, in the axisymmetric case the relative phases and the circulation constant m of a guided wave are known but the functions describing the field components in the r-z plane and the frequency are unknown. In this case the constant m is not artitrary but is related to the azimuthal

periodicity of the wave. In axisymmetric geometry attenuation in the  $\theta$ -direction cannot exist.

It is very important to realize that the character of a wave that can be supported in any given medium depends upon the form of the material property tensors describing the medium. In order for the equality in Maxwell's equations (2.1) and (2.2) to hold, there must exist a precise balance between the relative phases of the field vector components and the phases of the off-diagonal elements of the tensors  $\hat{\epsilon}$  and  $\hat{\mu}$ . For example, consider the three components of equation (2.1) in (x,y,z) coordinates, assuming that in the z-direction the wave varies as  $\exp(-\gamma z)$ 

$$\frac{\partial E_z}{\partial v} + \gamma \overline{E}_y = -j\omega(\mu_{xx}H_x + \mu_{xy}H_y + \mu_{xz}H_z)$$
 (3.1)

$$-\gamma E_{x} - \frac{\partial E_{z}}{\partial x} = -j\omega(\mu_{yx}H_{x} + \mu_{yy}H_{y} + \mu_{yz}H_{z})$$
 (3.2)

$$\frac{\partial E_{y}}{\partial x} - \frac{\partial E_{x}}{\partial y} = -j\omega(\mu_{zx}H_{x} + \mu_{zy}H_{y} + \mu_{zz}H_{z})$$
 (3.3)

If  $\gamma$  is replaced by an attenuation constant  $\alpha$ , then in a medium with real and symmetric permeability and permittivity tensors evanescent waves must be of the form

$$\overline{E} = \left[\overline{1}_{x} E_{x}(x,y) + \overline{1}_{y} E_{y}(x,y) + \overline{1}_{z} E_{z}(x,y)\right] \exp(j\omega t - \alpha z) \qquad (3.4)$$

$$\overline{H} = [\overline{1}_{x}H_{x}(x,y) + \overline{1}_{y}H_{y}(x,y) + \overline{1}_{z}H_{z}(x,y)] \exp(j\omega t - \alpha z \pm j\frac{\pi}{2})(3.5)$$

In other media, other types of evanescent waves may exist. If  $\gamma$  is replaced by  $j\beta$ , then only travelling waves of the . form

$$\overline{E} = \left[\overline{1}_{x} E_{x}(x,y) + \overline{1}_{y} E_{y}(x,y) + \overline{1}_{z} E_{z}(x,y) \exp(\pm j\frac{\pi}{2})\right] \exp(j\omega t - j\beta z)$$
(3.6)

$$\overline{H} = \left[\overline{1}_{x}^{H}_{x}(x,y) + \overline{1}_{y}^{H}_{y}(x,y) + \overline{1}_{z}^{H}_{z}(x,y)\exp(\pm j\frac{\pi}{2})\right] \exp(j\omega t - j\beta z)$$
(3.7)

may exist in media characterized by permeability and permittivity tensors of the following form.

$$\hat{\mu} = \begin{bmatrix} \mu_{xx} & \mu_{yx} + j\mu_{zx} \\ \mu_{yx} & \mu_{yy} + j\mu_{zy} \\ -j\mu_{zx} - j\mu_{zy} & \mu_{zz} \end{bmatrix}$$
(3.8)

$$\hat{\epsilon} = \begin{bmatrix} \epsilon_{xx} & \epsilon_{yx} + j\epsilon_{zx} \\ \epsilon_{yx} & \epsilon_{yy} + j\epsilon_{zy} \\ -j\epsilon_{zx} - j\epsilon_{zy} & \epsilon_{zz} \end{bmatrix}$$
(3.9)

respectively. These tensors are characteristic of transversely magnetized ferromagnetic materials and plasma [38,45-47]. The magnetization may be in any direction, but restricted to the x-y plane [48]. The waves described by (3.6) and (3.7) are linearly polarized with respect to the transverse plane.

Circularly polarized waves are also possible in waveguides [50]. For example, in an anisotropic waveguide with longitudinal magnetization [38,45], the medium is usually described by material property tensors of the form

$$\hat{\mu} = \begin{bmatrix} \mu_{xx} + j\mu_{yx} & \mu_{zx} \\ -j\mu_{yx} & \mu_{yy} - j\mu_{zy} \\ \mu_{zx} + j\mu_{zy} & \mu_{zz} \end{bmatrix}$$
(3.10)

$$\hat{\epsilon} = \begin{bmatrix} \epsilon_{xx} + j\epsilon_{yx} & \epsilon_{zx} \\ -j\epsilon_{yx} & \epsilon_{yy} - j\epsilon_{zy} \\ \epsilon_{zx} + j\epsilon_{zy} & \epsilon_{zz} \end{bmatrix}$$
(3.11)

The field vectors of circularly polarized travelling waves can be described as follows

$$\overline{E} = \left[\overline{1}_{x} E_{x}(x,y) + \overline{1}_{y} E_{y}(x,y) \exp(\pm j\frac{\pi}{2}) + \overline{1}_{z} E_{z}(x,y)\right] \exp(j\omega t - j\beta z)$$
(3.12)

$$\overline{H} = \left[ \overline{1}_{\mathbf{X}} \mathbf{H}_{\mathbf{X}}(\mathbf{x}, \mathbf{y}) \exp(\pm \mathbf{j} \frac{\pi}{2}) + \overline{1}_{\mathbf{y}} \mathbf{H}_{\mathbf{y}}(\mathbf{x}, \mathbf{y}) + \overline{1}_{\mathbf{z}} \mathbf{H}_{\mathbf{z}}(\mathbf{x}, \mathbf{y}) \exp(\pm \mathbf{j} \frac{\pi}{2}) \right].$$

$$\exp(\mathbf{j} \omega \mathbf{t} - \mathbf{j} \beta \mathbf{z})$$
(3.13)

Waves with complex propagation constants a+j\$ are also possible in lossless media [49], though they are usually considered only with lossy media.

In the following, only propagating waves of the type given in (3.6) and (3.7) and media described by tensors such as (3.8) and (3.9) will be considered. A similar analysis can be performed for other types of waves. In direct analogy with travelling waves in (x,y,z) coordinates, circulating waves in the  $(r,\theta,z)$  coordinate system are taken to be of the form

$$\overline{E} = \left[\overline{1}_{r}E_{r}(r,z) + \overline{1}_{\theta}E_{\theta}(r,z) + \overline{1}_{z}E_{z}(r,z)\exp(\pm j\frac{\pi}{2})\right] \exp(j\omega t - jm\theta)$$

$$\overline{H} = \left[\overline{1}_{r}H_{r}(r,z) + \overline{1}_{\theta}H_{\theta}(r,z) + \overline{1}_{z}H_{z}(r,z)\exp(\pm j\frac{\pi}{2})\right] \exp(j\omega t - jm\theta)$$

$$(3.14)$$

and the permeability and permittivity tensors are taken to be [51]

$$\hat{\mu} = \begin{bmatrix} \mu_{rr} & \mu_{\theta r} + j\mu_{zr} \\ \mu_{\theta r} & \mu_{\theta \theta} + j\mu_{z\theta} \\ -j\mu_{zr} - j\mu_{z\theta} & \mu_{zz} \end{bmatrix} = \text{Cartesian tensor}$$
at the plane  $\theta = 0$  (3.16)

- --

\*3

(3.18)

$$\hat{\boldsymbol{\epsilon}} = \begin{bmatrix} \boldsymbol{\epsilon}_{rr} & \boldsymbol{\epsilon}_{\theta r} + j\boldsymbol{\epsilon}_{zr} \\ \boldsymbol{\epsilon}_{\theta r} & \boldsymbol{\epsilon}_{\theta \theta} + j\boldsymbol{\epsilon}_{z\theta} \\ -j\boldsymbol{\epsilon}_{zr} - j\boldsymbol{\epsilon}_{z\theta} & \boldsymbol{\epsilon}_{zz} \end{bmatrix} = \text{Cartesian tensor} \quad (3.17)$$

Note that circulating waves are linearly polarized with respect to the r-0 plane and circularly polarized with respect to the r-z plane. The circulation constant m must be an integer (including zero).

# 3.2 Explicit Forms of the Functional for

## Travelling and Circulating Waves

Substituting a vector function  $\overline{\mathbf{u}}(\mathbf{x},\mathbf{y},\mathbf{z})$  of the form given in (3.6) or (3.7) and tensors  $\hat{\mathbf{p}}$  and  $\hat{\mathbf{q}}$  of the form (3.8) or (3.9) into the functional (2.70), an explicit form for  $F(\overline{\mathbf{v}})$  is obtained for travelling waves which are linearly polarized:

$$F(\overline{u}) = \frac{2\pi}{\beta} \int \int \left[ p_{xx} \left( \frac{\partial u_{\overline{z}} \pm \beta u_{y}}{\partial y} \right)^{2} + p_{yy} \left( \frac{\partial u_{z}}{\partial x} \pm \beta u_{x} \right)^{2} + p_{zz} \left( \frac{\partial u_{y}}{\partial x} - \frac{\partial u_{x}}{\partial y} \right)^{2} \right]$$

$$-2p_{yx} \left( \frac{\partial u_{z}}{\partial y} \pm \beta u_{y} \right) \left( \frac{\partial u_{z}}{\partial x} \pm \beta u_{x} \right)$$

$$\pm 2p_{zx} \left( \frac{\partial u_{y}}{\partial x} - \frac{\partial u_{y}}{\partial y} \right) \left( \frac{\partial u_{z}}{\partial y} \pm \beta u_{y} \right)$$

$$\pm 2p_{zy} \left( \frac{\partial u_{x}}{\partial y} - \frac{\partial u_{y}}{\partial x} \right) \left( \frac{\partial u_{z}}{\partial x} \pm \beta u_{x} \right)$$

$$-\omega^{2} / \left( q_{xx} u_{x}^{2} + q_{yy} u_{y}^{2} + q_{zz} u_{z}^{2} + 2q_{yx} u_{x} u_{y} + 2q_{zx} u_{x} u_{z}^{2} + 2q_{zy} u_{y} u_{z} \right)$$

$$+2 \left( f_{x} u_{x} + f_{y} u_{y} + f_{z} u_{z}^{2} \right) dx dy$$

The constant  $2\pi/\beta$  arises from the integration with respect to z, where the limits of integration are 0 and  $2\pi/\beta$ , i.e. the beginning and the end of a period in the direction of travel. The source function  $\overline{g}=\overline{f}(x,y,z)$  is assumed to be of the same form as the wave function  $\overline{v}=\overline{u}(x,y,z)$ .

A similar procedure for circulating waves produces the following functional form . . .

$$F(\overline{u}) = 2\pi \iint \left\{ p_{rr} \left( \sqrt{r} \frac{\partial u_{\theta}}{\partial z} \mp \frac{mu_{z}}{\sqrt{r}} \right)^{2} + p_{\theta\theta} r \left[ \left( \frac{\partial u_{r}}{\partial z} \right)^{2} + \left( \frac{\partial u_{z}}{\partial r} \right)^{2} \right] \right.$$

$$\left. + p_{zz} \left[ \left( \sqrt{r} \frac{\partial u_{\theta}}{\partial r} + \frac{u_{\theta}}{\sqrt{r}} \right)^{2} + \left( \frac{mu_{r}}{\sqrt{r}} \right)^{2} \right] + 2p_{\theta r} \frac{\partial u_{r}}{\partial z} \left( \pm mu_{z} + \frac{\partial u_{\theta}}{\partial z} \right) \right.$$

$$\left. + 2p_{zr} mu_{r} \left( \frac{\partial u_{\theta}}{\partial z} \mp \frac{mu_{z}}{r} \right) + 2p_{z\theta} \left[ \mp \frac{\partial u_{z}}{\partial r} \left( u_{\theta} + r \frac{\partial u_{\theta}}{\partial r} \right) - mu_{r} \frac{\partial u_{r}}{\partial z} \right] \right.$$

$$\left. - \omega^{2} r \left( q_{rr} u_{r}^{2} + q_{\theta\theta} u_{\theta}^{2} + q_{zz} u_{z}^{2} + 2q_{\theta r} u_{r} u_{\theta} \mp 2q_{zr} u_{r} u_{z} \mp 2q_{z\theta} u_{\theta} u_{z} \right) \right.$$

$$\left. + 2r \left( f_{r} u_{r} + f_{\theta} u_{\theta}^{2} + f_{z} u_{z} \right) \right\} dr dz \qquad m = 0, \pm 1, \pm 2, \pm 3, \dots$$

The  $\pm$  and  $\mp$  terms in the above arise from the fact that the z vector component may either lead or lag the other two components by a time phase of  $\frac{\pi}{2}$  radians. All quantities in (3.18) and (3.19) are real and the material property tensor elements that appear now designate magnitudes only.

It is clear from the expression (3.19) that when m=0 there is a  $1/\sqrt{r}$  singularity in terms involving  $u_0$  alone, but not in terms involving  $u_r$  or  $u_z$ . When  $m\neq 0$  the singularity also affects terms involving  $u_r$  and  $u_z$ . The physical significance of the singularities is that the azimuthal component of the field must always vanish along the z-axis if the axis is to be source-free [42]. The  $u_r$  and  $u_z$ 

components however, must vanish at r=0 only when they vary with the  $\theta$ -coordinate. In such case there is at least one null plane  $\theta$  = constant for these field components and again they must vanish at r=0 if the z-axis is to remain source-free. On the other hand, when there is no variation with  $\theta$  (i.e. m=0), finite non-zero values at r=0 are permitted for  $\mathbf{u_r}$  and  $\mathbf{u_z}$  and provided that they are continuous functions with continuous first derivatives, the z-axis will stay source-free.

In order to avoid difficulties in trying to integrate the terms in the functional (3.19) later, the singularities will be removed by transforming the components of the vector function [52]. In the case m=0 one introduces

$$u_{A} = \sqrt{r} h_{A}(r,z)$$
 (3.20)

$$f_{\theta} = \sqrt{r} d_{\theta}(r, z) \tag{3.21}$$

and consequently the functional given in (3.19) becomes

$$F(u_{r}, u_{z}, h_{\theta}) = 2\pi \int \int \{p_{rr}(r\frac{\delta h_{\theta}}{\delta z})^{2} + p_{\theta\theta}r[(\frac{\delta u_{r}}{\delta z})^{2} + (\frac{\delta u_{z}}{\delta r})^{2}] + p_{zz}(r\frac{\delta h_{\theta}}{\delta r} + \frac{3}{2}h_{\theta})^{2}$$

$$-2p_{\theta r}r\sqrt{r}\frac{\delta u_{r}}{\delta z}\frac{\delta h_{\theta}}{\delta z} \mp 2p_{z\theta}\sqrt{r}\frac{\delta u_{z}}{\delta r}(r\frac{\delta h_{\theta}}{\delta r} + \frac{3}{2}h_{\theta})$$

$$-\omega^{2}r(q_{rr}u_{r}^{2} + q_{\theta\theta}rh_{\theta}^{2} + q_{zz}u_{z}^{2} + 2q_{\theta r}\sqrt{r}u_{r}h_{\theta} \mp 2q_{zr}u_{r}u_{z}$$

$$\mp 2q_{z\theta}\sqrt{r}h_{\theta}u_{z}) + 2r(f_{r}u_{r} + rd_{\theta}h_{\theta} + f_{z}u_{z})\} dr dz$$

$$(3.22)$$

As can be seen, the  $1/\sqrt{r}$  singularity has disappeared. For reasons which will become clear later on, this form of F is only suitable for media in which  $p_{\theta r}$ ,  $p_{z\theta}$ ,  $q_{\theta r}$  and  $q_{z\theta}$  are zero [52]. Unfortunately the discretization procedure

employed requires that factors of the form  $\sqrt{r}$  should not appear in the functional. The only way out of this dilemma is to use the transformation

$$u_{\theta} = rh_{\theta}(r,z) \tag{3.23}$$

instead of the one given by (3.20). It then becomes possible to carry out the discretization, though the procedure is more involved and will not be pursued here.

When  $m\neq 0$  , in addition to the transformation given in (3.20) for  $u_\theta$  and  $f_\theta$  , the following transformations will also be used

$$u_r = \sqrt{r} h_r(r,z)$$
 (3.24)

$$\mathbf{f_r} = \sqrt{r} \, \mathbf{d_r(r,z)} \tag{3.25}$$

$$u_z = \sqrt{r} h_z(r, z) \tag{3.26}$$

$$\mathbf{f}_{\mathbf{z}} = \sqrt{\mathbf{r}} \, \mathbf{d}_{\mathbf{z}}(\mathbf{r}, \mathbf{z}) \tag{3.27}$$

The functional given in (3.19) now takes on the following form

$$F(\overline{h}) = 2\pi \int \int \left\{ p_{rr} \left( r \frac{\delta h_{\theta}}{\delta z} + mh_{z} \right)^{2} + p_{\theta\theta} \left[ \left( r \frac{\delta h_{r}}{\delta z} \right)^{2} + \left( r \frac{\delta h_{z}}{\delta r} \right)^{2} + rh_{z} \frac{\delta h_{z}}{\delta r} + \frac{1}{4} h_{z}^{2} \right] \right.$$

$$+ p_{zz} \left[ \left( r \frac{\delta h_{\theta}}{\delta r} + \frac{3}{2} h_{\theta} \right)^{2} + m^{2} h_{r}^{2} \right] + 2 p_{\theta r} r \frac{\delta h_{r}}{\delta z} \left( \pm mh_{z} - r \frac{\delta h_{\theta}}{\delta z} \right) \right.$$

$$+ 2 p_{zr} mh_{r} \left( r \frac{\delta h_{\theta}}{\delta z} + mh_{z} \right) + 2 p_{z\theta} \left[ \mp \left( \frac{1}{2} h_{z} + r \frac{\delta h_{z}}{\delta r} \right) \left( \frac{3}{2} h_{\theta} + r \frac{\delta h_{\theta}}{\delta r} \right) - mr h_{r} \frac{\delta h_{r}}{\delta z} \right]$$

$$- \omega^{2} r^{2} \left( q_{rr} h_{r}^{2} + q_{\theta\theta} h_{\theta}^{2} + q_{zz} h_{z}^{2} + 2 q_{\theta r} h_{r} h_{\theta} \mp 2 q_{zr} h_{r} h_{z} \mp 2 q_{z\theta} h_{\theta} h_{z} \right)$$

$$+ 2 r^{2} \left( d_{r} h_{r} + d_{\theta} h_{\theta} + d_{z} h_{z} \right) \right\} dr dz$$

$$m = \pm 1, \pm 2, \pm 3, \dots$$

$$(3.28)$$

In the following, only the functional forms given in (3.18) and (3.28) will be considered. The integrations involved will be performed over an arbitrary triangular region in the x-y' or the r-z plane. Over this region the magnitudes of the elements of the material property tensors are assumed to be constant.

## Discretization

The objective of this section is to discretize the two functionals which appear in equations (3.18) and (3.28) so that they can be written in matrix form. In the process, the vector fields are approximated by interpolation polynomials over a general triangular region in such a way that all geometrical information is separated from the process of integration. In other words, the integrations are performed once and only once, and geometrical information is added only when a specific problem is solved [24].

Examining each term in the integrands of the two functionals, one finds that many of the terms are similar to each other in form. There are six representative terms in each functional which must be discretized. The six representative integrals for the functional (3.28) are

1. 
$$\int \int h_1 h_2 dr dz$$

1. 
$$\int \int h_1 h_2 dr dz$$
 2.  $\int \int r h_1 \frac{\partial h_2}{\partial z} dr dz$  3.  $\int \int r h_1 \frac{\partial h_2}{\partial r} dr dz$ 

3. 
$$\int \int rh_1 \frac{\delta h_2}{\delta r} drdz$$

4. 
$$\iint r^2 \frac{\partial h_1}{\partial z} \frac{\partial h_2}{\partial z} drdz$$
 5.  $\iint r^2 \frac{\partial h_1}{\partial r} \frac{\partial h_2}{\partial r} drdz$  6.  $\iint r^2 h_1 h_2 drdz$ 

5. 
$$\int \int r^{2} \frac{\partial h_{1}}{\partial r} \frac{\partial h_{2}}{\partial r} dr dz$$

The subscripts 1 and 2 appear on the components of the vector h to signify that there may be two distinct components of h involved in the integration. The six representative integrals for the functional (3.18) are

1. 
$$\int \int u_1 u_2 dxdy$$

1. 
$$\iint u_1 u_2 dxdy$$
 2.  $\iint u_1 \frac{\partial u_2}{\partial y} dxdy$  3.  $\iint u_1 \frac{\partial u_2}{\partial x} dxd\hat{y}$ 

3. 
$$\iint u_1 \frac{\delta u_2}{\delta x} dxd\hat{y}$$

4. 
$$\iint \frac{\partial u_1}{\partial y} \frac{\partial u_2}{\partial y} dxdy$$
 5.  $\iint \frac{\partial u_1}{\partial x} \frac{\partial u_2}{\partial x} dxdy$  6.  $\iint \frac{\partial u_1}{\partial y} \frac{\partial u_2}{\partial x} dxdy$ 

5. 
$$\iint \frac{\partial u_1}{\partial x} \frac{\partial u_2}{\partial x} dxdy$$

6. 
$$\iint \frac{\partial u_1}{\partial y} \frac{\partial u_2}{\partial x} dxdy$$

The representative integrals 1 through 5 for each functional are analogous to one another. The sixth integral for travelling waves has no counterpart. This term would arise, however, in a functional for circulating waves if the phases of the field components were different and the form of the material property tensors were altered. The form encountered then would be

7. 
$$\iint r^2 \frac{\delta h_1}{\delta z} \frac{\delta h_2}{\delta r} dr dz$$

It turns out that one needs to work only on the representative integrals associated with the functional for circulating waves; the integrals in the functional for travelling waves can be derived from these integrals quite simply.

Consider now an axisymmetric electromagnetic field problem. The solution region in the r-z plane may have an arbitrary shape. In the triangular finite element method, one approximates the boundary of this region by a polygon as closely as possible and divides the interior of the polygon into triangles. This process is indicated in Figure 3.1. The triangles may be of

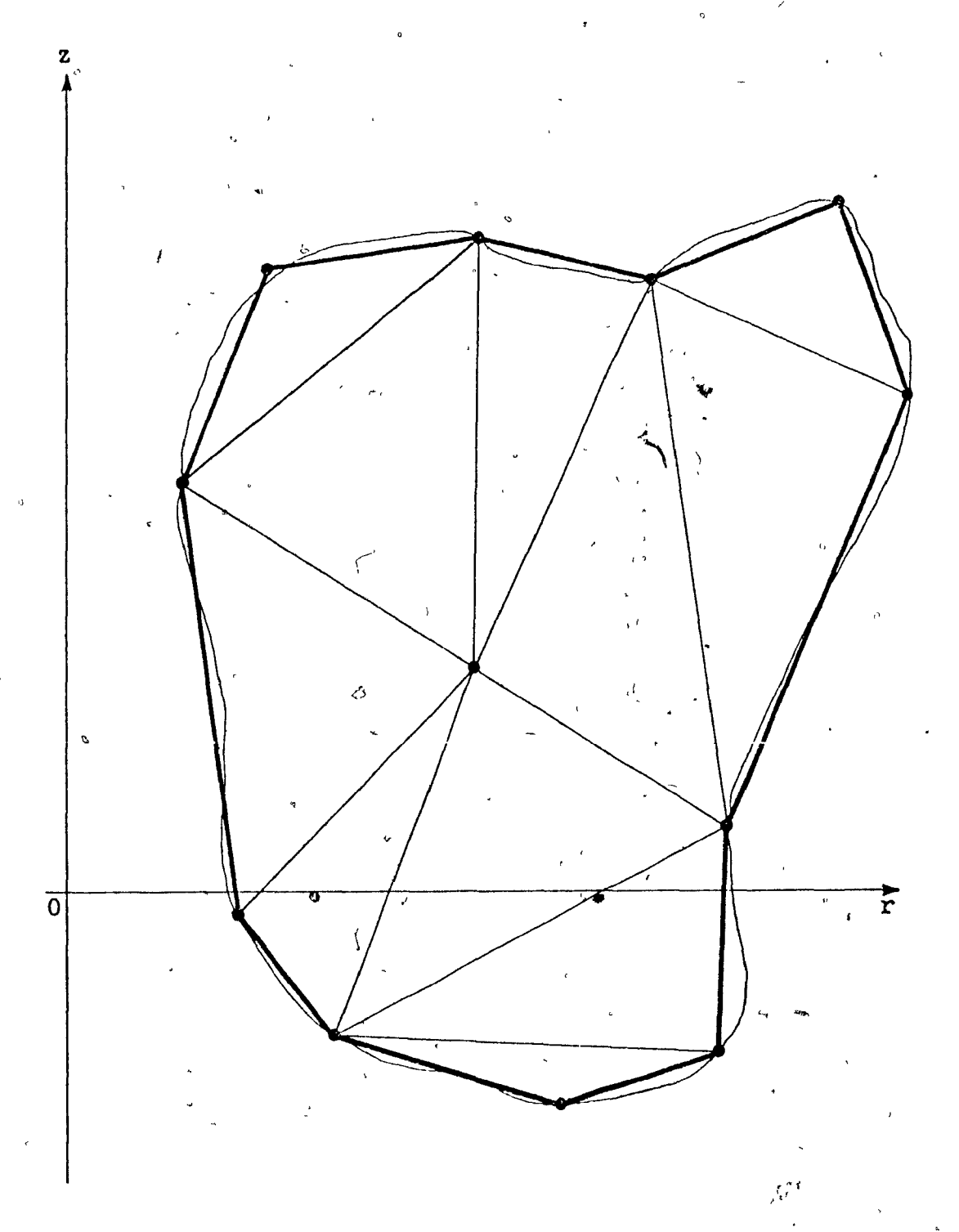


Figure 3.1

An arbitrary solution region approximated by a polygon and divided up into triangular subregions in the r-z plane.

different shapes and sizes. By selecting a general triangle and approximating each component of the vectors  $\overline{h}$  and  $\overline{d}$  by a complete set of n interpolation polynomials  $\{\alpha_i: i=1,2,3,\ldots,n\}$  each of degree N, the components of  $\overline{h}$  and  $\overline{d}$  are written in the form [24]

$$h_{r} = \sum_{i=1}^{n} v_{r}^{i} \alpha_{i}(5_{1}, 5_{2}, 5_{3})$$

$$h_{z} = \sum_{i=1}^{n} v_{z}^{i} \alpha_{i}(5_{1}, 5_{2}, 5_{3})$$

$$h_{\theta} = \sum_{i=1}^{n} v_{\theta}^{i} \alpha_{i}(5_{1}, 5_{2}, 5_{3})$$

$$d_{r} = \sum_{i=1}^{n} G_{r}^{i} \alpha_{i}(5_{1}, 5_{2}, 5_{3})$$

$$d_{z} = \sum_{i=1}^{n} G_{z}^{i} \alpha_{i}(5_{1}, 5_{2}, 5_{3})$$

$$d_{\theta} = \sum_{i=1}^{n} G_{\theta}^{i} \alpha_{i}(5_{1}, 5_{2}, 5_{3})$$

$$(3.32)$$

$$(3.33)$$

The interpolation polynomials  $\alpha_i$  are such that they evaluate to 1 at the i-th interpolation node and are zero at all other n-1 nodes [24]. Consequently, the coefficients  $V^i$  and  $G^i$  of the linear combinations represent the values of the components of  $\overline{h}$  and  $\overline{d}$  at each of the n interpolation nodes in the triangle. The interpolation polynomials are given as a function of the triangle area coordinates  $\gamma_1$ ,  $\gamma_2$ ,  $\gamma_3$ . These local coordinates are related to the global coordinates  $\gamma_1$ ,  $\gamma_2$ ,  $\gamma_3$ .

$$\beta_{i} = \frac{1}{24} (a_{i} + b_{i}r + c_{i}z)$$
  $i = 1, 2, 3$  (3.35)

where A is the area of the triangle and the coefficients  $a_i$  ,  $b_i$  and  $c_i$  are given by

12

$$a_i = r_{i+1}z_{i+2} - r_{i+2}z_{i+1}$$
 i cyclic mod 3 (3.36)

$$b_i = z_{i+1} - z_{i+2}$$
 i cyclic mod 3 (3.37)

$$c_i = r_{i+2} - r_{i+1}$$
 i cyclic mod 3 (3.38)

Here  $r_i$  and  $z_i$  are the radial and axial coordinates of the triangle vertices. Figure 3.2 shows a typical triangle and the n = (N+1)(N+2)/2 associated interpolation nodes and their local coordinates for the case N=5.

It should be noted that the radial coordinate r within a triangle can be expressed in terms of the local coordinates 5, and the vertex radial coordinates as the simple sum

$$\mathbf{r} = \sum_{i=1}^{3} \mathbf{r}_{i} \hat{\gamma}_{i} \tag{3.39}$$

It turns out that this is a very convenient expression to employ. No similar form exists for the square-root of r; this condition explains the stated difficulty with the factor  $\sqrt{r}$  in the functional (3.22).

In order to discretize the six representative integrals in the two functionals, the expression for  $r^2$  and the partial derivatives of the components of  $\overline{h}$  with respect to r and z are needed

$$r^{2} = \sum_{i=1}^{3} r_{i} \sum_{j=1}^{3} r_{j} \delta_{i} \delta_{j}$$
 (3.40)

$$\frac{\delta h_{i}}{\delta r} = \frac{1}{2A} \int_{j=1}^{3} b_{j} \frac{\delta h_{i}}{\delta \zeta_{i}} = \frac{1}{2A} \int_{j=1}^{3} b_{j} \int_{k=1}^{n} V_{i}^{k} \frac{\delta \alpha_{k}}{\delta \zeta_{j}}.$$
 (3.41)

$$\frac{\delta h_{i}}{\delta z} = \frac{1}{2A} \int_{j=1}^{3} c_{j} \frac{\delta h_{i}}{\delta \zeta_{j}} = \frac{1}{2A} \int_{j=1}^{3} c_{j} \sum_{k=1}^{n} v_{i}^{k} \frac{\delta \alpha_{k}}{\delta \zeta_{j}}$$
(3.42)

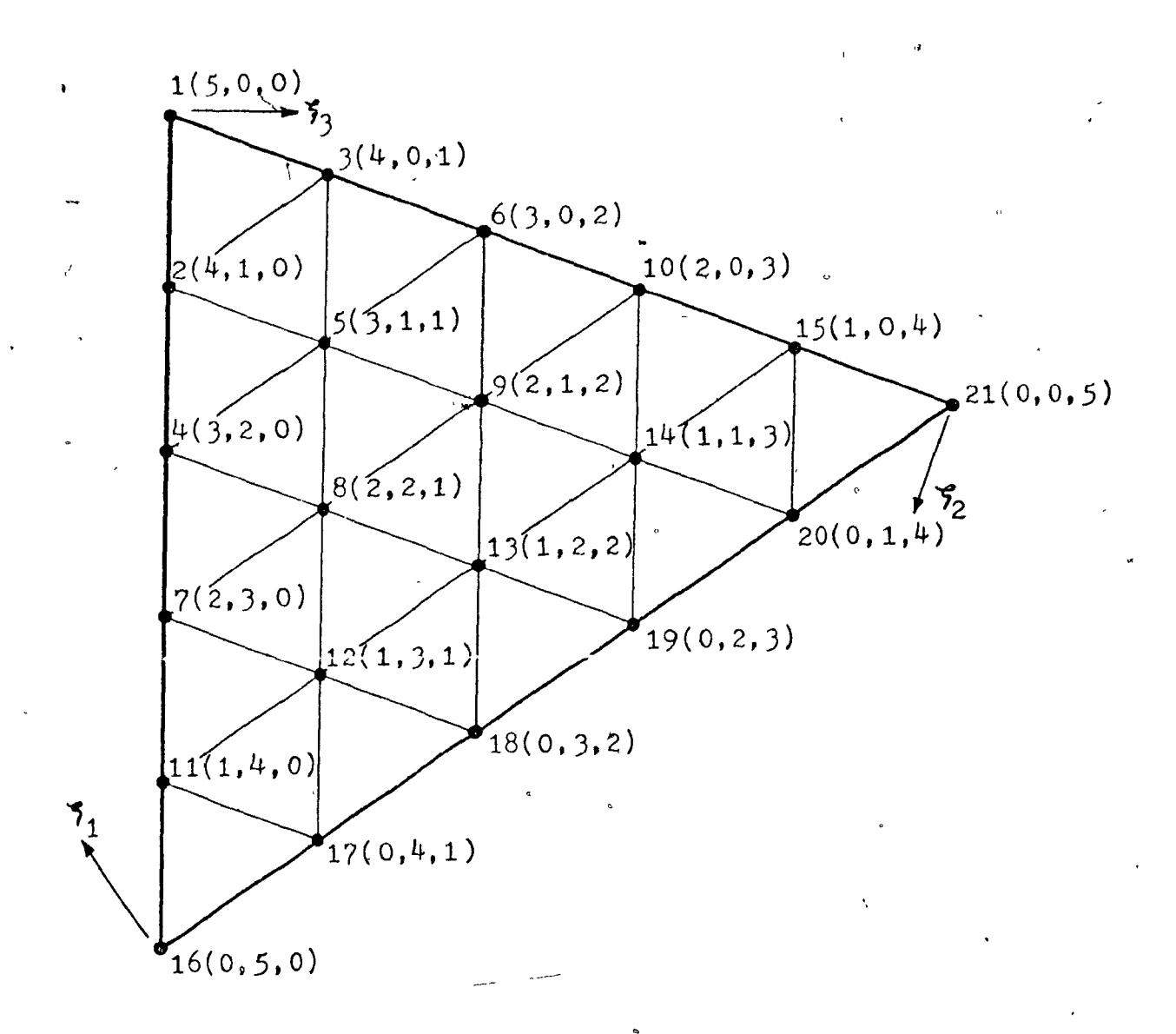


Figure 3.2

The 21 interpolation nodes in a 5-th order triangle (N = 5). The numbers in brackets represent the triangle area coordinates multiplied by N, i.e.  $(N \cdot 1, N \cdot 2, N \cdot 3)$ .

1

Consider first the discretization of integral number 6. One obtains

$$\iint r^2 h_1 h_2 \operatorname{drdz} \Rightarrow [V_1]^{t} [T] [V_2] \qquad (3.43)$$

where the column matrices  $[v_1]$  and  $[v_2]$  contain the n coefficients  $v_1^i$  and  $v_2^i$ , respectively, associated with the linear combinations of interpolation polynomials given in (3.29) through (3.31). The superscript t denotes transpose. The symmetric, n by n matrix [T] is given by

$$[T] = \sum_{i=1}^{3} r_{i} \sum_{j=1}^{3} r_{j} 2|A| [Y_{ij}]^{3}$$
 (3.44)

where the universally constant element matrices  $[Y_{ij}]$  have  $n^2$  elements, of which the (m,k)-th is given by the integral

$$Y_{i,j}^{(m,k)} = \frac{1}{2|A|} \int \int S_i S_j \alpha_m \alpha_k$$
 (3.45)

The integration is carried out over a triangular region.

Integral number 1 has the discretized form

where the symmetric, n by n matrix [R] is universally constant and has the following elements

$$R^{(m,k)} = \frac{1}{2|A|} \iint \alpha_m \alpha_k ds \qquad (3.47)$$

where the integration is over a triangle. One nice property of triangle area coordinates is that their sum is always equal to 1

$$\sum_{i=1}^{3} 5_i = 1 \tag{3.48}$$

as can be seen from equations (3.35) through (3.39). Due to

this property of the local coordinates, if the nine element matrices  $[Y_{ij}]$  are given, the element matrix [R] can be obtained from them by simply summing over the subscripts i and j

$$[R] = \sum_{i=1}^{3} \sum_{j=1}^{3} [Y_{ij}]$$
 (3.49)

This property explains the earlier remark that only the representative integrals associated with the functional for circulating waves need to be evaluated; the discretized forms of the representative integrals associated with the functional for travelling waves are derived from these values using equation (3.48).

Integral number 2 can be discretized as follows

$$\iint r h_1 \frac{\delta h_2}{\delta z} dr dz \Rightarrow \left[V_1\right]^{t} \left[J\right] \left[V_2\right]$$
 (3.50)

The non-symmetric, n by n matrix [J] is assembled from symmetric and antisymmetric constant element matrices  $[U_{ij}]$  and  $[\underline{U}_{ij}]$ , respectively, according to the rule

$$\begin{bmatrix} J \end{bmatrix} = \frac{|A|}{2A} \sum_{i=1}^{3} r_i \sum_{j=1}^{3} (r_{j+2} - r_{j+1}) \left\{ \begin{bmatrix} U_{ij} \end{bmatrix} + \begin{bmatrix} \underline{U}_{ij} \end{bmatrix} \right\}$$
(3.51)

The (m,k)-th element of the symmetric matrix  $[U_{ij}]$  are given by the following integral

$$U_{ij}^{(m,k)} = \frac{1}{2|A|} \int \int \beta_{i} (\alpha_{k} \frac{\partial \alpha_{m}}{\partial \beta_{j}} + \alpha_{m} \frac{\partial \alpha_{k}}{\partial \beta_{j}}) ds$$
 (3.52)

The antisymmetric matrices  $[\underline{\textbf{U}}_{i,j}]$  have elements given by

$$\underline{\mathbf{U}}_{\mathbf{i}\,\mathbf{j}}^{(m,k)} = \frac{1}{2|\mathbf{A}|} \int \int \hat{\mathbf{J}}_{\mathbf{i}} (\alpha_{\mathbf{k}} \frac{\delta \alpha_{\mathbf{m}}}{\delta \hat{\mathbf{J}}_{\mathbf{j}}} - \alpha_{\mathbf{m}} \frac{\delta \alpha_{\mathbf{k}}}{\delta \hat{\mathbf{J}}_{\mathbf{j}}}) \, ds$$
 (3.53)

Notice that (3.51) contains coefficients given in terms of the radial coordinates of the triangle vertices. The sign of the coefficients depends on the order of the vertices. However, the sign of the area vector A cancels this sign difference producing an expression which is invariant with respect to the ordering of the triangle vertices.

Discretization of the third integral produces results very similar to that of the second one

$$\int \int rh_1 \frac{\delta h_2}{\delta r} \, dr dz \Rightarrow \left[ V_1 \right]^{t} \left[ N \right] \left[ V_2 \right]$$
 (3.54)

Again, [N] is a non-symmetric, n by n matrix which is assembled from  $[U_{ij}]$  and  $[\underline{U}_{ij}]$  in the following manner

$$[N] = \frac{|A|}{2A} \sum_{i=1}^{3} r_i \sum_{j=1}^{3} (z_{j+1} - z_{j+2}) \{ [U_{ij}] + [\underline{U}_{ij}] \}$$
 (3.55)

The fourth integral can be transformed into the following matrix form

$$\int \int r^2 \frac{\delta h_1}{\delta z} \frac{\delta h_2}{\delta z} dr dz \Rightarrow [V_1]^t [D][V_2]$$
 (3.56)

where [D] is a symmetric, n by n matrix given by

$$[D] = \frac{1}{4A^2} \int_{i=1}^{3} r_i \int_{j=1}^{3} r_j \int_{1=1}^{3} r_j \int_{t=1}^{3} c_1 c_t [\iint \hat{S}_i \hat{S}_j \frac{\delta \alpha_k}{\delta \hat{S}_t} \frac{\delta \alpha_m}{\delta \hat{S}_t} ds] (3.57)$$

The symmetry of [D] is not obvious from (3.57). It appears however that the summation over the index t can be eliminated and the expression cast into the more revealing form

$$[D] = \frac{1}{2|A|} \sum_{i=1}^{3} r_{i} \sum_{j=1}^{3} r_{j} \sum_{l=1}^{3} (r_{l} - r_{l+2})(r_{l} - r_{l+1})[Q_{ijl}]$$
(3.58)

where  $[Q_{ij1}]$  are constant, symmetric matrices. The elements of  $[Q_{ij1}]$  are

$$Q_{ijl}^{(m,k)} = \frac{1}{2|A|} \int \int \tilde{\gamma}_{i} \tilde{\gamma}_{j} \left( \frac{\delta \alpha_{m}}{\delta \tilde{\gamma}_{1+1}} - \frac{\delta \alpha_{m}}{\delta \tilde{\gamma}_{1+2}} \right) \left( \frac{\delta \alpha_{k}}{\delta \tilde{\gamma}_{1+1}} - \frac{\delta \alpha_{k}}{\delta \tilde{\gamma}_{1+2}} \right) ds \quad (3.59)$$

where the integration is over a triangle. The subscript 1 is cyclic modulo 3.

An entirely analogous procedure for the fifth integral yields

$$\iint r^2 \frac{\delta h_1}{\delta r} \frac{\delta h_2}{\delta r} dr dz \Rightarrow [V_1]^{t} [E][V_2]$$
 (3.60)

where [E] is given by the same expression as [D]  $b_t$ . This expression again reduces to

$$[E] = \frac{1}{2|A|} \sum_{i=1}^{3} r_{i} \sum_{j=1}^{3} r_{j} \sum_{l=1}^{3} (z_{l} - z_{l+2})(z_{l} - z_{l+1})[Q_{ijl}]$$
 (3.61)

The discretization of the seventh integral requires more algebraic manipulation than the previous ones. As before, only the final result is reproduced here

$$\iint r^{2} \frac{\partial h_{1}}{\partial z} \frac{\partial h_{2}}{\partial r} drdz \Rightarrow \begin{bmatrix} v_{1} \end{bmatrix}^{t} [z] [v_{2}]$$
 (3.62)

where the non-symmetric, n by n matrix [Z] is given by

$$[z] = \frac{1}{4A^2} \sum_{i=1}^{3} r_i \sum_{j=1}^{3} r_j \sum_{l=1}^{3} \sum_{t=1}^{3} b_l c_t [\int \int f_i f_j \frac{\delta \alpha_k}{\delta f_l} \frac{\delta \alpha_m}{\delta f_t} ds] (3.63)$$

The matrix [2] can be split into symmetric and antisymmetric parts and the summation over the index t can be eliminated.

Then the following formula is obtained

E

$$[Z] = \frac{1}{4|A|} \sum_{i=1}^{3} r_{i} \sum_{j=1}^{3} r_{j} \sum_{1=1}^{3} (w_{1}[Q_{ij1}] + t_{1}[Q_{ij1}])$$
(3.64)

where w<sub>1</sub> and t<sub>1</sub> are coefficients given by

$$w_{1} = -(b_{1+1}c_{1+2} + b_{1+2}c_{1+1})$$

$$= (r_{1+1} - r_{1}) (z_{1} - z_{1+2}) + (r_{1} - r_{1+2}) (z_{1+1} - z_{1})$$

$$t_{1} = b_{1}c_{1+1} - b_{1+1}c_{1}$$

$$= (z_{1+1} - z_{1+2}) (r_{1} - r_{1+2}) - (z_{1+2} - z_{1}) (r_{1+2} - r_{1+1})(3.66)$$

The elements of the constant, symmetric matrices  $[Q_{ijl}]$  have already been defined in equation (3.59). The (m,k)-th element of the constant, antisymmetric matrices  $[Q_{ijl}]$  is given by

$$\underline{Q_{i\,j1}^{(m,k)}} = \frac{1}{2|A|} \int \int \zeta_{i} \zeta_{j} \left( \frac{\partial \alpha_{m}}{\partial \zeta_{1+1}} \frac{\partial \alpha_{k}}{\partial \zeta_{1}} - \frac{\partial \alpha_{m}}{\partial \zeta_{1}} \frac{\partial \alpha_{k}}{\partial \zeta_{1+1}} \right) ds \tag{3.67}$$

The subscript 1 is cyclic modulo 3.

One can now write down the discretized equivalent of the functional for circulating waves given in (3.28). The following matrix form is obtained

$$\begin{split} F(\overline{V}) &= 2\pi \Big\{ \big[ V_{\mathbf{r}} \big]^{t} \big( p_{\theta\theta} \big[ D \big] + 2m^{2} \big[ A \big] p_{\mathbf{z}z} \big[ R \big] - 2mp_{\mathbf{z}\theta} \big[ J \big] \big) \big[ V_{\mathbf{r}} \big] \\ &+ \big[ V_{\mathbf{z}} \big]^{t} \big( \pm 2mp_{\theta\mathbf{r}} \big[ J \big] + 4m^{2} \big[ A \big] p_{\mathbf{z}\mathbf{r}} \big[ R \big] \big) \big[ V_{\mathbf{r}} \big] \\ &+ \big[ V_{\mathbf{z}} \big]^{t} \big( p_{\theta\theta} \big[ E \big] + p_{\theta\theta} \big[ N \big] + \frac{1}{2} \big[ A \big] p_{\theta\theta} \big[ R \big] + 2m^{2} \big[ A \big] p_{\mathbf{r}\mathbf{r}} \big[ R \big] \big) \big[ V_{\mathbf{z}} \big] \\ &+ \big[ V_{\theta} \big]^{t} \big( 2mp_{\mathbf{z}\mathbf{r}} \big[ J \big]^{t} - 2p_{\theta\mathbf{r}} \big[ D \big] \big) \big[ V_{\mathbf{r}} \big] \\ &+ \big[ V_{\theta} \big]^{t} \big( 3 \big[ A \big] p_{\mathbf{z}\theta} \big[ R \big] + 3p_{\mathbf{z}\theta} \big[ N \big] + p_{\mathbf{z}\theta} \big[ N \big]^{t} + 2p_{\mathbf{z}\theta} \big[ E \big] + 2mp_{\mathbf{r}\mathbf{r}} \big[ J \big]^{t} \big) \big[ V_{\mathbf{z}} \big] \\ &+ \big[ V_{\theta} \big]^{t} \big( p_{\mathbf{r}\mathbf{r}} \big[ D \big] + p_{\mathbf{z}\mathbf{z}} \big[ E \big] + 3p_{\mathbf{z}\mathbf{z}} \big[ N \big] + \frac{9}{2} \big[ A \big] p_{\mathbf{z}\mathbf{z}} \big[ R \big] \big) \big[ V_{\theta} \big] \\ &- \omega^{2} \big( q_{\mathbf{r}\mathbf{r}} \big[ V_{\mathbf{r}} \big]^{t} \big[ T \big] \big[ V_{\mathbf{r}} \big] + 2q_{\mathbf{z}\mathbf{r}} \big[ V_{\mathbf{z}} \big]^{t} \big[ T \big] \big[ V_{\mathbf{r}} \big] + q_{\mathbf{z}\mathbf{z}} \big[ V_{\mathbf{z}} \big]^{t} \big[ T \big] \big[ V_{\mathbf{z}} \big] \\ &+ 2q_{\theta\mathbf{r}} \big[ V_{\theta} \big]^{t} \big[ T \big] \big[ V_{\mathbf{r}} \big] + 2q_{\mathbf{z}\theta} \big[ V_{\theta} \big]^{t} \big[ T \big] \big[ V_{\mathbf{z}} \big] + q_{\theta\theta} \big[ V_{\theta} \big]^{t} \big[ T \big] \big[ V_{\theta} \big] \big] \Big\} \\ &+ 2 \big( \big[ G_{\mathbf{r}} \big]^{t} \big[ T \big] \big[ V_{\mathbf{r}} \big] + \big[ G_{\mathbf{z}} \big]^{t} \big[ T \big] \big[ V_{\mathbf{z}} \big] + \big[ G_{\theta} \big]^{t} \big[ T \big] \big[ V_{\theta} \big] \big] \Big\} \end{aligned}$$

Using the properties of triangle area coordinates given in equation (3.48), the discretized forms of the six representative integrals in the functional for travelling waves are as follows

$$\int \int u_1 u_2 dx dy \qquad \Rightarrow 2 |A| [V_1]^{\dagger} [R] [V_2] \qquad (3.69)$$

$$\iint u_1 \frac{\delta u_2}{\delta y} dxdy \Leftrightarrow [V_1]^t [\mathfrak{F}][V_2]$$
 (3.70)

$$\int \left[ u_1 \frac{\delta u_2}{\delta x} \right] dx dy \Rightarrow \left[ v_1 \right]^t \left[ x \right] \left[ v_2 \right]$$
 (3.71)

$$\iint \frac{\partial u_1}{\partial y} \frac{\partial u_2}{\partial y} dxdy \Rightarrow [v_1]^t [\mathfrak{D}][v_2]$$
 (3.72)

$$\iint \frac{\delta u_1}{\delta x} \frac{\delta u_2}{\delta x} dxdy \Rightarrow [v_1]^{t} [\mathcal{E}][v_2]$$
 (3.73)

$$\iint \frac{\delta u_1}{\delta y} \frac{\delta u_2}{\delta x} dxdy \Rightarrow [V_1]^t [z] [V_2]$$
 (3.74)

where

$$[\mathcal{F}] = \frac{|A|}{2A} \sum_{j=1}^{3} (x_{j+2} - x_{j+1}) \{ [\underline{v}_j] + [\underline{v}_j] \}$$

$$(3.75)$$

$$[\mathbf{N}] = \frac{[\mathbf{A}]}{2\mathbf{A}} \sum_{j=1}^{3} (\mathbf{y}_{j+1} - \mathbf{y}_{j+2}) \left\{ [\mathbf{U}_j] + [\underline{\mathbf{U}}_j] \right\}$$
(3.76)

$$[\mathfrak{D}] = \frac{1}{2|\mathbf{A}|_{1}} \sum_{i=1}^{3} (\mathbf{x}_{1} - \mathbf{x}_{1+2}) (\mathbf{x}_{1} - \mathbf{x}_{1+1}) [\mathbf{Q}_{1}]$$
 (3.77)

$$[\mathcal{E}] = \frac{1}{2|\mathbf{A}|} \sum_{1=1}^{3} (\mathbf{y}_1 - \mathbf{y}_{1+2}) (\mathbf{y}_1 - \mathbf{y}_{1+1}) [\mathbf{Q}_1]$$
 (3.78)

$$[z] = \frac{1}{4|A|} \sum_{1=1}^{3} (w_{1}[Q_{1}] + t_{1}[Q_{1}])$$
 (3.79)

and

$$[U_{\mathbf{j}}] = \sum_{i=1}^{3} [U_{\mathbf{i}\mathbf{j}}]$$
 (3.80)

$$\left[\underline{\mathbf{U}}_{\mathbf{j}}\right] = \sum_{i=1}^{3} \left[\underline{\mathbf{U}}_{i\,\mathbf{j}}\right] \tag{3.81}$$

$$[Q_1] = \sum_{i=1}^{3} \sum_{j=1}^{3} [Q_{ij1}]$$
 (3.82)

(3.86)

$$[\underline{Q}_1] = \sum_{i=1}^{3} \sum_{j=1}^{3} [\underline{Q}_{ij1}]$$
 (3.83)

$$w_1 = (x_{1+1} - x_1)(y_1 - y_{1+2}) + (x_1 - x_{1+2})(y_{1+1} - y_1)$$
 (3.84)

$$t_1 = (y_{1+1} - y_{1+2})(x_1 - x_{1+2}) - (y_{1+2} - y_1)(x_{1+2} - x_{1+1})$$
 (3.85)

Again, the subscripts are cyclic modulo 3 and the subscripted x and y coordinates represent the vertex coordinates of the triangle. Using these results, the matrix form equivalent of the functional (3.18) can be written as

$$\begin{split} F(\overline{V}) &= \frac{2\pi}{6} \Big\{ \big[ V_x \big]^t \big( p_{zz} \big[ \mathcal{B} \big] + 2\beta^2 \big| A \big| p_{yy} \big[ R \big] \big) \big[ V_x \big] \\ &- \big[ V_y \big]^t \big( 2\beta p_{zx} \big[ \mathcal{F} \big] + 4\beta^2 \big| A \big| p_{yx} \big[ R \big] + 2p_{zz} \big[ \mathcal{Z} \big]^t + 2\beta p_{zy} \big[ \mathcal{F} \big]^t \big) \big[ V_x \big] \\ &+ \big[ V_y \big]^t \big( p_{zz} \big[ \mathcal{E} \big] + 2\beta p_{zx} \big[ \mathcal{F} \big] + 2\beta^2 \big| A \big| p_{xx} \big[ R \big] \big) \big[ V_y \big] \\ &+ \big[ V_z \big]^t \big( 2\beta p_{yx} \big[ \mathcal{F} \big]^t + 2p_{zx} \big[ \mathcal{E} \big] - 2\beta p_{yy} \big[ \mathcal{F} \big]^t - 2p_{zy} \big[ \mathcal{Z} \big]^t \big) \big[ V_x \big] \\ &+ \big[ V_z \big]^t \big( 2\beta p_{yx} \big[ \mathcal{F} \big]^t + 2p_{zy} \big[ \mathcal{E} \big] - 2\beta p_{xx} \big[ \mathcal{F} \big]^t - 2p_{zx} \big[ \mathcal{Z} \big] \big) \big[ V_y \big] \\ &+ \big[ V_z \big]^t \big( p_{xx} \big[ \mathcal{E} \big] + p_{yy} \big[ \mathcal{E} \big] - 2p_{yx} \big[ \mathcal{E} \big] \big) \big[ V_z \big] \\ &- \omega^2 \big( 2 \big| A \big| \big) \big( q_{xx} \big[ V_x \big]^t \big[ R \big] \big[ V_x \big] + 2q_{yx} \big[ V_y \big]^t \big[ R \big] \big[ V_x \big] + q_{yy} \big[ V_y \big]^t \big[ R \big] \big[ V_y \big] \\ &+ 2q_{zx} \big[ V_z \big]^t \big[ R \big] \big[ V_x \big] + 2q_{zy} \big[ V_z \big]^t \big[ R \big] \big[ V_y \big] + q_{zz} \big[ V_z \big]^t \big[ R \big] \big[ V_z \big] \big) \\ &+ 4 \big| A \big| \big( \big[ G_x \big]^t \big[ R \big] \big[ V_x \big] + \big[ G_y \big]^t \big[ R \big] \big[ V_y \big] + \big[ G_z \big]^t \big[ R \big] \big[ V_z \big] \big) \Big\} \end{split}$$

The column matrices  $[v_x]$ ,  $[v_y]$ ,  $[v_z]$ ,  $[G_x]$ ,  $[G_y]$  and  $[G_z]$  in (3.86) contain the coefficients of the linear expansions

$$u_{x} = \sum_{i=1}^{n} V_{x}^{i} \alpha_{i}$$

$$u_{y} = \sum_{i=1}^{3} V_{y}^{i} \alpha_{i}$$
(3.87)
$$(3.88)$$

$$u_z = \sum_{i=1}^{3} v_z^i \alpha_i$$
 (3.89)

$$\mathbf{f}_{\mathbf{x}} = \sum_{i=1}^{n} \mathbf{G}_{\mathbf{x}}^{i} \alpha_{i} \tag{3.90}$$

$$\mathbf{f}_{\mathbf{y}} = \sum_{i=1}^{n} G_{\mathbf{y}}^{i} \alpha_{i} \tag{3.91}$$

$$\mathbf{f}_{\mathbf{z}} = \sum_{i=1}^{n} \mathbf{G}_{\mathbf{z}}^{i} \alpha_{i} \tag{3.92}$$

The discretized functionals (3.68) and (3.86) can be constructed for a triangle of arbitrary shape provided that the vertex coordinates are known and the constant matrices  $[Y_{ij}]$ ,  $[U_{ij}]$ ,  $[U_{ij}]$ ,  $[Q_{ij1}]$  and  $[Q_{ij1}]$  are given. There are 81 such constant matrices, all involving various integrals of the interpolation polynomials  $\alpha_i$ . In the next section, it will be demonstrated that only 14 of these matrices are independent, the remaining 67 being obtainable by row and column permutations, and the procedure for computing these 14 matrices will be indicated.

# 3.4 The Element Matrices

In order to compute the element matrices, an explicit definition of the interpolation polynomials  $\alpha_{\hat{\bf i}}$  must be given. The polynomials

$$\alpha_{i} = \alpha_{(j,k,1)} = P_{j}(5_{1}) P_{k}(5_{2}) P_{1}(5_{3})$$
  $j+k+1=N$  (3.93)

where

$$P_{m}(7) = \frac{m}{n} (\frac{N7 - n + 1}{n})$$
 for  $m \ge 1$ 

$$= 1$$
 for  $m = 0$ 

have been used extensively in recent years to generate

high-order polynomial triangular finite elements [24]. The triple set of subscripts (j,k,l) in (3.93) correspond to the product of N times the triangle area coordinates at the i-th interpolation node, i.e.  $(N\S_1,N\S_2,N\S_3)$ . Figure 3.2 demonstrates the case N=5.

Substituting these interpolation, polynomials into the right-hand sides of equations (3.45), (3.52), (3.53), (3.59) and (3.67), yields expressions in which the integrands are polynomials in triangle area coordinates. A typical term in these polynomials is of the form

where C is a different constant for each term. The integral of this monomial over a triangle of area A is given by [53,54]

$$\int \int (C_{1}^{m} \gamma_{2}^{j} \gamma_{3}^{p}) ds = 2 C |A| \frac{m! j! p!}{(m+j+p+2)!}$$
 (3.95)

Although straightforward, the integrations in equations (3.45), (3.52), (3.53), (3.59) and (3.57) cannot be carried out by hand, except in the case N=1 or 2, due to the large number of algebraic operations required. However, using an IBM PL/I FORMAC compiler the polynomial expressions may be manipulated and integrated symbolically rather than numerically [55] (see Appendix I). Even so, it has required several hours of computing time on an IBM 360/75 computer to obtain the independent matrices for polynomial orders up to and including 6.

From equations (3.45), (3.59) and (3.67) it is apparent that there is symmetry of the elements with respect to the indeces i and j in the matrices  $[Y_{ij}]$ ,  $[Q_{ijl}]$  and  $[Q_{ijl}]$ . Exploiting this symmetry property reduces the required

number of matrices from 81 to 54. Furthermore, it is apparent from Figure 3.2 that a three-fold symmetry exists between the triplet  $(N_{1},N_{2},N_{3})$ . For example, node numbers 3, 11 and 20 in Figure 3.2 are all permutations of (4,0,1). This symmetry diminishes the required number of matrices further by a factor of 3; instead of 54 only 18 matrices are now required. In addition, two additional matrices may be removed from each of the sets  $[Q_{ij1}]$  and  $[Q_{ij1}]$  due to a symmetry with respect to the subscript 1. Therefore only the following 14 independent matrices remain

Symmetric matrices: 
$$[Q_{111}]$$
,  $[Q_{121}]$ ,  $[Q_{221}]$ ,  $[Q_{231}]$ ,  $[U_{11}]$ ,  $[U_{21}]$ ,  $[Y_{11}]$ ,  $[Y_{21}]$ 

'Antisymmetric matrices: 
$$[\underline{Q}_{111}]$$
,  $[\underline{Q}_{112}]$ ,  $[\underline{Q}_{121}]$ ,  $[\underline{Q}_{231}]$ ,  $[\underline{U}_{21}]$ ,  $[\underline{U}_{21}]$ 

The numerical values of the symmetric matrices appear in Table 3.1 for N=1 and N=2. These were obtained in connection with the formulation of triangular finite elements for the generalized Bessel equation of order m and have been published elsewhere [52]. The permutation operations which must be applied to obtain the entire set of symmetric element matrices, appear in Table 3.3. The numerical values of the independent, antisymmetric matrices are listed in Table 3.2 for N=1 and N=2. The permutation rules for generating the entire set are shown in Table 3.4. Higher-order matrices (N=3 through 6) are not reproduced here since they require considerable space. In actual practice, the numbers are handled by two computer programs called block data generators,

## First-order matrices

Q <sub>111</sub>	Q <sub>121</sub>	<sup>Q</sup> 221	Q <sub>231</sub>	Y <sub>11</sub>	Y <sub>21</sub>	<sup>U</sup> 11	<sup>U</sup> 21
0 0 1 1 0 -1 1 denom = 12	0 1 $0 - 1 1$ denom = $24$	0 0 1 0 -1 1 denom = 12	0 $0 -1$ $0 -1$ $1$ $0 = 24$	12 3 2 3 1 2 denom = 360	3 2 3 1 1 1 denom = 360	1 0 1 0 0 denom = 24	2 2 0 1 0 0 denom = 24
Second-ord	er matrices	*				,	
Q <sub>111</sub> " •		Q <sub>121</sub>	. }	, Q <sub>221</sub>	<i>.</i>	Q <sub>231</sub>	
0 96 0 96 0 -96 96 0 -12 12 0 0 0 0 0 0 0 0 0 0 0 0 0 0 0 0 0	7 -8 16 1 -8 7	0 48 0 -48 48 0 8 -8 7 0 -16 16 -0 8 -8 denom = 360	·20 32 5 <b>-</b> 12 %	0 0 16 0 -16 16 0 12 -12 0 -16 16 - 0 4 4 denom = 180	39 48 64 9 -16 7		15 16 32 1 -16 15
<u>Y</u> 11	•	Y <sub>21</sub> =	•	U <sub>11</sub>	•	U <sub>21</sub>	
24 12 48 12 24 48 -3 -6 -6 0 12 12 - -3 -6 -6 denom = 252	2 2 8 1 -2 2	3 0 36 0 12 12 -1 0 -2" -2 12 8 0 -4 -2 denon = 252	3 0 12 0 -2 1	36 24 64 24 32 64 -5 0 -4 0 4 16 16 0 -5 -4 0 0 denom = 360	0	-8 48 32	0 0 0

Table 3.1

The first- and second-order, independent, symmetric element matrices are given as integer quotients brought to a common denominator. Only the lower triangle portions are reproduced. The mapping operations to obtain the remaining symmetric matrices are given in Table 3.3.

First-order matrices

<u>Q</u> 111	<u>Q</u> 112	<u>Q</u> 121	<u>Q</u> 231	<u>U</u> 11	<u>U</u> 21
0 -1 · 0 1 0 0	0 0 0 0 0 -1 0 1 0	0 -1 0	$\begin{array}{cccc} 0 & -1 & 0 & , \\ 1 & 0 & 0 & , \\ 0 & 0 & 0 & . \end{array}$	0 1 1 -1 0 0 -1 0 0	0 ·2 1 -2 0 0 -1 0 0
$\frac{0}{\text{denom}} = 12$	$\frac{1}{\text{denom}} = 12$	$\frac{1}{\text{denom}} = 24$	denom = 24	denom = 24	denom = 24

Second-order matrice's

Table 3.2

The first- and second-order, independent, antisymmetric element matrices are given as integer quotients brought to a common denominator. The mapping operations to obtain the remaining antisymmetric element matrices are given in Table 3.4.

Matrix		j = 1		j = 2			j = 3 ·		
Q <sub>ij1</sub>	1 = 1	1 = 2	1 = 3	1 = 1	1 = 2	1 = 3	1 = 1	1 = 2	1 = 3
i = 1	q <sub>111</sub> given	Q <sub>112</sub> = RFQ <sub>221</sub>	Q <sub>113</sub> = R <sup>2</sup> Q <sub>221</sub>	Q <sub>121</sub> given	Q <sub>122</sub> = FFQ <sub>121</sub>	Q <sub>123</sub> = R <sup>2</sup> Q <sub>231</sub>	Q <sub>131</sub> = FQ <sub>121</sub>	Q <sub>132</sub> = RQ <sub>231</sub>	Q <sub>133</sub> = R <sup>2</sup> Q <sub>121</sub>
i = 2	Q <sub>211</sub> = Q <sub>121</sub>	Q <sub>212</sub> = RFQ <sub>121</sub>	Q <sub>213</sub> ,= R <sup>2</sup> Q <sub>231</sub>	Q <sub>221</sub> given	Q <sub>222</sub> = RQ <sub>111</sub>	Q <sub>223</sub> = R <sup>2</sup> FQ <sub>221</sub>	q <sub>231</sub> given	Q <sub>232</sub> = RQ <sub>121</sub>	Q <sub>233</sub> = R <sup>2FQ</sup> 121
i = 3	9311 = FQ121	Q <sub>312</sub> = RQ <sub>231</sub>	Q <sub>313</sub> = R <sup>2Q</sup> 121	Q <sub>321</sub> = Q <sub>231</sub>	Q <sub>322</sub> = XQ <sub>121</sub>	Q <sub>323</sub> = R <sup>3</sup> FQ <sub>121</sub>	<sup>Q</sup> 331 = <sup>FQ</sup> 221	Q <sub>332</sub> = RQ <sub>221</sub>	Q <sub>333</sub> = R <sup>2</sup> Q <sub>111</sub>

Matrix Y	, j = 1	j = 2	j = 3
i = 1	Y. 11 given	Y <sub>12</sub> = Y <sub>21</sub>	Y <sub>13</sub> = Y <sub>31</sub>
i = 2	Y 21 given	Y <sub>22</sub> = RY <sub>11</sub>	Y <sub>23</sub> = Y <sub>32</sub>
i = 3	Y <sub>31</sub> = FY <sub>21</sub>	Y <sub>32</sub> = RY <sub>21</sub>	Y <sub>33</sub> = R <sup>3</sup> Y <sub>11</sub>

R: Rotation permutation operator

F: Flip permutation operator

£<sup>2</sup>: ₽ R

Matrix <sup>U</sup> ij	j = 1	j = 2	j =*3
i = 1	U 11 given	U <sub>12</sub> = RFU <sub>21</sub>	U <sub>13</sub> = ° R <sup>3</sup> U <sub>21</sub>
i = 2	U <sub>21</sub>	υ <sub>22</sub> =	U <sub>23</sub> =
	given	<i>Զ</i> υ <sub>11</sub>	L <sup>3</sup> FU <sub>21</sub>
i = 3	U <sub>31</sub> =	U <sub>32</sub> =	U <sub>33</sub> =
	FU <sub>21</sub>	RU <sub>21</sub>	R <sup>aU</sup> 11

Table 3.3

Permutation operations for the symmetric element matrices

•		,	·	3 - 1 - 1					
Matrix		j = 1	7		j = 2			j = 3	
<u>Q</u> ij1	1 = 1	1 = 2	1 = 3	1 = 1	1 = 2	1 = 3	1 = 1	1, = 2	1 = 3
i = 1	Q <sub>111</sub> given	Q <sub>112</sub> given	Q <sub>113</sub> = . -FQ <sub>111</sub>	Q <sub>121</sub> given	$\frac{Q_{122}}{-R^3 \mathcal{F} Q_{231}}$	Q <sub>123</sub> = +2 <sup>2</sup> Q <sub>231</sub>	$\frac{Q_{131}}{-\mathcal{R}\mathcal{F}Q_{231}}$	$\frac{Q_{132}}{+RQ_{231}}$	9 <sub>133</sub> = +2°9 <sub>121</sub>
i = 2	Q <sub>211</sub> = Q <sub>121</sub>	$\frac{Q_{212}}{-R^2 F Q_{231}}$	$\frac{Q_{213}}{+x^2Q_{231}}$	$\frac{Q_{221}}{-\mathcal{R}^{\mathcal{F}}Q_{111}}$	, Q <sub>222</sub> = +RQ <sub>111</sub>	$\frac{Q_{223}}{+\mathcal{R}_{2}^{Q}} = 112$	9 <sub>231</sub> given	Q <sub>232</sub> = +RQ <sub>121</sub>	Q <sub>233</sub> = -FQ <sub>231</sub>
i = 3	<sup>Q</sup> 311 = -78 <sup>F</sup> Q231	\frac{Q}{312} = +\pi\text{Q}{231}	Q <sub>313</sub> = + <b>A</b> <sup>2</sup> Q <sub>121</sub>	Q <sub>321</sub> = Q <sub>231</sub>	$\frac{Q}{322} = \frac{1}{2}$	Q <sub>323</sub> = -FQ <sub>231</sub>	$\frac{Q_{331}}{+\mathcal{R}^2Q_{112}}$	9332 = -x <sup>3</sup> 79 <sub>111</sub>	9 <sub>333</sub> = + <b>R</b> <sup>2</sup> 9 <sub>111</sub>

Rotation
permutation
operator

F: Flip permutation operator

 $\mathcal{R}^{\mathbf{a}}:\mathcal{R}\mathcal{R}$ 

Matrix <u>U</u> ij	j = 1	j = 2	$\tilde{j} = 3$
i = 1	U11 given	$\begin{array}{c} \underline{\mathbf{U}}_{12} = \\ + \mathcal{R} \mathbf{F} \underline{\mathbf{U}}_{21} \end{array}$	<u>U</u> <sub>13</sub> = + R <sup>3</sup> <u>U</u> <sub>21</sub>
i = 2	U <sub>21</sub> given	<u>U</u> 22 = +¤ <u>U</u> 11	$\frac{U_{23}}{+\mathcal{R}^2\mathcal{F}U_{21}} =$
i = 3	<u>U</u> 31 = +3 <u>U</u> 21	<u>U</u> 32 = +R <u>U</u> 21	$\begin{array}{c} \underline{U}_{33} = \\ + \mathcal{R}^3 \underline{U}_{11} \end{array}$

Table 3.4

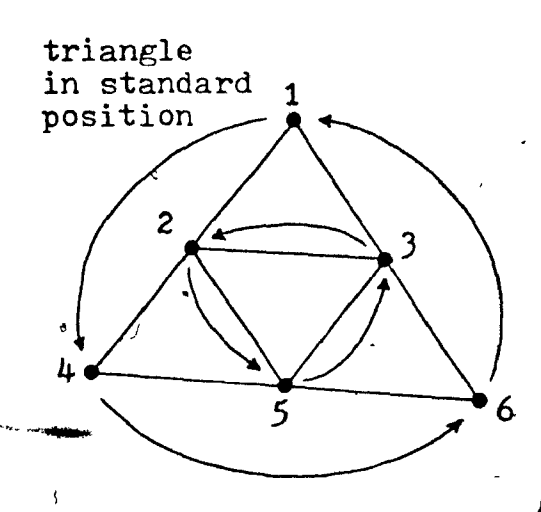
Permutation operations for the antisymmetric element matrices

which store all 14 independent matrices as integer quotients with common denominators and generate single precision block data statements containing the matrices. The block data generator programs are listed in Appendix II and Appendix III. The block data generator program in Appendix III also performs the summations indicated in equations (3.49) and (3.80) through (3.83). Thus, the element matrices required by the discretized functional (3.86) for travelling waves, are also produced. The permutation rules for these element matrices may be derived from the rules in Tables 3.3 and 3.4. It should be noted here  $[Q_1]$  have originally been that the element matrices [R] and given for polynomial orders 1 through 4 by Silvester [24], the antisymmetric matrix  $[Q_1]$  has been given independently by Csendes [7,12] and by Daly [9,25] and the matrices  $[U_1]$  and  $[\underline{U}]$  have been computed by Stone [23,26] for N=1 through 4.

The permutation rules in Tables 3.3 and 3.4 have been discussed in detail elsewhere [24,55-57]. A brief explanation of these rules will however be given for sake of completeness.

There are two basic kinds of permutation rules for element matrices. One corresponds to a mapping of the interpolation node numbers by a rotation of the triangle counter-clockwise until the last node number occupies the relative location of the first one. For a second-order triangle, the required mapping is shown in Figure 3.3. The permutation rule associated with this mapping operation is called the rotation permutation rule and is denoted by the letter  $\mathcal{R}$ . In Figure 3.3, the relative positions of the nodes of the triangle in the rotated position match the relative positions of the nodes of the nodes of the

27



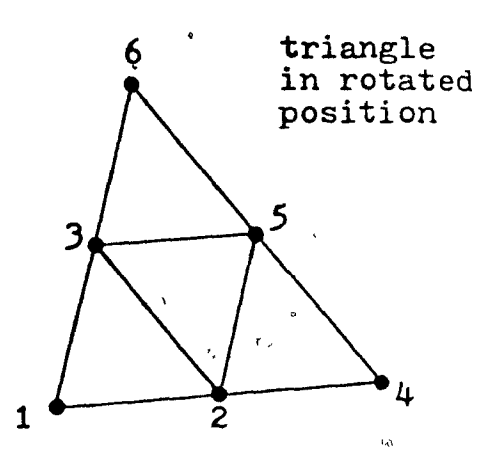


Figure 3.3

Mapping of the interpolation nodes of a secondorder triangle by a counter-clockwise rotation.

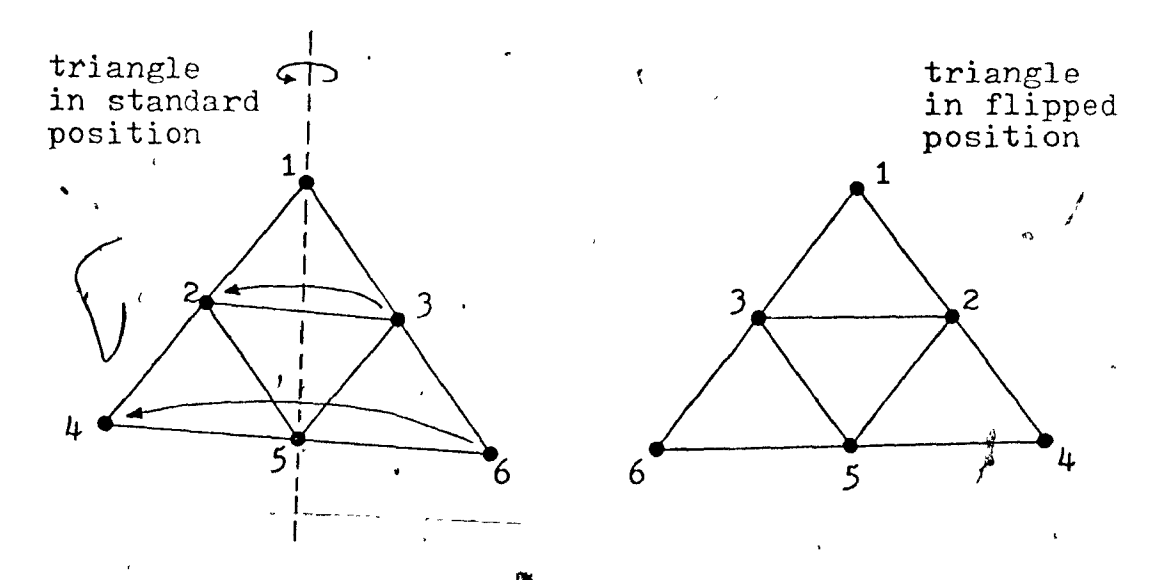


Figure 3.4

Mapping of the interpolation nodes of a second-order triangle by a flip-over about an axis in its plane.

triangle in the standard position. The node numbering sequence of the triangle in the standard position corresponds to the row and column sequence of the independent element matrices of Tables 3.1 and 3.2. In the rotated position, the sequence becomes 6,3,5,1,2,4. For example, if the rows and columns of the  $Q_{111}$  matrix are permuted in the sequence in which the nodes of the rotated triangle match the nodes of the triangle in the standard position, the resulting matrix is  $Q_{222}$ . Therefore, one obtains

Q <sub>222</sub>	C O L U	M N S	Q <sub>111</sub>	C 0 L U	M N S
6 R 3 0 5 W 1 S 4	7 -12 -8 -12 96 0 -8 0 16 0 0 0 12 -96 0 1 12 -8	$ \begin{array}{cccccccccccccccccccccccccccccccccccc$	1 R 2 W 4 S 6	0 0 0 0 0 0 0 0 96 -96 -12 0 -96 96 12 0 -12 12 7 0 0 0 -8 0 12 -12 1	0 0 12 0 -12 -8 1 16 -8 7
			(	,	(3.96)

This result appears in Table 3.3. When applied twice to the same matrix, the permutation operation  $\mathcal{R}$  results in a second counter-clockwise rotation of the rotated triangle in Figure 3.3. The doubly rotated triangle's node sequence is 4,5,2,6,3,1.

The second type of permutation rule corresponds to the mapping of the interpolation node numbers by 'flipping' the triangle about an axis in its plane, as illustrated in Figure 3.4. The flip permutation rule is denoted by the letter  $\mathcal{F}$ . As an example, consider the  $Q_{113}$  matrix which according to Table 3.4 is equal to  $-\mathcal{F}Q_{111}$ . One obtains the following:

113	<u>C</u>	3	2	6	M 5	N S	<u>-</u>	9	111	1	2	<u> </u>	4	<u>M</u> 5	<u>N</u> 6
1 3 2 6 5 4	0 0 -60 0 -12	0 0 -24 0 -16 4	60 24 0 0 -8	0 0 0 0 0	12 16 8 0 0	-9 -4 0 0	= <b>-</b> F	R O W S	123456	0 60 0 -9 12 0	-60 0 -24 4 8 0	0 24 0 -4 16	944000	-12 -8 -16 0 0	0 0 0 0 0

It can be seen from Tables 3.3 and 3.4 that the permutation, rules are also needed for the combinations  $\mathcal{RF}$  and  $\mathcal{RF}$ . In these cases, the  $\mathcal{R}$  and  $\mathcal{F}$  permutation rules are applied consecutively. Fortran function subroutines implementing the permutation rules and their combinations have appeared elsewhere [56].

# 3.5 <u>Minimization of the Discretized Functionals</u> over a Compound Triangular Region

With the independent element matrices, the matrix forms (3.68) and (3.86) representing the discretized equivalents of the functionals (3.18) and (3.28), can be constructed for any given triangular region. In any collection of connected triangles such as the one in Figure 3.1, the discrete matrix equation for each triangular subregion can be generated.

Assuming continuity of the electromagnetic vector fields from triangle to triangle, the local functionals can be assembled into a global matrix form. In order to achieve this, it is required that contributions from each triangle be properly identified and connected together. The trial functions must have continuity from element to element in order to

satisfy the functional and, therefore, the adjacent potential or wave function values are set equal.

The assembly process is usually performed theoretically with connection matrices [31,58]. In most applications however, they are seldom needed explicitly [57]. It is sufficient to employ a global numbering sequence for the interpolation nodes in a compound region. Provided that the local functionals are constructed using the global node identifiers, the proper location of the element in the global matrix is determined. In form, the matrices in (3.68) and (3.86) are unchanged in global interpretation. For example, the column matrix  $[v_r]$ of equation (3.68) in globally form simply contains the coefficients  $V_{f r}^{f l}$  from all of the triangles in the sequence in which the nodes are numbered. Similarly, the matrices [T] are in global form the sum [E], [N]and of the individual contributions of each triangle assembled by the connection matrices.

Under a global interpretation of the discretized functionals (3.68) and (3.86), one can proceed to minimize them by differentiating the functionals with respect to each of the coefficients  $v_r^i$ ,  $v_z^i$ ,  $v_z^i$  and  $v_x^i$ ,  $v_z^i$ ,  $v_z^i$  respectively, and equating each of the results to zero. Three matrix equations with three unknown column matrices result for each functional; the three equations can be combined into a single large matrix equation with a single unknown column vector.

For the functional for circulating waves, equation (3.68), one obtains

$$[s_c][v_c] - \omega^2[T_c][v_c] = -[T_{cd}][G_c]$$
 (3.98)

where the column matrices  $[V_c]$  and  $[G_c]$  are given by

$$\begin{bmatrix} \mathbf{v}_{\mathbf{c}} \end{bmatrix} = \begin{cases} \begin{bmatrix} \mathbf{v}_{\mathbf{r}} \end{bmatrix} \\ \begin{bmatrix} \mathbf{v}_{\mathbf{c}} \end{bmatrix} \end{cases}$$
 (3.99)

and

$$\begin{bmatrix} G_{\mathbf{c}} \end{bmatrix} = \begin{bmatrix} G_{\mathbf{r}} \end{bmatrix}$$

$$\begin{bmatrix} G_{\mathbf{g}} \end{bmatrix}$$

$$\begin{bmatrix} G_{\mathbf{g}} \end{bmatrix}$$
(3.100)

and the symmetric matrices [Sc], [Tc] and [Tcd] are given by

$$\begin{bmatrix} 2q_{rr}[T] & \mp 2q_{zr}[T] & 2q_{\theta r}[T] \\ \\ \mp 2q_{zr}[T] & 2q_{zz}[T] & \mp 2q_{z\theta}[T] \\ \\ 2q_{\theta r}[T] & \mp 2q_{z\theta}[T] & 2q_{\theta\theta}[T] \end{bmatrix}$$
(3.102)

$$[T_{cd}] = \begin{bmatrix} 2[T] & 0 & 0 \\ 0 & 2[T] & 0 \\ 0 & 0 & 2[T] \end{bmatrix}$$
 (3.103)

For the functional for travelling waves, equation (3.86), one obtains

$$[s_{t}][v_{t}] - \omega^{s}[T_{t}][v_{t}] = -[T_{td}][G_{t}]$$
 (3.104)

where the column matrices  $\left[\mathbf{V_{t}}\right]$  and  $\left[\mathbf{G_{t}}\right]$  are given by

$$\begin{bmatrix} v_{t} \end{bmatrix} = \begin{bmatrix} v_{x} \end{bmatrix}, \\ \begin{bmatrix} v_{y} \end{bmatrix} \\ \begin{bmatrix} v_{z} \end{bmatrix} \end{bmatrix}$$
 (3.105)

and

$$\begin{bmatrix} G_{\mathbf{t}} \end{bmatrix} = \begin{bmatrix} G_{\mathbf{x}} \end{bmatrix}$$

$$\begin{bmatrix} G_{\mathbf{y}} \end{bmatrix}$$

$$\begin{bmatrix} G_{\mathbf{z}} \end{bmatrix}$$

$$(3.106)$$

and the symmetric coefficient matrices  $[S_t]$ ,  $[T_t]$  and  $[T_{td}]$  are given by

	2p <sub>zz</sub> [\$]	-28p <sub>zx</sub> [3] <sup>t</sup>	=2βp <sub>yx</sub> [3]
	+482 A Pyy [R]	$-4\beta^2 A p_{yx}[R]$	∓2p <sub>zx</sub> [\$]
	+28p <sub>zy</sub> ([3]+[3] <sup>t</sup> )	-2p <sub>zz</sub> [z]	±2βp <sub>yy</sub> [N]
!	-0	-28p <sub>zy</sub> [N]	±2p <sub>zy</sub> [2]
:	-2 <sub>βPzx</sub> [7]	2p <sub>zz</sub> [&]	∓2βp <sub>yx</sub> [ <b>N</b> ]
-	-4β2   A   p <sub>yx</sub> [R]	$+2\beta p_{zx}([N]+[N]^t)$	
[s <sub>+</sub> ] =	-2p <sub>zz</sub> [Z] <sup>t</sup>	,	±2βp <sub>xx</sub> [3]
	$-2\beta p_{zy}[\mathcal{N}]^{t}$		$\pm 2p_{zx}[z]^{t}$
•			
	∓2βp <sub>yx</sub> [Ϡ] <sup>t</sup>	<b>∓</b> 2βρ <sub>γχ</sub> [[] <sup>t</sup>	2p <sub>XX</sub> [Ø]
	≠2p <sub>zx</sub> [\$]	≠2p <sub>zy</sub> [&]	+2p <sub>yy</sub> [&]
	±28p <sub>yy</sub> [N] <sup>t</sup>	±2βp <sub>xx</sub> [7] <sup>t</sup>	$-2p_{yx}([x]+[x]^{t})$
``.	±2pzy[Z] <sup>t</sup>	$\pm 2p_{zx}[z]$	
		<b>v</b>	(3.102)

(3.107)

$$\begin{bmatrix}
2q_{xx}[R] & 2q_{yx}[R] & \mp 2q_{zx}[R] \\
2q_{yx}[R] & 2q_{yy}[R] & \mp 2q_{zy}[R]
\end{bmatrix}$$

$$\mp 2q_{zx}[R] & \mp 2q_{zy}[R] & 2q_{zz}[R]$$
(3.108)

$$[T_{td}] = (4|A|) \begin{bmatrix} [R] & 0 & 0 \\ 0 & [R] & 0 \\ 0 & 0 & [R] \end{bmatrix}$$
(3.109)

The matrix equations (3.98) and (3.104) reduce to matrix eigenvalue equations whenever the right-hand sides are sourcefree. The eigenvalues of the equations are  $\omega^2$  and the eigenvectors are the nodal values of the vector fields. For every value of the propagation constant β; or of the circulation constant m, an eigenvalue-eigenvector spectrum set can be obtained. When the frequency  $\omega$  is set to zero, and the righthand sides are non-zero, a system of linear equations results for the vector potential function. In the eigenvalue problem, the eigenfunctions represent either the magnetic or the electric field intensity vectors depending on the choice of p and a and the boundary conditions. The size of the coefficient matrices for a single triangle fitted with polynomials of degree and having n interpolation nodes, is 3n x 3n; for an assembly of triangles with a total of n+ interpolation nodes, the size of the coefficient matrix will be  $3n_{t} \times 3n_{t}$ .

The solutions of equation (3.98) must be retransformed into the original variables in accordance with equations (3.20), (3.24) and (3.26).

Finally, it should be pointed out that although the material property tensors are assumed to be independent of the frequency  $\omega$  in the formulation given here, there is no theoretical reason why the  $\omega$  dependence could not be taken care of. With the material property tensor elements given in terms of the frequency, the matrix eigenvalue equation can be

1 **8** 3

rewritten as a matrix polynomial equation in  $\omega$ . The solution of such an equation is a problem in numerical analysis, not in electromagnetic theory. Moreover, the problem can be turned around by assuming that  $\omega$  is given and the propagation constant  $\beta$  or the circulation constant m is unknown. In the coefficient matrix  $[S_t]$  there are terms with  $\beta$  and  $\beta^2$ . Thus the equation could be written right away as a second degree, matrix polynomial equation in the propagation constant.

1%

## CHAPTER IV

### COMPUTER PROGRAM, RESULTS AND APPLICATIONS

# Summary

A computer program is presented which implements the triangular finite element method for linearly polarized travelling waves. For demonstrative purposes, the first problem solved is that of an empty square waveguide. In addition, more complicated problems such as the half-filled dielectric loaded rectangular waveguide, enclosed single microstrip and anisotropic waveguides are also solved in order to illustrate potential applications. A detailed analysis of theoresults is carried out in each case.

## 4.1 The Three-Component Magnetic Field Vector Program

A computer program which assembles the matrices  $[S_t]$  and  $[T_t]$  (given by equations (3.107) and (3.108) respectively) for a collection of triangles in the x-y plane has been written. A double precision version of this program is listed in ... Appendix IV. The basic components of the matrix assembly are carried out in the subroutine ASSEMB. In essence, this subroutine is a Fortran language equivalent of equations (3.75) through (3.79), (3.84) and (3.85), Tables 3.3 and 3.4, and equations (3.107) and (3.108). The summations in equations (3.80) through (3.83) have been performed by the block data generator program given in Appendix III. Thus, the matrices

[U<sub>1</sub>], [U<sub>1</sub>], [Q<sub>1</sub>] and [Q<sub>1</sub>], together with the matrix. [R], are stored in five block data subprograms (BLOCK1, BLOCK2, BLOCK3, BLOCK4, BLOCK5) which are accessible to the subroutine ASSEMB. The permutation rules required in the assembly process are performed by the function subroutines ROTAT1 and ROTAT2. The matrices are stored in linear arrays by rows of their lower triangle; the function subroutine LOCATE provides the necessary address conversion.

All necessary geometric information about triangle coordinates and interpolation node locations are supplied to ASSEMB by the subroutine READIN. This subroutine processes the input data consisting of a list of the triangle vertices and coordinates and also a list of the triangles. Using this information, READIN generates additional points corresponding to the desired polynomial approximation over each triangle. The relative locations of these points are mapped approximately on the line printer by the subroutine MAP.

After assembling the global [ $S_t$ ] and [ $T_t$ ] matrices, the MAIN program calls subroutine EIGVAL and EIGVEC to solve the matrix eigenvalue equation .

$$[s_t][v_t] = k^2[T_t][v_t]$$
 where  $k \neq \omega \sqrt{\mu_o \epsilon_o}$  (4.1)

for all of the eigenvalues and eigenvectors desired. Subroutine EIGVAL uses the Choleski method to decompose the positive definite matrix  $[T_t]$  into lower and upper triangular factors and to cast the matrix eigenvalue equation (4.1) into standard form. Householder's method and a modified Sturm sequence

<sup>1</sup>see also section 5 in Chapter V.

-4

procedure are employed to compute the eigenvalues. The eigenvectors are computed in the subroutine EIGVEC by Wielandt iteration and are properly transformed to give the eigenvectors of equation (4.1).

The eigenvectors of equation (4.1) can be interpreted either as the approximate nodal values of the magnetic field  $\overline{H}$  within a region bounded by a perfect electric conductor or as the approximate nodal values of the electric field  $\overline{E}$  in a region bounded by a perfect magnetic conductor. Since the curlcurl equation in terms of  $\overline{E}$  or  $\overline{H}$  does not represent Maxwell's equations at zero frequency, solutions at k=0 are not possible.

With the eigenvector interpreted as a magnetic field, the material property tensor  $\hat{p}$  in equation (3.107) represents the inverse of the permittivity tensor. On the other hand, the tensor  $\hat{q}$  in the expression for  $[T_t]$  in equation (3.108), must be taken to be the permeability tensor of the medium. These tensors must be constant in every triangular subregion, although different triangles may have different permittivities.

Boundary conditions are not enforced by the computer program since the condition

$$\overline{n} \times \hat{\epsilon}^{-1} \operatorname{curl} \overline{H} = 0$$
 (4.2)

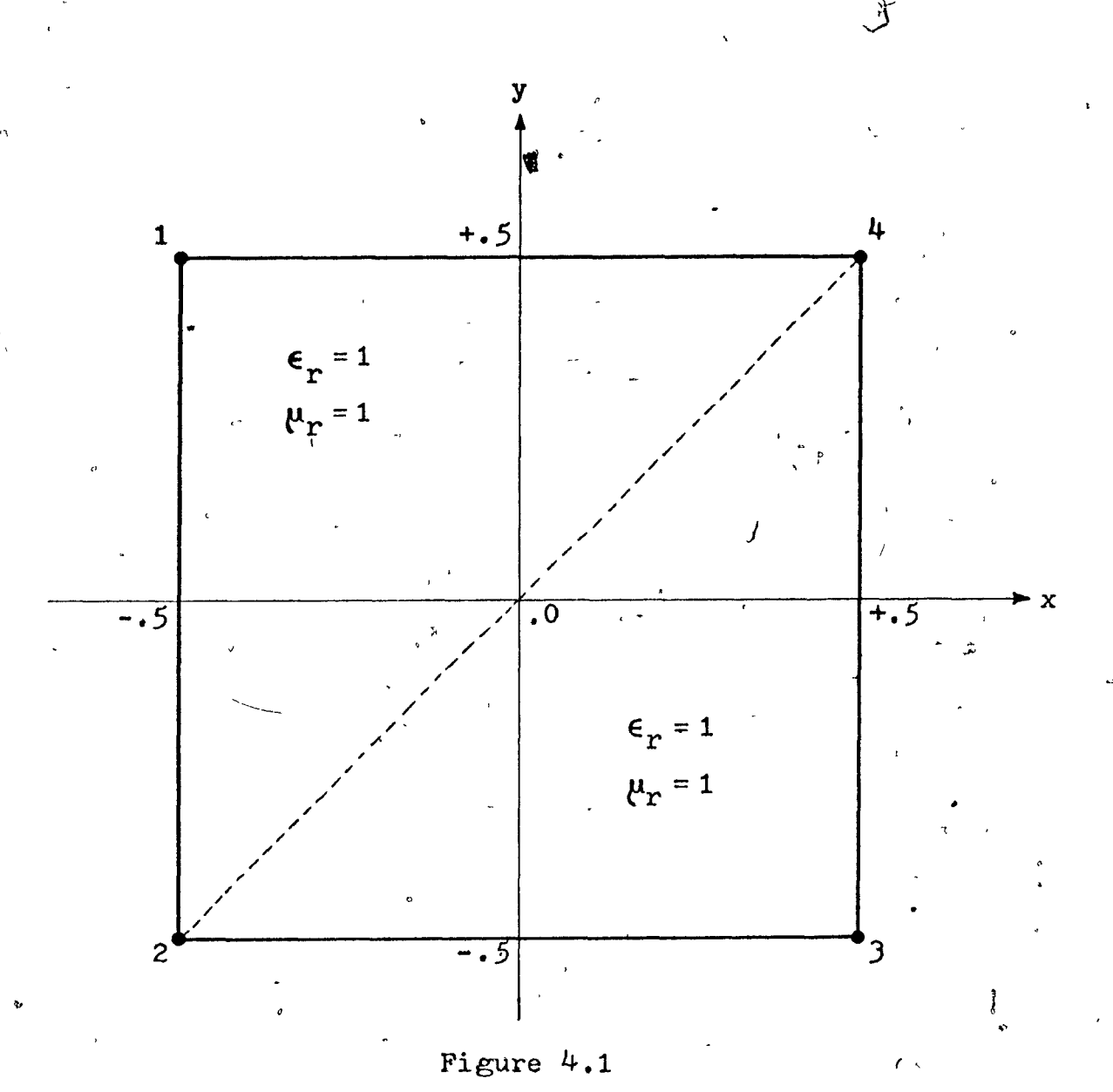
is a natural one for the functional and it will be satisfied automatically by the eigenvectors.

Due to the generality of the finite element formulation on which the program is based, solutions can be obtained for a variety of problems that normally are given special treatment.

The simplest category is the isotropic, homogeneous waveguide problem. In the next section solution is given to the empty square waveguide in order to demonstrate how the program works and also to illustrate the generality of the method. Results have been obtained with both a single precision version of the program and with a double precision version. Comparison of results helps to ascertain the amount of round-off error in the single precision results.

#### 4.2 Solution to a Homogeneous, Isotropic Waveguide Problem

Consider the square waveguide shown in Figure 4.1. The region has been divided into two triangles whose vertices have been numbered. The input data cards to the program have been rep#oduced in.Figure. 4.2. The first card contains an asterisk in column 1, followed by the problem title. The X after the title specifies that no punched output is desired (a P would cause the program to punch out the eigenvalues and eigenvectors on cards). The two numbers following the X are the x and y coordinate scale factors (taken here as unity). The -2.000 after the scale factors is the starting value of the desired propagation constant  $\beta$ . This value of  $\beta$  is to be incremented by 1.000 (the next number on the data card) until 8 different values of \$ (ranging from -2.000 to +5.000) are used, as indicated by the last number on data card number 1. The minus sign in column 72 signifies that the H<sub>2</sub> magnetic field component should have a phase factor  $\exp(-j\frac{\pi}{2})$  relative to the other two field components.



Cross-section of an empty square waveguide. The region has been divided into 2 triangles and the vertices numbered 1 to 4.

```
_x 1.00 1.00 -2.000
                 1.0000
                          C.CCCC
                                   0.0000 . 1.0000
                                                    0.0000 20 25 CARTGCC2
        c.ccc
1.0000
                    0.50000
       -0.50000
       -C.5CCCC
                   -0.50000
                                                                    CARECCC4
                   -0.50000
        C.50000
                                                                    CARECCO5
                    0.50000
                                                                    CARCCOC6
         C.5CCCC
                                                                    CAPECCC7
                                                                    CAPECCE9
             1.0000
                     0.0000
                                                 0.0000 . 1.0000
                                                                    CARCCOLO
```

Figure 4.2

Input data cards which describe the empty square waveguide problem to the three-component magnetic field vector program.

The second data card again contains an asterisk in column 1. The purpose of these asterisks is to provide the program with a means of detecting the first two cards of a data set in a long stream of data. The six numbers following the asterisk on the second data card are the xx, yx, yy, zx, zy and zz components of the magnitudes of the permeability tensor of the medium filling the waveguide. The figures given represent the relative permeability tensor of free space. The final number, 0.0000, following the tensor components has no bearing on an empty waveguide\_problem. In a ferrite filled waveguide problem, it is used to indicate the direction of the external magnetizing field with respect to the y-coordinate axis. The last two integer numbers on this data card request the program to compute 25 modes starting with mode number 20. It turns out that the first 21 modes returned by the program for this problem are non-physical solutions associated with zero frequency. Their number can be estimated from the number of boundary nodes; hence the figure 20 used on the data card to specify the first mode to be returned.

The next four data cards (cards No.3 through No.6) contain the x-y coordinates of the triangle vertices and the numbers assigned to them in Figure 4.1. The blank card following these indicates the end of the input point list to the program.

defining the problem region as well as information pertaining to the type of triangle employed. The first figure on card number 8 indicates that the triangle is to be fitted with a 4-th order interpolation polynomial for all field components.

The next three numbers, 1, 2 and 4, define a triangle with vertex numbers 1, 2 and 4. The six numbers after that are the magnitudes of the xx, yx, yy, zx, zy and zz components of the relative permittivity tensor of the medium contained by the region defined by the triangle. As was the case with the permeability tensor, the numbers here represent the permittivity tensor for free space. Card number 9 contains similar information for a triangle whose vertices are numbered 3, 2 and 4. The polynomial order and the permittivity tensor elements have not been punched since the program automatically uses the values from the previous card. The list of triangular elements is terminated by a blank card (card No.10).

The program supplements the list of input points with a full set of interpolation nodes which it generates in each triangle. In this case, since there are 15 interpolation nodes in each 4-th order triangle, of which 5 nodes are common, the total number of points obtained is 25. Since three components of the magnetic field vector are associated with each node, the number of unknowns, and hence the matrix size, for this problem will be 75 x 75.

The output from the program consists first of all of a restatement of the input point and triangle lists. This is followed by an approximate map of the input points, assembled point and triangle lists, a second map, this time of the assembled points, a page providing an error code and problem size information, and finally, the wave-numbers and eigenvectors requested. A portion of the output from the single precision version of the program appears in Figures 4.3 through 4.7.

EMPTY SCLARE HAVEGLICE 1.00 HCRIZCNIAL S. - SCALE = 1.CC > VEPTICAL ~ \*\*\* INPLT PCINT LIST \*\*\* VERT-ICAL PCINT **FCRIZCNTAL** CCCPCINATE CCCRCINATE NC. . 0.50000 -0.50000 -C.50000 -C.SCCCC, 0.50000 -Q.5CCCC C.FCCCC C.5CECC \*\*\* INPLT ELEMENT LIST \*\*\* CACER PERMITTIVITY TENSOR COMPONENTS: EXX FYX (-J)E2X (-J)EZY EYY

C.C

C.C

1.CCCC

1.0000

C.C

C . C

0:0

C.C

Figure 4.3

I.CCCC

1.0000

TRIDICLE

NC.

1.

Output from the three-component magnetic field vector program - list of the input points and triangles.

EZZ

1.0000

1.CCCC

TRIPNOLE CRIEF POINT POINT

PCINA

MC.

?. 4. HE917CATAL

CCCRCINATE

-0.\*(.c. 1000;.0 2000;.0

-0.40000

-0.25000

NC+ N NC+1 NC+2 NC+2 NC+4 NC+5 NC+6 NC+7 NC+6 NC+5 NC+10 NC+11 NC+12 NC+13 NC+14 NC+15 NC+16 CP 17 CR 16 CP 17 CR 16 CP 20 CR 21 CR 22 CR 23 CR 24 CR 25 CR 26 CR 27 CR 27 CR 26 CR 27 CR 27 CR 26 CR 27 CR 27 CR 26 CR 27 CR 26 CR 27 CR 26 CR 27 CR 26 CR 27 CR 27 CR 26 CR 27 CR 27 CR 26 CR 27 CR

\*\*\* ASSEMBLED FLEMENT LIST \*\*\*

EMPTY SCLARE WAVEGUICE

Figure 4.4

Output from the three-component magnetic field vector program - list of the assembled points and triangles.

,

	****ENP	TY SCLARE WAVEGU	ICE	<b>* * * *</b> .
	*** MVD CE	THE ASSEMBLED	PCINTS ***	
1	6	9	13	4
,	<u></u>	•	-	, 4
5	8	12 ~ ~	16	°∈ 25
7	11	15	24	21
			-	
10	. 14	<sub>1</sub> 23 _	20	18 .
	,		ŧ	
2	. 22	-19	17	3
1	Output from the to vector program - assembled points.	∽ apdroximate ma	nagnetic field	ld

```
EMPTY SCLARE WAVEGLICE
      *** CIMENSIONS OF THE PROPLEM ***
ERRCR CCDE:
                           "MISTAK" =
TOTAL NO. OF POINTS:
PERMISSIPLE AC. OF PEINTS:
                             "LNGT" =
                                             57
NC. OF TRIANGULAR ELEMENTS: "NELMT" =
                                              2
PECUTRED "5"-MATPIX: ,
                           "LENGTH" =
                                           2850
AVAILABLE "S"-MATRIX:
                           "LCNGST" =
                                          14706
NC. OF ENTRIES IN "NVTX":
                            "INCIC" =
                                             31
AVAILARLE "NVTX" SIZE:
                            "LNVTX" =
                                            301
MATPIX SIZE:
PREPACATION CONSTANT:
PERMEABILITY TENSOR ELEMENTS: "PXX" =
                                          1.CCC
                                          C.C
                                          1.CCC
                                          0.0
                          (-J)"PZX" =
                          (-J)"PZY" =
                                          C.C
                                          1.000
```

#### Figure 4.6

Output from the three-component magnetic field vector program - problem statistics (variable names used in the program appear in quotation marks).

Figure 4.7

Output from the three-component magnetic field vector pragram: modes No. 32 and 35. These are the  $TE_{01}$  and  $TM_{11}$  modes at cut-off. The true solutions for the wave-numbers are  $\pi$  and  $\sqrt{2}\pi^{\frac{1}{2}}(=4.4428^{\frac{1}{2}})$  respectively. The round-off errors in these single precision results are less than 0.001%.

The eigenvalues k obtained from the program are plotted in Figure 4.8 as a function of the propagation constant  $\beta$ . It is apparent from this plot that the  $TE_{mn}$  and  $TM_{mn}$  modes familiar from analytical solution of the empty square waveguide problem [38] are correctly returned by the program both for positive and for negative values of the propagation constant. Table 4.1 shows the errors in the wave-numbers computed for the waveguide modes. Degenerate modes (e.g.  $TE_{01}$  and  $TE_{10}$ ) produce a single curve on the k- $\beta$  diagram, but, although the program returns two almost identical eigenvalues, the eigenvectors are a linear combination of the associated eigenfunctions. The TE and TM modes can be easily distinguished by inspecting the eigenvectors returned for  $\beta = 0$ : for TM modes the  $H_Z$  component is zero while the  $H_X$  and  $H_V$  components vanish for TE modes.

The waveguide modes described above are not the first eigenfunctions of the matrix eigenvalue equation. In this case for example, the TE<sub>01</sub> and TE<sub>10</sub> modes are the thirty-second and thirty-third respectively. The first 31 modes represent 'spurious' solutions of the waveguide problem. The present method is not the first to generate more modes than desired [5,7-12]; many other formulations [5-12,59], particularly those involving inhomogeneous waveguide and microstrip problems, are plagued by the occurrence of spurious modes.

It can be seen from Figure 4.8 that modes No. 26 through 31 have  $k-\beta$  curves which are straight lines at  $\pm 45$  degrees with respect to the axis, with the hyperbolas describing the behaviour of the waveguide modes being asymptotic to these lines.  $k-\beta$  curves at a  $\pm 45$  angle are characteristic of TEM modes. The occurrence of these modes in the solution is

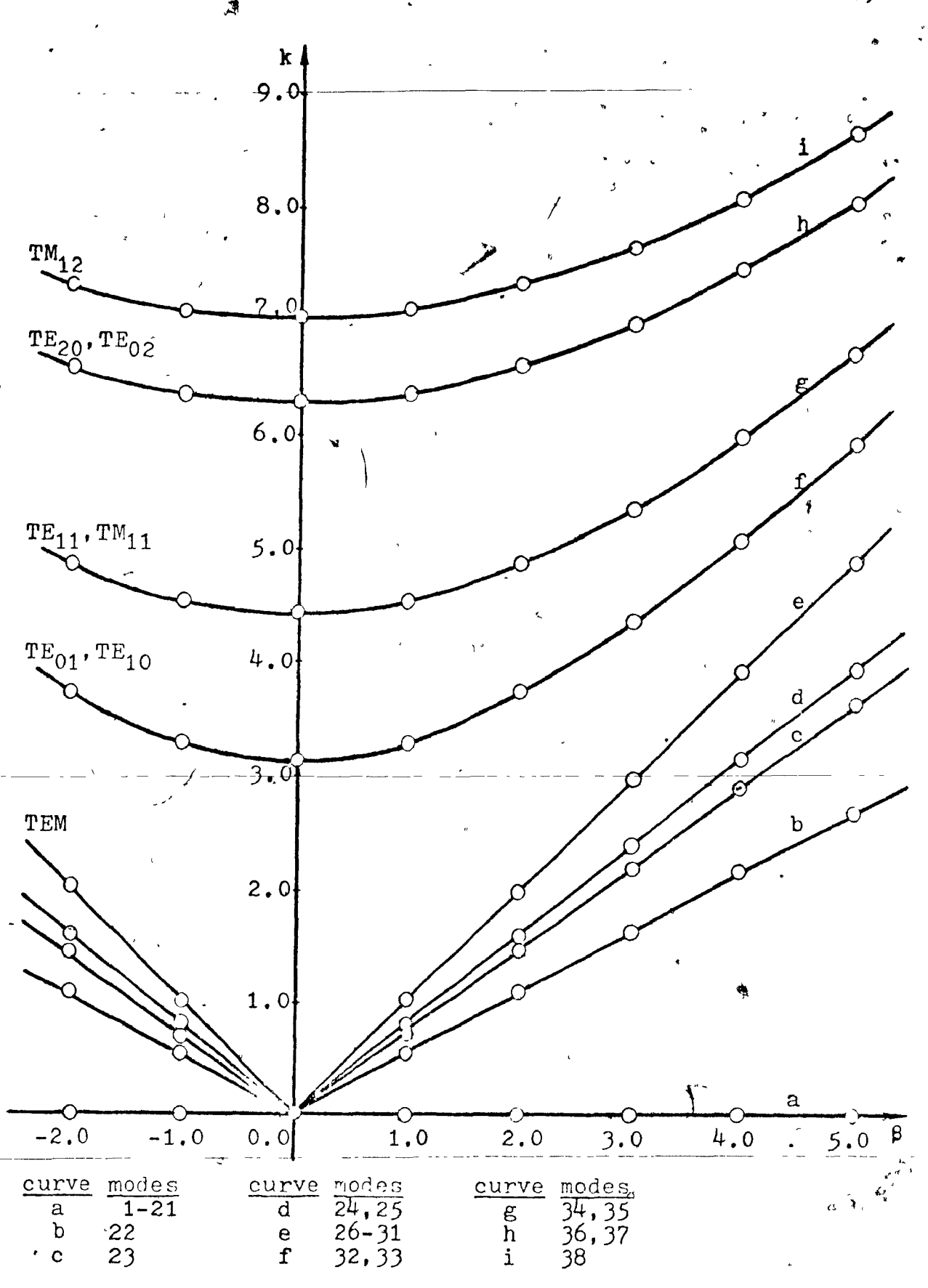


Figure 4.8

k-β diagram for the empty, square waveguide problem prepared from the output of the single precision version of the three-component magnetic field vector program.

Ca

	lode	β =	= 0	β	= 1	β:	= 2 ·
No.		k	%error	k	%error	k	%error
32.	"	3.14206	0.0149	3.29736	1	3.72459	0.0107
33.	TE10	3.14234	0.0238	3.29764	0.0222	3.72481	0.0166
34.	TE <sub>11</sub>	4.44656	0.0827	4.55763	0.0790	4.87562	0.0683
35.	TM11	4.45974	0.3794	4.57047	0.3609	4.88766	0.3155
36.	<sup>TE</sup> 20	6.30590	0.3615	6.38472	0.3529	6.61548	0.3285
37.	TE <sub>02</sub>	6.30594	0.3621	6.38474	0.3532	6.61550	0.3288
38.	TM12	7.05432	0.4200	7.12479	0.4109	7.33213	0.3855
39.	<sup>TM</sup> 21	7.17106	2.0818	7.24043	2.0406	7.44473	1.9271
40.	TE <sub>12</sub>	7.18927	2.3411	7.25850	2.2953	7.46228	2.1674
41.	TE <sub>21</sub>	7.59589	8.1294	7.66031	7.9581	7.85053	7.4830
42.	T₽22	9.30165	4.6803	9.35523	4.6229	9.51422	4.4593
43.	ZM <sub>Z</sub> 2	9.56880	7.6868	9.62021	7,5862	9.77285	7.2989
3.0							
$\frac{No}{No}$	ode	ع ا	Terror	k   k	= 4	B =	= 5
32.	Type TE <sub>01</sub>	4.34423	0.0072	5.08647	%error 0.0049	5.90526	%error 0.0036
-		1 1 2 1 1 1 2 2	0.0072	5.00047	0.00.49	1 7.70 7.60	0.0000
33.	(DI)	11 2000		2 00770		20017	
	<sup>ТЕ</sup> 10	4.34449	0.0132	5.08669	0.0093	5.90546	0.0069
34.	TE <sub>11</sub>	5.36391	0.0562	5.98090	0.0447	6.69110	0.0353
35.	TE <sub>11</sub>	5.36391 5.37488	0.0562	5.98090 5.99075	0.0447	6.69110	0.0353
35. 36.	TE <sub>11</sub> TM <sub>11</sub> TE <sub>20</sub>	5.36391 5.37488 6.98317	0.0562 0.2608 0.2948	5.98090 5.99075 7.46756	0.0447 0.2095 0.2575	6.69110 6.69993 8.04763	0.0353 0.1673 0.2215
35. 36.	TE <sub>11</sub> TM <sub>11</sub> TE <sub>20</sub> TE <sub>02</sub>	5.36391 5.37488 6.98317 6.98318	0.0562 0.2608 0.2948 0.2949	5.98090 5.99075 7.46756 7.46759	0.0447 0.2095 0.2575 0.2579	6.69110 6.69993 8.04763 8.04765	0.0353 0.1673 0.2215 0.2217
<ul><li>35.</li><li>36.</li><li>37.</li><li>38.</li></ul>	TE <sub>11</sub> TM <sub>11</sub> TE <sub>20</sub> TE <sub>02</sub>	5.36391 5.37488 6.98317 6.98318 7.66524	0.0562 0.2608 0.2948 0.2949 0.3489	5.98090 5.99075 7.46756 7.46759 8.10866	0.0447 0.2095 0.2575 0.2579 0.3074	6.69110 6.69993 8.04763 8.04765 8.64550	0.0353 0.1673 0.2215 0.2217 0.2664
<ul><li>35.</li><li>36.</li><li>37.</li><li>38.</li><li>39.</li></ul>	TE <sub>11</sub> TM <sub>11</sub> TE <sub>20</sub> TE <sub>02</sub> TM <sub>12</sub> TM <sub>21</sub>	5.36391 5.37488 6.98317 6.98318 7.66524 7.77329	0.0562 0.2608 0.2948 0.2949 0.3489 1.7634	5.98090 5.99075 7.46756 7.46759 8.10866 8.21121	0.0447 0.2095 0.2575 0.2579 0.3074 1.5759	6.69110 6.69993 8.04763 8.04765 8.64550 8.74207	0.0353 0.1673 0.2215 0.2217 0.2664 1.3864
35. 36. 37. 38. 39. 40.	$TE_{11}$ $TM_{11}$ $TE_{20}$ $TE_{02}$ $TM_{12}$ $TM_{21}$ $TE_{12}$	5.36391 5.37488 6.98317 6.98318 7.66524 7.77329 7.79010	0.0562 0.2608 0.2948 0.2949 0.3489 1.7634 1.9835	5.98090 5.99075 7.46756 7.46759 8.10866 8.21121 8.22712	0.0447 0.2095 0.2575 0.2579 0.3074 1.5759 1.7728	6.69110 6.69993 8.04763 8.04765 8.64550 8.74207	0.0353 0.1673 0.2215 0.2217 0.2664 1.3864 1.5598
35. 36. 37. 38. 39. 40.	$TE_{11}$ $TM_{11}$ $TE_{20}$ $TE_{02}$ $TM_{12}$ $TM_{21}$ $TE_{12}$	5.36391 5.37488 6.98317 6.98318 7.66524 7.77329 7.79010	0.0562 0.2608 0.2948 0.2949 0.3489 1.7634 1.9835	5.98090 5.99075 7.46756 7.46759 8.10866 8.21121 8.22712	0.0447 0.2095 0.2575 0.2579 0.3074 1.5759 1.7728	6.69110 6.69993 8.04763 8.04765 8.64550 8.74207	0.0353 0.1673 0.2215 0.2217 0.2664 1.3864 1.5598
35. 36. 37. 38. 39. 40. 41. 42.	TE <sub>11</sub> TE <sub>20</sub> TE <sub>02</sub> TM <sub>12</sub> TM <sub>21</sub> TE <sub>12</sub> TE <sub>21</sub> TE <sub>22</sub>	5.36391 5.37488 6.98317 6.98318 7.66524 7.77329 7.79010 8.15808	0.0562 0.2608 0.2948 0.2949 0.3489 1.7634 1.9835 6.8009 4.2109	5.98090 5.99075 7.46756 7.46759 8.10866 8.21121 8.22712 8.57076 10.1252	0.0447 0.2095 0.2575 0.2579 0.3074 1.5759 1.7728 6.0237 3.9059	6.69110 6.69993 8.04763 8.04765 8.64550 8.74207	0.0353 0.1673 0.2215 0.2217 0.2664 1.3864 1.5598 5.2437 3.5737

Table 4.1.

Percent errors in the wave-numbers k of the waveguide modes computed by the single precision version of the three-component magnetic field vector program for the homogeneous, square waveguide problem.

puzzling since TEM modes are known to exist on transmission lines but may not exist in hollow waveguides.

In order to explain the occurrence of modes No. 26 through 31, the behaviour of the field solutions must be examined. The magnetic field vectors returned by the program for these modes have a constant  $H_Z$  component at  $\beta=0$  and a vanishing one at other  $\beta$  values. The  $H_X$  and  $H_Y$  components display an unusual spatial dependence and do not resemble any known field configuration; it appears from the output that the eigenfunctions associated with these modes do not satisfy the requirement that the magnetic field be tangential to the boundary surface. It therefore appears that modes No. 26 to No. 31 do not represent a physical solution of the waveguide problem, only a mathematical solution of the eigenvalue problem. Moreover, the number of such modes which occur in the output varies with the number of degrees of freedom in the finite element model.

A similar situation exists for modes No. 22 through No. 25, which have k-B curves that are characteristic of slow waves. The latter are known to exist only in periodic homogeneous structures, not in hollow waveguides. Modes No. 1 through No. 21 are again spurious, although in this case they may be easily dismissed on the grounds that the curlcurl equation does not represent Maxwell's equations at zero frequency.

To obtain the values plotted in Figure 4.8 the computer program required 2 minutes and 41 seconds of CPU (Central Processing Unit) time to execute 182 K bytes of dynamic core

<sup>&</sup>lt;sup>1</sup>An IPM Portion IV H compiler generated object code was used.

<sup>2</sup>An IEM 360/75 computer was used.

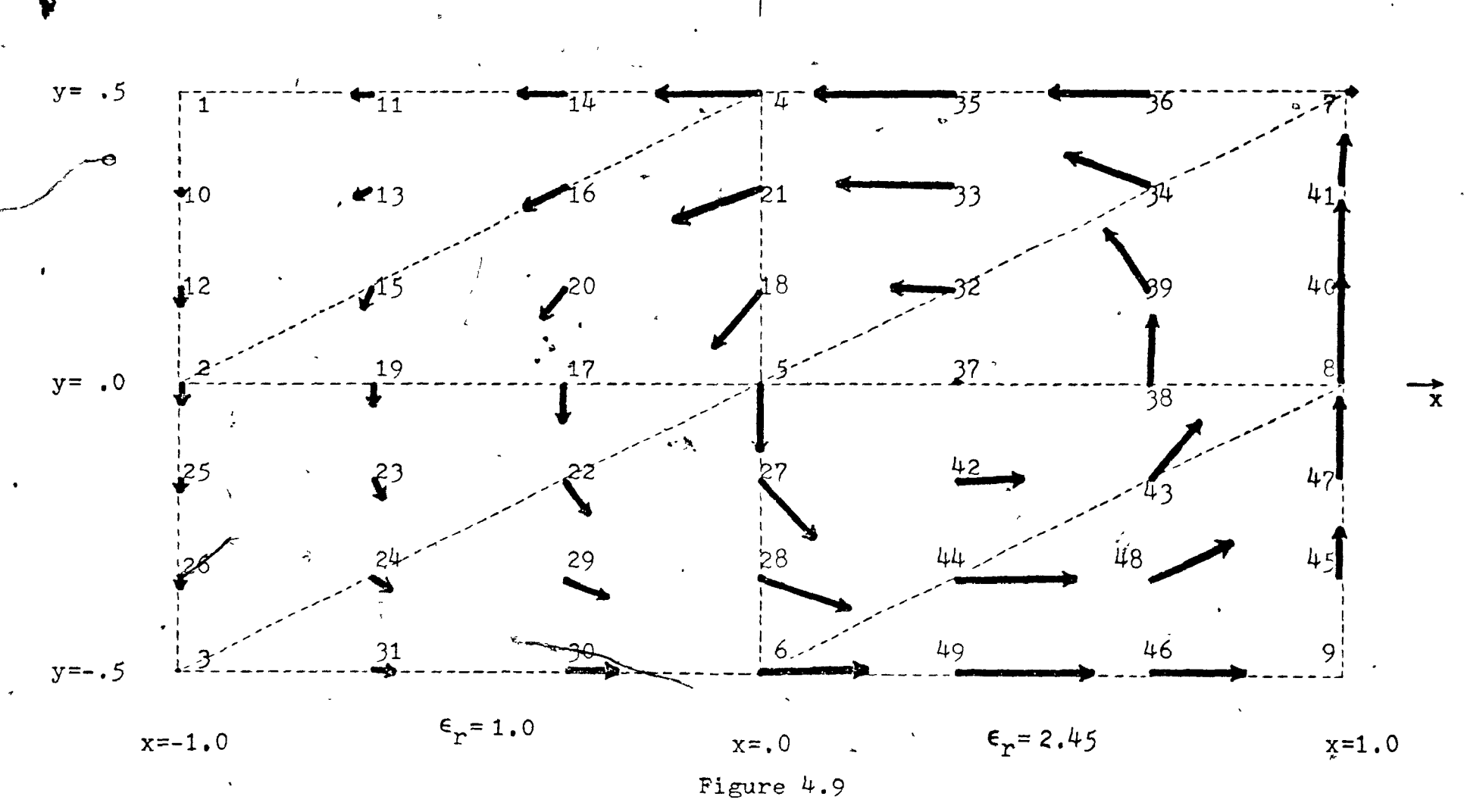
is required by the program, although the program is dimensioned for much larger problems than this example. In view of the complexity of the method and the program, the computing time given here and the accuracy shown in Table 4.1 compare quite favourably with those of other numerical methods [17,18].

The empty, square waveguide problem has also been solved with the double precision version of the program. There was no significant increase in computing time, but storage requirements were nearly doubled. Comparison of the results showed that round-off errors in the single precision results are of the order of 0.001%. The errors shown in Table 4.1 may therefore be attributed to discretization error.

# 4.3 An Inhomogeneous, Isotropiq Naveguide Problem

Figure 4.9 shows the dimensions, triangulation and partial solution of a rectangular waveguide half-filled with a dielectric material of relative permittivity 2.45. Figure 4.10 displays the data cards for this problem and the program output for the TM<sub>11</sub> mode (the 54-th eigenvector) is reproduced in Figure 4.12. The k-B diagram appears in Figure 4.11.

The modes in Figure 4.11 and 4.16 have been designated. TE and TM according to the field vector components present at cut-off. It is understood that these designations do not have the same meaning as in the case of the empty waveguide modes since above cut-off all electric and magnetic field components are present. The 56-th and 58-th eigenfunctions are difficult to classify since they possess three non-vanishing vector components even at cut-off. The k-B curve corresponding to

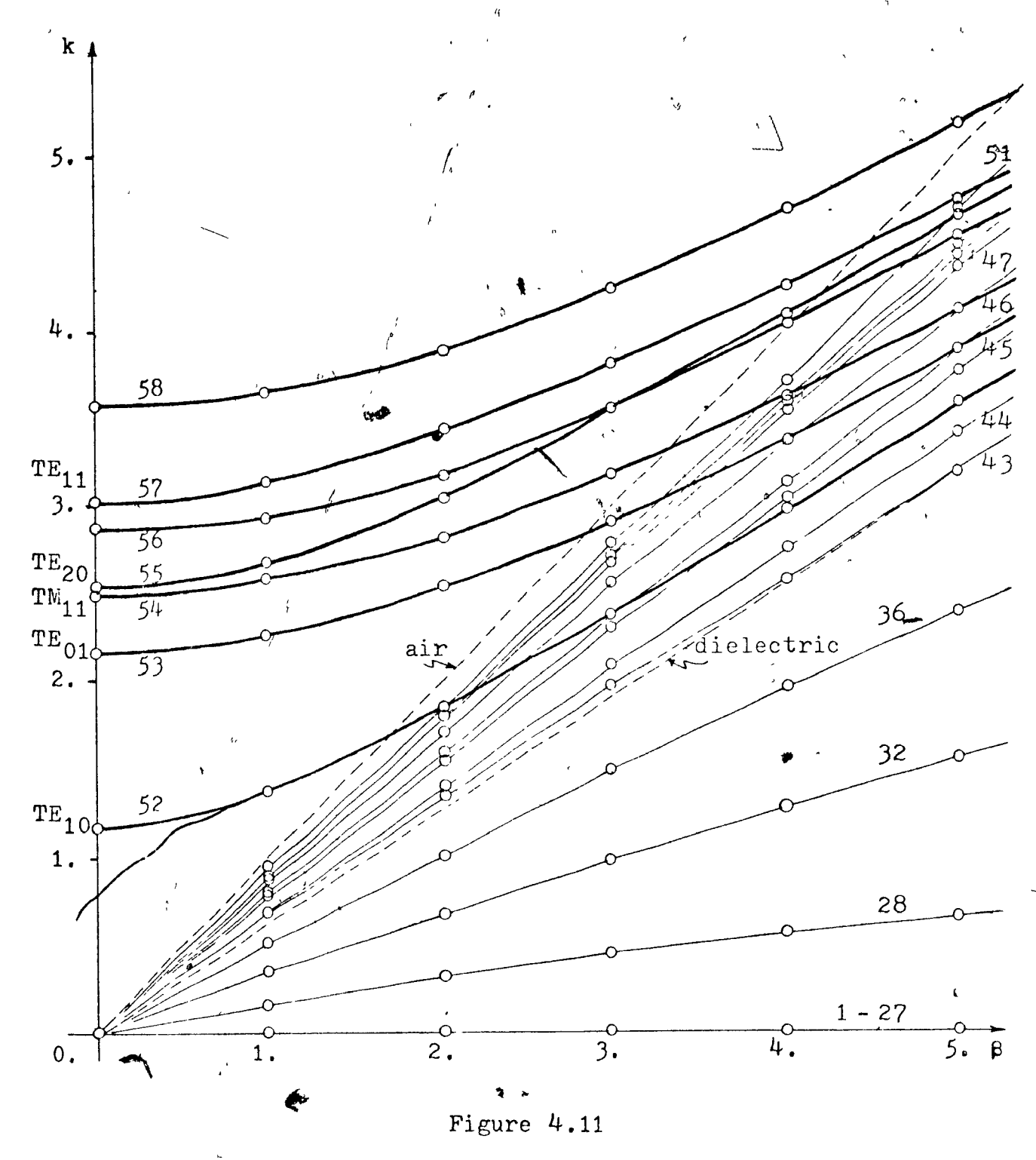


Dimensions and triangulation of a rectangular waveguide half-filled with a dielectric. The interpolation node numbers generated by the program are shown together with the magnetic field vector H for the  $TM_{11}$  mode at cut-off obtained from the program (see Figure 4.12). The concentration of the field in the dielectric material is noticeable.

*	_HALF-FI	LLED,	RECTAN	GULAR WAVE	EGU I DE	X 1.00	1.00 0	-000 1-0	0000 6-CARD0001
4	1.0000	0.0	000 1	.0000 0.	.0000 0	0000	1.0000	0.0000	26 35 CARD0002
	1	<b>-1.</b> 9	00 <b>0C</b>	0.50000					CARD0003
	2	-1.0	0000	0.00000					GARD0004
	3	-1.0	6000	-0.50000					CARDOOD5
	4	0.0	0000	0.50000			,		CAHDOOG6
	\$	0.0	Ú000	0.00000					CARDOOCT
	6	0.0	0000	-0.50000		.5			CARDOOO8
•	7	1.0	000 <b>C</b>	0.50000		4		•	CARD0009
	ರ	1.0	6366	0.00000					CARDOO10
	9 ~	1.0	0000	-0.50000					CARD0011
-									CARD0012
3	1 2	4	1.0000	0.0000	1.0000	0.000	0.00	00 1.00	000 CARCO013
	5 2	4			•				CARDCO14
	5 .2	~3			* 1		٥	<b>1</b> 6	CAR D0015
	ە 5	3	_		4			<b>*</b> c	CARDOO16
	5 4	7	2 • 45 0 0	0.0000	2.4500	0.000	0.00	00 2.49	500 CARD0017
	5 ′ ່ 8	7`				•			'CARD0018
	ნ ძ	Ö							_ CARD0019
	9 8	6							CARD0020
							•		CAR D0 0 2 1

Figure 4.10

Data cards for the inhomogeneous, isotropic, rectangular waveguide problem.



k-B diagram for the rectangular waveguide half-filled with a dielectric material of relative permittivity 2.45. The diagram was prepared from the output of the three-component magnetic field vector program listed in Appendix IV.

......... B BAY MUMILER # 0.248671F401 MUDE NU . 54 BETA= 0.000 MAGNETIC FIELD INTENSITY AT THE INTERPOLATION NODES 1. -0.4101/ve-02 0.13434E-01 -C.43/24E-05 18. -0.4444601 -0.51561E+01 -0.50060E-04 35. -0.11951E+02 +0.20648E+00 0.60237E-08 2. -0.203786.00 -0.100091.01 C.p7748E-04 19. 0.718171-01 -0.20739E-01 0.36210E-04 36. -0.86346E-01 -0.11227E-00 -0.32643E-04 J. 0.15455€.00 0.11130E+00 6.1943JE+63 20. -0.23J44E+01 +0.28157E+01 +0.33424E+04 37. +0.89250E+01 0.89059E+00 0.01269€-04 4. -8.y0#fet+01 0.15832E-01 -C.01/32E-04 21. -0.78051E+01 -0.27500E+C1 -C.55101E-04 38. 0.10340E+00 0.62108E+01 0.45701E-04 5. 0.727372-01 -0.502-JE+01 -0.277536-04 22. 0.231996+01 -0.28727E+01 -0.387646-04 39. -0.408196+01 0.543936+01 0.21277E-04 6. 0.88927E+01 0.33731E+30 -0.9013EE-C4 23. 0.911GCE+00 -0.17282E+01 0.80500E-04 40. 0.10116E+00 0.70601E+01 -0.18807E-03 7. C.d5:80c+00 -0.515.0E-01 -0.27030c-03 24. 0.10200E+01 -0.11040E+01 0.88380c-04 41. 0.28714E+00 0.44577E+01 -0.23745E+03 0. -0.214136+00 0.04 JUE+01 -0.407050-U4 25- -0.014446-02 -0.143436+01 0.108056-03 42. 0.505406+01 0.431706+00 0.406608-44 9. -0.176265-00 -0.428475-01 -0.427415-04 26. G.118675-00 -0.431205+00 G.158055-03 43. 0.427915-01 0.4427855-01 0.442787575-04
10. 0.545875-01 -0.401495+03 0.444475-05 27. 0.444495+01 -0.507285+01 -0.705085-04 44. 0.104685+02 0.114885+00 0.314965-04 11. -0.187946-01 -0.136196-01 -c.260406-04 28. 0.784956-01 -0.286906-01 -0.895066-04 45. -0.594326-01 0.440456-01 -0.334716-04 12. 0.7155E-01 -0.1475/E-01 C.3418CE-04 24. 0.37434E-01 -0.15786E+01 -0.35295E-04 46. 0.833E9E+01 -0.44287E-01 0.27067E-84 13. -Q.184528+01 -0.102401+01 -0.012786-05 JO. 0.450386+01 -C.145508+60 -0.350718-04 47. -Q.180686+CQ 0.759788+01 -0.493158-84 14. -6.450216-01 0.112116-03 -0.417-06-04 11. 0.153366-01 -0.157056-00 0.101406-03 48. 0.718756-01 0.32038-01 0.164818-04 18. -0.,4900k+01 -0.17206E+01 -0.3037CE-04 33. -0.10233E+02 0.19984E+00 0.28498E-04 17. -0.246912-01 -0.31411E+01 -0.30702E-04 34. -0.72533E+01 0.29285E+01 -0.13939E-04

\_HALF-FILLED. RECTANGULAR FATEGUIDE\_

Figure 4.12

Output from the single precision version of the three-component magnetic field vector program; the 54-th eigenvector corresponding to the TM<sub>11</sub> mode of the rectangular wave-(, suide half-filled with a dielectric material of relative permittivity 2.45 as in ? Figure 4.9. The magnetic field vector H presented here is plotted in Figure 4.9.

the TE<sub>10</sub> dominant waveguide mode (curve 52 in Figure 4.11) agrees very well with the analytical solution [37,41,59]. The k-\$\varphi\$ curve of the dominant mode is obtained by solving the following transcendental equation [59,60]

$$k_{\bullet} \tan(k_{\bullet}) = -k_{\bullet} \tan(k_{\bullet}) \qquad (4.3)$$

where

$$k_a^o = k_a - \beta_a \tag{4.4}$$

and

$$k_1^2 = k^2 \in r - \beta^2 \tag{4.5}$$

Table 4.2 contains the analytical solution as well as the values of k obtained from the single and the double precision versions of the three-component magnetic field vector program. Two single precision results are given in Table 4.2; the second set was obtained by replacing the four third-order triangles in the dielectric region by two sixth-order ones, causing the matrix size to increase from 147 to 210. According to established theory, the accuracy of the solution should improve with increasing order and increasing matrix size [58]. The percent errors in Table 4.2, however, indicate a decline in the accuracy. This can only be attributed to accumulated round-off error in the single precision version of the program, an error which may be expected to increase with larger matrix size. This observation is further substantiated since the double precision results are the most accurate.

Spurious modes appear in this problem as they had before in the homogeneous waveguide problem. The  $k-\beta$  diagram in

C/r.

B	k analytical solution	k double N = 3 n = 147	% error in k	k single N = 3 n = 147	% error in k	k single N = 3&6 n = 210	% error in k
0.0	1.1216905	1.17179 +0	.008492	1.17209	+0.034096	1.16948	-0.188659
1.0	- 1.3787439	1.37885 +0	.007695	1.37914	+0.028729	1.37687	-0.135914
2.0	1.8473069	1.84745 +0	.007746	1.84761	+0.016408	1.84250	-0.260211
3.0	2.4025974	2.40266 +0	.002606	2.40275	+0.006351	2.40001	-0.107692
4.0	2.9837841	2.98362 -0.	.005500	2.98366	-0.004159	2.98245	-0.044732
5.0	3.5765880 ~	3.57612 -0.	.013085	3.57615	-0.012246	3.57587	-0.020075

N: the degree of the interpolation polynomials used n: matrix size

#### Table 4.2

Values of k obtained from the single and the double precision versions of the three-component magnetic field vector program for the dominant mode of the rectangular waveguide half-filled with a dielectric material of relative permittivity 2.45 .

Figure 4.11 shows that the waveguide mode  $k-\beta$  curves No. 52 through 58 intersect with curves No. 28 through No. 51 which represent spurious modes. These intersections result in a change in the sequence in which the eigenvalues and eigenvectors appear for different values of  $\beta$ . The eigenfunctions change very slowly with changes in  $\beta$  and it is therefore evident which discrete values of the output in the  $k-\beta$  plane should be joined. Note that this problem can only occur in inhomogeneous waveguides since the  $k-\beta$  curves intersect only in the region between the air and the dielectric lines.

The magnetic field for the  $TM_{11}$  mode plotted in Figure 4.9 illustrates the accuracy with which the natural boundary conditions are satisfied. The mode pattern presented there preserves its character above cut-off, but the  $H_z$  field component grows as '\$\beta\$ increases.

To obtain all of the points plotted on the k-ß diagram, 9 minutes 34 seconds of computer time was required with the double precision program and 10 minutes 11 seconds with the single precision program. Storage requirements were 100 K and 50 K single precision words respectively. The Fortran IV H compiler and the IBM 360 Model 75 computer were used. When the matrix size was increased from 147 to 210, the single precision program required 31 minutes 45 seconds (CPU) to solve the same problem. While these computing times are considerable, the results are necessary in order to understand the method.

### 4.4 A Microstrip Problem

The problem of an enclosed microstrip supported by a dielectric slab is essentially just another form of the inhomogeneous isotropic waveguide problem. However, a microstrip can support low frequency propagation due to the presence of two conductors and has generated considerable interest in recent years [5,6,9-11,61-64].

In order to illustrate how a microstrip problem can be solved by the finite element method presented\here consider the microstrip treated by Daly [9]. The dimensions and triangulation are shown in Figure 4.13; the data cards are listed in Figure 4.14.

Daly has also solved this problem by a high-order polynomial triangular finite element method [9,24,58], using a longitudinal electric and magnetic field vector components (E<sub>z</sub> and H<sub>z</sub>) formulation. None of the modes reported by Daly are labeled non-physical, although he presents results for three different mode types: the quasi-TEM mode, a "low-loss surface wave" and the first waveguide mode. His results using a 4-th order polynomial approximation have been plotted in Figure 4.15 in order to compare them with the results obtained by this method. Daly's surface wave has been dismissed by Corr and Davies [5], by Bird [65] and by Krage and Haddad [10] as a "spurious mode". The results shown in Figure 4.15 substantiate this finding since no k-β curves appear which match Daly's points for the surface wave.

It is apparent from Figure 4.15 that Daly's quasi-TEM solution is fairly close to mode number 38 obtained by this

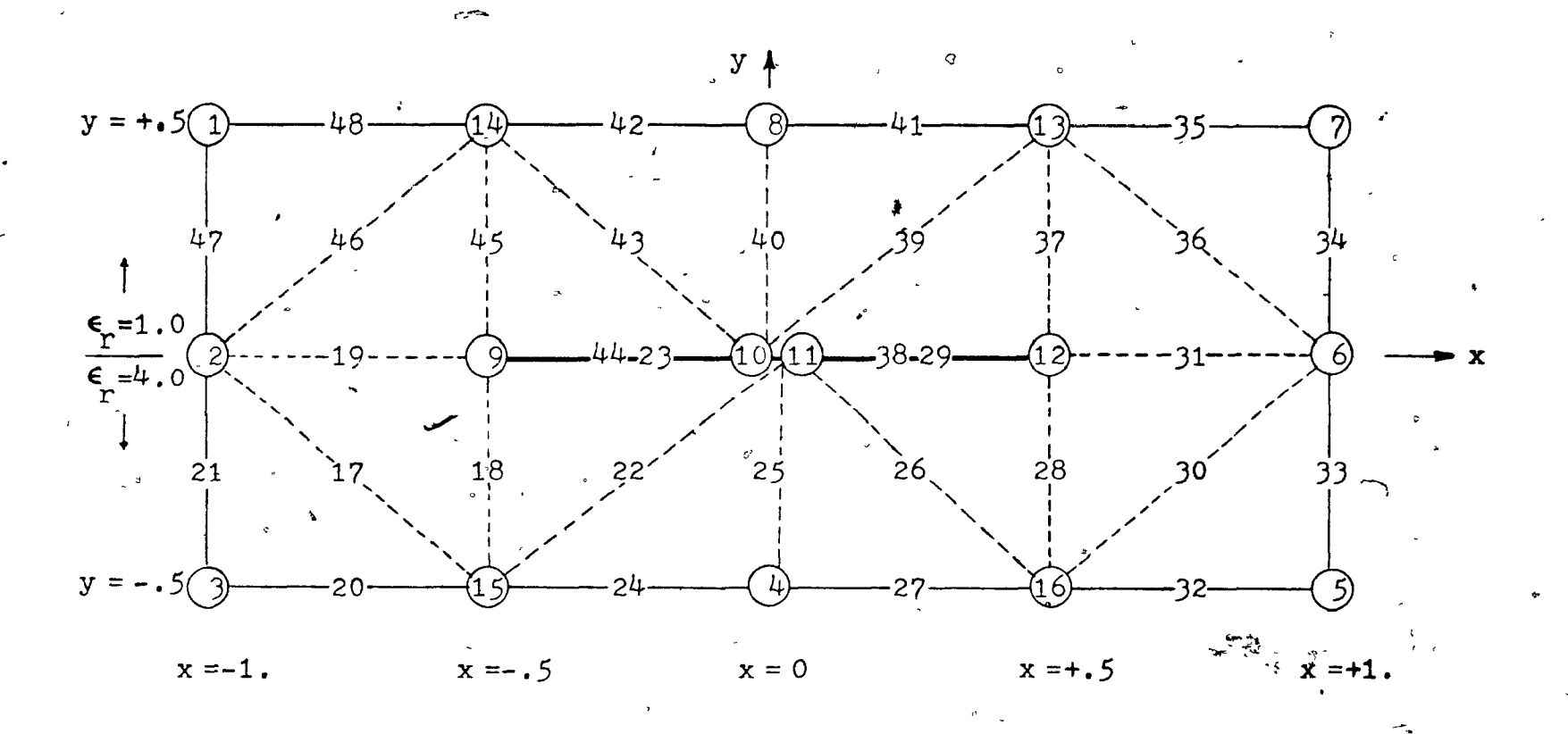
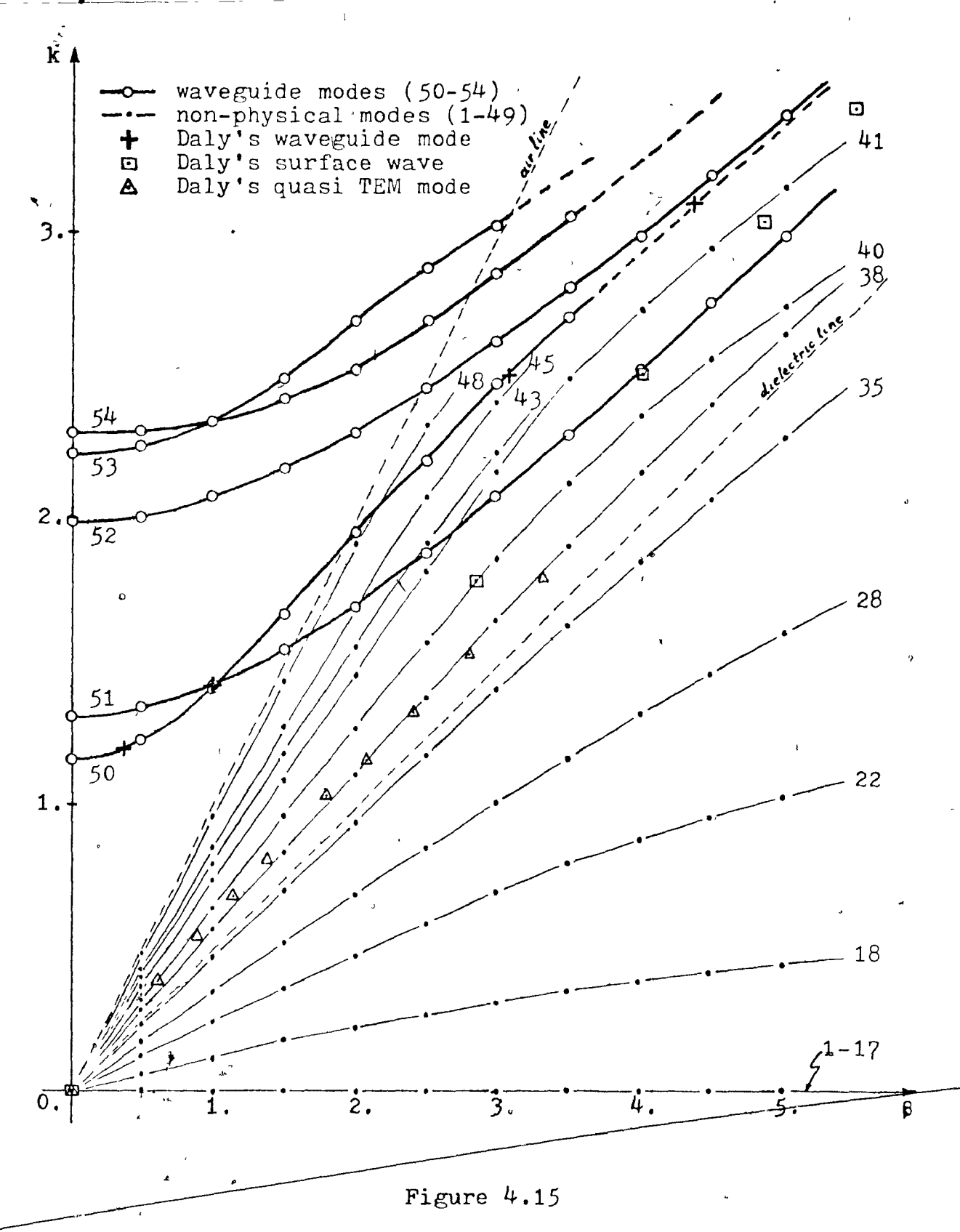


Figure 4.13

The dimensions and triangulation of Daly's closed, supported, single microstrip problem. The encircled node numbers represent the input points. The strip is of zero thickness and is located between nodes 9 and 12. The relative permittivity of the dielectric support is 4. The uncircled node numbers are generated by the program using a second-order polynomial approximation.

```
.DALY'S CLOSED, SINGLE MICROSTRIP....X
                                                          1.00
                                                   1.00
                                                                         0.500 11-CARECCO1
       1.CCCC
                 0.0000
                           1.CCCO
                                     C.0000
                                               O.CCCC
                                                          1.CCCC
                                                                    0.0000
                                                                            17 B3 CARECOO2
                -1.CCCCC
                            . C.5CCCC
                                                                                   CARCODO3
        2
                -1.CCCCC
                              C.CCCC
                                                                                   CARCOOO4
                -1.CCCCC
                             -C.50CCC
                                                                                   CARCCOO5
                 C.CCCC
                             -C.5GCCC
                                                                                   CARCCCC6
                 1.00000
                             -C.5CCCC
                                                                                   CARCOOC7
                              C.CCCCC
                 1.CCCCC
                                                                                   CAREGOOS
                 1.CCOCO
                              0.50000
                                                                                   CARCCCC9
                 C.CCCCC
                              C.5CCCC
                                                                                   CAREGGIG
                -0.5CCCC
                              C.CCCCC
                                                                                   CAREGOI1
       10
                -C.01CCO
                              0.00000
                                                                                   CARCCC12
-0 ¥ -*
       11
                 C.CICCC
                              0.00000
                                                                                   CARCOO13
       12
                 C.5CCCC
                              C.COCCO
                                                                                   CARCOO14
       13
                 C.5CCCC
                              0.50000
                                                                                   CARCOO15
       14
                -C.5CCCC
                              0.50000
                                                                                   CARCCO16
       15.
                -0.5CCCC
                             -C.50000
                                                                                   CARCOO17
       16
                 0.50000
                             -C.5CCCC
                                                                                   CAREGO18
                                                                                   CARECCI9
                     4.CCCO - C.COOC
       15
                                          4.0000
                                                    0.0000
                                                              0.0000
                                                                        4.0000
                                                                                   CARCCC20
       15
            2
                 3
                                                                                   CARCOO21
       15
           11
                 9
                                                                                   CARECC22
       15
           11
                                                                                   CAREGO23
       16
           11
                                                                                   CARCOO24
           11
       16
                12
                                                                                   CARCG025
                12
       16
            6
                                                                                   CARCC026
      ,16
            6
                 5
                                                                                   CARCOO27
                13
            6
                     1.CCCO
                               C.0000
                                          1.CCCG
                                                                                   CARCO028
               13
       12
            6
                                                                                   CARECO29
       12
          → 1 C
                13
                                                                                   CARCCO30
           10
                13
                                                                                   CARECO31
           1 C
               14
                                                                                   CARECO32
         4 1 C
                14
                                                                                   CAREGO33
               14
            2
                                                                                   CAREGO34
               14
            2
                                                                                   CARECO35
                                                                                   CARCC036
                                           Figure 4:14
```

Data cards used with the program of Appendix IV to solve Daly's microstrip problem.



k-8 diagram for Daly's microstrip problem prepared from the output of the double precision version of the three-component magnetic field vector program. Some of the non-physical modes have been left out for clarity. The solution obtained by Daly has also been plotted for comparison.

method. However, the eigenfunction associated with this mode has all of the features of a non-physical mode, e.g. the boundary condition  $\overline{n}.\overline{H}=0$  is not satisfied. Conclusive evidence that this mode is not the quasi-TEM wave can be obtained by proceeding on theoretical grounds; the number of spurious modes with non-zero eigenvalues (32 in this problem) always equals the number of boundary nodes (32 in this problem) which in this case includes the nodes on the microstrip. This number corresponds to the number of rows and columns that would be eliminated from the assembled finite element matrices if the boundary condition  $\overline{n}.\overline{H}=0$  were rigidly imposed at all the boundary nodes.

The agreement between the first waveguide mode obtained by this method (curve number 50 in Figure 4.15) and the four points plotted by Daly is very good. Geometrically, the problem is a difficult one [66] since second-order interpolation polynomials cannot easily approximate the true fields which are singular at the edges of the microstrip. For higher values of B and k it is very difficult, indeed at times impossible to ascertain which points are to be joined on the k-B diagram. Where the curve is doubtful, the k-B curves have been drawn as a dotted line in Figure 4.15. In all probability, this problem would not arise with a more accurate discretization. However, increasing the matrix size from second to thitd order is prohibitive since with second-order triangles used there were 48 nodes, resulting in a matrix size of 144 and an execution time-of 20 minutes and 39 seconds (CPU). With thirdorder triangles the matrix order would have been 288.

. It is interesting to note that the first two waveguide modes of the microstrip problem have  $k-\beta$  curves which cross at about  $\beta=1$ . Both of these modes have only a longitudinal magnetic field component at cut-off and are therefore labeled as TE modes. The difference between the two modes is that  $H_Z$  is antisymmetric about the y-axis for the first one (curve number 50 in Figure 4.15) and symmetric for the second one (curve number 51). The next three higher-order modes are also characterized as TE modes at cut-off.

#### 4.5 The Origin of the Spurious Modes

The results shown in Figure 4.11 for the dielectric loaded waveguide have been replotted as  $\beta/k$  versus k in Figure 4.16. Axis of this type are commonly used in the literature since  $\beta/k$  is a less sensitive parameter than  $\beta$ . In the present case, notice that in addition to crossing the wavefulde mode curves in the region  $1.0 < (\beta/k) < (1/\sqrt{2.45})$ , the curves associated with the spurious modes are nearly parallel to each other and are closely spaced.

Several finite difference and finite element formulations of the inhomomeneous, isotropic waveguide and microstrip problems have been established [5-12] some of which give rise to spurious modes similar to those obtained by the finite element method presented in this thesis. In most cases, the formulation is given in terms of the  $E_{\mathbf{z}}$  and  $H_{\mathbf{z}}$  field components. It is an annoying feature of all of these formulations (including the present one) that the spurious modes are

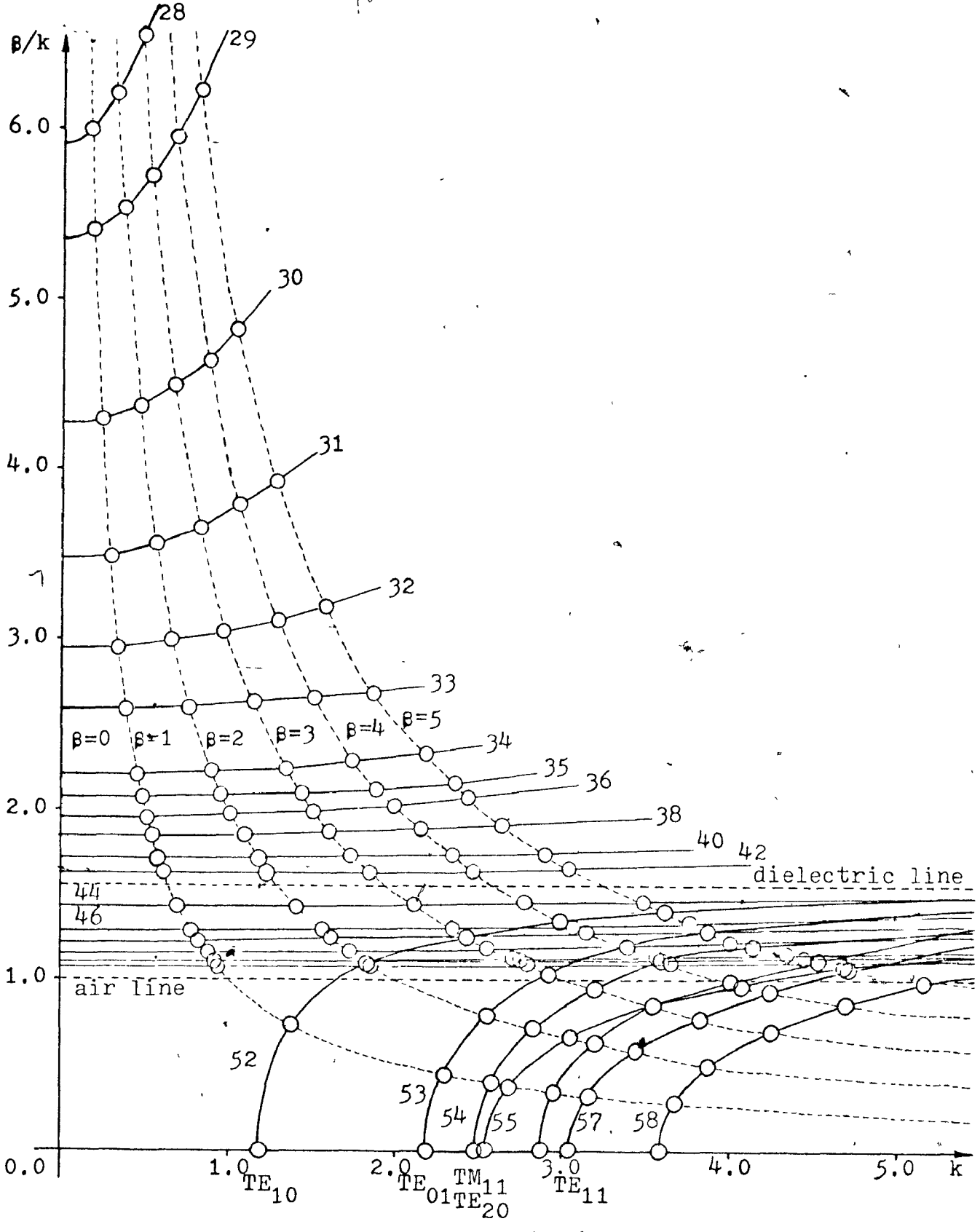


Figure 4.16

Plot of B/k versus k for the rectangular waveguide half-filled with a dielectric material of relative permittivity 2.45. The diagram was prepared from the output of the three-component magnetic field vector program listed in Appendix IV. The curves are designated as in Figure 4.11.

difficult to separate from the physical solutions since the dispersion curves contain two intersecting classes of modes.

According to Corr and Davies [5]

"The cause of these spurious solutions is believed to be in the indefinite nature of the variational expression, (7). Similar extraneous solutions are reported by Harrington [34] that occur for an indefinite system but not for a definite system. The identification of the spurious mode class was made by investigation of slab-loaded waveguide structures. The modes which propagate on this type of structure are well known 32. however using the formulation described, it was found that as well as these physical modes, spurious modes were also present of identical appearance to those in Fig. 11. It was found that the number of these modes was equal to the number of mesh points on the airdielectric interface, and that each mode could be characterized by the number of changes of sign of the values of ø across the interface. Again, this number of spurious solutions agrees with Harrington's findings [34], where one free boundary point gave rise to one spurious solution, and two points to two spurious solutions."

"Apart from the considerations given, it would be very difficult to account for these modes physically; their number, absence of low-frequency cutoff, and their rapid spatial dependence of field components along the dielectricair interface all point to their being nonphysical."

Corr and Davies derived finite difference equations from "the variational expression for an inhomogeneously filled structure" originally given by Berk [13]. Berk's variational expression is in fact an energy functional in terms of the longitudinal field components  $E_z$  and  $H_z$ . This functional is then modified by applying the "divergence theorem" [5] in order to remove the second derivative terms. Although not mentioned by the authors, the procedure involves the secting of a surface integral to zero, and hence introduces natural boundary conditions into the finite difference equations.

<sup>1</sup> equation numbers, figure numbers and reference numbers refer to those given in the paper by Corr and Davies (reference [5])
2 a slip of the tongue by the authors; it is in fact Green's first identity that is applied

The results in this thesis do not support forr and Davies' conclusion that the cause of spurious modes is the nature of the functional 1. The functional used in the present method is clearly definite, or possibly positive semidefinite, for isotropic media. The number of spurious modes emerging from the solution of the matrix eigenvalue equation varies with the matrix size regardless of the formulation used. Since the spurious modes have no low frequency cut-off, one possibility is that they are non-unique solutions. On the other hand, one accepts without hesitation the increase in the number of emerging waveguide modes. The reader is reminded here of the uniqueness proof given in section 4 of Chapter II. According to this section all solutions are unique, except the ones for which the frequency is zero, provided that the surface integral in equation (2.66) vanishes for certain boundary conditions. These conditions were given in equations (2.67) through (2.69) and were obtained under the assumption that the surface integral vanishes if the integrand vanishes. In the functional (2.37) for the curlcurl equation, a similar surface integral was set to zero and resulted in the natural boundary conditions given in section 3 of Chapter II. These natural boundary conditions were the same as those which occured in the analysis of uniqueness. However, it should be pointed out that in order for the relevant surface integral term to vanish over the boundary surface as a whole, the integrand need not be identically zero everywhere on the boundary. It is possible to have a non-zero integrand and still obtain an integral of zero, providing of

<sup>&</sup>lt;sup>1</sup>the indefinitness in the  $E_z$ ,  $H_z$  formulations arises in conjunction with a singularity at the air and dielectric lines on the dispersion diagram.

course that the integrand changes sign. In such a situation, the solution would be unique, but would satisfy some boundary conditions which are not desired. Physically, the solutions obtained with such boundary conditions would satisfy the condition that no net power may flow across the boundary surface, but that power may flow inward or outward over partial sections of the boundary. Solutions of this type satisfy Maxwell's quations and the curlcurl equation, of course, but they do not satisfy the electromagnetic boundary conditions associated with perfect conductors.

To illustrate the above argument, consider for example mode No. 22 obtained for the empty square waveguide problem discussed in section 4.2. The  $H_{\rm x}$ ,  $H_{\rm y}$  and  $H_{\rm z}$  values at the interpolation nodes for eigenfunction No. 22 at  $\beta=1$  (see curve b in Figure 4.8) are shown in Figures 4.17a through 4.17c as they were produced by the three-component magnetic field vector program of Appendix IV. The magnitude and direction of the transverse component of  $\overline{H}$  at the interpolation nodes are shown in Figure 4.18. It is clear that  $\overline{H}$  is not tangential at the side walls of the guide.

Consider now the surface integral S.I. around the guide walls which was set equal to zero in deriving the natural boundary conditions. For a unit length in the z-direction one obtains

S.I. = 
$$\mathcal{F}[\overline{H}^*x(\hat{\epsilon}^{-1}\text{curl}\overline{H})].\overline{n}\,dS$$
  
=  $-\mathcal{F}[\overline{n}x(\hat{\epsilon}^{-1}\text{curl}\overline{H})].\overline{H}^*dl$  (4.6)

Since the medium in this problem is two-dimensional empty space

#### Figure 4.17a

Values of H returned by the three-component magnetic field vector program for mode No.22 of the empty square wavefulde problem. The values are shown at the interpolation nodes.

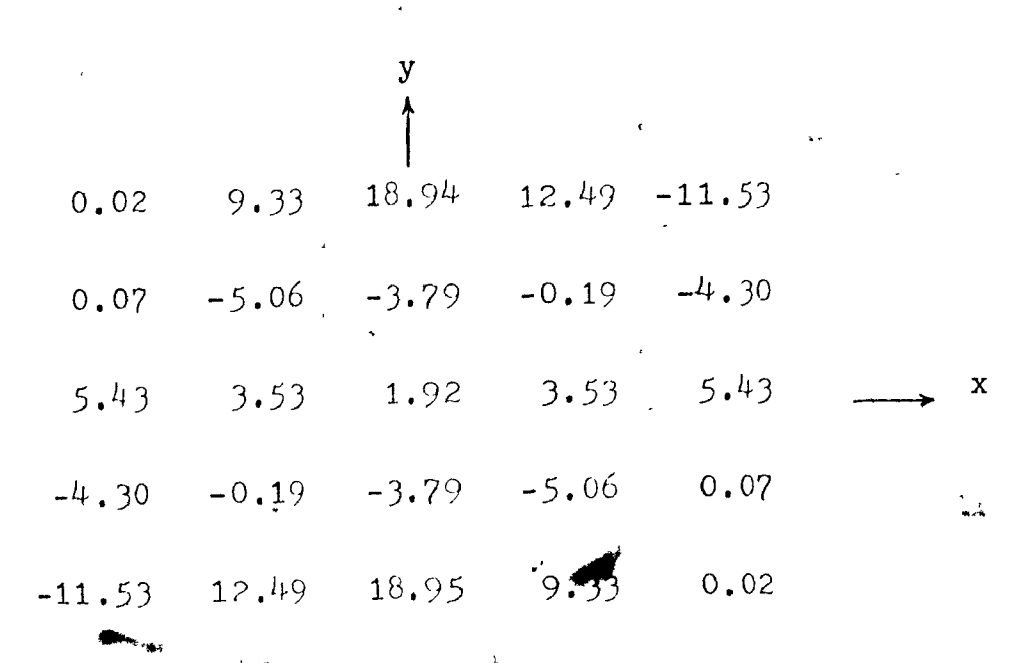


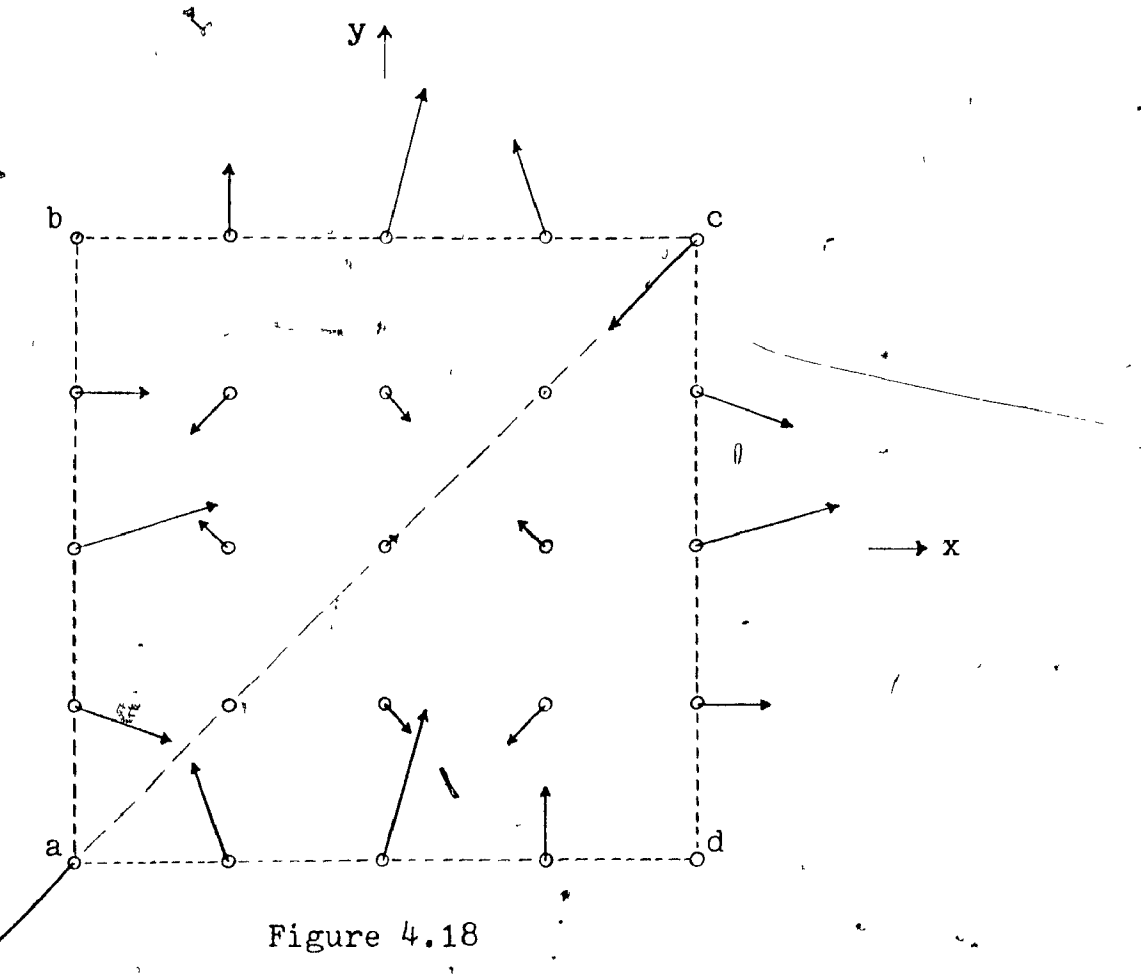
## Figure 4.17b

Values of H<sub>V</sub> returned by the three-component magnetic field vector program for mode No.22 of the empty square waveguide problem. The values are shown at the interpolation nodes.

*		y ,	,	gue . *		
0.00	-0.32	0.06	0.74	-2.00		•
0.32	0.00	-0.22	0.87	0.74	· ,	
-0.06	0.22	0.00	-0.22	.0.06		x
-0.74	-0.87	` 0.22	0.00	-0.32		
2.00	-0.74	-0.06	0.32	0.00	<b>\</b>	•

### Figure 4.17c

Values of  $\rm H_{\rm Z}$  returned by the three-component magnetic field vector program for mode No.22 of the empty square wavecuide problem. The values are shown at the interpolation nodes.



Magnitude and\_direction of the transverse component of H at the interpolation nodes for mode No. 22 of the empty square waveguide problem. See also Figures 4.17a & b.

and since  $H_{\mathbf{x}}(\mathbf{x},\mathbf{y}) = H_{\mathbf{y}}(\mathbf{y},\mathbf{x})$  according to the results shown in in Figures 4.17a and 4.17b, the z-component of curl  $\overline{H}$  and hence  $E_{\mathbf{z}}$  must vanish at the boundary. Therefore, the surface integral can be rewritten as

S.I. = + 
$$\int \left[ n_x (\beta H_x + \frac{\partial H_z}{\partial x}) + n_y (\frac{\partial H_z}{\partial y} + \beta H_y) \right] H_z d1$$
 (4.7)

In order to evaluate this integral, the partial derivatives of  $H_Z$  need to be evaluated at the interpolation nodes by differentiating the interpolation polynomials over each triangle; the results of such differentiation are shown in Figures 4:19a and 4.19b. Notice that there is a discontinuity in the first derivative of the solution at the common triangle edge. The integration can be carried out for each side of the square by using the 4-th order Newton-Cotes quadrature formulae for one-dimensional integration. Starting with the corner labeled a in Figure 4.18 and going clockwise, one obtains

S.I. = 
$$-\int_{1}^{b} (H_{x} + \frac{\partial H_{z}}{\partial x}) H_{z} dy + \int_{b}^{c} (\frac{\partial H_{z}}{\partial y} + H_{y}) H_{z} dx$$
  
 $+\int_{1}^{c} (H_{x} + \frac{\partial H_{z}}{\partial x}) H_{z} dy - \int_{1}^{a} (\frac{\partial H_{z}}{\partial y} + H_{y}) H_{z} dx$   
=  $+6.43 + 6.43 - 6.43 - 6.43$   
= 0 (4.8)

Therefore it can be seen that the surface integral vanishes for the entire boundary but not for each individual triangle edge. The integrals on the common triangle edge have been found to be equal, i.e.

$$\int_{c}^{a} \left[ n_{x} \left( H_{x} + \frac{\delta H_{z}}{\delta x} \right) - n_{y} \left( \frac{\delta H_{z}}{\delta y} + H_{y} \right) \right] H_{z} d1 =$$

$$\int_{c}^{c} \left[ n_{x} \left( H_{x} + \frac{\delta H_{z}}{\delta x} \right) - n_{y} \left( \frac{\delta H_{z}}{\delta y} + H_{y} \right) \right] H_{z} d1$$
(4.9)

•		†		ţ	v	
, . <b>0 . 01</b> . (	-0.68	3.49	`-0.58	-25.99 2.01		
3.42	-2.99	2.02	5.36 -6.87	10.98		
9.26	-2.87	2.99 2.99	-2.87	9.26		x
10.98	-6.87 5.36	2.02	-2.99	3.42		
2.01 -25.99	-0.58	3.49	-0.68	0.01		

#### Figure 4.19a

Values of  $\partial H_z/\partial x$  at the interpolation nodes for the empty square waveguide problem. The derivative is discontinuous at the common triangle edge and hence two values are shown.

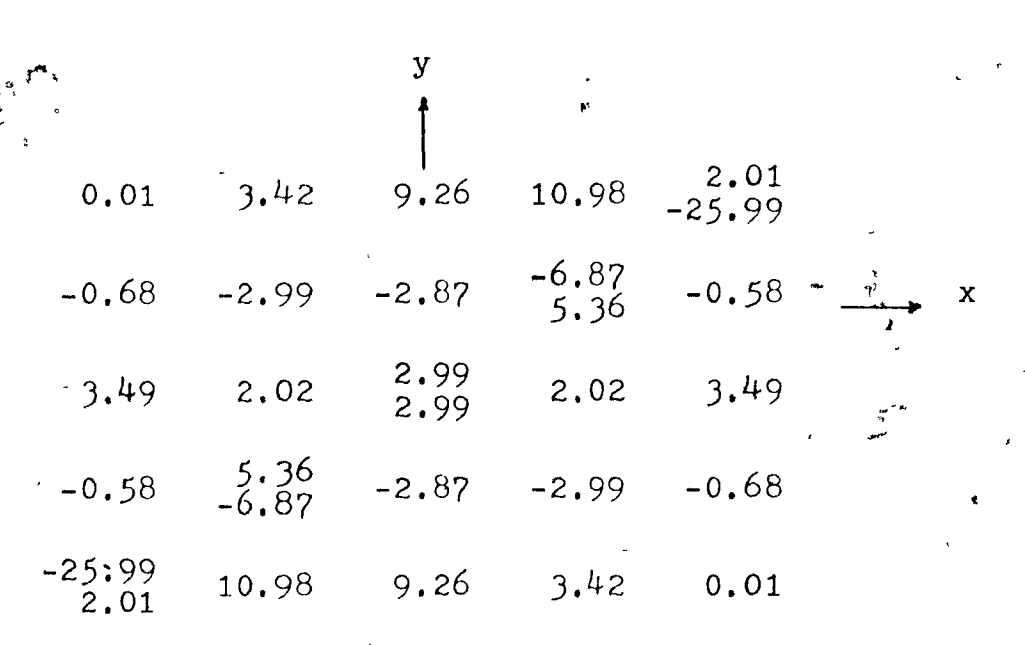


## Figure 4.19b

Values of  $\delta \rm{H_{Z}/\delta y}$  at the interpolation nodes for the empty square waveguide problem. The derivative is discontinuous at the common triangle edge and hence two values are shown.

E.

The higher order spurious modes returned by the program have similar properties in this case as well as for the dielectric loaded waveguide problem of section 4.3. There is no doubt that these modes are non-physical solutions, and they appear only as mathematical solutions. It appears - however, that not enough is known about the variational finite element method with respect to the ways in which natural boundary conditions are derived. No treatment of the finite element method [29-35,67] known to this author mentions the possibility of non-physical solutions arising from the dropping of the surface integral term in the way indicated above. It is likely that in  $E_z$  and  $H_z$  finite difference and finite element formulations of the dielectric loaded waveguide and microstrip problems the spurious modes reported by the authors occur for reasons similar to that given here [16].

Assuming that the occurrence of spurious modes is caused by the reason given above, it should be a relatively easy task to filter out the non-physical solutions. In the present method one could enforce the boundary condition  $\overline{n}.\overline{B}=0$  explicitly at each boundary point by eliminating rows and columns from the matrix eigenvalue equation. Thus, for the empty square waveguide problem with 16, boundary interpolation nodes, 10 independent conditions can be added due to the symmetry of the problem. Ten rows and columns and hence 10 modes would be eliminated. In this way the spurious modes No. 22 through No. 31 could be eliminated from the spectrum since they do not satisfy these conditions.

The elimination of spurious modes No. 1 through No. 21 requires a different treatment. These solutions satisfy the

condition  $\operatorname{curl} \overline{H} = 0$  on the boundary and belong to the null space of the curlcurl operator, but are not valid solutions since they occur with zero corresponding eigenvalue. They may therefore be eliminated by finding the rank of the coefficient matrix  $[S_t]$  in equation (4.1) and retaining only the independent rows and columns.

It is interesting to note that non-physical modes have not been reported in vector variational formulations using a restricted set of trial functions which satisfy the boundary conditions over rectangular and circular regions [19-21].

## 4.6 A Homogeneous, Magnetically Anisotropic Waveguide Problem

Consider a rectangular waveguide with a 2:1 width to height ratio completely filled with a ferrite material characterized by a relative permittivity of 2.0 and a relative permeability tensor  $\hat{\mu}_r$  given by

$$\hat{\boldsymbol{\mu}}_{\mathbf{r}} = \begin{bmatrix} 3.0 & 0.0 + j0.8 \\ 0.0 & 1.0 + j0.0 \\ -j0.8 - j0.0 & 3.0 \end{bmatrix}$$
 (4.10)

It is assumed here that the electromagnetic properties of the material do not vary with frequency, although this assumption is not valid in general for ferrites [45-47].

Data cards to solve this problem using the computer program in Appendix IV are shown in Figure 4.20. A map of the assembled points is presented in Figure 4.21 indicating the relative locations of the interpolation nodes in the two sixth-order triangle finite element model. The program output

```
7-CARD0001
FERRITE-FILLED RECTANGULAR WAVEGUIDE . X
3.0000
          0.0000
                    1.0000 * 0.8000
                                       0.0000
                                                 3.0000
                                                                      25 CARDO002
                                                                         E000GRAD
         -1.00000
                       C.50006
                                                                         CARDOOO4
         -1.60000
                     . -0.50000
                      -0.50000
                                                                         CARDOOG 5
          1.00000
                                                                        .. CARD0006
          1.00000
                       0.50000
                                                                         CARCOOO7
                                                                         CARDUO08
                        0.0000
                                                                         CARD0009
                                                                          CARDOO10
```

Figure 4.20 p

Data cards for the ferrite-filled rectangular waveguide problem.

\*\*\*\* ••FERRITE-FILLED RECTANGULAR WAVEGUICE•• \*\*\*\*

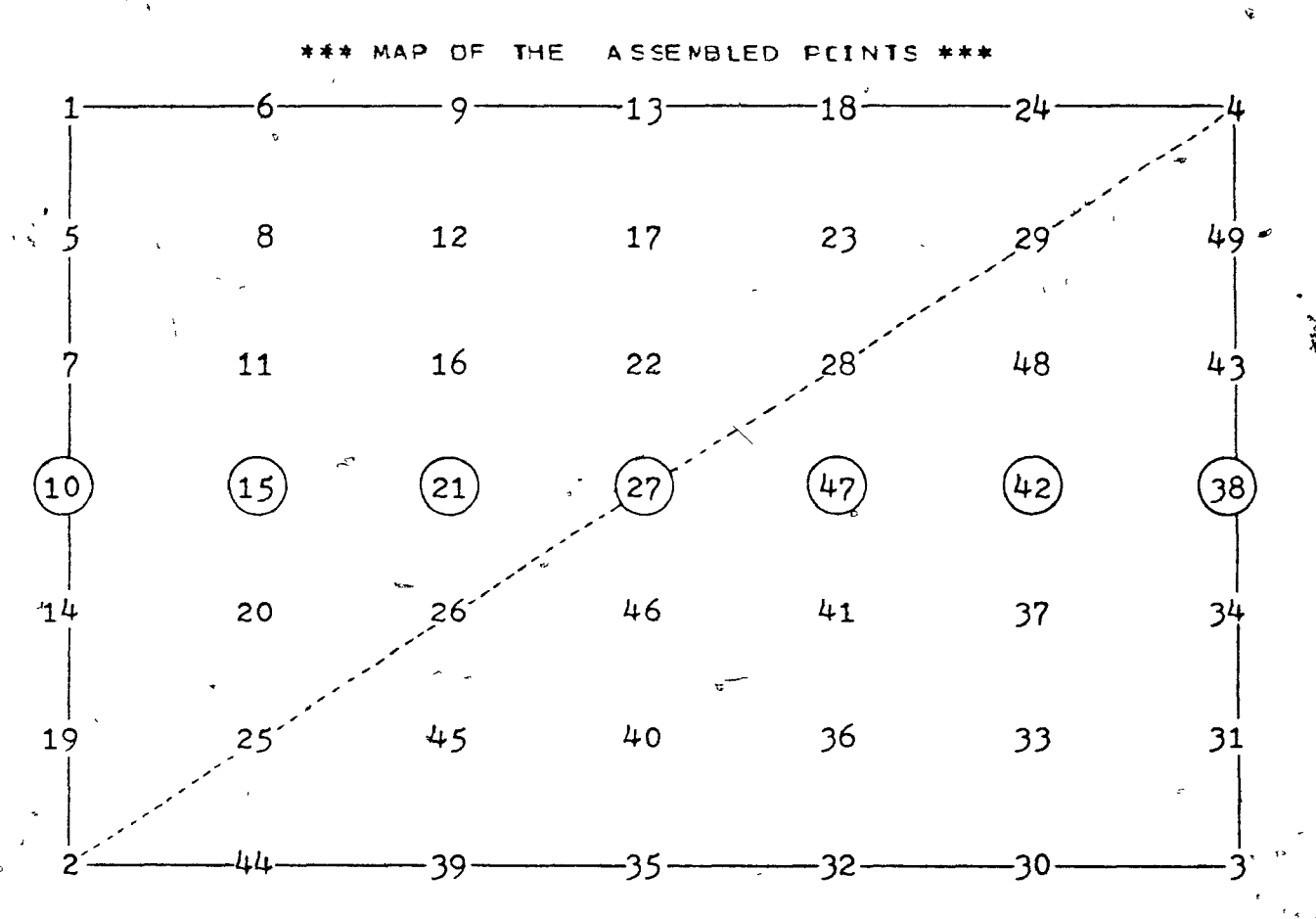


Figure 4.21

The map of the assembled points returned by the three-component magnetic field vector program showing the approximate locations of the finterpolation nodes. The problem solved is a ferrite-filled rectangular waveguide using two sixth-order triangles. The circled nodes lie on the x-axis.

for the 58-th eigenvector is reproduced in Figure 4.22 for  $\beta=1$ . The complete k- $\beta$  diagram prepared from the program output is shown in Figure 4.23.

Analytical solution can be obtained for the dominant waveguide mode and also for some of the higher-order modes.

A characteristic of these modes is the lack of an Hy field component. On the k-8 diagram these modes are nymbered 58, 60 and 64 respectively. The procedure to obtain the analytical solution for these modes follows.

The curlcurl equation in terms of the magnetic field  $\overline{H}$  is given by

$$\operatorname{curl}(\hat{\epsilon}^{-1}\operatorname{curl}\widetilde{H}) - \omega^2 \hat{\mu}\widetilde{H} = 0 \tag{4.11}$$

The following assumptions may be made:

- a)  $H_{y} = 0$ ;
- b) no variation occurs with respect to y;
- c) the fields vary as  $exp(-j\beta z)$  in the z-direction;
- d)  $H_z$  has a phase factor  $\exp(-j\frac{\pi}{2})$  relative to  $H_x$  and  $H_y$ . The relative permittivity is 2.0 and the relative permeability tensor is given in equation (4.10). Equation (4.11) then reduces to

$$\beta^{2}H_{x} - \beta \frac{\partial H_{z}}{\partial x} - k^{2}2(3H_{x} + 0.8H_{z}) = 0$$
 (4.12)

$$\beta \frac{\partial H_{x}}{\partial x} - \frac{\partial^{2} H_{z}}{\partial x^{2}} - k^{2} 2(0.8 H_{x} + 3 H_{z}) = 0$$
 (4.13)

Substituting for  $H_{\mathbf{X}}$  in equation (4.13) from equation (4.12) and collecting terms, yields the following second-order differential equation in  $H_{\mathbf{Z}}$ 

$$\frac{\partial^2 H_z}{\partial x^2} + (\frac{16.72}{3} k^2 - \beta^2) H_z = 0 \qquad (4.14)$$

\*\*\*\* .. FERRITE-FILLED RECTANGULAR DAVEGUIDE.. \*\*\* # #AVENUMBER # 6.7887580+66 # MODE NO. ER PET ## 1.000 1. 0.117340+C1 C.1CCF1C-02 -0.43373C+01 18. +0.29674C+01 0.24412C-02 0.26029C+01 35. +C.27f74C+C1 C.26526C-C2 C.73549C+08 2. 0.114970+01 C.945000-C2 -C.422270+01 15 0.115180+01 -0.19993C-02 -0.43323C+01 36. -0.296610+01 0.471280-C3 C.28C270+01 3. -0.115696-01 0.101966-02 0.413276-01 10. -0.378160+66 0.111430-02 -0.338450+01 37. -0.237996-01 -0.153176-03 0.411996-01 0.10234D-01 0.403376-01 (2). -0.181150+01 -0.11461D-02 -0.15280+01 (2). -0.185720+01 -0.266786-03 0.433236-01 0.10234D-01 0.266786-03 0.433236-01 0.45691D-03 0.735386+00 25. -0.181220+01 0.275900-02 -0.182450+01 6. -0.37869(-00 0.139350-02 -0.22840+01 22- -0.288700+01 -0.96483D-04 0.280290+01 40. -0.275725+01 0.473540+03 0.725640+00 

Figure 4.22

-0.378590+00 -0.613770-02 -0.338450+C1 32- -0.89660C+01 0.22577C-02 0.28027C+01 49. -0.11565C+01 -0.206520-CE 0.433220+CE

63. -0.378590+00 -0.013770-02 -0.331850+01 322 -0.00000170 0.201930-03 0.411990-01 0. 0.201930-03 0.411990-01 0.201930-03 0.411990-01 0.201930-03 0.431230-01 0.431230-01

17. -0.27571C+01 0.46633C-03 0.73528C+00 34. -0.115720+C1 -0.26528D-03 0.43323D+C1

Output from the three-component magnetic field vector program of Appendix IV showing the 58-th eigenvector at  $\beta = 1$  for the ferritefilled rectangular waveguide problem. The circled point numbers correspond to the circled nodes in Figure 4.21.  $\rm H_X$  and  $\rm H_Z$  at these points are plotted in Figures 4.24 and 4.25 respectively.

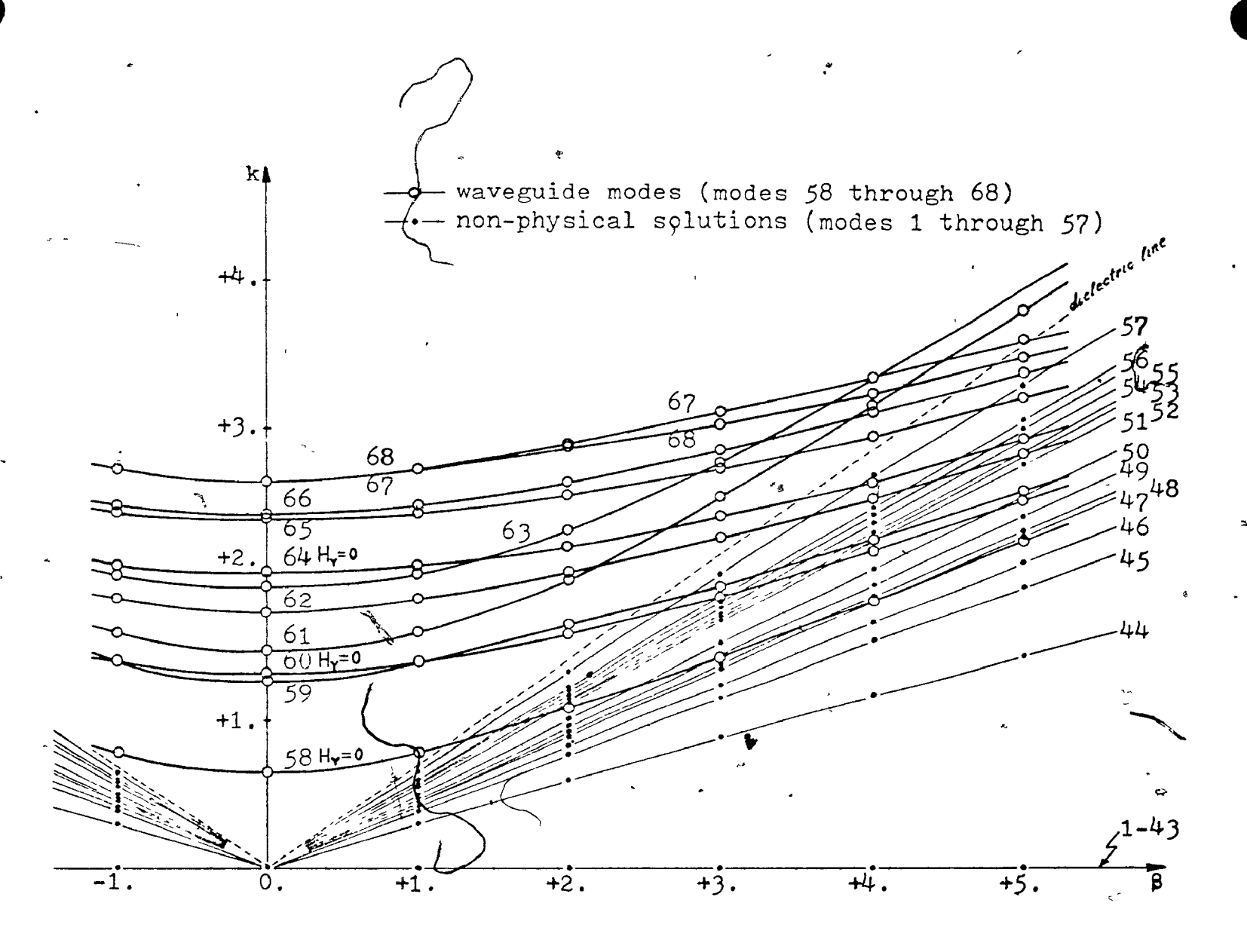


Figure 4.23

k-8 diagram prepared from the output of the three-component magnetic field wector program for the ferrite-filled rectangular waveguide problem.

The boundary condition on  $\overline{H}$  is given by equation (4.2); under the assumptions listed above, this reduces to

$$\frac{\partial H_z}{\partial x} + \frac{0.8}{3} \beta H_z = 0 \tag{4.15}$$

and must be satisfied at  $x = \pm 1$ . Assuming a solution of the following form

$$H_z = A \sin(\frac{1}{2}n\pi x) + B \cos(\frac{1}{2}n\pi x)$$
  $n = 1, 2, 3, ...$  (4.16)

in equation (4.14), the following dispersion relation is obtained

$$k^2 = \frac{3}{16.72} \left[ \beta^2 + (n\frac{\pi}{2})^2 \right]$$
  $n = 1, 2, 3, ...$  (4.17)

A comparison of the analytic solution with the finite element solution has been made. The percent errors in the wave-numbers computed by the finite element method are given in Table 4.3 for the dominant mode (n = 1) and two higher-order modes (n = 2 and 3).

The values of  $H_z$  at the interpolation nodes which have been circled in Figures 4.21 and 4.22 are listed in Table 4.4 for various values of the propagation constant. To obtain the analytical solution, substitute for  $H_z$  in equation (4.15) from equation (4.16) and set  $x = \pm 1$ ; one obtains

$$B = (1.6\beta/3\pi)A$$
 for  $n = 1$  (4.18)

$$B = -(3\pi/0.8\beta)A$$
 for  $n = 2$  (4.19)

$$B = (1.6\beta/9\pi)A$$
 for  $n = 3$  (4.20)

where A. is an arbitrary constant. Thus, for n=1 (dominant mode) the longitudinal magnetic field is given by

β	k <sub>1</sub>	% error*	k <sub>2</sub>	% error*	k <sub>3</sub>	% error*
-1	0.788758	1.74x10 <sup>-4</sup>	1.39655	1.64x10 <sup>-3</sup>	2.06006	0.956
σ	0.665367	2.56x10 -4	1.33076	1.70x10 <sup>-3</sup>	2.01606	0.999
+1	0.788758	1.74x10	1.39655	1.64×10 <sup>-3</sup>	2.06006	0.956
+2	1.07723	2.42x10	1.57754	1.35x10 <sup>-3</sup>	2.18662	0.838
+3	1.43441	3.89x10,	1.84005	1.32x10 <sup>-3</sup>	2.38326	0.717
+4	1.82031	0.06x10	2.15448	1.17x10 <sup>-3</sup>	2.62255	0.164
+5	2.21999	0.59x10 <sup>-4</sup>	2.50133	1.15x10 <sup>-3</sup>	2.92135	0.378

\*analytical solution:  $k_n^2 = \frac{3.0}{16.72} \left[8^2 + (n\frac{\pi}{2})^2\right]$ 

#### Table 4.3

The wave-numbers k1, k2 and k3 returned by the three-component magnetic field vector program (modes No. 58, No. 60 and No. 64 respectively in Figure 4.23) for the ferrite-filled rectangular waveguide problem. The percent errors are given.

$$H_z = A[\sin(\frac{1}{2}\pi x) + (1.6\beta/3\pi)\cos(\frac{1}{2}\pi x)]$$
 (4.21)

The arbitrary constant A may be chosen in such a way that the finite element solution matches the analytical solution at x=+1. The percent errors so obtained are also given in Table 4.4. The agreement of the two solutions is quite good.

The  $H_{\mathbf{X}}$  and  $H_{\mathbf{Z}}$  values at the interpolation nodes circled in Figure 4.21 have been plotted in Figures 4.24 and 4.25 from the program output. Apparently  $\overline{H}$  is not tangential at the metal boundary and shows a reciprocal behaviour for  $\beta = \pm 1$ . Fields of this type are expected from ferrite-filled waveguides with transverse magnetization [45].

The magnetic flux density vector components are given by

$$B_{x} = 3.0 H_{x} + 0.8 H_{z}$$
 (4.22)

$$B_{V} = H_{V} = 0$$
 (4.23)

$$B_z = -j(0.8 H_x + 3.0 H_z)$$
 (4.24)

Using the results from the finite element program,  $B_{x}$  and  $B_{z}$  have been calculated from  $H_{x}$  and  $H_{z}$  at the interpolation nodes and the results are plotted in Figures 4.26 and 4.27. Note that  $B_{x}$  is zero at  $x=\pm 1$ , i.e. the condition  $\overline{n}.\overline{B}=0$  is satisfied at the metal boundary.

The matrix size for the ferrite-filled rectangular wave-guide problem was 147 and required 9 minutes-43 seconds to obtain all of the points on the  $k-\beta$  diagram.

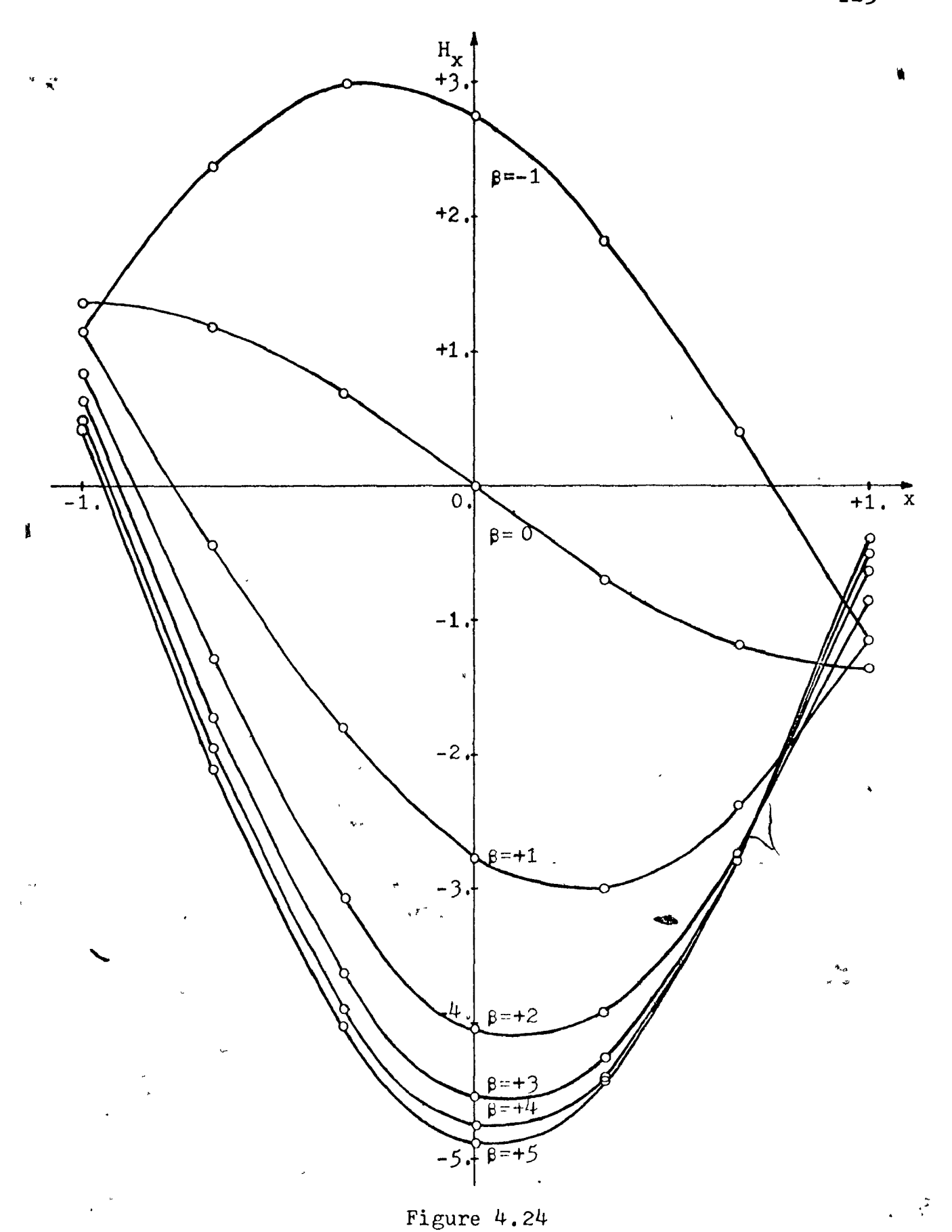
The example given here shows that the three-component magnetic field vector program is capable of solving homogeneous,

β	H <sub>z</sub> (x=-1) and % error*	$H_{z}(x=-\frac{2}{3})$ and $\%$ error*	$H_z(x=-\frac{1}{3})$ and % error*	H <sub>z</sub> (x= 0) and % error*	$H_z(x=+\frac{1}{3})$ and % error*	$H_z(x=+\frac{2}{3})$ and % error*	H <sub>z</sub> (x=+1) and % error*
-1	-4.3323	-4.1199	-2.8028	-0.73543	+1.5289	+3.3845	+4.3323
	0.000	-0.007	0.010	0.006	0.020	-0.010	- 0.000
0	-5.1357	-4.4480	-2.5674	+0.00006	+2.5676	+4.4481	+5.1358
	0.002	-0.006	0.019		0.012	-0.008	0.000
	-4.3323	-3.3845	-1.5289	+0.73546	+2.8028	+4.1199	+4.3323
+1	0.000	-0.010	0.020	0.002	0.010	-0.007	0.000
	-3.1721	-2.2089	-0.65313	+1.0771	+2.5187	+3.2859	+3.1721
+2	0.000	-0.013	0.029	-0.007	0.003	-0.008	0.000
	-2.3821	<b>-1.</b> 4568	-0.14028	+1.2133	+2.2418	+2.6700	+2.3821
+3	0,000	-0.030	0.081	-0.009	0.001	-0.017	0.000
	-1.8767	-0.98929	+0.16511	+1.2757	+2.0424	+2.2640	+1.8775
+4 .	0.043	-0.080	0.162	-0.060	0.023	-0.025	0.000
	-1.5391	-0.67965	+0.36195	+1.3064	+1.9012	+1.9862	+1.5389
+5	-0.013	-0.008	-0.040	-0.011	-0.026	-0.017	0.000

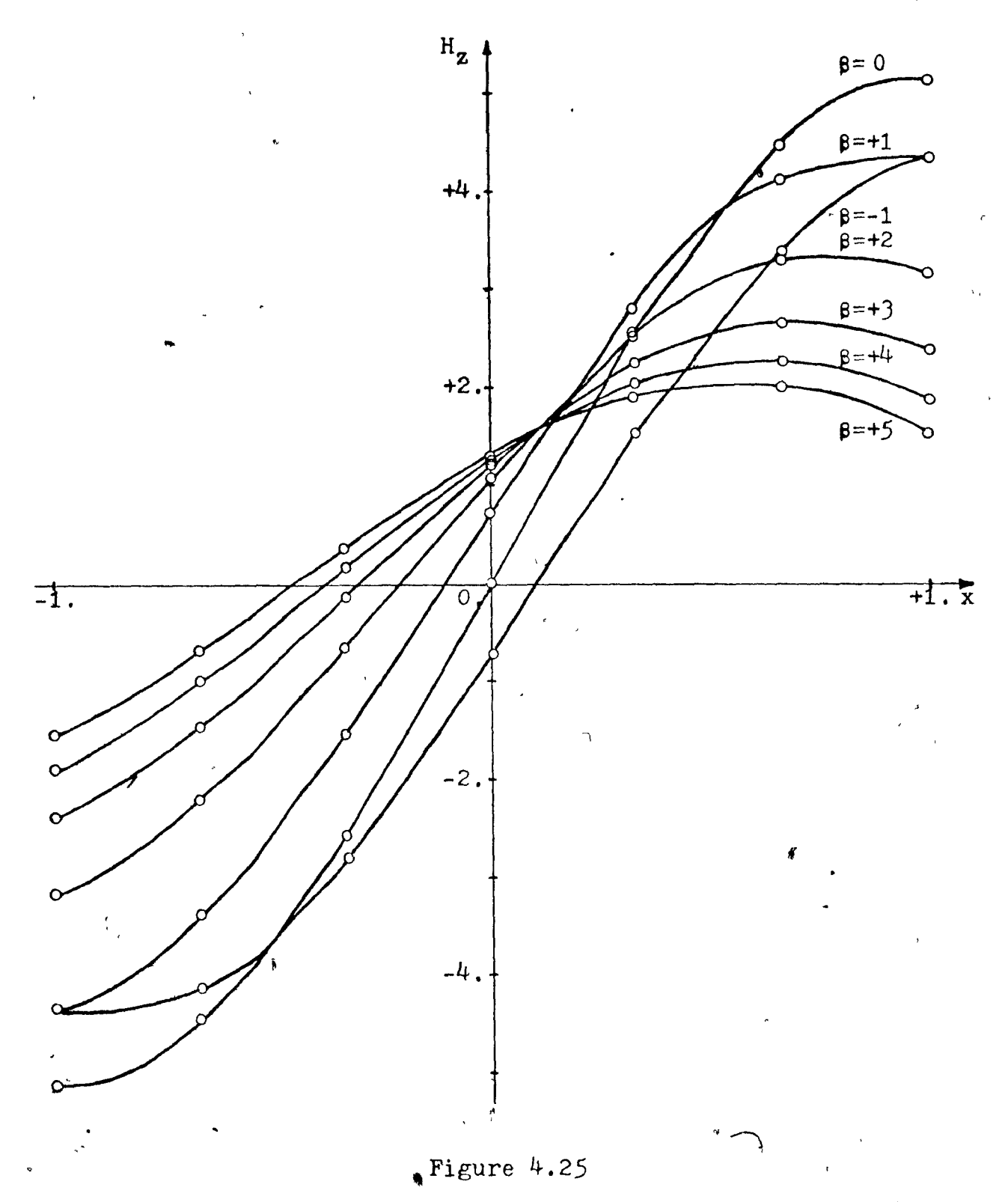
<sup>\*</sup>analytical solution:  $h_z = A[\sin(\frac{1}{2}\pi x) + (1.6\beta/3\pi)\cos(\frac{1}{2}\pi x)]$  where A has been chosen in such a way that the percent error in the computed values  $H_z(x=+1)$  is zero.

#### Table 4.4

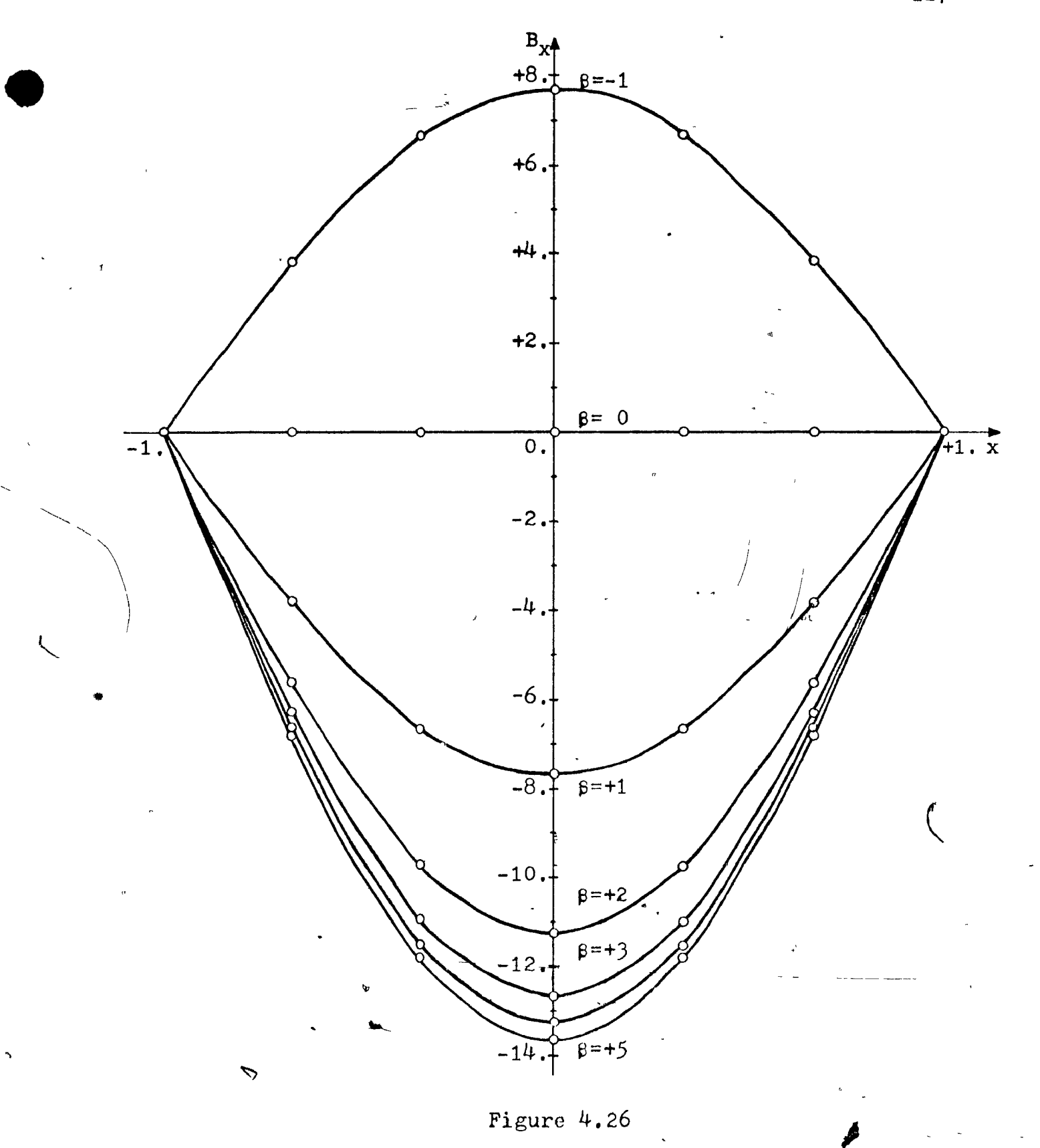
Values of  $H_Z$  returned by the program of Appendix IV at the interpolation nodes circled in Figures 4.21 and 4.22. The percent errors are also shown.



Values of  $\rm H_{x}$  at the interpolation nodes circled in Figure 4.21, for the ferrite-filled rectangular waveguide problem.



Values of  $\rm H_{2}$  at the interpolation nodes circled in Figure 4.21. for the ferrite-filled rectangular waveguide problem.



Values of B at the interpolation nodes circled in Figure 4.21, for the ferrite-filled rectangular waveguide problem. The values have been calculated from  $H_{\mathbf{x}}$  and  $H_{\mathbf{z}}$  obtained from the finite element program of Appendix IV.

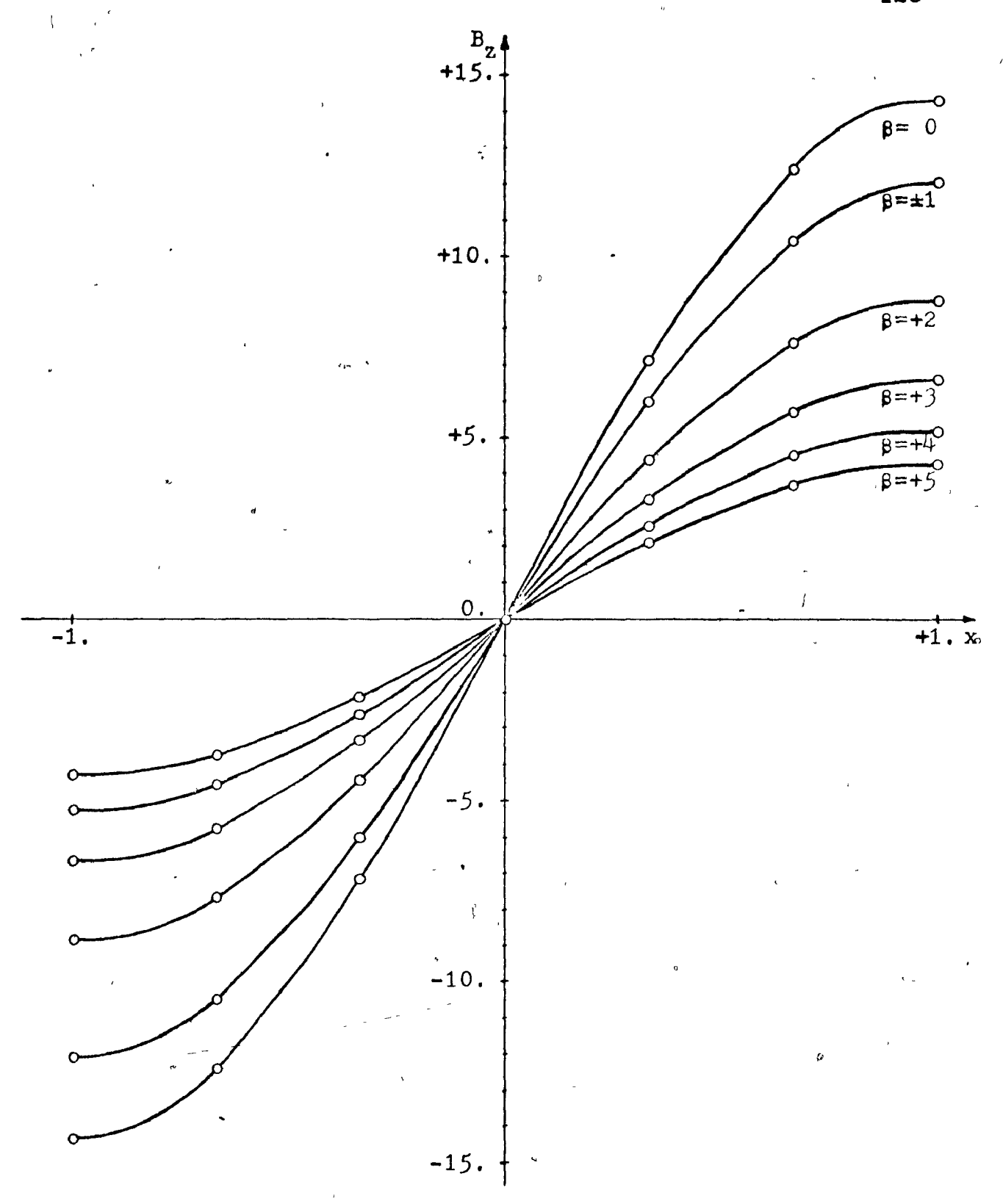


Figure 4.27

Values of B<sub>z</sub> at the interpolation nodes circled in Figure 4.21, for the ferrite-filled rectangular waveguide problem. The values have been calculated from H<sub>x</sub> and H<sub>z</sub> obtained from the finite element program of Appendix IV.

ath

magnetically anisotropic waveguide problems with very good accuracy. Although the present program is limited to frequency independent material property tensors, the program can be extended to deal with frequency dependent tensors as well by solving a matrix polynomial equation in k iteratively.

Inhomogeneous, magnetically anisotropic waveguide problems occur in a large number of practical applications, perhaps even more than the homogeneous ones. In order to treat such problems, it is best to solve for  $\overline{E}$  rather than for  $\overline{H}$  since  $\overline{H}$  is discontinuous if the permeability is discontinuous. In order to convert the present program into an  $\overline{E}$ -field solving program, the boundary condition  $\overline{n} \times \overline{E} = 0$  must be added to the program. This would result in eliminating certain rows and columns associated with boundary nodes from the global coefficient matrices assembled by the program.

# 4.7 Homogeneous and Inhomogeneous, Electrically Anisotropic Waveguide Problems

Consider again a rectangular waveguide with a 2:1 width to height ratio and filled with an anisotropic dielectric material which is characterized by a relative permeability of 1.0 and a relative permittivity tensor  $\hat{\epsilon}_r$  given by

$$\hat{\epsilon}_{r} = \begin{bmatrix} 2.5 & 0.0 + j0.75 \\ 0.0 & 1.0 + j0.0 \\ -j0.75 - j0.0 & 2.5 \end{bmatrix}$$
 (4.25)

Tensor permittivities of this type are characteristic of

transversely magnetized plasmas, although in general plasmas have a frequency dependent permittivity tensor [38,68].

The data cards for this problem are shown in Figure 4.28. The assembled point map is the same as for the ferrite-filled rectangular waveguide problem of the previous section and is given in Figure 4.21. The wave-numbers for the first six physically meaningful modes are given in Table 4.5 and the corresponding k- $\beta$  curves appear in Figure 4.29. These modes are the 58-th through 63-rd in sequence at  $\beta=0$ , the first 57 modes being non-physical modes. It is interesting to note that in this case the first 30 modes have imaginary values of k corresponding to negative eigenvalues  $k^2$ . This indicates that for electrically anisotropic problems the functional (3.18) may become negative.

The program output for the 59-th eigenvector at  $\beta=1$  corresponding to the second waveguide mode is reproduced in Figure 4.30. The transverse magnetic field vector at the interpolation nodes has been plotted from this output in Figure 4.31. In this figure, the effect of anisotropy of the medium on the magnetic field is clearly visible. Notice that the boundary condition  $\overline{n}.\overline{H}=0$  is satisfied approximately but accurately at the waveguide walls.

Due to the particular form of the permittivity tensor given in equation (4.25) the dominant waveguide mode as well as some higher-order modes are not affected by the anisotropy of the medium and these modes behave as if the medium was empty space. The following assumptions may be made:

a)  $H_{y} = 0$ ;

b) no variation occurs with respect to y;

```
.PLASMA-FILLED, RECTANGULAR WAVEGUIDE..X 1.00 1.00 -1.000
                                                                       7-CARD0001
                    1.0000
           5.0000
                             0.0000
                                       0.0000
                                                                   1 99 CARD0002
                                                1.0000
         -1.00000
                       0.50000
                                                                         CARD0003
          -1.60000
                      -0.50000
                                                                         CARD0004
                      -0.5000C
           1.00000
                                                                         CARD0005
           1.5000,0
                       0.50000
                                                                         CARDOUG6
                                                                         CARDOGO7
               2.5000
                        0.0000
                                  1.0000
                                           0.7500
                                                                         CARDOO08
                                                                         CARD0009
                                                                         CARD0010
```

Figure 4.28

Data cards for the plasma-filled rectangular waveguide problem.

Mode sequence No. at cut-off	Wave No. k for β = 0	Wave No. k for β =±1	Wave No.  k  for $\beta = 2$	Wave No.  k  for  β = 3	Wave No. k for \$ = 4	Wave No.  k  for $\beta = 5$
58.	1.57079	1.86209	2.54311	3.38635	4.29737	5.24094
59.	1.84347	1.98158	2.31568	2.74757	3.23586	3.76164
60.	2.41193	2.45579	2.68605	3.06212	3.52855	4.22407
61.	2.49244	2.70275	3.13139	3.54555	3.97489	4.43659
62.	3.07893	3.15321	3.42275	4.00935	4.78733	5.64304
63.	3.14165	3.29696	3.72424	4.34395	5.08625	5.90508

Table 4.5

Wave-numbers for the first six physically meaningful modes returned by the program of Appendix IV for the plasma-filled rectangular waveguide problem. The  $k-\beta$  curves are plotted in Figure 4.29.

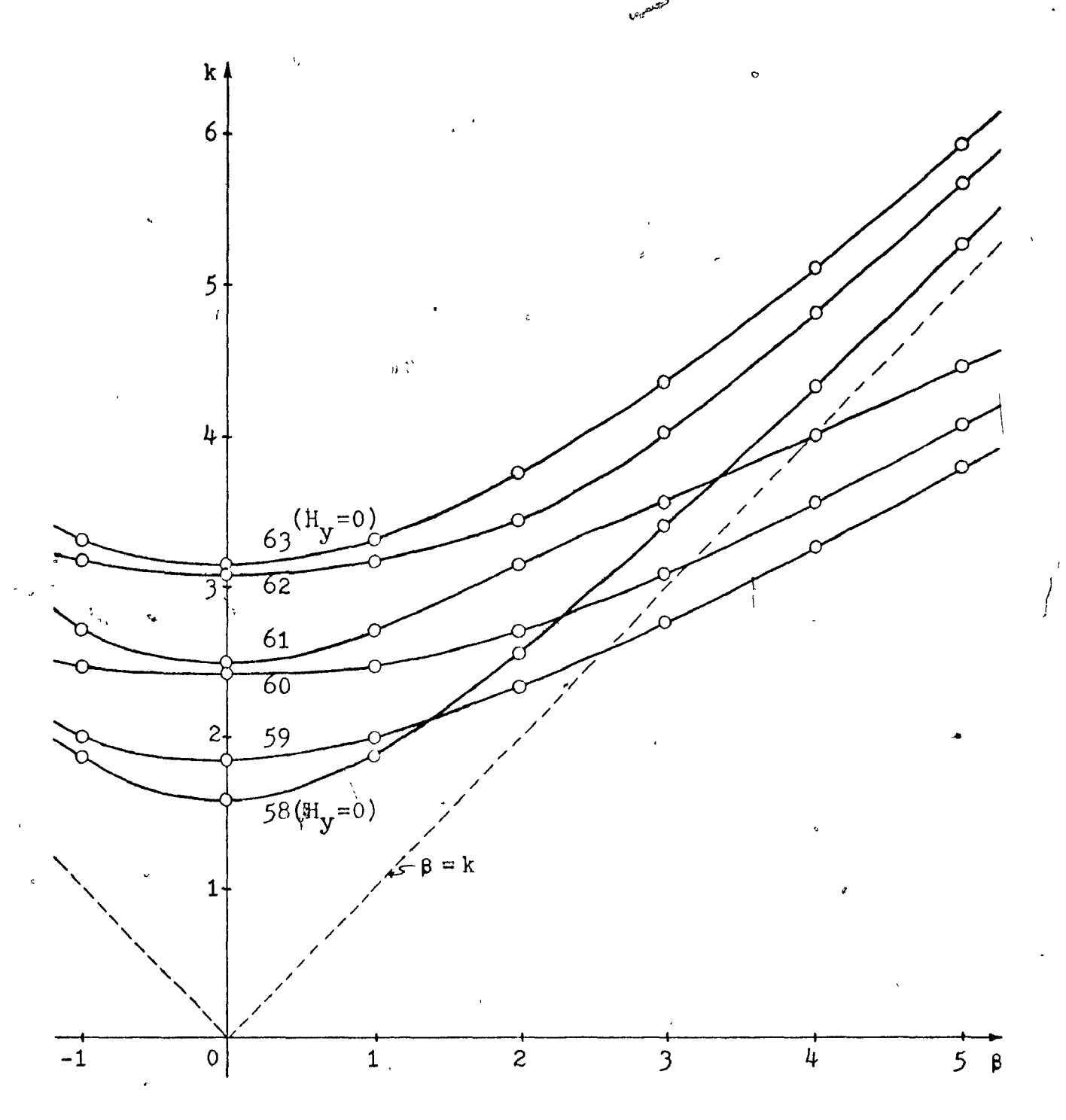


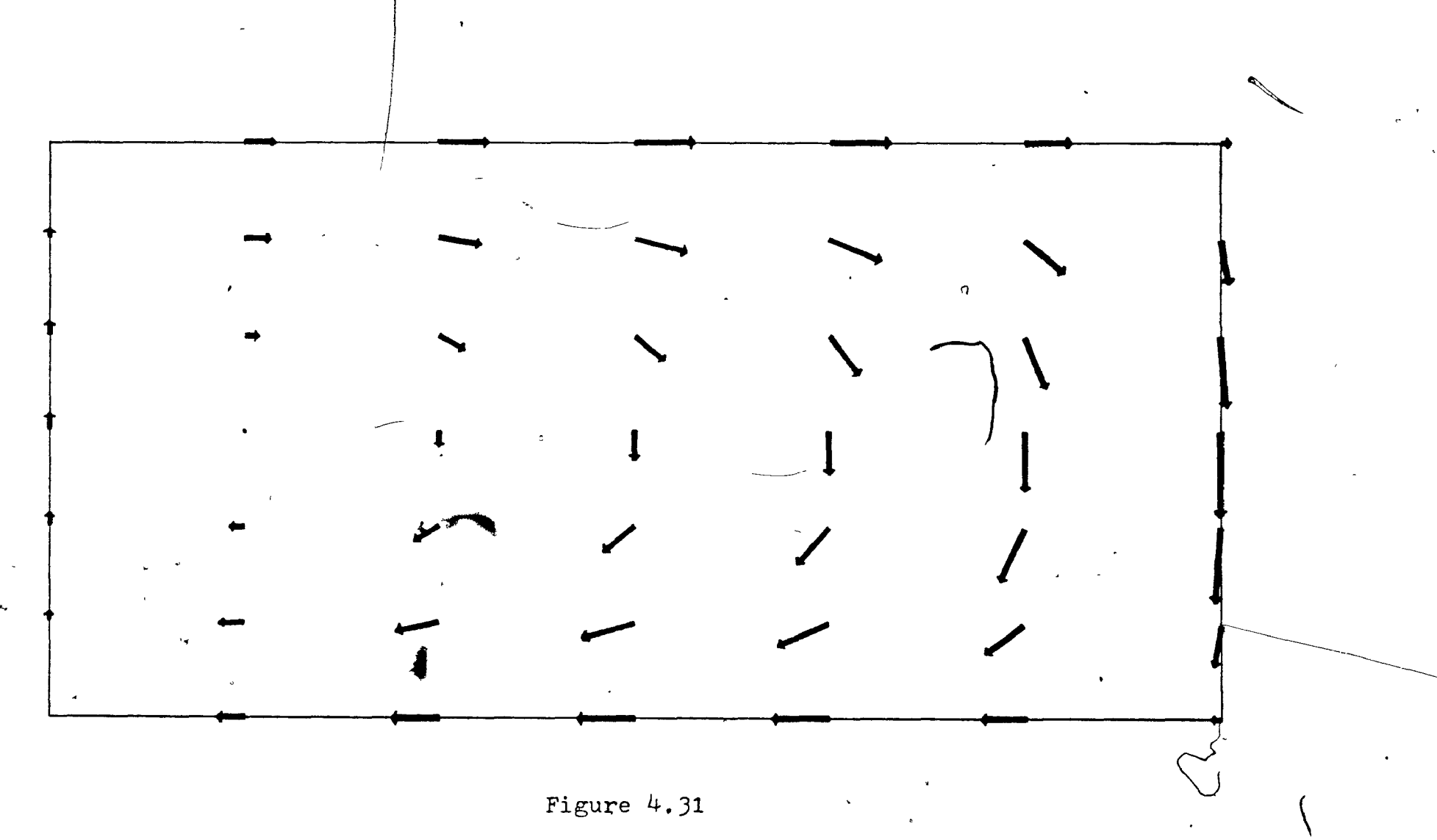
Figure 4.29

k-β diagram prepared from the output of the three-component magnetic field vector program for the plasma-filled rectangular waveguide problem. Only the first six physically meaningful k-β curves are shown.

#### ...PLASMA-FILLED, RECTANGULAR WAYEGUIDE: #### MUDE NUL 54 BETA: 1.000 MAGNETIC FIELD INTENSITY AT THE INTERPCLATION NODES ... 1. -7.134780+07 -0.925440-03 0.449313+01 2. 0.12001000 -0.113 20-01 -0.00001001 10. 0.122270000 0.63800000 -0.02420001 36. -0.02400001 -0.177510001 -0.63750001
3. -0.76360000 -0.264000-02 -0.0760001 20. -0.07670001 -0.635110-01 -0.26014000 37. -0.18760001 -0.02210001 -0.01750001 4. 0.754522-C +0.195240-U1 0.474344+71 21. 0.105140-02 -0.124 SUPOL 0.116430-02 10. 0.544440-02 -0.723640-01 -0.448190-03 \$. -0.118730+0<sup>6</sup>> (,,634.90+u) (.4243U0+01 24. 0.2437W0+01 -0.20324D+01 0.340480+01 39. -0.402₹50+01 -0.691400-0≥\<u>-0.9</u>#3410+01 10. -0.623230-0\$ 0.127490+01 1.276180-03 27. 0.102433-v2 -0.234640+01 0.284443-03 46. -0.240320+01 -0.696190-02 -0.28190+01 11. 0.12/130+0\$ -0.824423-01 3.2002403-01 28. 0.244780+41 -0.307884+81 0.382784+01 65. -0.348400+01 -0.625110+08 -0.813980-01 18. 0.148360+C1 -C.624110+00 L.513840+v1 29. 0.125160+01 -0.252740+01 0.724380+01 44. -0.241760+01 -0.201760+01 -0.201760+01 -0.201760+01 83. 9.487790+01 -0.439c0-03 0.64f270+01 30. -0.17500+01 -0.127400-02 -0.835980+01 -7. 0.742300-04 -0.354580+01 -0.491170-03 14. 0.70176D-04 2 11(600-01 -C.204 003-01 31. -0.001200-00 -0.351850-01 -0.76170-01 48. 0.187650-01 -0.438520-01 0.417950-01 18. 0.35747D-01 -C.946.90-01 C.11775D-C2 JZ. -0.489630-01 0.21272D-03 -0.76427D-01 49. 0.65466D-00 -0.341600-01 0.704110-01 \$6. \$.201C30+04 -C.1C8 #0+01 U-240040+01 J3- -0.3251+0+01 -8-25305U+81 -8-72408U+81 "kt. 0.622540+04 -n.117540+01 0.5dv26D+01 34. -0.37977D+00 -0.62678Dey1 -0.43×43D+01

Figure 4.30

Output from the three-component magnetic field vector program of Appendix IV showing the 59-th eigenvector at  $\beta=1$  for the plasma-filled rectangular waveguide problem. For the location of the 49 nodes see Rigure 4.21. The plot in Figure 4.31 has been prepared from this output.



The transverse magnetic field vectors at the interpolation nodes for the second waveguide mode of the plasma-filled rectangular waveguide ( $\beta=1$ ). The program output for this mode is reproduced in Figure 4.30; the node numbers are as shown in Figure 4.21.

- c) the fields vary as exp(-j\$z) in the z-direction;
- d)  $H_z$  has a phase factor  $\exp(-j\frac{\pi}{2})$  -relative to  $H_x$  and  $H_y$ . Under these conditions, curl  $\overline{H}$  has only a y-component

$$(\operatorname{curl} \overline{H})_{y} = \overline{1}_{y}(-j\beta H_{x} + j\frac{\partial H_{z}}{\partial x})$$
 (4.26)

Since the inverse of the permittivity tensor is given by

$$\hat{\epsilon}^{-1} = \underbrace{\begin{array}{c} 2.5 & 0.0 & -j0.75 \\ \hline 0.0 & 5.6875 & -j0.0 \\ \hline +j0.75 & +j0.0 & 2.5 \end{array}}_{(4.27)}$$

the curlcurl equation (4.11) reduces to the following two / differential equations

$$(\beta^2 H_x - \beta \frac{\partial H_z}{\partial x}) - k^2 H_x = 0$$
 (4.28)

$$\left(\frac{\partial^2 H_Z}{\partial x^2} - \beta \frac{\partial H_X}{\partial x}\right) + k^2 H_Z = 0 \tag{4.29}$$

Eliminating  $H_{\mathbf{x}}$  from these equations results in the familiar hollow waveguide equation

$$\frac{\partial x^2}{\partial x^2} + (k^2 - \beta^2) H_Z = 0 (4.30)$$

The boundary condition on  $\overline{H}$ , given by equation (4.2), is the simple homogeneous Neumann boundary condition

$$\frac{\partial H_z}{\partial x} = 0 \quad \text{at} \quad x = \pm 1.0$$

The solution of equations (4.30) and (4.31) is

$$H_z = A \sin(n \frac{\pi}{2} x)$$
  $n = 1, 2, 3, ...$  (4.32)

The dispersion relation is the familiar hyperbolic one

$$k^2 = (n \frac{\pi}{2})^2 + \beta^2$$
  $n = 1, 2, 3, ...$  (4.33)

It can be seen from Table 4.5 and Figure 4.29 that modes No. 58 and No. 63 correspond to the above analytical solutions for n=1 and n=2 respectively.

As for the ferrite-filled waveguide problem, the matrix size for this problem was 147 and the execution time was 15 minutes 47 seconds.

Consider now the same rectangular waveguide but/having only one half filled with the anisotropic material, the remaining half being completely empty. The data cards for this problem are given in Figure 4.32; the triangulation is the same as the one in Figure 4.9. The program output for the 53-rd eigenvector corresponds to the second waveguide mode 8=1 and is reproduced in Figure 4.33. The transverse magnetic field vector at the interpolation nodes is plotted from this output in Figure 4.34. This mode is analogous to the one shown in Figure 4.31 for the entirely filled waveguide. Notice that the inhomogeneity of the medium causes H, a discontinuity in the first derivative in the x-direction. The effects of the anisotropy of the medium are also evident in Figure 4.34. The components of the electric flux, density vector  $\overline{D}$  are given by the components of Maxwell's curl equation

$$D_{x} = \frac{\delta H_{z}}{\delta y} - \beta H_{y}$$
 (4.34)

$$D_{y} = \beta H_{x} - \frac{\partial H_{z}}{\partial x}$$
 (4.35)

$$D_{z} = \frac{\partial H_{y}}{\partial x} - \frac{\partial H_{x}}{\partial y} \tag{4.36}$$

In order to determine the electric field, two calculations

*	INHOM	OGE	NECU	S, ANTS	SCIRCPIC	WAVEGUI	DEX	1.00	1.CC	+1.000	0.000	1-CARECOOL
*	1.00	CO	0.	CCOC	1.0000	0.0000	0.00	CC 1	1.0000	C.C	CCO 4C	2C CARCCCC2
	1		-1.	ccccc	C.5CC	CC						CARCCCC3
	2 -		-1.	CCCCC	0.000	CC						CARECOC4
	3		-1.	CCOCO	-0.500	CC				,		CARECCC5
	4		· C-	CCCCC	C.5CC	CC						CARECCC6
	5 -	-	C.	ccccc	0.000	CC						CARECCC7
	6		C -	CCOCO	-C.5CC	CC						CARCCCC8
	7		1.	ccccc	C.500	CC						CARCCCCS
	8		1.	ccccc	C.CCC	CC						CARECCIO :
	9		1.	CCOCO	-0.500	CC						CARCCCII
												CARECG12
3	1	2	4	1.000	0.00	CC 1.	CCCC	C.CCC	0 C.	CCCG	1.CCCC	CARECO13
	5	2	4									CARCCC14
	5	2	3					,				CARECO15
	5	6	3	$\wedge$								CARECO16
	5	4	7	/2 J5C	c.co	CC 1.	CCCO	C.75C	c c.	CCCC	2.5000	CARECO17
€. 4	5	9	7	' '					-			CARCCO18
	5	8	6									CAREGO19
	9	3	6									CARECCEC
												CARCCO21

Figure 4.32 ·

Data cards for the inhomogeneous anisotropic rectangular waveguide problem.

& 3

Figure 4.33

Output from the three-component magnetic field vector program of Appendix IV shows the 53-rd eigenvector at  $\beta=1$  for the inhomogeneous anisotropic rectangular wave-guide problem. The locations of the 49 nodes are shown in Figure 4.9. The plot in Figure 4.34 has been prepared from this output.

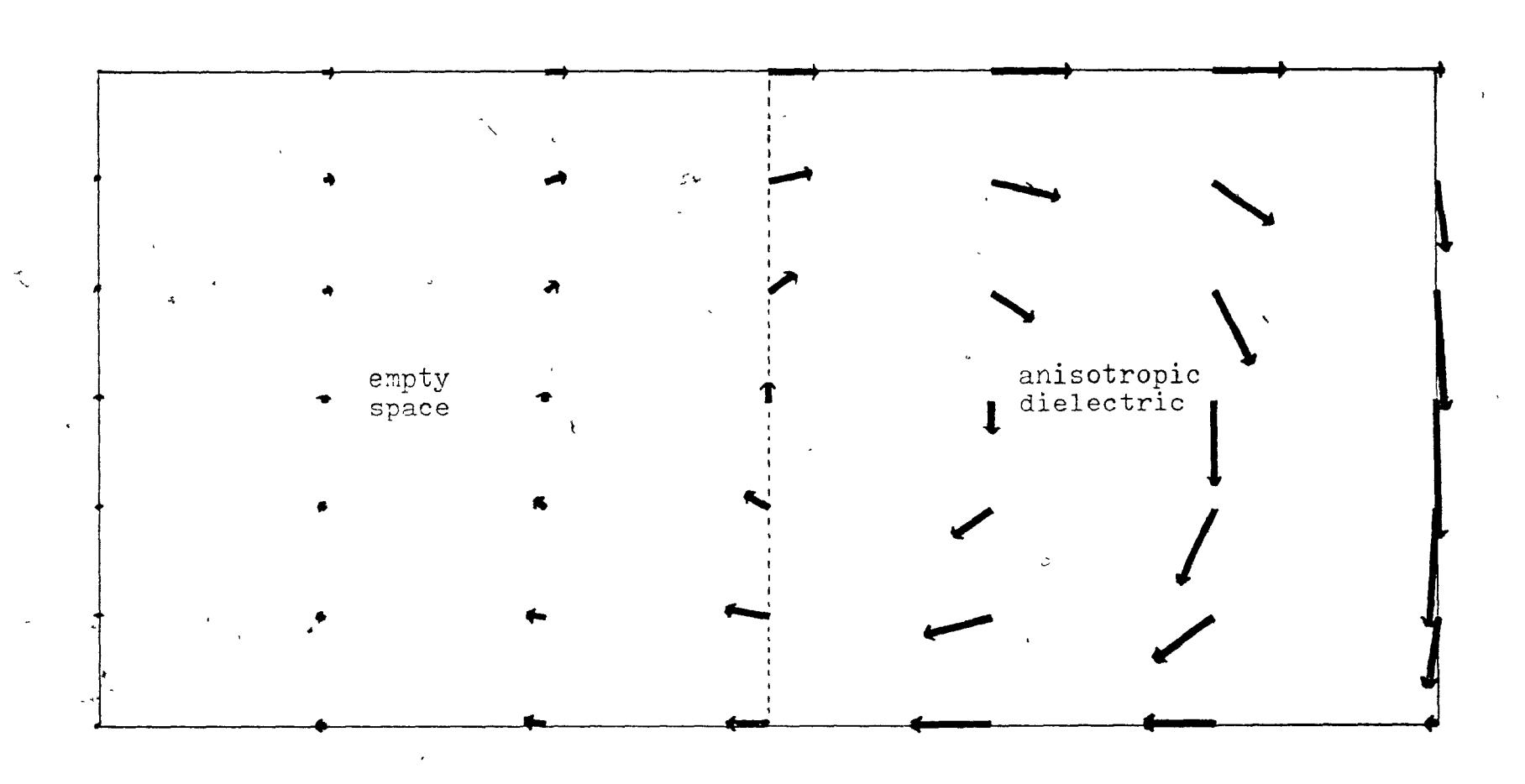


Figure 4.34

The transverse magnetic field vectors at the interpolation nodes for the second waveguide mode at  $\beta=1$  for the inhomogeneous anisotropic rectangular waveguide problem. The corresponding program output is presented in Figure 4.33; the node numbers are as those in Figure 4.9.

are necessary. In the empty space region  $\overline{D}$  is proportional to  $\overline{E}$ ; in the anisotropic dielectric region the components of  $\overline{E}$  are given by

$$E_{x} = (2.5D_{x} + 0.75D_{z})/5.6875\epsilon_{o}$$
 (4.37)

$$E_{y} = D_{y}/\epsilon_{o} \tag{4.38}$$

$$E_{z} = (0.75D_{x} + 2.5D_{z})/5.6875\epsilon_{o}$$
 (4.39)

Table 4.6 contains the components of  $\overline{D}$  at the interpolation nodes at the dielectric interface. The values have been computed according to equations (4.34) through (4.36). The derivatives of the components of  $\overline{H}$  have been computed by exact\_differentiation of the interpolation polynomials. Bearing in mind that differentiation is an unstable numerical process, the results indicate that the continuity condition for the normal component of  $\overline{D}$  at the interface is satisfied. Table 4.7 contains similar results for  $\overline{E}$ . The continuity condition on the tangential component of  $\overline{E}$  at the interface is also very approximately satisfied. Reference [69] contains an excellent example of a practical application of inhomogeneous, anisotropic waveguide problems.

Node number	Ď	$^{\mathrm{D}}\mathbf{x}$	$^{\mathrm{D}}\!\mathrm{y}$	$D_{y}$	Ďz	$D_{\mathbf{z}}$
at the inter-	left of inter-	right of inter-	left of inter-	right of inter-	left of inter- face	right of inter-
						,
. 4	-0.2214	-0.2214	+7.9665	+7.6845	+0.5018	-0.8695
· 21	-6.7360	-6.7360	+5.5114	+6.6692	+3.9843	+11.230
· 18	-11.066	-11.066	+2.9857	+4.0549	+6.3331	+19.447
5 5	-13.439 -13.625	-13.439 -13.625	-0.0147 -1.2328	-0.5633 +0.1390	+7.5481 +8.0882	+23.781 +21.076
27	-11.204	-11.204	-4.2428	-3.8580	+6.2077	+18.262
28	-6.6048	-6.6048	-6.0229	<b>-7.</b> 2389	+3.6322	+10.048
.6	+0.4487	+0.4487	-7.0958	-10.528	+0.3614	-8,6531

Table 4.6

The components of  $\overline{D}$  at the interpolation nodes at the dielectric interface for the inhomogeneous anisotropic rectangular waveguide problem. The first four nodes belong to one triangle, the other four nodes to an adjacent triangle (see Figure 4.9).

Node number at the inter- face	€E °x left of inter- face	Fight of inter-face	€Ey left of inter- face	€.Ey right of inter- face	&E <sub>z</sub> left of inter-face.	€E <sub>z</sub> right of inter- face
4	-0.2214	-0.2120	+7.9665	+7.6845	+0.5018	-0.4114
21	-6.7360	-1.4800	+5.5114	+6.6692	+3.9843	+4.0481
18	-11.066	-2.3000	+2.9857	+4.0549	+6.3331	+7.0889
5 5	-13.439 -13.625	-2.7713 -3.2100	-0.0147 -1.2328	-0.5633 + <b>0.</b> 1390	+7.5481 +8.0882	+8.6810 +7.4675
27	-11.204	-2.5168	-4.2428	-3.8580	+6.2077	+6.5497
28	-6.6048	-1.5782	-6.0229	-7.2389	+3.6322	+3.5456
- 6	+0.4487	-0.9438	-7.0958	-10.528	+0.3614	-3.7444

Table 4.7

The components of  $\overline{E}$  at the interpolation nodes at the dielectric interface for the inhomogeneous anisotropic rectangular waveguide problem. The first four nodes belong to one triangle, the other four nodes to an adjacent triangle (see Figure 4.9).

#### CHAPTER V

# LACC: A LINEAR ACCELERATOR CAVITY CODE BASED ON THE FINITE ELEMENT METHOD

#### Summary

Linear Accelerator Cavity Code (LACC) is a Fortran IV computer program written especially for the numerical calculation of electromagnetic fields in linear accelerator (linac) cavities by the high-order, polynomial, triangular finite element method. The program input consists chiefly of the cavity geometry and the finite element triangulation of the solution region. The output contains the normalized longitudinal and transverse components of the electric field intensity, the normalized peripheral magnetic field intensity and also global quantities, such as the Q factor, stored energy, power loss, and shunt impedance.

## 5.1 Introduction

The LACC computer program is a specialized version of the general, axisymmetric, one-component vector, finite element computer program AXISYMM-VECTOR-HELMHOLTZ-FINTEL6 [36]. The latter was developed in order to solve boundary value problems described in one form or another by the generalized Bessel equation of order m

$$\frac{1}{r} \cdot \frac{\partial}{\partial r} \left( r \cdot \frac{\partial A}{\partial r} \right) + \left( k^2 - \frac{m^2}{r^2} \right) A + \frac{\partial^2 A}{\partial z^2} = g$$
 (5.1)

subject to the boundary conditions normally derived for scalar potentials, vector potentials or field intensities at conducting surfaces [52]. The AXISYMM-VECTOR-HELMHOLTZ-FINTEL6 program returns only the wave-number k and unnormalized values of the wave function or potential.

The present program, LACC, bridges the gap between a purely mathematical solution and the computation of parameters relevant to linac cavity design. The program is in no way restricted to only linac cavities. It will perform equally well for many other types of cavities which operate at microwave frequencies.

#### 5.2 The Linac Cavity Electromagnetic Field Problem

The classical electromagnetic field problem of the empty resonator with conducting walls is governed by Maxwell's equations [38]. For time-harmonic fields the equations are

$$\operatorname{curl} \overline{E} = -j\omega\mu_{\alpha}\overline{H} \tag{5.2}$$

$$\operatorname{curl} \overline{H} = +j\omega \epsilon_{\bullet} \overline{E}$$
 (5.3)

Due to the identity divcurl (any vector) = 0, the above equations automatically guarantee the divergenceless nature of the electric and magnetic field intensity vectors  $\overline{E}$  and  $\overline{H}$ . In order to obtain an equation in terms of  $\overline{H}$ , alone, one can take the curl of both sides of (5.3) and then substitute for curl  $\overline{E}$  from equation (5.2). This yields

curl curl 
$$\overline{H} - \omega^2 \mu_{\bullet} \in \overline{H} = 0$$
 (5.4)

The quantity  $\omega \sqrt{\mu_{\rm e} \epsilon_{\rm e}}$  will be denoted by the letter k and

referred to as the wave-number. Since the divergence of  $\overline{H}$  is identically zero, equation (5.4) can also be written in terms of the Laplacian operator

$$\nabla^2 \overline{H} + k^2 \overline{H} = 0$$
 (5.5)

Equation (5.5) is the familiar Helmholtz equation.

Once  $\overline{H}$  is known,  $\overline{E}$  can be obtained from (5.3) in terms of  $\overline{H}$ . Assuming cylindrical symmetry and taking  $\overline{H}$  to be purely peripheral, one obtains

$$E_{r} = \frac{+j}{\omega \epsilon_{0}} \left( \frac{\delta H_{\theta}}{\delta z} \right) \tag{5.6}$$

$$E_{z} = \frac{-j}{\omega \epsilon_{o}} \left( \frac{\partial H_{\theta}}{\partial r} + \frac{H_{\theta}}{r} \right)$$
 (5.7)

where the imaginary unit j merely denotes a  $\frac{\pi}{2}$  time phase difference between the components of  $\overline{E}$  and  $H_{\theta}$ . The singularity at r=0 in equation (5.7) immediately raises a question: Is  $E_z$  singular along the axis of symmetry? Since  $\overline{H}$  is solenoidal, application of L'Hospital's rule to the limit of  $H_{\theta}/r$  as r approaches zero, leads to the following expression for  $E_{\theta}$  along the z-axis

$$E_{\mathbf{z}}\Big|_{\mathbf{r}=\mathbf{0}} = \frac{-2\mathbf{j}}{\omega \epsilon_{\mathbf{0}}} (\frac{\partial H_{\mathbf{0}}}{\partial \mathbf{r}})$$
 (5.8)

Figure 5.1 shows the outlines of a typical axisymmetric linac cavity. Along the metal walls of the cavity the electric field intensity vector  $\overline{E}$  must be normal everywhere to the surface, i.e.

$$\overline{n} \times \overline{E} = 0$$
 (5.9)

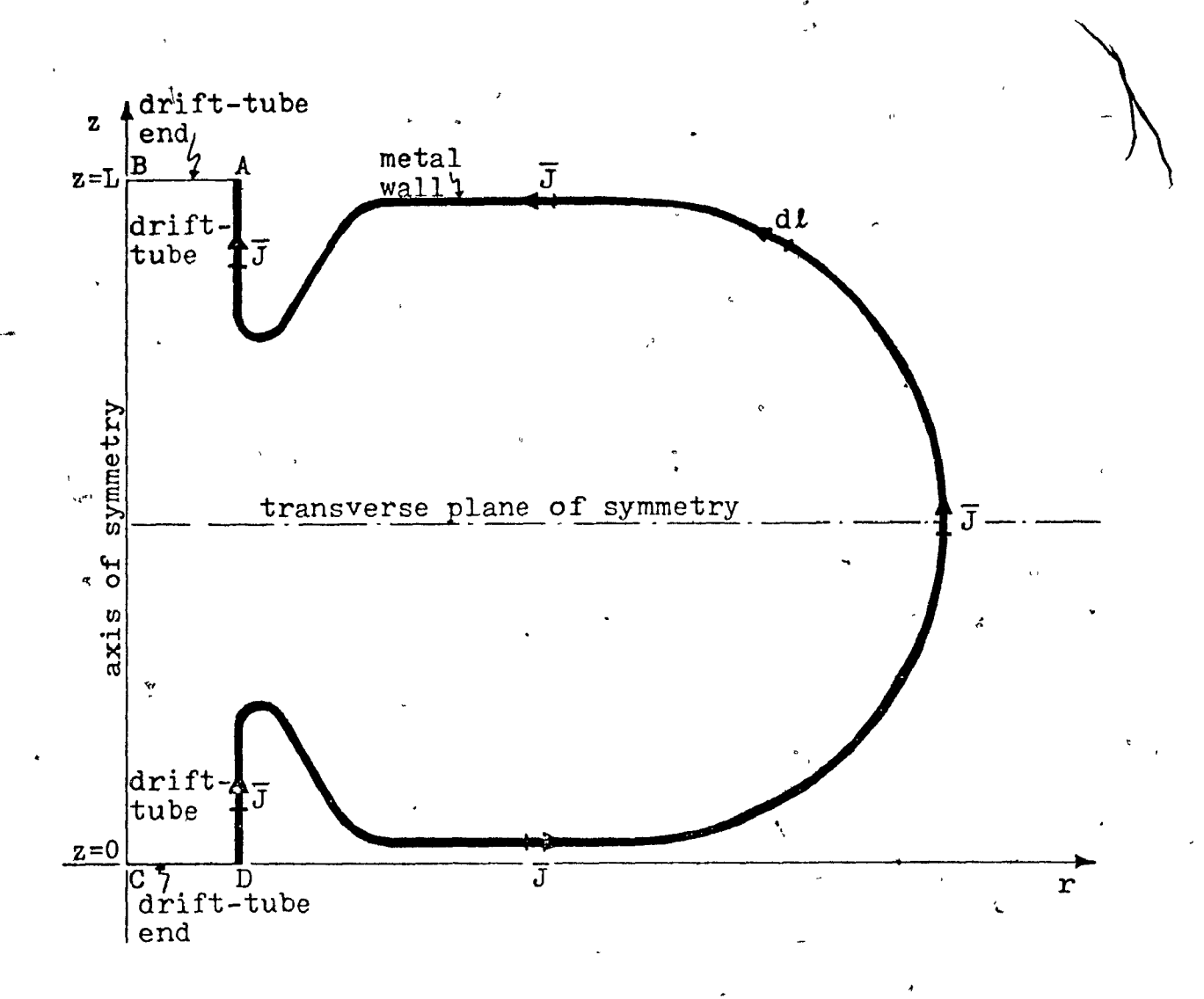


Figure 5.1

A typical linear accelerator cavity

where  $\overline{n}$  denotes the outward normal unit vector to the perfectly conducting metal surface.

Substituting  $\overline{E}$  from equation (5.3) into equation (5.9), one obtains the boundary condition for  $\overline{H}$  at the conducting surface

$$\overline{n} \times \text{curl } \overline{H} = 0$$
 (5.10)

This can be shown to be equivalent to the following impedance-type boundary condition for  $H_{\theta}$ 

$$\frac{\partial H_{\theta}}{\partial n} = -\frac{H_{\theta}}{r} \frac{dr}{dn}$$
 (5.11)

The net displacement current  $(I_d)$  flowing through a transverse cross-sectional portion of the cavity is obtained by applying Ampère's law. According to this law, the integral of the magnetic field intensity  $H_\theta$  over any closed circular path, r=R around the axis of the cavity is

$$I_{d}\Big|_{r=R} = \int_{0}^{2\pi} (H_{\theta}r) d\theta \Big|_{r=R} = 2\pi r H_{\theta}\Big|_{r=R}$$
 (5.12)

Notice that the integrand is  $rH_{\theta}$  rather than just  $H_{\theta}$  alone. Let  ${\mathfrak S}$  denote  $rH_{\theta}$ .  ${\mathfrak S}$  will be called the displacement current distribution. The boundary condition equivalent to (5.11) in terms of  ${\mathfrak S}$  can be written as

$$\frac{\partial s}{\partial n} = \mu_{\bullet} H_{\theta} \frac{dr}{dn} + \mu_{\bullet} r \frac{\partial H_{\theta}}{\partial n} = \mu_{\bullet} (H_{\theta} \frac{dr}{dn} - H_{\theta} \frac{dr}{dn}) = 0 \qquad (5.13)$$

Therefore the displacement current distribution function of satisfies the homogeneous Neumann boundary condition at the cavity walls. This makes of attractive to work with in finite difference formulations of the linac cavity field problem [70, 71].

Another important observation is that along a line z = constant, the right-hand side of equation (5.11) vanishes because dr/dn (i.e. the cosine of  $\frac{\pi}{2}$ ) vanishes. Therefore, for a cavity which displays symmetry about such a line, it is possible to solve for the fields in only one half of the region by treating the plane of symmetry as if it were a metal wall.

The boundary condition for Ha on the axis of symmetry (z-axis) is always homogeneous Dirichlet, i.e.  $H_e = 0$  at r = 0. This is due to the fact that the magnetic field vector is solenoidal. The last boundary condition one needs to consider is identified as the drift-tube end in Figure 5.1. Before stating the boundary condition however, the operation of linac cavities [72,91] must be described. Linac cavities are used in a chain, connected to each other at the ends of the drift-tubes, forming a long structure. Such structures have the property that they are able to propagate waves with phase velocities which are lower than the speed of light. This property is ideally suited for the acceleration of elementary particles since protons and electrons must travel at speeds less than that of light and can only 'ride' on a wave which has a low phase velocity. The resonant frequency of the cavities shifts along the chain and consequently the particles accelerate as they travel along the structure.

The mode in which the electromagnetic wave propagates along the structure can be any one of several different kinds. When the electric fields in adjacent cavities are oppositely directed, and the particles pass through the cavity in one

half of a cycle, the operation of the accelerator is said to be in the  $\pi$ -mode. It is clear that the axial field  $E_z$  in  $\pi$ -mode operation must have a null-plane between cavities if it is to change sign from cavity to cavity. This implies from equation (5.8) that  $H_\theta$  must be a constant at the plane at the end of the drift-tube. The value of  $H_\theta$  has already been fixed at one point on this plane, namely at r=0, therefore  $H_\theta$  must be zero at the end of the drift-tube in  $\pi$ -mode. operation. It should be pointed out that the purpose of the drift tubes is to concentrate the electric field near the center of the cavity and away from the drift-tube ends. The particles are in the drift-tubes when the axial electric field of the cavity changes sign and becomes decelerative.

When it takes a particle an entire cycle to pass through a cavity and the electric fields in adjacent cavities maintain the same direction, one says that the accelerator is operating in the  $2\pi$ -mode. In this instance, the particles 'hide' in the drift-tubes and are shielded from the influence of the electric fields when they are decelerative. It is easy to see that in  $2\pi$ -mode operation,  $E_z$  has no null-planes at the drift-tube ends. However,  $E_r$  must be zero there if the electric flux lines are to continue from cavity to cavity. This implies that the boundary conditions (5.9) and (5.10) or (5.11) must be satisfied. Therefore, in  $2\pi$ -mode operation, one can regard the drift-tube ends as being scaled-off by infinitely thin metal plates.

There is an infinite number of both  $\pi-$  and  $2\pi-$ modes in accelerator cavities which differ in the radial variations of

the fields. Accelerators generally operate in the fundamental  $\pi$ - or  $2\pi$ -mode which are well separated in frequency from the next lowest order modes. Sometimes however, higher order modes may become excited in the cavities and interact with the particles to produce undesirable effects.

#### 5.3 Finite Element Method

# for the Computation of the Magnetic Field Intensity

With the assumption that  $\overline{H}$  has only an  $H_{\theta}$  component which does not vary with  $\theta$ , it can be shown that equation (5.5) takes the following form in cylindrical coordinates

$$\frac{1}{r}\frac{\partial}{\partial r}\left(r\frac{\partial H_{\theta}}{\partial r}\right) + \left(k^2 - \frac{1}{r^2}\right)H_{\theta} + \frac{\partial^2 H_{\theta}}{\partial z^2} = 0 \tag{5.14}$$

It can also be shown that the Euler equation associated with the energy-related functional

$$F(\mathcal{H}_{\theta}) = 2\pi \int \left\{ r \left[ \left( \frac{\partial \mathcal{H}_{\theta}}{\partial z} \right)^{2} + \left( \frac{\partial \mathcal{H}_{\theta}}{\partial r} \right)^{2} - k^{2} \mathcal{H}_{\theta}^{2} \right] + \frac{\mathcal{H}_{\theta}^{2}}{r} + 2\mathcal{H}_{\theta} \frac{\partial \mathcal{H}_{\theta}}{\partial r} \right\} dr dz$$
(5.15)

is equation (5.14). The natural boundary conditions associated with (5.15) are of the homogeneous Dirichlet type or of the impedance type as given in equation (5.11) [73].

It is known that the function which extremizes F is a solution of the Euler equation and satisfies the natural boundary conditions of the functional [34,40]. Instead of the true solution, an approximate solution to equation (5.14) is sought. The approximate solution has the form

$$H_{\theta} = \sum_{i=1}^{n} H_{\theta}^{i} (\sqrt{r}/\sqrt{r_{i}}) \alpha_{i}$$
 (5.16)

over triangular elements in the region of solution. The  $\alpha_i$  form a complete set of local interpolation polynomials over a triangle. Each  $\alpha_i$  evaluates to 1 at the interpolation node and to 0 at all other nodes. The  $H_{\theta}^i$  are coefficients to be determined for each of the n interpolation nodes and represent the local values of  $H_{\theta}$ . In a triangle fitted with N-th degree polynomials there are n=(N+1)(N+2)/2 interpolation nodes which are located so that any three adjacent nodes are vertices of a triangle similar to the original one. Figure 5.2 shows the locations of the 28 interpolation nodes in a 6-th order triangle. The  $r_i$  in equation (5.16) represents the radial coordinates of the interpolation nodes.

Denoting  $H_{\theta}^i/\sqrt{r_i}$  by  $V_i$  the functional F can be discretized to yield the matrix quadratic form

$$F(V_i) = \pi \left\{ [V]^t [S][V] - k^2 [V]^t [T][V] \right\}$$
 (5.17)

where [V] is the column matrix of the quefficients  $V_i$  and the superscript t denotes transpose. The matrices [S] and [T] are symmetric and given by

$$[S] = 2[C] + 9|A|[R](+ 3[W])$$
 (5.18)

$$[T] = 4|A|[P] \qquad (5.19)$$

where A denotes the triangle area. The symmetric matrices [C], [W] and [P] can be assembled from universal, constant, symmetric, element describing matrices  $[Q_{ijl}]$ ,  $[U_{ij}]$  and  $[Y_{ij}]$  respectively, as given in the formulae below:

$$[c] = \sum_{i=1}^{3} r_{i} \sum_{j=1}^{3} r_{j} \sum_{l=1}^{3} \cot(\beta_{l}) [Q_{i,j1}]$$
 (5.20)

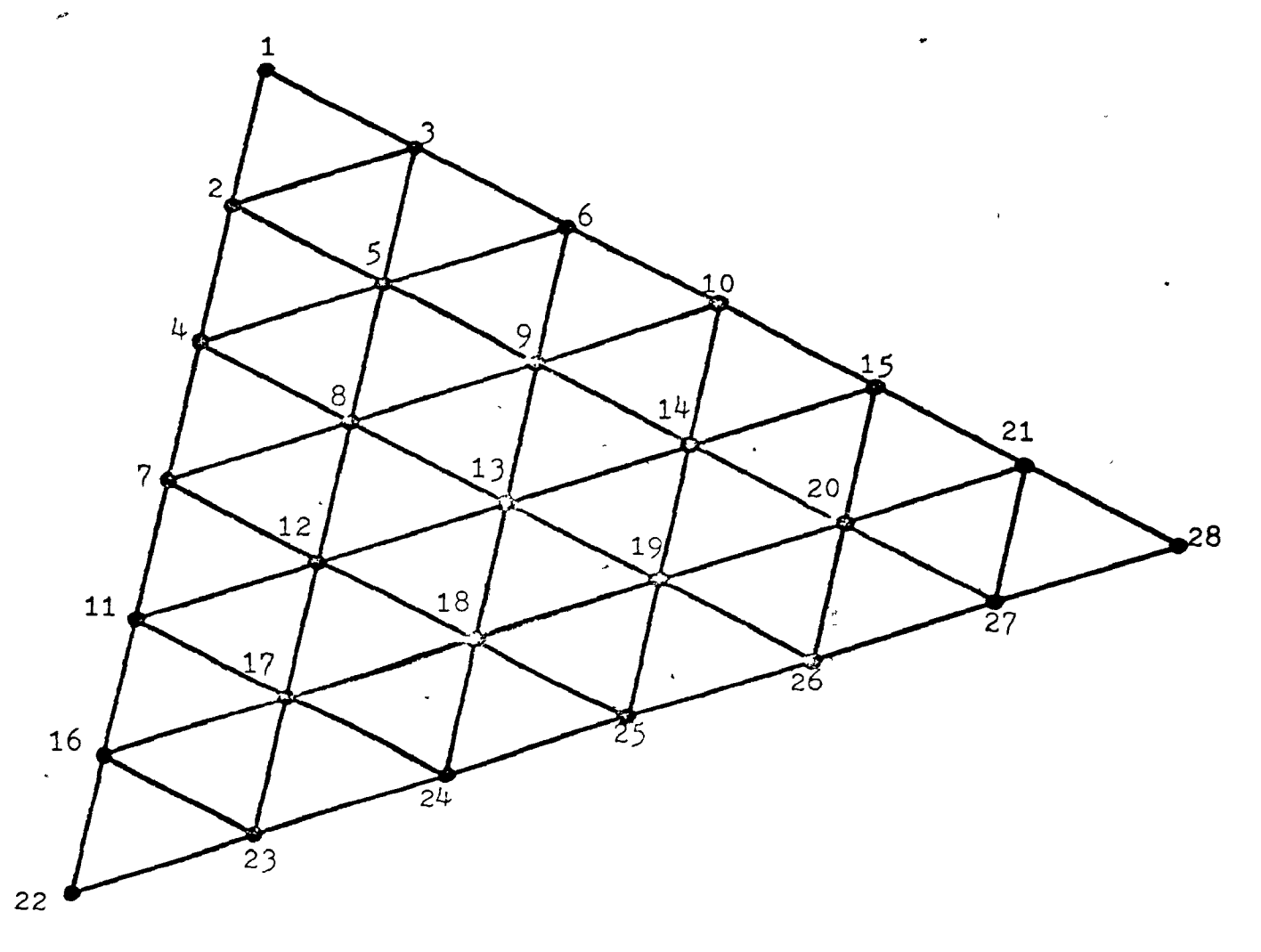


Figure 5.2

The locations of the 28 interpolation nodes in a 6-th order triangle

$$[W] = \frac{A}{|A|} \sum_{i=1}^{3} r_{i} \sum_{j=1}^{3} (z_{j+1} - z_{j-1}) [U_{ij}]$$
 (5.21)

$$\begin{bmatrix} P \end{bmatrix} = \sum_{i=1}^{3} r_i \sum_{j=1}^{3} r_j \begin{bmatrix} Y_{ij} \end{bmatrix}$$
 (5.22)

The  $\beta_1$  represents the interior angles at the triangle vertices while  $r_1$ ,  $r_2$ ,  $r_3$ ,  $z_1$ ,  $z_2$  and  $z_3$  are the radial and axial coordinates of each of the vertices respectively. The subscript j in equation (5.21) is cyclic modulo 3. The total number of Q-matrices is 27; there are nine U-matrices and nine Y-matrices; there is only one R-matrix. Of these 46 matrices only [R],  $[Q_{111}]$ ,  $[Q_{221}]$ ,  $[Q_{121}]$ ,  $[Q_{231}]$ ,  $[U_{11}]$ ,  $[U_{21}]$ ,  $[Y_{11}]$  and  $[Y_{21}]$  are independent, the remaining matrices can be obtained from these nine by row and column permutations which have been described in detail elsewhere [24, 52, 55, 56].

The discretized functional (5.17) yields the following matrix equation when differentiated with respect to the coefficients  $V_{i}$ 

$$([S] - k^{2}[T])[V] = 0$$
 (5.23)

Equation (5.23) is the discrete form of (5.14). The individual equations for a many triangle region may be combined to form one large global matrix equation for the overall region. The impedance boundary condition (5.11) is automatically satisfied at all unconstrained boundary nodes because this is the natural boundary condition of the functional. The coefficients  $V_i$  are zero at all boundary nodes constrained by the homogeneous Dirichlet boundary condition. Thus the rows and columns associated with these coefficients must be removed from equation (5.23).

The LACC computer program assembles the matrices [S] and [T] of equation (5.23) from the nine given universal element matrices stored in the program. It separates the unconstrained coefficients from the constrained ones and solves the matrix eigenvalue problem for the unconstrained coefficients  $V_i$  (the eigenvector) and the wave-number k (the square-root of the eigenvalue). The coefficients  $V_i$  computed by LACC are transformed into  $H^i_\theta$  according to the equation

$$H_{\theta}^{i} = \sqrt{r_{i}} V_{i} \tag{5.24}$$

The coefficients  $H_{\theta}^{i}$  provide values of the magnetic field intensities in various modes at the nodal points. The computer program then uses these coefficients to compute global linac cavity parameters.

## 5.4 Special Quantities Related to Linac Cavity Design

The criterion for an optimal accelerator cavity design is high operational efficiency. The operational efficiency of a cavity depends upon two factors: (1) the gain in kinetic energy of a particle passing through the cavity and (2) the power lost in the cavity walls. The designer must therefore obtain from the calculated magnetic field intensity performance measuring quantities which allow him to choose between competitive designs. Such quantities are the transit time factor T, the shunt impedance Z and the Q factor.

Faraday's law of electromagnetic induction can be used to obtain the electromotive force V induced across a cavity by

a changing magnetic field in the cavity. The total flux  $\emptyset$  through the longitudinal cross-section of the cavity is found by integrating the flux density  $B_{\theta} = \mu_{\bullet} H_{\theta}$  over the surface of the cross-section

$$\emptyset = \mu_{\bullet} \iint \dot{H}_{\theta} \, dr \, dz \tag{5.25}$$

Then, according to Faraday's law

$$V = -d\emptyset/dt = -j\omega\mu_{\theta} \int \int H_{\theta} dr dz \qquad (5.26)$$

The imaginary unit j indicates that there is a time phase difference of  $\frac{\pi}{2}$  between  $H_{\theta}$  and V. For a cavity operating in the  $\pi$ -mode, V represents the unnormalized voltage between points A and D in Figure 5.1, whereas for a cavity operating in the  $2\pi$ -mode, V is the voltage between points B and C.

The electromotive force V can also be found by computing the work done in carrying a unit charge completely around the loop bounding the longitudinal cross-section of the cavity.

Thus, using the designations in Figure 5.1, one has

$$V = \oint \overline{E} \cdot d\overline{\ell} = \int_{C}^{B} E_{z} dz + \int_{B}^{A} E_{r} dr + \int_{A}^{D} \overline{E} \cdot d\overline{\ell} + \int_{D}^{C} E_{r} dr$$
 (5.27)

The line integral between points A and D along the metal surface vanishes since  $\overline{E}$  is everywhere normal to  $d\overline{\ell}$ . The integrals from B to A and from D to C are obviously equal.

The electromotive force varies harmonically with time in phase with  $E_z$  and lagging  $H_\theta$  by  $\frac{\pi}{2}$  radians. If no time were required for the particle to travel through the cavity, then the particle would traverse a potential difference given by .

$$V_{BC} = \int_{C}^{B} E_{z} dz \qquad (5.28)$$

and it would be accelerated by the maximum axial electric field. However, the particle is traveling with finite velocity and takes a finite amount of time to travel through the cavity. Assuming that its velocity is constant and that it enters the cavity at the beginning of a cycle (i.e. it enters at time t=0) and leaves it after one-half cycle ( $t=\pi/\omega$ ) when the cavity is operating in the  $\pi\text{--mode}$  or after a complete cycle  $(t=2\pi/\omega)$  when the cavity operates in the  $2\pi$ -mode, the particle traverses the following potential differences:

$$\mathbf{v}_{BC}^{(\pi)} = \int_{C}^{B} \mathbf{E}_{z} \sin(\pi z/L) dz \qquad (\pi\text{-mode}) \qquad (5.29)$$

$$\mathbf{v}_{BC}^{(\pi)} = \int_{C}^{B} \mathbf{E}_{\mathbf{z}} \sin(\pi z/L) dz \qquad (\pi\text{-mode}) \qquad (5.29)$$

$$\mathbf{v}_{BC}^{(2\pi)} = -\int_{C}^{B} \mathbf{E}_{\mathbf{z}} \cos(2\pi z/L) dz \qquad (2\pi\text{-mode}) \qquad (5.30)$$

Here L is the length of the cavity (the distance between points B and C in Figure 5.1).

The ratio of the voltage given by (5.29) or (5.30) to that given by (5.28) is called the transit time factor T and is of great significance to the linac cavity designer [72]. This factor indicates the effect on the particle of not being subjected to the maximum value of the field at all times during its passage through the cavity. The energy gained by a particle of charge  $\,$  q  $\,$  is thus given by the product  $\,q\,v_{BC}^{}T$ instead of simply by  $qv_{\begin{subarray}{c} \end{subarray}}$  which would result if the electric field was static.

The maximum energy U stored in a cavity can be obtained from the magnetic field in the following way

$$U = \frac{1}{2} \int \overline{B} \cdot \overline{H} \, dv = \frac{1}{2} \mu_{\bullet} \int \int \int H_{\theta}^{2} r \, dr \, dz \, d\theta = \pi \mu_{\bullet} \int \int r H_{\theta}^{2} \, dr \, dz \quad (5.31)$$

Thus the volume integration reduces to an integral over the longitudinal cross-section.

One can obtain the capacitance of the cavity at resonance from the stored energy and the electromotive force in the cavity from the relation

$$C_{\bullet} = 2 U / V^{2} \tag{5.32}$$

If the walls of the cavity are perfect conductors, there is no loss and the cavity behaves in a purely reactive manner. The inductance at resonance can be determined if the wall currents are known.

In order to find the currents on the walls of a cavity, one can use the " $\overline{n} \times \overline{H}$ " rule. Thus, the tangential current density  $\overline{J}$  is equal in magnitude to the tangential magnetic field intensity  $H_{\theta}$  but it has a different direction, as indicated in Figure 5.1. One obtains

$$\overline{J} = \overline{n} \times \overline{H} = H_{\theta} \left( -\frac{dz}{dn} \overline{1}_{r} + \frac{dr}{dn} \overline{1}_{z} \right) = H_{\theta} d\overline{\ell}$$
 (5.33)

The magnitude of the current density along the cavity valls is therefore described by the function  $H_{\pmb{\rho}}$ .

One can now obtain the cavity inductance at resonance from the stored energy and the integral of the square of the wall current

$$L_{o} = 2U / \int_{0}^{2\pi} \int_{D}^{A} r \, dl \, d\theta = U / \pi \int_{D}^{A} r \, H_{\theta}^{2} \, dl \qquad (5.34)$$

Thus, the components of a loss-less parallel LC circuit can

be determined which describe the behaviour of the linac cavity at resonance. The displacement current flows through a capacitance  $C_{\bullet}$  and the surface current flows through an inductance  $L_{\bullet}$ .

If the cavity walls have a finite conductivity, the fields penetrate the conductor surface and transfer net power into the cavity, walls, in addition to the inductive effects of the conductor. The calculation of losses in the metal walls is relatively easy if one assumes that the currents in the lossy walls are identical to the loss-free currents. Then the average power loss at any given point on the surface is given by the expression

$$p = \frac{1}{2} R_{S} J^{2}$$
 (5.35)

where R<sub>s</sub> is the surface resistivity. Integrating this over the entire metal surface, one obtains the total average power loss

The internal impedance per unit area of conductor surface is given by [38]

$$Z_s = (1 + j) R_s$$
 (5.37)

where

$$R_{s} = 1/\sigma \delta = \sqrt{\pi f \mu_{o}/\sigma} = \sqrt{\omega \mu_{o}/2\sigma}$$
 (5.38)

Here  $\sigma$  is the conductivity of the metal and  $\delta$  is the skin depth. Therefore the power loss is

$$P = \pi \sqrt{\omega \mu_{\bullet}/2\sigma} \int_{D}^{A} r H_{\theta}^{2} d\ell \qquad (5.39)$$

The apparent shunt impedance of the cavity may be defined as

$$Z = V^2/P \qquad (5.40)$$

According to equation (5.40), shunt impedance and power loss are in inverse proportion. Linac cavity designers endevour to build linac cavities with a high shunt impedance. One of the most important performance figures in linac cavity design is the quantity  $ZT^2$  which includes transit time effects.

The quality factor Q of the linac cavity is defined by

$$Q = \frac{\omega_o(\text{maximum stored energy})}{\text{average power loss}} = \omega_o U/P$$
 (5.41)

Q describes the sharpness of resonance and is a measure of the persistance of the oscillation.

Not all of the quantities mentioned in this section are computed by the LACC computer program, simply because not all of them are needed. Some of them have been mentioned merely to shed more light on the physical behaviour of the device.

## 5.5 Numerical Methods Used in the LACC Computer Program

As mentioned at the end of section 5.3, the computer program LACC assembles the matrices [S] and [T] of the matrix eigenvalue equation (5.23). The whole matrix assembly procedure is carried out by the subroutine ASSEMB. The nine

independent element matrices ([R], [Q<sub>111</sub>], [Q<sub>221</sub>], [Q<sub>121</sub>], [Q<sub>231</sub>], [U<sub>11</sub>], [U<sub>21</sub>], [Y<sub>11</sub>] and [Y<sub>21</sub>]) are stored in five BLOCK DATA subprograms in single precision. The assembly of [S] and [T] is carried out in double precision in order to minimize the introduction of round-off error.

The choice of the method used to solve the matrix eigenvalue equation (5.23) is entirely traditional [57.58.74.75].

It permits the computation of all eigenvalues and all eigenvectors directly. The eigenvalues are computed in the subroutine EIGVAL. All operations are carried out in double
precision. A brief description of the procedure follows.

The positive definite, symmetric matrix [T] is first decomposed into a lower and an upper triangular matrix by the Choleski method, with the upper triangular factor equal to the transpose of the lower triangular factor, i.e.

$$[T] = [L][U] = [L][L]^{t}.$$
 (5.42)

The inverse of [L] is easy to obtain [76,p.446]. Consequently, equation (5.23) is recast in the form

$$[L]^{-1}[S][L]^{-1}^{t}[L]^{t}[V] - k^{2}[L]^{-1}[L][L]^{t}[L]^{-1}^{t}[L]^{t}[V] = 0$$
(5.43)

which is reduced to the form of the standard eigenvalue problem

$$[Z][X] - k^{2}[X] = 0$$
 (5.44)

if the notations

$$[Z] = [L]^{-1}[S][L]^{-1}^{t}$$
 (5.45)

$$[x] = [L]^{t}[v]$$

(5.46)

Subroutine EIGVAL computes and stores the matrix [Z] and then tridiagonalizes [Z] by Householder's method. The desired number of eigenvalues  $k^2$  are computed from the stored diagonal and subdiagonal elements by a modified Sturm sequence procedure. Sixty bisections are carried out for each eigenvalue.

The computation of the corresponding eigenvectors [X] is also carried out in double precision arithmetic by the subroutine EIGVEC. According to the matrix size, two or more Wielandt iterations are performed to produce eigenvectors of the tridiagonal matrix. The eigenvectors of the matrix [Z] are obtained from the eigenvectors of the tridiagonal matrix by an inverse Householder transformation. These eigenvectors are then scaled and premultiplied by [L]<sup>-1t</sup> in order to obtain the eigenvectors [V] of the original problem, equation (5.23).

The most time-consuming part of the above method is the Householder tridiagonalization [76] which is performed only once for each problem. In view of the fact that any of the eigenvalues and eigenvectors of (5.23) can be obtained by this method, it is very effective. On the other hand, since the first two eigenvalues are widely separated, matrix powering or inverse iteration [76] could be used as an alternative when only the first eigenvalue is required.

Once the eigenvector [V] has been computed, the stored energy  $U^-$  may be computed as given in equation (5.31). Under

the transformation (5.24) the discretized version of equation (5.31) can be written as

$$U = \pi \mu_{\bullet} \iint \mathbf{r}^{2} V^{2} \, d\mathbf{r} \, d\mathbf{z} \implies \pi \mu_{\bullet} \left[V\right]^{t} \left[T\right] \left[V\right] \tag{5.47}$$

The matrix [T] is stored in LACC and the computation of the product [V]<sup>t</sup>[T][V] is accomplished when the eigenvector [V] is determined. Since [V] is not normalized at this point in the program, the stored energy obtained in this calculation is unnormalized.

The program next transforms [V] according to equation (5.24) and overwrites the values of [V] with the result. In the remainder of this section, the notation [H $_{\theta}$ ] will be used in order to avoid confusion.

In order to obtain the total emf from equation (5.26),  $H_{\theta}$  must be integrated over the longitudinal cross-section of the cavity. Given the coefficients  $H_{\theta}^{i}$  at the interpolation nodes, the integration is carried out using the Newton-Cotes quadrature formulae for triangles [77]. This process amounts to replacing the integration in (5.26) by two summations

$$\iint H_{\theta} dr dz = \sum_{s=1}^{m} |A_s| \sum_{i=1}^{n} c_i H_{\theta}^{i,s}$$
 (5.48)

The first sum in (5.48) is calculated over the m triangles that subdivide the region of solution in the r-z plane and is weighted by the surface area  $A_s$  of each triangle. The second summation extends over the n interpolation nodes of a triangular finite element of order N. The quantities  $c_i$  are the closed Newton-Cotes quadrature weights for triangles

$$c_{i} = \frac{1}{|A|} \int \int \alpha_{i} dr dz \qquad (5.49)$$

where the integration is over a triangular region. These weights have been calculated for a general triangle and their values are stored in the subroutine AINTEG.

It should be pointed out that the total emf obtained in this manner is unnormalized and, for a cavity operating in the  $\pi$ -mode, it does not equal the potential difference along the z-axis. In order to find the axial potential difference, the off-axis contributions across the drift-tubes must be subtracted from the total emf. For this purpose, the line integrals in equation (5.27) need to be evaluated. These integrations however, involve electric field components rather than  $H_{\theta}$ . In order to obtain  $\overline{E}$ , one must use equations (5.6) through (5.8), all of which involve derivatives of  $H_{\theta}$ .

 $H_{\theta}$  is given in the solution in terms of interpolation polynomials  $\alpha_{i}$  over triangular regions. The differentiation of these polynomials is relatively straightforward [39,78,79]; by the chain rule of differentiation, for a single triangle there results

$$\frac{\partial H_{\theta}}{\partial z} = \sum_{i=1}^{r} H_{\theta}^{i} \frac{\partial \alpha_{i}}{\partial z} = \sum_{i=1}^{r} H_{\theta}^{i} \sum_{j=1}^{r} \frac{\partial \alpha_{i}}{\partial \beta_{j}} \frac{\partial \beta_{j}}{\partial z}$$
 (5.50)

The  $\gamma_j$  represent the three triangle area coordinates in terms of which the interpolation polynomials  $\alpha_i$  are given. The area coordinates  $\gamma_j$  are related to the r and z coordinates by the following expression

$$S_{j} = \frac{1}{2A} [(r_{j+1}z_{j+2} - r_{j+2}z_{j+1}) + (z_{j+1} - z_{j+2})r + (r_{j+2} - r_{j+1})z]$$

$$(5.51)$$

where the subscript j is cyclic modulo 3 and the subscripts on r and z represent the vertices of the triangle. Hence, one may write

$$\frac{\partial \hat{S}_{j}}{\partial z} = (r_{j+2} - r_{j+1})/2A$$
 (5.52)

If  $\alpha_i$  is an interpolation polynomial of degree N, then its first derivative is of degree N-1. Since the set of all polynomials of degree N-1 or less is embedded in the set of polynomials of degree N or less, one may express the derivative of the  $\alpha_i$  in terms of the polynomials  $\alpha_i$  themselves without introducing any approximation

$$\frac{\partial \alpha_{i}}{\partial \hat{\gamma}_{j}} = \sum_{k=1}^{n} G_{j}^{(i,k)} \alpha_{k}$$
 (5.53)

The coefficients  $G_j^{(i,k)}$  are simply the values of the derivative at the k-th interpolation node. One can also regard  $G_j^{(i,k)}$  as the (i,k)-th entry of a n by n matrix  $[G_j]$ . Three such matrices exist, one for each value of the subscript j. These are row and column permutations of each other and therefore only one (say  $[G_1]$ ) needs to be computed. As with the interpolation polynomials  $\alpha_k$ , the differentiation matrices  $[G_j]$  are independent of triangle size and geometry and need to be computed only once [39,78,79].

Equation (5.50) may now be written as

$$\frac{\partial H_{\theta}}{\partial z} = \sum_{k=1}^{n} \sum_{i=1}^{n} H_{\theta}^{i} \sum_{j=1}^{3} \left(\frac{r_{j+2} - r_{j+1}}{2A}\right) G_{j}^{(i,k)} \alpha_{k} \qquad (5.54)$$

In matrix notation this is simply

$$\left[\left(\frac{\delta H_{\theta}}{\delta z}\right)^{k}\right] = \sum_{j=1}^{3} \left(\frac{r_{j+2} - r_{j+1}}{2A}\right) \left[G_{j}^{(i,k)}\right] \left[H_{\theta}^{i}\right]$$
 (5.55)

A similar derivation for partial derivatives yields

$$\left[\left(\frac{\partial H_{\theta}}{\partial r}\right)^{k}\right] = \sum_{j=1}^{3} \left(\frac{z_{j+1} - z_{j+2}}{2A}\right) \left[G_{j}^{(i,k)}\right] \left[H_{\theta}^{i}\right]$$
 (5.56)

The non-zero values of matrix  $[G_1]$  are stored in a block data subprogram (BLOKK1) for polynomial approximations up to and including 6th order. Since the last N+1 rows and the lower triangle portion of  $[G_1]$  are zeros, little storage space is required. The matrix multiplication and additions required by equations (5.55) or (5.56) are performed by the subroutine DERIV [79].

It should be noted that due to the piecewise continuous nature of  $H_{\theta}$  obtained in the finite element method, the functions  $E_{r}$  and  $E_{z}$  are discontinuous at inter-element edges. Since differentiation is a difficult numerical procedure, the electric field values at triangle edges will not be as accurate as those in the approximation of the magnetic field. The discontinuities in the electric field values can be smoothed by averaging the values obtained at common edges or at vertices. LACC prints the discontinuous values of the  $\overline{E}$  field triangle by triangle only upon request; otherwise it simply returns the smoothed approximation to  $\overline{E}$ .

of particular interest are the axial electric field values and the off-axis values of  $E_{\mathbf{r}}$  along the radius of the drift-tube end in the  $\pi$ -mode case. The integration of  $E_{\mathbf{z}}$  along the edges of triangles which lie along the z-axis is performed according to equation (5.28). Along each edge, the values of  $E_{\mathbf{z}}$  are known at equally spaced intervals; the number of these intervals depends upon the order of the

polynomial approximation in that triangle. Since the approximation is made with polynomials and the nodes are equispaced on triangle edges, the method of integration used is the one-dimensional, closed Newton-Cotes integration formula [76]

$$\int_{z_1}^{z_2} E_z dz = \int_{i=0}^{N} h_i E_z \left[ z_1 + i \left( \frac{z_2 - z_1}{N} \right) \right]$$
 (5.57)

There is no error term in the right-hand side since the integration formula is exact for polynomials of degree N or less. The weights  $h_i$  are available [76.p.116] and are stored in the program (BLOKK2 block data subprogram). The quantities  $\mathbf{z}_1$  and  $\mathbf{z}_2$  are the z-coordinates of the vertices of a triangle edge lying on the axis. The summation in equation (5.57) is performed in the subroutine COTES1 for any given side of a triangle of order N. Note that it makes no difference which segment end-point is taken first since the integration formula is symmetric with respect to the weights.

The integral of  $E_r$  along the drift-tube end is obtained in the same way as the integration of  $E_z$  along the axis. Contributions from all of the triangles lying along the path of integration must of course be accumulated. For a cavity in  $\pi$ -mode operation, the emf contributions from the drift-tube ends are subtracted from the total emf obtained via Faraday's law in order to arrive at the net emf across the cavity. This emf value is expected to be more accurate than the one obtained by the line integral method since the latter involves more differentiation.

The line integral method must be used however, in computing the transit time factor. The denominator of the

transit time factor has already been calculated. The numerator is given by equation (5.29) or (5.30) and may be evaluated by the Newton-Cotes integration. The only requirement before calling the subroutine COTES1 is to multiply the values of  $E_z$  by the proper trigonometric function. The error in  $E_z$  is somewhat smoothed in the integration and there is a tendency for these errors to diminish when taking ratios [80]. Thus, the transit time factor may be expected to be accurate even if the emf values are in error.

It is necessary to compute the transit time factor in order to arrive at a realistic normalization factor for the field values. Linac cavity designers prefer to have the field magnitude such that the emf per unit axial distance is 1 MegaVolt/meter. This figure includes transit time effects. Consequently, the normalization factor of can be determined from the following relationship between of, the axial emf V, the transit time factor T and the cavity length L

nf V T/L = 1 MegaVolt/meter  $\rightarrow$  nf = L/VT (5.58)

All of the results printed by LACC are normalized.

The final calculation is the value of the integral in the power loss calculation in equation (5.39). The integration in (5.39) involves the square of a function which has been approximated by a polynomial of degree N. The square of  $H_{\theta}$  is therefore a polynomial of degree 2N. One could simply take the square of the nodal values of  $H_{\theta}$  and then use the one-dimensional Newton-Cotes formula to perform the integration. However, this would involve the approximation of a polynomial

of degree 2N by one of degree N. In order to avoid this approximation the following procedure is used. Consider a triangle edge along a metal wall of the linac cavity. The magnetic field along the edge is given. Thus one can write  $H_{\theta}$  along the triangle egde as a linear combination of one-dimensional interpolation polynomials  $\alpha_i^1$ 

$$H_{\theta} = \sum_{i=1}^{N+1} H_{\theta}^{i} \alpha_{i}^{1}$$
 (5.59)

where  $H_{\theta}^{i}$  represents the (N+1) nodal values of the field along the triangle edge. The power loss P specified by equation (5.39) therefore becomes

$$P = \pi \sqrt{\omega \mu_{c}/2\sigma} \sum_{i=1}^{A} \sum_{j=1}^{N+1} (\sqrt{r_{i}} H_{\theta}^{i}) \frac{1}{s} \int_{s} \alpha_{i}^{1} \alpha_{j}^{1} d\ell (\sqrt{r_{j}} H_{\theta}^{j})$$

$$(5.60)$$

The first summation is over the triangle edges coincident with metal boundaries of the cavity in Figure 5.1. The letter is denotes the length of the triangle edge and N is the polynomial degree. The subscripted radial coordinates  $r_i$  and  $r_j$  refer to the coordinates of the interpolation nodes along the triangle edge. The symmetric N+1 by N+1 matrix [T1] may be regarded as the metric of the interpolation polynomials  $\alpha_i^1$ . These matrices are available for polynomial degrees beyond 6 [81] and are independent of the length and position of a triangle edge. LACC stores the matrices [T1] up to and including the matrix corresponding to polynomials of degree 6 in a block data subprogram (BLOKK3). Subroutine COTES2 performs the matrix multiplication required by equation (5.60).

## 5.6 Input/Output Features of the LACC Computer Program

In this section, the input procedures of the LACC computer program are described for a practical linac cavity and the output obtained from the program is explained. Consider again the linac cavity in Figure 5.1. Due to symmetry about a transverse plane, only one half of the clongitudinal cross-section of the cavity need to be considered. Figure 5.3 shows the triangulation of the upper half of the cavity cross-section. Curved sections of the boundary are approximated by straight line segments, while sections which are straight lines are modeled exactly. All triangle edges that appear along the problem boundary lie entirely along it. unlike the usage in the AXISYMM-VECTOR-HELMHOLTZ-FINTEL6 program. This is because LACC identifies boundaries by labelling triangle sides, so that any edge of a triangle must either lie entirely along a boundary, or else entirely inside the cavity. Also note that in some cases triangle edges are matched to two equal triangle edges along. Such triangles are fitted with different polynomial orders with coincident nodes [57,75] and are accepted by LACC.

The triangle vertices in Figure 5.3 have been numbered in an arbitrary sequence. Given the r and z coordinates of each vertex point, an input point list is prepared and punched out on data cards, one point number and the associated coordinates per card. These cards are reproduced in Figure 5.4a where they are preceded by a data header card containing an asterisk, the problem title and the r and z scale factors. The input point list is terminated by a blank card.

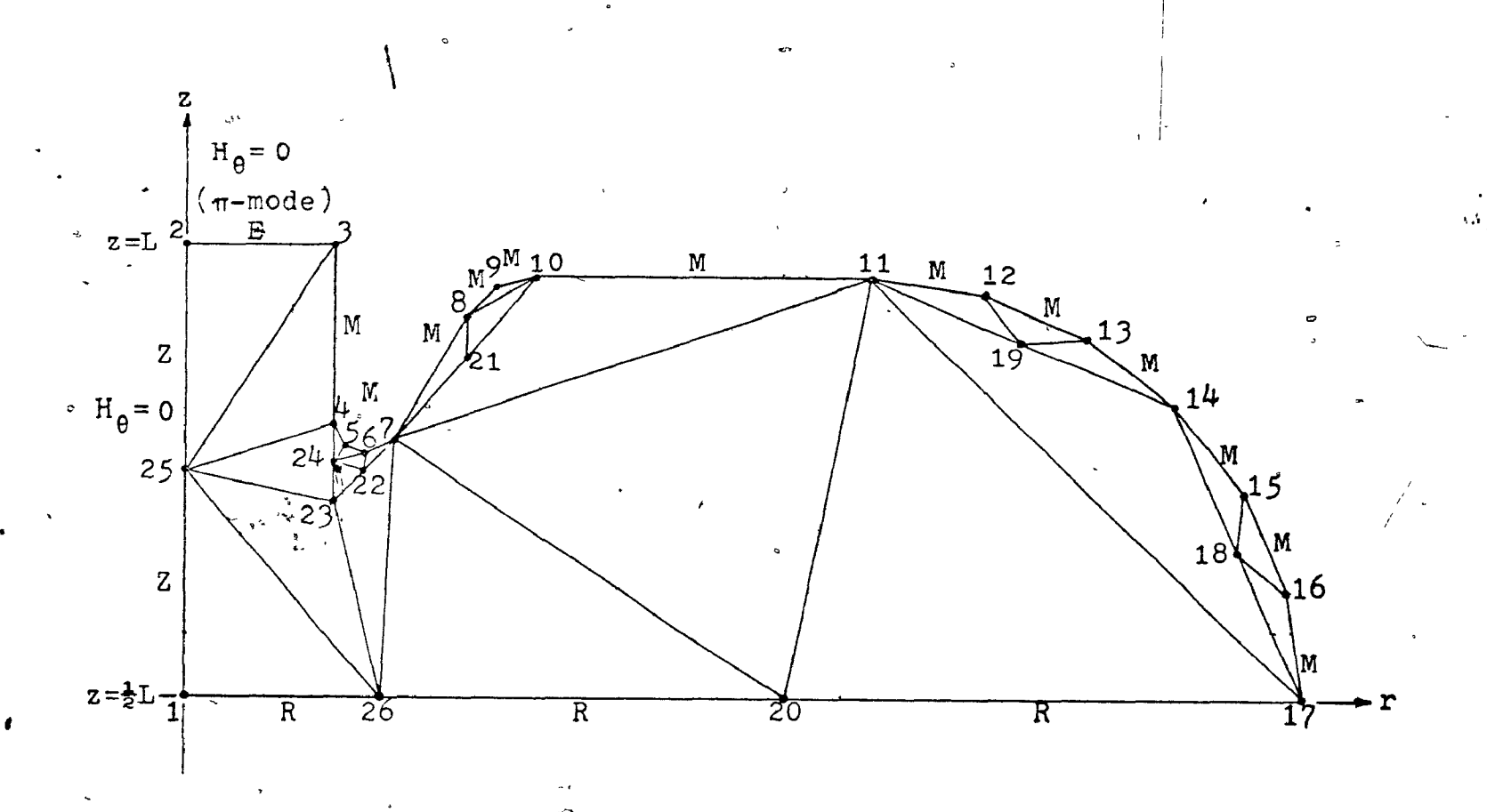


Figure 5.3

Triangulation of the upper half of the cavity cross-section of Figure 5.1.

in the second

*HCYT'S	805MHZ SHAPED PROTONALINAC	CAVITY - 1.00 1.4	CARECCC1
9	1	0.0	6.05172CARCCCO2
, ,	. 2	C • C	12.10344CAREOCC3
₩	3	1.90000	12-TC344CA9CCCC4/
	4 .	1.90000	9.69074CAPDCCC5
•	5 .	2.01715	9.40789CAPECOC6
	. 6	° 2 • 3.0 0 0 0	9° 29074CAPCCCC7
	7	7.64641	9.49C74CARDCCCP
P	8	3.59121	11.12719CAPECCO9
· -	, ,	3.95724	11.49322CARCUCIO
	, 16	. 4.45724 <sup>3</sup>	11.62719CARECC11
•	11_	8.57903	- 11.62719CARCCO12
. â	. 12 \	10.02207	11.43723CARCCO13
	13	11.36676	10.88C24CARCC014
•	14	12.52150	9.99419CARCCC15
	15	13.40755	8.83945CA°CCC16
•	16	13.96454 ; *	7.49476CARCCC17
	17	14.15450	6.05172CARD6018
•	18.	13433800	_8_02295CARCCC19 -
•	19	10.55026	10.81C69CARCC020
3	3 20	7.50 <del>€</del> 0	6.05172CARDCC21
	. 21	3.55102	. 10.55896CARCC022
į	22	2.2732C	9.09074CARC0023
* *	23	1.90000	8.69C74CAFEC024
	24	1.90000	9.19C74CARDC-C25
	25 ,	0.0	9.07758CAPCC026
	<b>?</b> 5	2.50000	6.05172CARCC027
	•		CARDCC28
			· ·

Figure 5.4a

Data cards containing the input point list. The coordinate dimensions are in centimeters.

Figure 5.4b shows the remaining data cards required by LACC. It presents the input element list, one triangle per card. The first number on every card specifies the polynomial order in the element and the next three numbers specify a triangle by its vertex numbers. An arbitrary sequence may be used to specify these vertices; however, once specified, an implicit order, A B C, is defined for the vertices.

the fifth, sixth and seventh numbers on each data card designate boundary conditions for sides AB, BC and AC respectively, of the triangle defined on that card by vertex numbers A, B and C. There are three types of boundary conditions for triangle edges:

- (1) Interelement continuity;
- (2) The impedance boundary condition given in equation (5.11) at boundary edges (this includes the transverse plane of symmetry);
- (3) The homogeneous Dirichlet boundary condition on boundary edges (this includes the axis of symmetry). There is no distinction in the treatment of the first two of these and both are communicated to the program using the character 0. The third type of edge condition is specified in the data by the character 1. These characters are called constraint numbers; a constraint number of 0 refers to triangle edges where the  $H_{\theta}$  values are free prior to the solution of the problem, while a constraint number of 1 designates triangle sides where  $H_{\theta}$  values are fixed to be zero.

The 8-th, 9-th and 10-th entries on each card are alphanumeric characters called segment identifiers. They identify

•							_		س	
. 4	25	2	3	_ 1	. 1	0	٠ ٧	Ε	*	CARECO29
L,	3	, 4	25	~ C	0	С	þ	*	* *	CARECC30
4	25	4	23	0	0	C	*	. ≉	*	CARECE31
4	25	26	23	C	0	C	, *	<b>,</b> *	*	CARDOC32
4	`25	· 1	2.46	1	. С	C	* Z	R	#	CARECO33
4	23	7	26	O	C	С	*	*	*	CAPECC34
4	26	7	20	e - C	) C	C	*	*	R	CARDCC35
4	11	7	2Ĉ	0	0	C	*	*	<b>*</b>	CARDO036
4		7	10	0	0	, C	*	*	M	CAPDCC37
4	1 <u>1</u> 1 1	17	2 C	C	C	0	*	* Ř	*	CARDC038
4	l.l	14	17	C	C	- C	*	° <b></b>	*	CAPEO039
<b>*</b> **	4	5	24	C	0	С	M	*	*	CAPECC40
2	5	6	£ 24	C	0	С	M	*	<b>*</b>	CARCCC41
<b>~</b> 2	<b>.</b> 6	, 7	- 22	C	0	C	۲	*	*	CAPFO042
2.	6	24	22	C	C	C	*	. *	*	CARCC043
2	23	24	22	O	0	0	*	*	*	CARCCC44
2	7	٠, ۶ -	. 21	C	C	C	۲	۰ 🖈	*	CARCCC45
2	10	8	21	C	C	Co	*	*	- *	CARECU46
2	ឧ	, 3	10	, O	_ 0	C	м	μ	*	CAPCCC47
2 2	11	- 12	15	C		, 0	٧	*	*	CARDC048
2	12	13	19	,	C	C	M	*	<b>,</b> *	CARC0049
2	13	14	19	O	0	С	M	*	*	GARCC050
2	14	15*	0 1 2	. 0	0	C	×	*	*	CARCCC51
2	15	16	18	O	0	С	٧	*	*	CARECO52
7 -	16	17 .	18	C	C	C	þ	*	*	CARCCO53
					/					CAPCCC54
U,XX,	1 1	۵			٠	•			1	CARCC055
		·			•	-				

Figure 5.4b

Data cards containing the input element list.

triangle sides along the 'z-axis (Z), along the end of the drift-tube (E), along the transverse plane of symmetry (R) and along the metal walls of the cavity (M). The sequence in which they appear on each card is the same as the sequence used for constraint numbers. An asterisk has been used for triangle edges that do not belong to any of the four categories. mentioned above.

The primary role of the segment identifiers Z, E and M. is to identify the line segments where various line integrals will be evaluated. Thus, Z identifies the path of integration for the computation of the emf across the cavity by the line integral method. The identifier E indicates the integration path along the drift-tube end radius where the computation of the emf contribution by the line integral method is also required. M identifies the metal walls of the cavity where the power loss must be computed. The identifier R merely communicates to the program the existence of a transverse plane of symmetry. In addition, the identifiers serve the purpose of checking the correctness of the triangulation and the geometry of the problem, as discussed below in the description of the data processing. The cavity defined by the data in Figures 5.4a and 5.4b will operate in the π-mode since a homogeneous Dirichlet boundary condition is specified at the end of the drift-tube. This is identified by the segment identifier E. If the cavity is to operate in the  $2\pi$ -mode, a constraint number of 0 should be assigned to the drift-tube end, and the segment identifier E omitted, since in 2π-mode operation the drift-tube end may be regarded as being sealedoff.

The input element list is also terminated by a blank data card. One additional data card is required, providing two optional code words, the sequence number of the first mode desired and the total number of modes to be returned by the program. The optional code word PU specifies that the results should be punched out on cards and the optional code word EF specifies that a list of the electric field values for each triangle is to be printed out separately. XX is used in Figure 5.4b instead of EF, indicating that such a listing is not required.

All data cards are processed by the subroutine READIN. This subroutine reproduces the input point and element lists in the output. Subroutine MAP produces a crude diagram of the locations of input points on the line printer. This is useful for checking errors in the data cards. A number of errors in the data are also automatically checked by the subroutine READIN [57,75].

From the input point and element lists READIN generates an assembled point list and an element list (see Figures 5.5a and 5.5b). The assembled point and element lists are generated when interpolation nodes are added to the input point list. The points in the assembled list are renumbered and rearranged in such a way that fixed points (i.e. points with Dirichlet boundary condition) appear at the end of the assembled point list. A second map of the points is produced on the line printer by the subroutine MAP (see Figure 5.6), this time with the assembled points. READIN also prints an error code and the required and available size of certain primary arrays, as well

				•				
PERAT	+CRT7CATAL	WANT SCAL	PCIAT	PERMITE	VERTICAL	POINT	+ CREZCATAL	VERFICAL
4C.	CCCTCINATE	CEUACIVATE	<b>NC.</b>	CCCGC 17 911 .	CCCACIVALL	Nr.	E E CAL IVATE	CCCRCENATE
1.	1.90000	9464614	•c.	1.72900	7.46 854	59.	11.09701	7.44559
2.	2.01715	3.40149	51.	1.57500	P.12765	100.	5.4111	7.44559
٦,	33030	5.29674	57.	2.15000	f.7k147	101.	12.49068	6.2112
4.	2.4641	9.411.74		2.70000	7, 1712 1	167.	10.42175	6.0417
5.	9,59121	11.12714	54.	2.04000	P. Carse	101	9.16363	6.05172
4.	8.05774	11.45327	55.	0.62500	7.56465	iĉ4.	9. * 6 4 6 *	1 11.21654
١.	4.45774	11.47719	54.	0.42400	6.60818	165.	10.45**1	9.87467
A.	P. * 74" 1	11.02013	57.	1.73060	F. PCP1 P	1/6.	11.53500	10.46244
4.	10.07701	11.43773	54.	0.62500	6.65172	107.	11.54413	5.41662
10.	11.14676	4 . 41774	49.	1.75000	6.05172	1(8.	17.35 224	**4*120
H.	12.42140	9.95411	£¢.	1.07500	6.05177	169.	12. 12.115	9 ( ( + 5 )
12.	12.4.755	F. + 1745	61.	2.09660	P. 69C74	110.	13.14424	1, (1)14
1.	1 . 50444	7.45476		2.73660	8.23098	111.	1,24.47	5,1451
14,	14.154*(	4.05172	41.	7.45581	8.29074	117.	11.9000	5.251.11
15.	13,33800	0.72745	- 64.	7.47120	4.49064	1111	2.12312	5,14542
ie.	10.55 21	10. 110/4	65.	2.18660	7.571.23	114.	2.107	1,24014
17.	7.5000/	4.06177		2.60941	P. CICAP	115.	7.47171	5,15014
12.	*.551*2	£7.5444A	67.	2.57326	7, 17123	116.	3.7511	9.13074
15.	7.17176	9.09014	6.	2.53660	6.51147	117.	2.65116	5.14(74
2C.	1.7707	*. 4 C74	49.	3.75000	6.05172	110.	1,11401	10.10850
21.	1.506-0	9.1-674	70.	3. 77666	4.51147	iis.	1, 11112	10. 44703
22.	7.14.000	4.75000	71.	5.00000	6.65172	170	4. (242)	11.17715
?*.	C.475CF	9	77.	3.47320	7,77173	171.	1, 114, 1	11.71000
74.	C.475CC	10.43041	73.	5.03000	1.51147	122.	4.20774	11.50020
25.	0.55000	10.59051	14.	6.75000	6.65177	123.	9. 10 ( ) 1	11.57221
?€.	FLATREE	11.24152	75.	3.25921	P.6309P	174.	10.25414	31-12356
77.	~.94^[~	11.74658	76.	5.01320	7,77123	125.	10.49447	11,15 = 74
79.	1.42500	11.7469#	77.	4.2P+6C	(.51147	126.	10.05 ** 1	10.44447
79.	1.50000	11.5/07	70.	7.099#	11.0530#	127.	11.56419	10.41762
10.	9 1.9000	10.85709	79.	P. 10977	10.21112	12**	12-26452	5.416.67
71.	1.47500	1^.74380	*r.	5.61777	10.15854	125.	13,3337#	P.4712C
١7.	1.90001	10.25111	•1.	6.42612	5.65921	1.0.	12.0000	1,10710
* * * * * * * * * * * * * * * * * * * *	1-42500	17.14(**	• 2 .	P.C3952	P. P1945	111.	13,611/3	7.7***
34.	0.95000	9.94714	91.	4.12957	10.07485	112.	14.0542	7 1.7.1324
,*5.	E-4750C.	9.51745		5.14294	9.1451C	133.	C.C	4.04177
₹6.	C.45CCC	9. 34416	•5.	6.55616	P. 20534	1140	0.0	17.10144
37.	F-415FF	4.326.63	***	7.71974	1,44459	135.	1,50001	12.16144
7×.	C-47500		47.	7.54856	11.67715	1 *6.	C. C	9.07150
19.	C. 95CCC	9.17416	**.	6.76541	11.09*0#	117.	i.c	9,00404
40.	C • 950°C	P. # + 4 * #	mg,	F.51P14	11.67719:	130.	C.C	10.59041
41.	1.42*00	9.7*145	90.	4.47277	12.44#5#	119.	1 0.0	11 34404
42.	1.47500	9.0 9745	41.	5.03494	45003.11	141.	33*56.3	(")
47.	1-47500	4.77745	97.	5.41769	11.62719	141.	6.4466	12.10 *44
44.	1.9000	9.4467# 1	97.	1.05917	10.024#5	142.	1.47501	12.16344
45.	1.90000	P. 941 74	94.	4.06451	\11.C937P	143.	(	6, 12112
44.	Caezacc	4.72112	59.	* 4.97790	4 10.23132	i		7,46464
47.	P+25000	7.56465	44.	*** 11.76617	P. 87944	3 144.	3.3 C	91924.9
49.	1.10000	P+27441	47.	9,70314	P.P.945		,	
49.	1-87500	4.80818		19 14041			,	

Figure 5.5a The assembled point \list.

OLON PETTS BOSHIT SHAPEE PRETH LING CAVITY SON

TRIBACLE DICER | PEINT | PCINT | PCINT

Figure 5.5b

The assembled element list.

# \*\*\* FCYT'S BCSMF2 SHAFFE PRETCH LINAC CAVITY \*\*\*\* \*\*\* MAP OF THE ASSEMBLED POINTS \*\*\*

Figure 5.6

Map of the assembled point set. Point numbers of interpolation nodes which are situated too close over-write each other. They can be recovered from the assembled point and element lists shown in Figures 5.5a and 5.5b. as a list of points with Dirichlet boundary conditions (see Figure 5.7).

Vsing the information passed on by READIN, subroutine FINDIT determines the cavity length L by reviewing all segment identifiers. It verifies that the segment identifiers E and R refer to horizontal line segments only, and that the identifier Z refers to vertical segments. Any deviation from this condition causes the program to abandon the data set and to print an appropriate error message.

Another check of the data performed by FINDIT concerns the triangulation of the region. In m-mode operation the magnetic field is zero both along the z-axis and along the end of the drift-tube. Thus the field values are very low in the corner defined by the axis and the drift-tube end radius. Better results are obtained in differentiating H<sub>0</sub> in this case if the 90° corner belongs to one triangle. Consequently, subroutine FINDIT detects any subdivision of the corner and abandons the data set, printing an appropriate error message. A similar check is made for the 90° angle made by the z-axis and the transverse plane of symmetry.

Subroutines FINDIT and LINAC, along with the MAIN program produce the global quantities discussed in section 5.4 and print them as in Figure 5.8. The computed resonant frequency and the field values are printed by the subroutine OUTPUT. Figure 5.9 shows the normalized values of  $H_{\theta}$  and  $rH_{\theta}$  at the interpolation nodes for the problem at hand. Figure 5.10 contains the list of normalized and averaged values of  $E_{\mathbf{r}}$ .  $E_{\mathbf{r}}$  and  $|\overline{E}|$  at the nodes. These results were also punched on

#### \*\*\* DIMENSIONS OF THE PROBLEM \*\*\*

ERROR CODE:	"PISTAK"	=	, o	
NC. CF FIXED POTENTIALS:	"NF I X"	<b>÷</b>	13	
NC. CF FREE PCTENTIALS:	"NFREE"	=	132	
TOTAL NO. OF POINTS:	"NSUP"	=	145	
PERMISSIPLE, NC. OF POINTS	: "LNG,T"	=	5 C C	
NC. CF TRIANGLLAR ELEMENT	S:"NELMT"	=	25	
REQUIRED "S"-MATRIX:	"LENCTH"	=	e វ 7 e	
AVAILABLE "S"-MATRIX	·ULCNGST"	=	12246	
NC. CF ENTRIES IN "NVTX":	"INC I C"	=	250	
AVAILABLE "NVTX" SIZE:	uFV^LXu	=	349	

\*\*\* PCINTS WITH FOMOGENFOUS DIRICHLET BOUNDARY CONCITION \*\*\*

POINT		WΛ	VE-
NO.		FUNC	TICN:
-		۲	₽≉H
133.		C • C	C • C
134.		C.C	C.C
135.	3	0.0	0.0
136.		C • C	$C \cdot C$
137.		o.c	$C \cdot C$
138.		$C \cdot C$	0 • C
139.		C. • C	$G \cdot C$
140.	6.	0 • C	$C \cdot C$
141.		0.C	0.0
142.		0.0	$O \cdot C$
1,43.		$C \cdot C$	$C \cdot C$
144.		0 • Ç	$C \cdot C$
145.		0.0	0.0

## Figure 5.7

Subroutine READIN prints out an error code and the required and available size of certain arrays; a list of points with Pirichlet boundary condition also appears in the output.

### \*\*\*\* HCYT'S 805MHZ SHAPED PROTON LINAC CAVITY \*\*\*\*

B

#### \*\*\* CHARACTERISTICS OF THE LINEAR ACCELERATOR CAVITY \*\*\*

```
CAVITY LENGTH:
                                      "CL" =
                                               0.1210340+00 METERS
COMBINED DRIFT-TUBE-END RADII:
                                   "CDTER" =
                                               C.38CCCCD-01 METERS
RADIAL SYMMETRY FACTOR:
                                      "RS" =
                                                  (2 FCR SYMMETRY)
NUMBER OF NODES ON RERMIN:
                                  "KTRACK" =
                                               9
                                                            D-LESS
MAXIMUM 7-CCCRCINATE ON R=PMIN:
                                    "ZMAX" =
                                               0.121C34D+02 CENTIM
MINIMUM 7-COCRDINATE ON RERMIN:
                                    "ZMIN" =
                                               C.6051272D+C1 CENTIM
("ZVAX"-"7VI\")*"RS"/1CO =
                                   "CHECK" =
                                               C.121C34D+CC METERS
MINIMUM R-CCCRDINATE:
                                    "RMIN" =
                                                            CENTIM
PARTICLE VELCCITY/LIGHT VELCCITY: "RETA" =
                                               C.653C67D+CC D-LESS
MODE NO.
                                   "KCUNT" =
                                                            D-LESS
MODE TYPE:
                                     "TYP" =
                                              0.3141590+01 DelESS
SURFACE INTECRAL OF HTETA:
                                     "SUM" =
                                              C.1503150+06
                                                             VCLIS
CCRRECTED: VOLTAGE ("SUN"-"DELTAV"):"SHO" =
                                              C.1485540+06
                                                             VCLIS
LINE-INTEGRAL OF EZ ALONG AXIS: WIVEZINTI = JO.1443140+06
                                                             VCLTS
TRANSIT TIME FACTOR NUMERATOR:
                                  "TEZINT" =
                                              C.11758CD+06
INTECRAL OF ER (REAM FOLE):
                                  "CELTAV" =
                                              C.1760560+04
                                                             VCLIS
POWER LOSS IN METAL WALLS:
                                  "PCWLCS" =
                                              C.2691750+04
                                                             WATTS
CONDUCTIVITY OF THE METAL:
                                  "CENDUC" =
                                              C.5910160+08 MFCS/M
TRANSIT TIME FACTOR:
                                     "TTF" = - C.814750D+00 D-LFSS
SCALE FACTOR (=CL/(SMC*TTF)):
                                      "SF" = -0.5324060+04 D-LESS
SQUARE OF THE SCALE FACTOR:
                                     "SF2" = '
                                              0.283456F+08 C-LESS
1CO*("SMC"-"VEZINT")/"SMC":
                                    "QLTY" =
                                              C.28542CD+C1 PERCNI
FNERGY STURED IN THE CAVITY:
                                     "VTV" =
                                              C.147713D-C1 JULLES
Q-FACTOR (CMEGA*VIV/PCWLCS):
                                  "CFACTR" =
                                              0.278872C+05 D-LESS
SHUNT IMPERANCE:
                                  "ZIMPED" =
                                              C.819848D+07
                                                              CHMS
"71PPEC"*"TTE"#*2
                                     "7T2" =
                                              C+54423CD+C7
                                                              CHMC
SHUNT IMPEDANGE PER UNIT LENGTH: "ZOVERL" =
                                              0:67736FC+08 CFMS/M
"7T2"/"CL"
                                   "7T2CL" =
                                              C.449649C+08 CHMS/M
"ZCVERL"/"GFACTR"
                                    "ZCLQ" =
                                              C. 2428560+04 CHMS/M
"ZT2CL"/"CFACTR"
                                  "Z72CLC" =
                                              C.1612390+04 CHMS/M
```

#### Figure 5.8

Joint output from subroutines FINDIT and LINAC and the MAIN program containing the global quantities discussed in section 5.4.

BAVEMINARRIZZEN - C. [693]10-cc

	•			12 4.2				
	•••	*** 1117 (* 1			ZEC MAYF-FUNCTIO			
					211 #-41-10-(11()	. ANECEST	•••	
						Ĩ.		
PCIAL	+ BAYF-	Bor baye-	PERA	M #44F-	#4F b#4F-	PCANT	b. 5.4.15	
AC.	FLACTICAL	FUNCTION !	Nr.	FUNCTION	FLACTICAL		H MAYF-	BAL PARE-
	APF/PE1ER	BAREALS		AMP/PF TER	AMPERES	> . N.C.	FUNCT (CN: #P#/PETF#	FUNCTIONS
							***/** 11 *	*****
١.	-2.1777116.02	-C.71471AC+C1	44.	-C. 86244 804C1	-0.1401030+07	85.	0.3144446444	-0.13591=0+03
7.		-C.1434640407	Ae.		-C.1e21e20e01	90.		-C.1CE45E+C*
٠.	-0.1277141.404	-0.2436360402	47.		-0.655116461	91.		
4.	-0.1756444664	-C.4/19791&^?	40.	*-C.47801 1F+C3		97.		-C.110075(+C)
٩.	-0.25 140 16 404	-C C754 71 +C2	49.		-0.1565097402	91.		-C.68416CE+CZ
' e.	-0.2490541404	44587667 }	50.		-0.1701440+02	54.		-C. (4*22E+C2
٠.	-6.5155136464	-C.1(441>"+C = 4	51.		-0.1102515462	9.		-0.2101450+07
٠.		1 3743F AC 1	47		-C.237415F+C2	96.		-F.216764F4F4
٠.	+0.000	-C+21 17747+63	53.	J-C.9541030+C1		97,		-6.7646911.063
10.		-F.235*5#( +F %	544	-0.9292276461	-0.1904520+02	9.5		-0.2534425.00
11.		-0.74 7/3/463	••.		-0.1688600001	99.		-C.214114F+L1
12 •	-9.E#K5211 404		***	40.2714110+0+	-0.1/57576+01	100.	-0 2155951 +04	
17.		-0.756 ALC + C +	57.	-0.5425156+01	-0.67#174[+61	101.	-0.761*#20+64	
14.		-0 * 3 < %@∰ ¥ C • C ±	5.	-0.27033AP+C3	-0.1+#397r+C1	102.	-C.21*1**[+C4	
15-	-5*140111L*U4		55.	-C.535#0404C4C3	130364649.30	103.	-1.210170 044	
16.	-0.2056441404		er.	-0.7971576+01		104.	-0.2055711+04	
17.	-6.562634 +6+		41.	-0.9F375FF+C3	-0.2057190+02	10.	-C.2CF2CFF+C4	
14.	-0.2132747.464		47.	+2+1131131.3-	-0.2*659*6*6*	ICA.	-0.1964C71+C4	
15.	-C.1171C4/+/4		A 7.		-0.1565966462	107.	404 11E JOS 0-	-C-219515(+C)
76.	-0.4625600.403		64.		-0.27##C#6+62	ice.	-0.199*****(4	
21.	-1.7157476467		**.	+0.104219/464	-0.7487250+02	104.	-1.1417447 +C4	
27.8	-C.1C36411+C4		66.		-6.1+12546465	Hic.	-C+1#744F1+C4	-042574951461
24	-0.5197416464		67.	40.112972FeC4			-1,4714717461	-0.1024461+02
75.	-0.41010107			-C*10441404L4		112.	-6.1*70756.00	
20.	-C.45417464C2 -C.117764F+C2		49.	-0.14*C9PD+C4		117.		
27.	-0.2944441 +62		<u></u>	-C. [48954[4C4		114.	-1.5%*(641+6*	
20.	-0.3377141.62		71.	-0.1744441.04		114.	-0.15*7441+04	
29.	-0.232445[+0>		77. 71.	-0.1444010+04		116.	-1.1194941 +64	
10.	-C.ece27*( +C2		74.	-0.1705561+04		117.	- C • 4 * 14 1 41 • C *	
31.4	-0.8484847			-0.1944070+04		110.	-0.240+911+64	
12.	-C. 14 17 141 +F +		70.	• -C.1702620+C4		117.	-0.7496496.04	
*3.	-0.119454511461		77.	-0.1997476404		120.	-(.)44#5#1+04	
34.	-0-1717740-03		76.	-C.2139#9B+C4		121.	+1+7619170+64	
35.	-0.9466065 +04		19.	-0.7144470+04		1224	-0.2399961404	
71	-0.2635550467		40.	-0.2117110+04		123.	-0.2105440.404	
17,	-C-11#197F+C1		ř1.	-0.7109790+04		124.	-0.2059727064	
38.	-0-1550190-01		87.	-C. 2141C4C+C4		126.	-0.7079641.004	
34.	+0-32AC4CE+C+		P7.	-0.7111411+04		127.	*0.72774C+04	
40.	-0.1500940+01		Re.	-6.1996676464		1274	+0.19*94([+04	
41.	-C.4710570+C1		4 99 .	-0.2046990+04		179.	-0.1757676.7-	
42.	-0.54174/1+04	-C.771987C+C1	et.	-0.2117270+04		130.	-C.184741C+C4	
43.	-0.58477CD+01		87,	-0.2155720+04		131.	-C+1#127#E+04	
44.	-0-6027470+67	-C-1145220+C2		-0.2114640-04		132.	-(.1636130+64	
			=		,	4 / 4 4	- ( ) ( ) ? ( ) ( ) ( ) ( )	

# Figure 5.9

The normalized values of  $H_{\theta}$  and  $rH_{\theta}$  at the interpolation nodes.

5 B

\*\*\* LIST OF POINTS WITH MORPALITED, ELECTRIC FIELD VALLET ! \*\*\*

	* * *!*( * * *!*(		FI WAVE- FUNCTIONS VOLTS/P	FLACTICAT VCLTS/#	PCINT	FR WAYE- FUNCTIONT VOLTS/#	EZ WAYF- FLXCTTENT VCLTS/#	TEL BAVE- FLACTIONT VCLTS/P	PCINT NC.	FR BAVF- FLACTICAT VELTS/P	E7	IFI WAVE~ - FLACTICAT VCLTS/P
	1) 1.71		2.3+370+05	1.47350+06		-5. 28560+04	1.42491 +C6	1.9740[004	551	3.816CF+C#	2,544****(5	2.4444000
	73 7.447		3,44441 406	4.#3410+CA		-1.42350+32	5.03400.404	7.07675+04	1071	#.#52F1+C*	4.61.16.64	4.01750+04
		, , ,	5.3434D+36	5.76471+C6		-4.29446464	1. W. Jecour	1-43436404		.1.1.1(+0)	1.43411.474	1.51525+05
	43 - 1 1/7		2. 21.71 + 26	1.12407.06		-1.42441+05	1.94611464	1.93141464	1071	2.40445463	%, %# 6 #[ # 7 % # _ 4 # % % 7 # C #	4.4+46.45
			4,6117 406	7.88597+C5 5.27077+85		-1.49250+05 -1.45220+05	2.154 11 + CE	Z.16010406 [.945*[.06	1041	5.918+1+64	* 74+4[ • C*	* 15*10*0*
	# } " \ \		- 4. * 2 * 17 * 7 \$ - 5. 5 * 6 * 6 * 6 * 6 5 .			-7.30350+03	1.97491 006	1.97690 +56	1641	7. 6 17 16 . 64	2.66 866 475	7.7757[+64
			4.695+6+05	4.09447.05		-2.47410.04	1.91450 +FE	1.51465464	icei	1.0,150.00	1. ** 4* 1 + 5 *	7.14746.664
	4) - 1-		1.71717 + 25	1.19147454		-9.94777407	1.91716+66	1.91700+06	1011	F. 141 114C4	1 . * * * * * * * * *	1.52540+64
	1 1 1 14		1. 27/11 005	2.24740+05		A. 157104C1	1.6*23C*Ce	1.08340406	10-1	4.27171+14	1.47*****	1.02547.465
	<b>1</b> 00 1 1 1		1.0315 +05	1.51040 +05		-4.44550+03	1.83090+06	1.** (50.00	1091	*.47721 + (4		1.15100.00
	177	-	4.441 11464	9.41747464		-4.4555+64	2.00435.00	30+36178.5	1101	3,03301.004	7.44111 074	4.243/1454
	1 1 4,41		1.015.0404	4.67#10+04	621 -	-1" 0 3 K Y L + C K	2.01600+04	7.54415404	1111	2.31.61.66	1.7477 .ce	2.41545454
	141 1-14	. 1	- 1.4 4- 1	2 #5120# 3	411	-1.32675.05	*.+1077+re	7.844.10404	1121	1.67876 . ( .	3. +4416.41+	1.10756+06
	141 4.5	* ***	A	P. 46 36 30 CA	641	-1.84190+05	2.21145456	7.74145476	1131	1. *** 1 4 E	4.110/ 406	4412455466
	14) 4,2**		3.7. Pr. 475	3.910,1006	A5) -	-1.43375 +05	1.*1*70*06	1.47240+06	114)	# . 31 77( +1 5	*, 1936[ * (*	******( * ( 6
	. 71 -5.457	6 + 73	7. 7 1, 21 4 25	7.85370.655	649 -	· 6 . 8 1 4 8 7 4 7 5 1	7.11910.00	3.32*10*04	11*)	-1.71 841 4(4	1.41161166	4, 1174( 106
	18154		7.3 31/405	630nn935.I		-1.87555+05	6.44545406	1.45715.406		->.14=41.41=	********	******
	1-1 -1. 11	* C * C 5	3 4774 6	3. 19147 + 01		-4.04030+04	1.04430+06	1.848 [476		1 state over	* , 7* * ** 4 ( #	37 24361 4 6 4
	253 4-163		9 10 30 6 30 0	2.23795.66		2.25756+64	1.4973/406	1.49340404		1.51940+04		1. 191 17 • 04
	211 2114		7.4407 + 25	7.04535 404		-1.21417.75	1.50700.404	1.50700 +0+		-7.6477(+(*		5.65777.654
	23 - 1, 5		1.71927-06	1.7367 +CA		3.74 /47 0 74	1.75776164	1.71777.436			* 1 (25) * (*	##C1141 #C# ##90#01 #C#
	271) 7 744		3.44210+05	9.51031.675		-1.97476-04	1.51450.06	1.52730404		-4.4441464	4,51171.005	4.03(4)404
		1'	4.75120.05	4.47145.65		-1.0024F+05 3.6123F+C4	1.2157 *06	9-94200406	1277	-5,71191+(4 -5,11141+141	1. 61161 464	3,44410464
	*** ****	1" • " 5	- የፈጻለራ ጥቀርኝ - 1 ፈናለማየጠቀጣኝ	1.44140405		-4.64.44.44	1.4774 • 66	1.61000+76	1241	P.40141404	7.0 ******	********
				1.40730.05		-1.34-40-05	1-19775	1-10-10-04	12.1	1.00411 5	***********	7.440.500
			4.47.20073	1. 23 110 + 05		-1.11446474	4.75011 475	g. 74 4 Frank	1261	13/42 27 464	7.1445(40#	7.4744 464
		31.475	1.30271005	2.23010.0		-1.72130+04	A. 91 PPI + 75	6.9109(+05	1271	1.11#7/405	1 . 4 + 7 = 1 + C =	1. * 4 * * ( * 2 _
		F + 15	1.10170434	1.71170405	73)	7.66030+07	4.42511464	*,40977059	1281	5.40135466	7.57485464	1.27340.405
	311 2.774	10.05	1.31171.75	1.71475 105	401	-1.4721(+05	7.78741405	3.9144606	1251	7.(* 79[ * [ 4	4.44CF1 +C4	#. 4114F + C4
	17) 4,"44	. + - " 5	-A. **     ** r4	5.(*7*^*(5	- €11 ·	- A. 23910+04	7. * 16.75 + 15	7.87175 404	1361	4.40,95054	7.05751-64	7.51315454
	337 5,113	11+75	4.11211.475	6.54140+05	871 -	-1.73636+64	e. e e e el e c e	6.4472C+05	1311	4.15/11+04	1,4194(4(4	e.2142C+C4
	749 7,514	77+05	7.7.575.405	4.61240405		-6.2427[+65	1.04925466	1,7381[+06	1171	7.24145454	5.07676464	2.29821 + 64
			1.14.46.464	1.411574CA		-2.30340+55	9.92101455	1.01441.404	1,,,	C.^	1.92540.66	1.57840.00
		77.475	1-42517455	1.44447.00		-7,34100+04	P. R. LAL + C.S.	******	1341	C.C		C.C
		****	1.2.447.34	1.4 437474		-2.1111 +04	1.7********	1.77140.00		4.10250+64	5.4110000	7.04717.064
	31 3	* *15	1.47715.65	1.57*75*66		-7.78745+64	6,371 (404	6.34637.00		-3.5762***(4	1.24664464	1.24027404
				1.44750+54		-2,28055+04	7.50480+05	7,50270405		¢.c	9. 17/// +C*	9.37447464
		, ***	1.777.0076	1.47230.434		-3.53/75064	7.45**********	7,4347[4/3	1371	c.c	4.6^17[+05	4.6(775+65
	42, 7, -7	475	1.47140+04	1.7#M9M+CA 1.94740+CA		-1.95000000 -1.08030005	# <sub>*</sub> 10qx0x05 7 <sub>*</sub> 24790x05	7.42426405	1953	1.E 4.G794[+C4	1.76420465	1.1647[+[*]
	4") 4, "		1.9.747.036	2.03140+SA		1.1895L+C4	1.15191.05	7. 15840404	1411	6. 171AC +C4		6-111FF-64
		+03	1.44777476	7.43417.05		-1.81777-76	1.17410.00	1.971+1466	1421	434315454	č.c	*-6471F+C4
e	4-1 37		7.5745 +CA	7.46400+06		-4.19570+05	6.15400-05	7.56271.05	1431	C.C	1.7100000	1.71++0.00
	44) 5.12.		1.#31*0.08	1.49747.00	951	5.40#AT+C4	3.64.25.664	9. 70500 405		C.C	1.4*77E+Ce	1.43270+04
	473 -2.14		A0+30+24	1,95410406	961	6.00404	2.465* - 29	2.57270405	1441		1.96775.66	F.4677C+C6
	4"3 4. 1		1.55517+06	1.55 .17 .08	973	1,07 ****	4.1777645	4, 19 - 17 173	• • •	•••		
	491 -4.347	3. + 34	1.87751 406	1.03000.00	923	3.28745 .64	1.201221.5	1.26667405				

Figure 5.10

The list of normalized  $\mathbf{E_r}$ ,  $\mathbf{E_z}$  and  $|\overline{\mathbf{E}}|$  values at the nodal points.

cards and used as input to a modified version of the finite element field plotting program FINPLT [82]. This program uses a CALCOMP digital plotter to draw lines of constant  $H_{\theta}$ ,  $rH_{\theta}$ ,  $E_{r}$ ,  $E_{z}$  and  $|\bar{E}|$ . The plots produced are given in Figures 5.11a through 5.11e. These plots reveal that the E-field values are less accurate than the H-field values. Nevertheless, these plots indicate very well the nature of the field configuration in the cavity and the locations of the maximum field values.

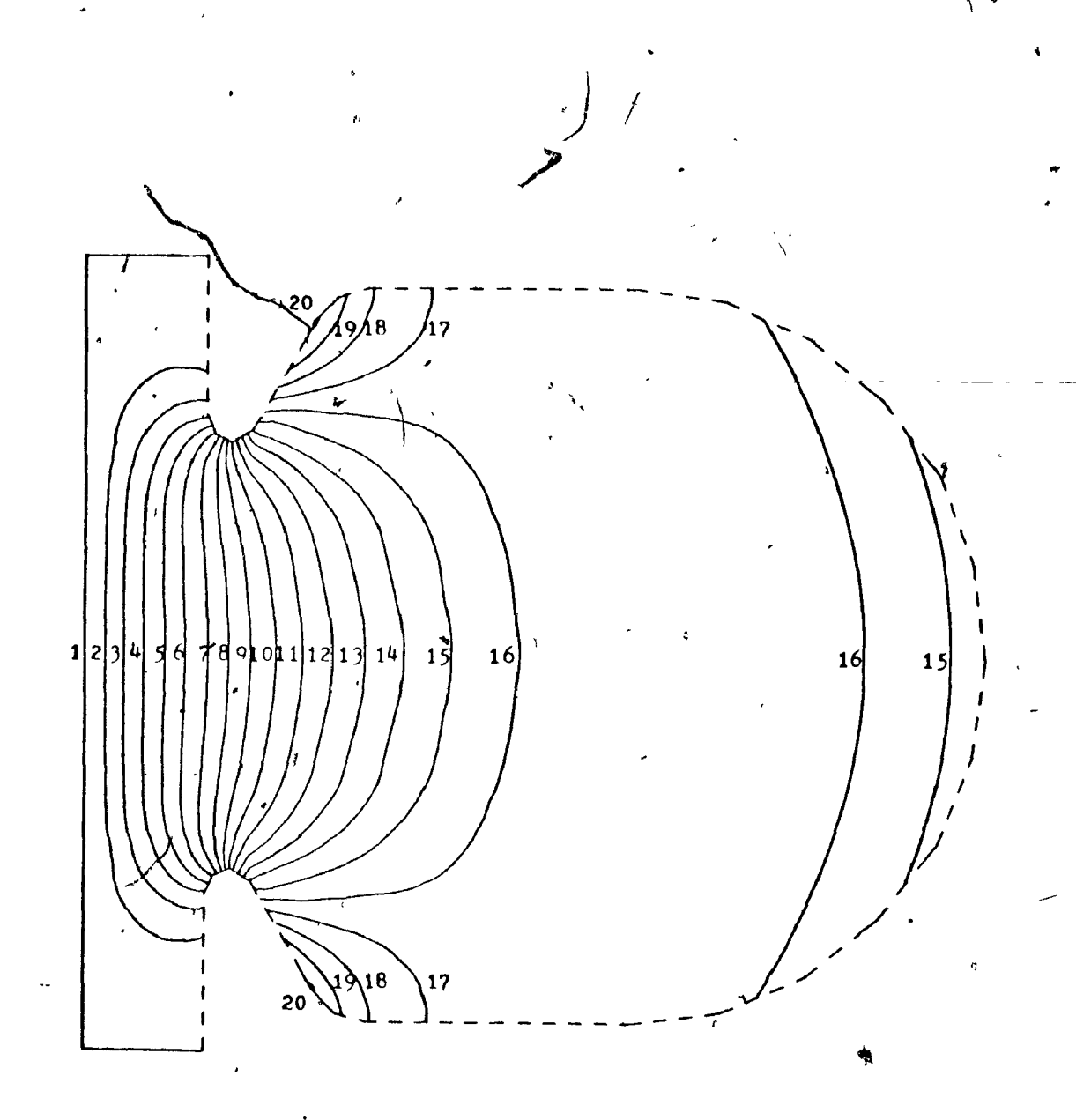


Figure 5.11a

Lines of constant H, for the fundamental mode (808.799 MHz). The values range from 0.0 to 2576.0 Ampères/meter in steps of 135.58 Ampères/meter. These are normalized values such that the emf across the cavity is 1 MV/m including the transit time factor.

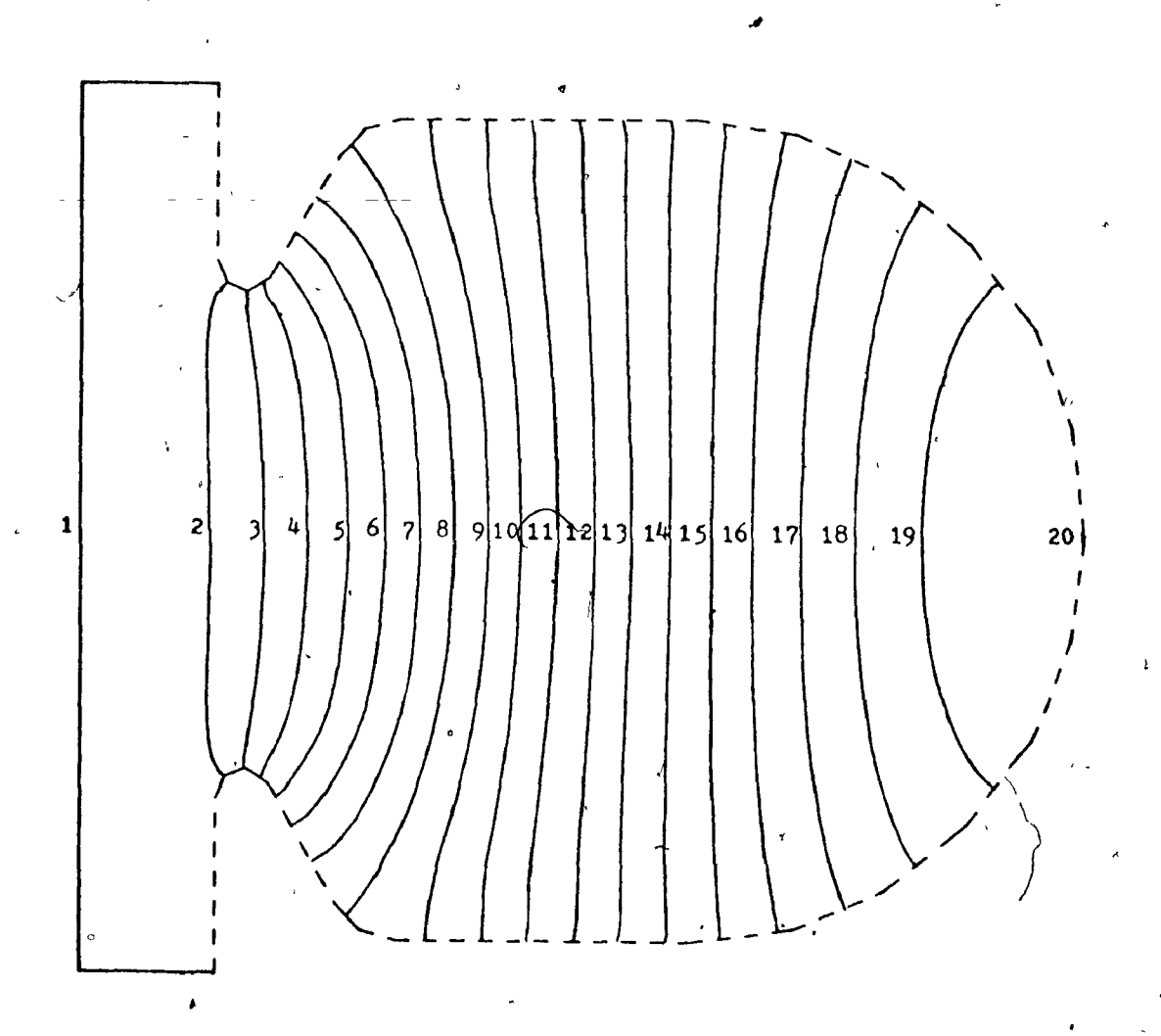


Figure .5.11b

Lines of constant \$ (=rH<sub>0</sub>) for the fundamental mode (808.799 MHz). The values range from 0.0 to 2590.0 Ampères in steps of 136.31 Ampères. The values are normalized as for H<sub>0</sub>:

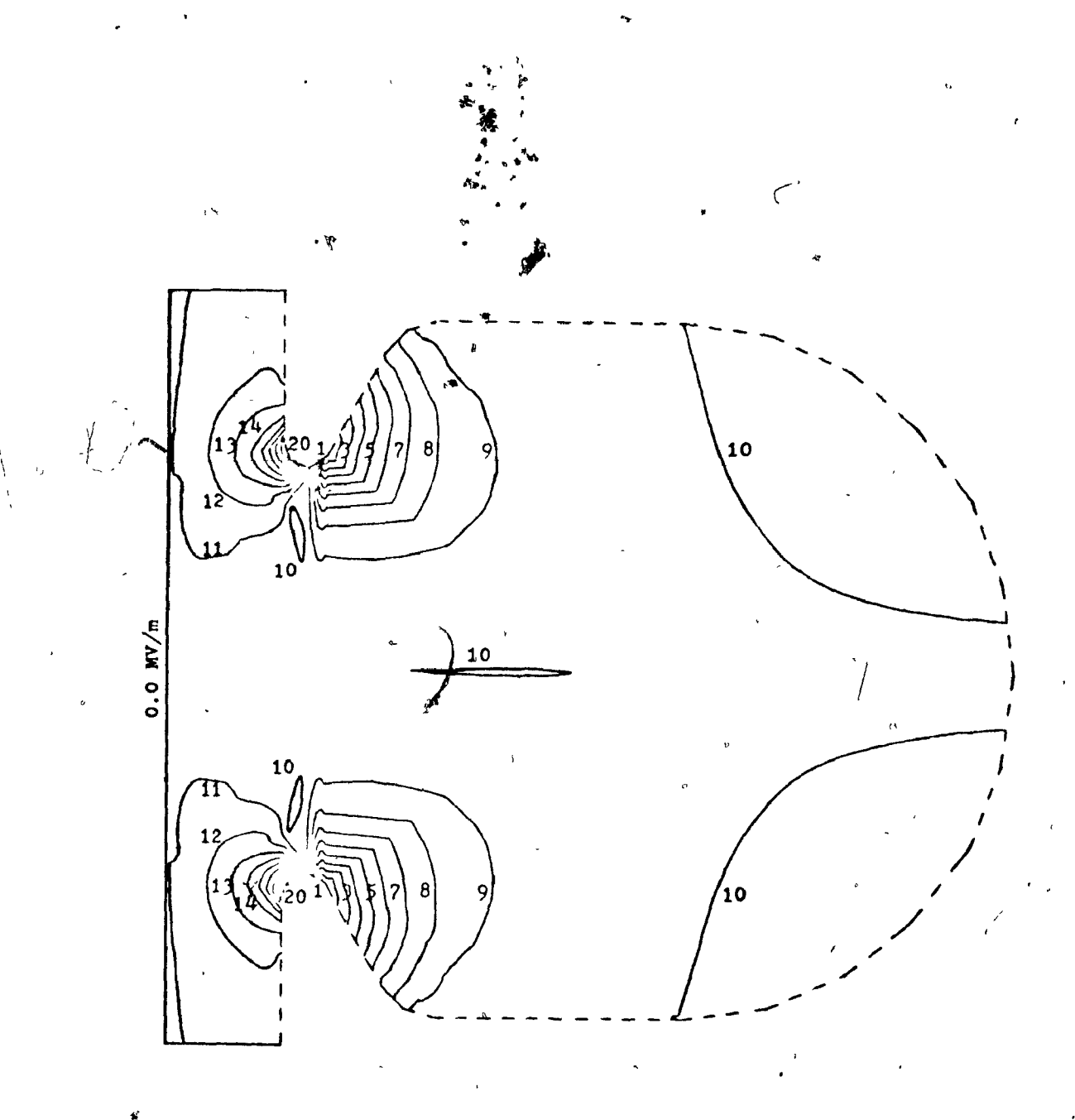
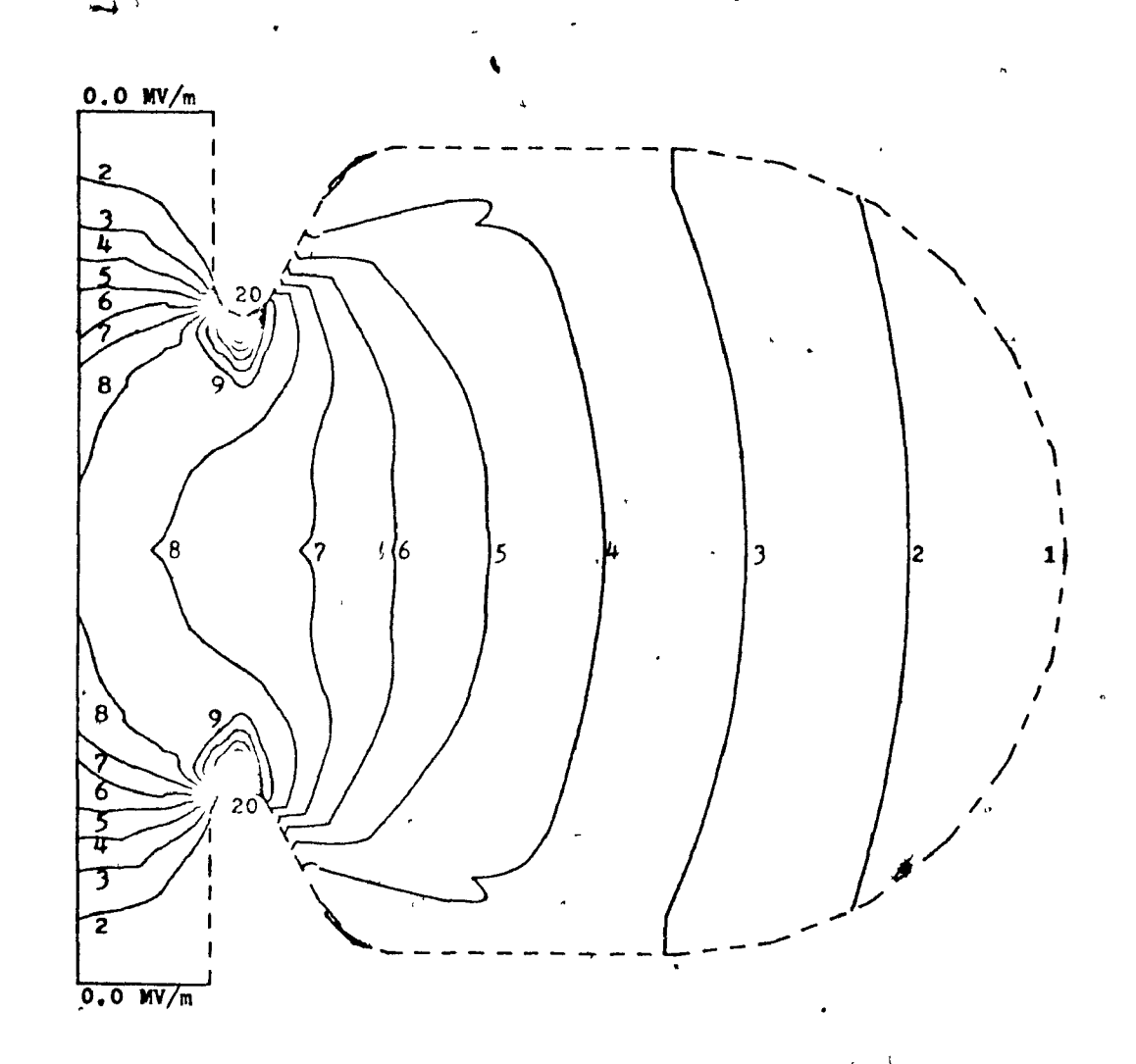


Figure 5.11c

Lines of constant E<sub>r</sub> for the fundamental mode (808.799 MHz). The values range from -2.1479 to +2.4431 MegaVolts/meter in steps of 0.2416 MV/m. The values are normalized as for H<sub> $\theta$ </sub>.



2

Figure 5.11d

Lines of constant E for the fundamental mode (808.799 MHz). The values range from -0.0655 to +5.2636 MegaVolts/meter in steps of 0.2805 MV/m. The values are normalized as for  $\rm H_{\theta}$ .

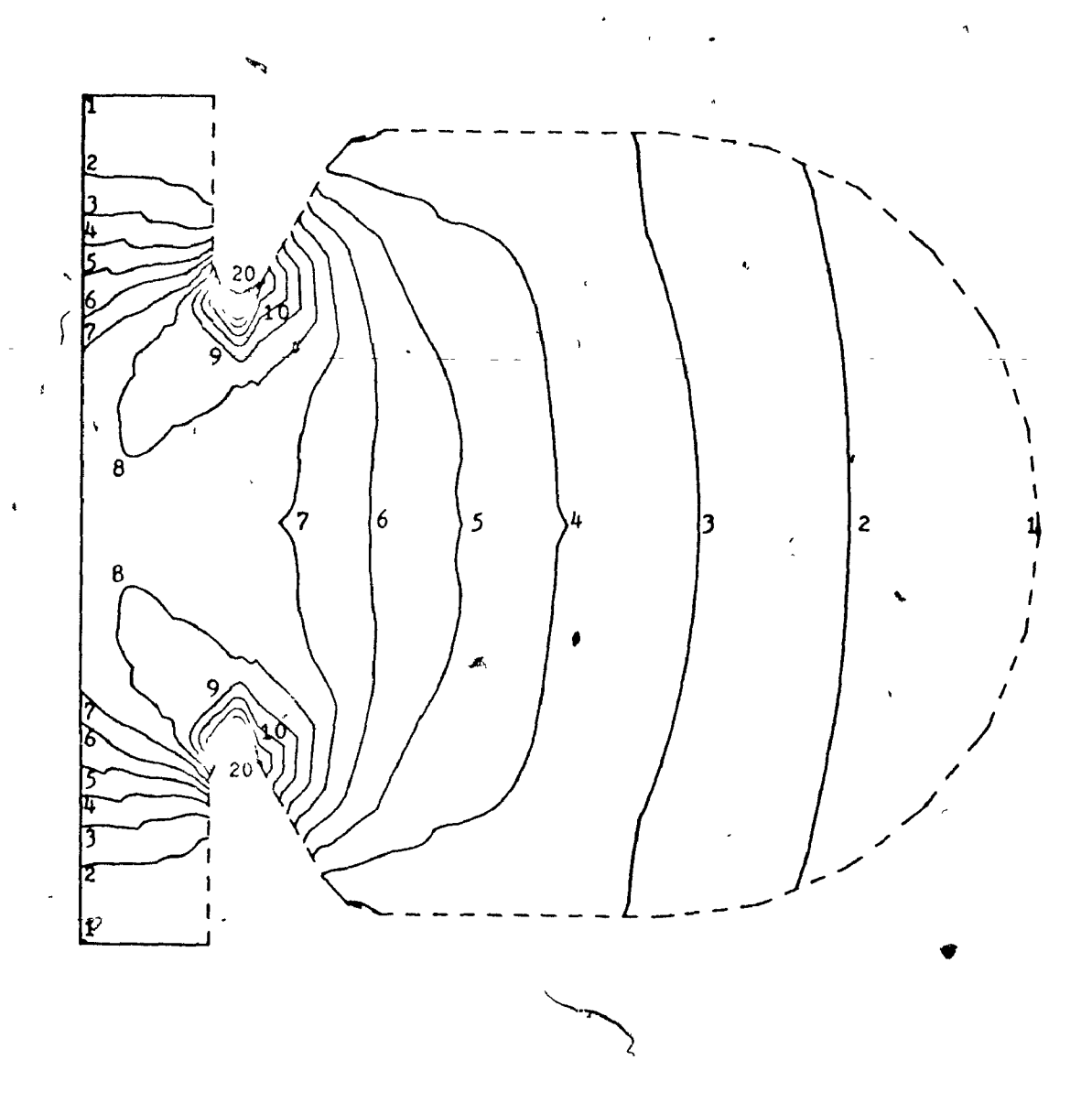


Figure 5.11e

Lines of constant  $|\overline{E}|$  for the fundamental mode (808.799 MHz). The values range from 0.0 to 5.2647 MegaVolts/meter in steps of 0.2771 MV/m. The values are normalized as for H $_{\theta}$ .

# 5.7 Accuracy, Speed, Convergence and

#### a Comparison with the LALA Program

The problem treated in the previous section has been solved by Hoyt, Simmonds and Rich [70] in 1965 using a computer program (LALA) based on finite difference methods. In order to make a meaningful comparison between their results and the finite element solution, their method must be explained briefly [70,80,83].

The LALA program works with the function  $S = rH_{\theta}$  as has been discussed in section 5.2. The numerical method employed is successive point over-relaxation. A square mesh is used and a nine-point difference equation is derived for interior points from a variational formulation. At the boundary, a special set of boundary difference equations are used, which according to the authors satisfy the homogeneous Neumann boundary condition for S on the actual cavity boundary. In Hoyt's words [83]

"The LALA program uses a zig-zag approximation to the actual boundary. This zig-zag boundary lies either on or outside the actual boundary. The calculation is carried out for the region inside the zig-zag boundary. The equations used to compute the values of F for the zig-zag boundary points are derived so as to satisfy physical boundary conditions on the actual boundary."

The LALA program determines the dominant eigenvalue by means of the Rayleigh quotient. An initial guess is made for the eigenvalue and for the function \$\mathbf{F}\$, followed by an iterative procedure to produce a new \$\mathbf{F}\$ and a new eigenvalue. The process is repeated until the values settle down to small changes.

 $<sup>^{1}</sup>$  F denotes  $rH_{\theta}$  in Hoyt's paper.

Using this method, the resonant frequency of the cavity as produced by LALA is 804.80 MHz. According to the paper given in reference [70], "the computed frequency probably is within 0.1%". The frequency computed by the finite element program is 808.799 MHz. This figure is approximately 0.5% off of the frequency computed by Hoyt, Simmonds and Rich; hence, either the authors of LALA have underestimated the error in LALA solutions or the finite element program is highly inaccurate.

Details of the computational tests performed with the AXISYMM-VECTOR-HELMHOLTZ-FINTEL6 finite element computer program have been published elsewhere [52]. They indicate that the agreement between analytical solutions and the wave-numbers of the dominant modes computed by AXISYMM-VECTOR-HELMHOLTZ-FINTEL6 for cylindrical resonators is Netter than 0.1%. In view of the fact that LACC works in double precision arithmetic whereas AXISYMM-VECTOR-HELMHOLTZ-FINTEL6 is written in single precision, the agreement for the same test cases is better than 0.01%. Table 5.1 shows the resonant frequencies of cylindrical cavities with various radio as computed by LALA and by LACC. The percent errors in these results are also given. They indicate that both programs produce accurate results for cylidrical cavity problems.

Considering that the matrix size for the linac cavity problem of section 5.6, is 132 (a large value by finite element standards) and that second—and fourth-order elements are used in the approximation, it is very unlikely that the frequency returned by LACC could be in error by as much as 0.4%. In

cavity radĭus in cm	analytical frequency in MHz	LALA* freq. in MHz	% error in LALA freq.	LACC freq. in MHz	% error in LACC freq.
14.96	766.9962	767.04	+0.00571	766.951	-0.00589
14.98	765.9722	766.04	+0.00885	765.926	-0.00603
15.00	764.9509	764.92	-0.00404	764.905	٥-0،00600
15.02	763.9323	763.93	-0.00030	763.886	-0.00606
15.04	762.9165	762.94 .	+0.00308	762.870	-0.00609
15.06	761.9033	761.95	+0.00613	761.856	-0.00621

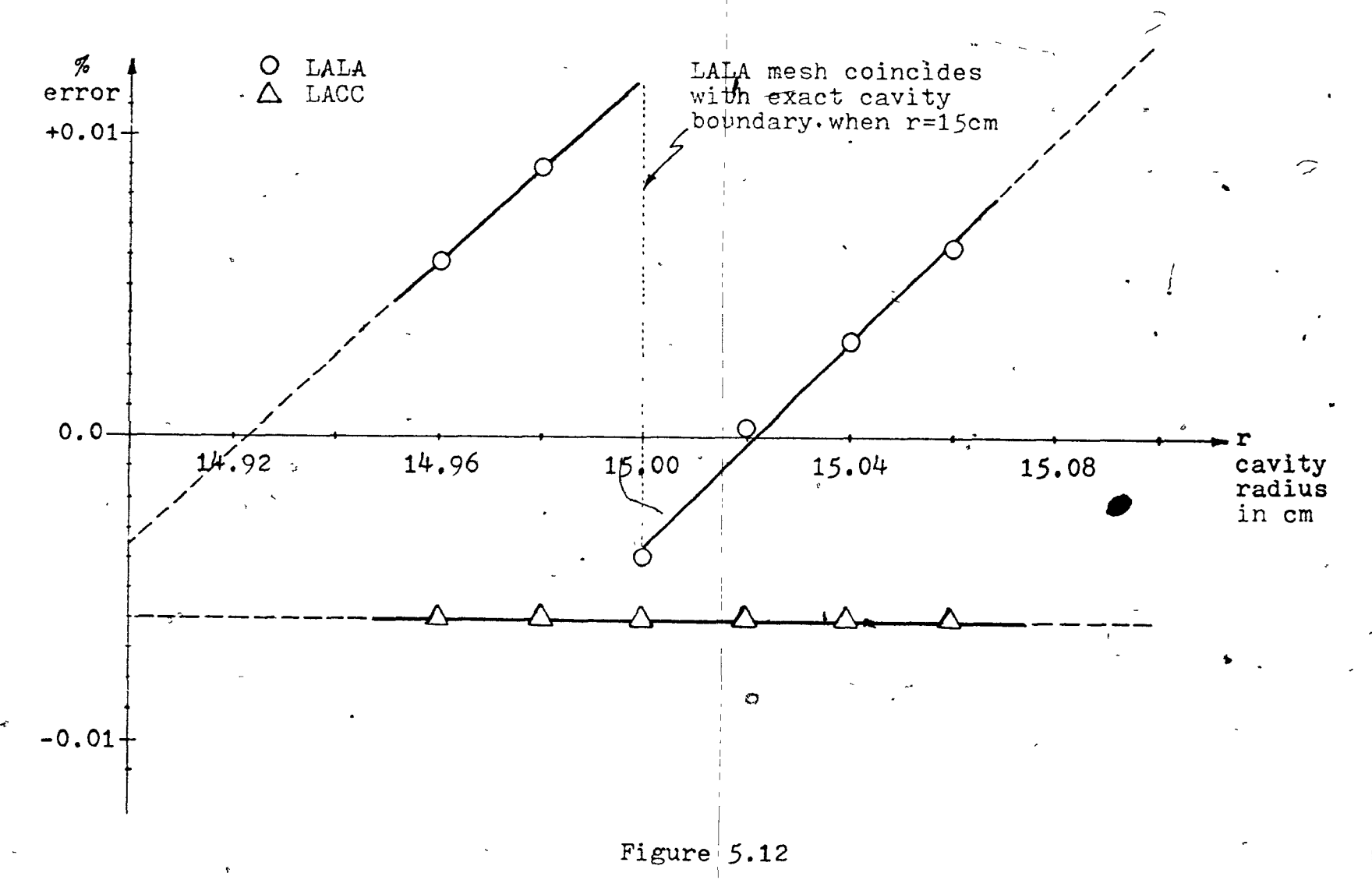
\*LALA results courtesy of Dr. K. Mittag [84]

#### Table 5.1

The resonant frequencies of cylindrical cavities with various radii as computed by LALA and by LACC. The LALA program used a rectangular mesh comprising 3171 mesh points to solve the cylindrical cavity problem. The LACC program solved the same problem with sixth-order polynomial approximation using 84 nodes. The percent errors shown indicate that both programs produce accurate results for cylindrical cavity problems. In Figure 5.12 the percent errors are plotted against the cavity radii.

the author's opinion, the discrepancy between the LALA and the LACC results can only be attributed to serious shortcomings in the methods used by the originators of LALA. In LALA, the Neumann boundary condition is imposed by setting the function values on the zig-zag boundary equal to values obtained by linear interpolation between points of a cell just inside the actual boundary. This can lead to an uncertainty in the precise location of the point where the Neumann condition is satisfied, of approximately one mesh length (≈1 mm). This uncertainty is clearly reflected in the variation of the percent errors in the LALA results with cavity radius for the cylindrical cavity problem (see Table 5.1 and Figure 5.12). In order to further substantiate this point, the radial coordinates of the input points No. 11 through No. 19 in Figures 5.3 and 5.4a were increased by 0.455 millimeter (this corresponds to a mere 0.32% increase in the maximum cavity radius) and the problem was solved again. The resonant frequency computed by LACC for this cavity is 806.370 MHz. This figure is substantially closer to the LALA resonant frequency and is 0.30% lower than the LACC result for the smaller cavity. A further increase of 0.7281 millimeter in the z- $\phi$ oordinates of the input points No. 8 through 16 (see Figures 5.3 and 5.4a) results in a resonant frequency of 802.384 MHz. Since for the zig-zag boundary the resonant frequency obtained by the LALA program for this problem lies somewhere between the values obtained by LACC for the original contour (Figure 5.3)\and\the slightly enlarged one, it must be concluded that the zig-zag boundary used in LALA introduces an appreciable error in the resonant frequencies computed by it.

3



The variation of percent errors in the LALA and the LACC resonant frequencies of cylindrical cavities with the cavity radius. The fluctuations in the LALA % error are due to the way LALA handler, the boundary condition.

The agreement between other quantities computed by the two computer programs is fairly good. The results are summarized in Table 5.2. The close agreement of the Q-factor calculations can be attributed to the stationary property of this quantity. The axial emf, power loss and stored energy in the cavity are not given in Hoyt's paper [70].

There are a number of mesh iteration computer programs for linac cavity applications on the market [85-88]. Of these, LALA is probably the most widely used and accepted. With the number of mesh points ranging between 5000 and 15000 LALA can solve a linac cavity problem in 10 to 20 minutes on an IBM 7094 computer [70]. The size of the eigenvalue problem in the example in the previous section was 132. Using an IBM Fortran IV H compiler and an IBM 360/75 computer, the problem solution required 57 seconds (CPU) of arithmetic computing time with LACC. At least 60% of this time was spent on solving the matrix eigenvalue cauation proper. Although it is impossible to make a precise comparison regarding speed, LACC is estimated to be roughly 5 times faster than LALA [89].

require convergence to solve the large, sparse matrix eigenvalue equation with which these programs are associated. However, this convergence should not be confused with convergence to the true solution of the problem; an iterative procedure may converge very nicely to a wrong answer. Another type of convergence is related to the nature of the subspace in which the approximation occurs. This type of convergence has been presented elsewhere [56,58] and is usually illustrated by a

Computer program	Cavity size	Freq. fin MHz	Axial emf V in MegaVolts	Power loss P in Watts	Transit time factor T	Q factor	ZT²/L in Mn/m	Stored energy U in Joules
LACC	original	808.799	148.554	2691.75	0.81475	27887.2	44.965	0.01477
LACC	enlarged in the r direction	806.370	148.563	2696.76	0.81470	27900.9	44.881	0.01485
LACC	enlarsed in the r&z directions	802.384	148.591 ·	2663.31	0.81455	27973.9	45.445	0.01478
LALA*	original	804.80	-	-	0.8180	27890.0	44.04	<b>'-</b>

<sup>\*</sup>LALA results are taken from reference [70]

Table 5.2

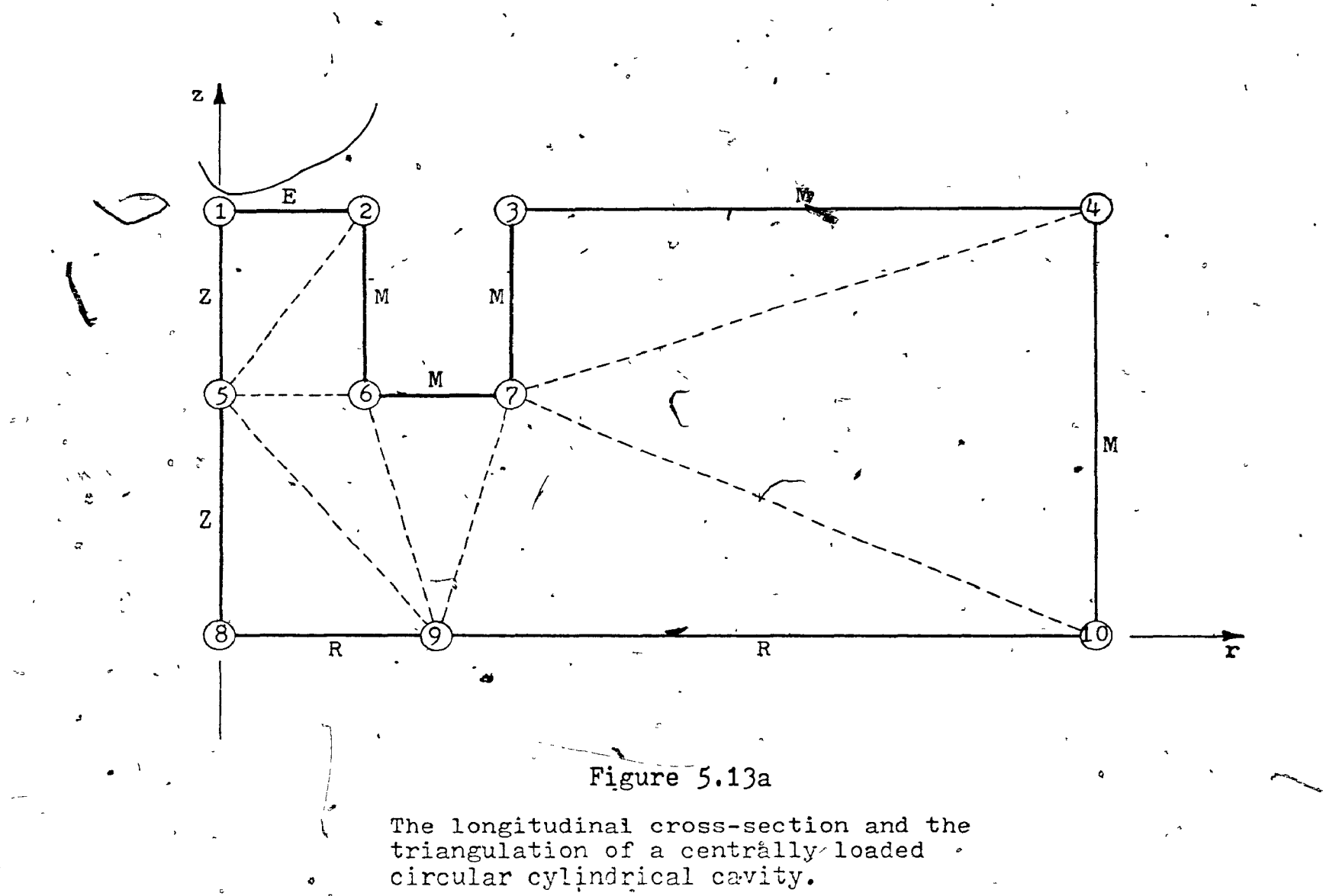
Comparison of the results returned by LACC and by LALA for Hoyt's linac cavity.

plot of the error in the eigenvalues of an analytically solvable problem versus matrix size on a semilogarithmic scale. Curves are often plotted for various orders of polynomial approximation. The results are also valid for the LACC program.

In order to illustrate the accuracy of the LACC program with triangles of various orders, two simple problems will be considered here. The first one consists of a centrally loaded, circular cylindrical cavity similar to the one given in a paper by Hoyt [83]. The longitudinal cross-section of the cavity, the triangulation and the input point and element lists for this problem appear in Figures 5.13a and 5.13b. The second problem is illustrated in Figures 5.14a and 5.14b. In this case there is no sharp re-entrant corner at the drift-tube. The results to these problems are given in Tables 5.3 and 5.4 respectively, where the computing times required are also indicated.

It is evident from the results displayed in Tables 5.3 and 5.4 that the solutions improve with increased matrix size and higher polynomial degree. It is also apparent that the rate of convergence is influenced by the geometry of the problem. The re-entrant corner at the drift-tube walls for the cavity of Figure 5.13a reduces the convergence of the solution since the solution is singular at re-entrant corners. The less pronounced the bend is, the faster the rate of convergence.

For quantities other than frequency and Q, the convergence is not uniform. The nonuniformity is most pronounced in the potential difference V across the cavity. The explanation of this is that the components of  $[H_{\theta}]$  from which V is derived.



\*\*\* INPUT POINT LIST \*\*\*

POINT NO.	HORIZONTAL COORDINATE (CENTIMETER)	VERTICAL COORDINATE (CENTIMETER)
1.	0.0	5.71500
2.	1.90000	5.71500
3.	3.80000	5.71500
4.	11.43000	5.71500
4 • 5 •	0.0	3.21500
6.	1.90000	3.21500
7.	3 - 80000	3.21500
8.	0.0	0.0
9.	2.85000	0.0
10.	11:43000	0.0

# \*\*\* INPUT ELEMENT LIST \*\*\*

								7		
TR	IAVGLE	٧	ERTICES	:		RICHL			GME	
•	NO.	A	В	С		STRAI B_C.		IDEN A_B	B_C	IERS, A_C
	1.	1	2	5	* 1	0	, 1	E	, #	Z
7	2.	6	7	٠ 5	0	0	0	M	*	*
	3.	6	, 9	5	0	0	0	*	*	*
	4.	8	9	5 ۰	0	0	1	R	*	7.
	5 · \ \\ \tau_{\tau}	6	7.	9	0	· C .	0	M.	*	*
	6.	9 (	10	7	, 0	0	0 "	R	*	*
	7.	4	10	7	0	n	0	H	*	<b>*</b> ,
	8•	7	3 \	4	0	0	O' ,	M	M	*

# Figure 5.13b

Input point and input element lists for a centrally loaded circular cylindrical cavity (see Figure 5.13a).

	•		,			
N	1	2	3	4	5	.6
n	6 •	20 .	42	72	110	156
t(sec) ·	4.2	4.8	7.0	14.1	34.7	83.0
f(MHz)		876.545	848.488	837.671	834.109	832.773
· <u>V(MV</u> olts)		ı		`		
	2506.31	•				i
T		1	.808113			
U(Joules)	.011912	.011178	.012838	.012736	.012799	.012819
Q	27291.6	23237.6	22167.4	21517.5	21409.2	21341.0
ZT2/L (M1/m)	45.6049	43.1424	37.0194	36.6893	36.4817	36,3665

N: the degree of the interpolation polynomials used

n: the size of the eigenvalue problem

t: computing time (CPU)

#### Table 5.3

Results obtained for the centrally loaded circular cylindrical cavity described in Figures 5.13a and 5.13b. The computing times required are indicated.

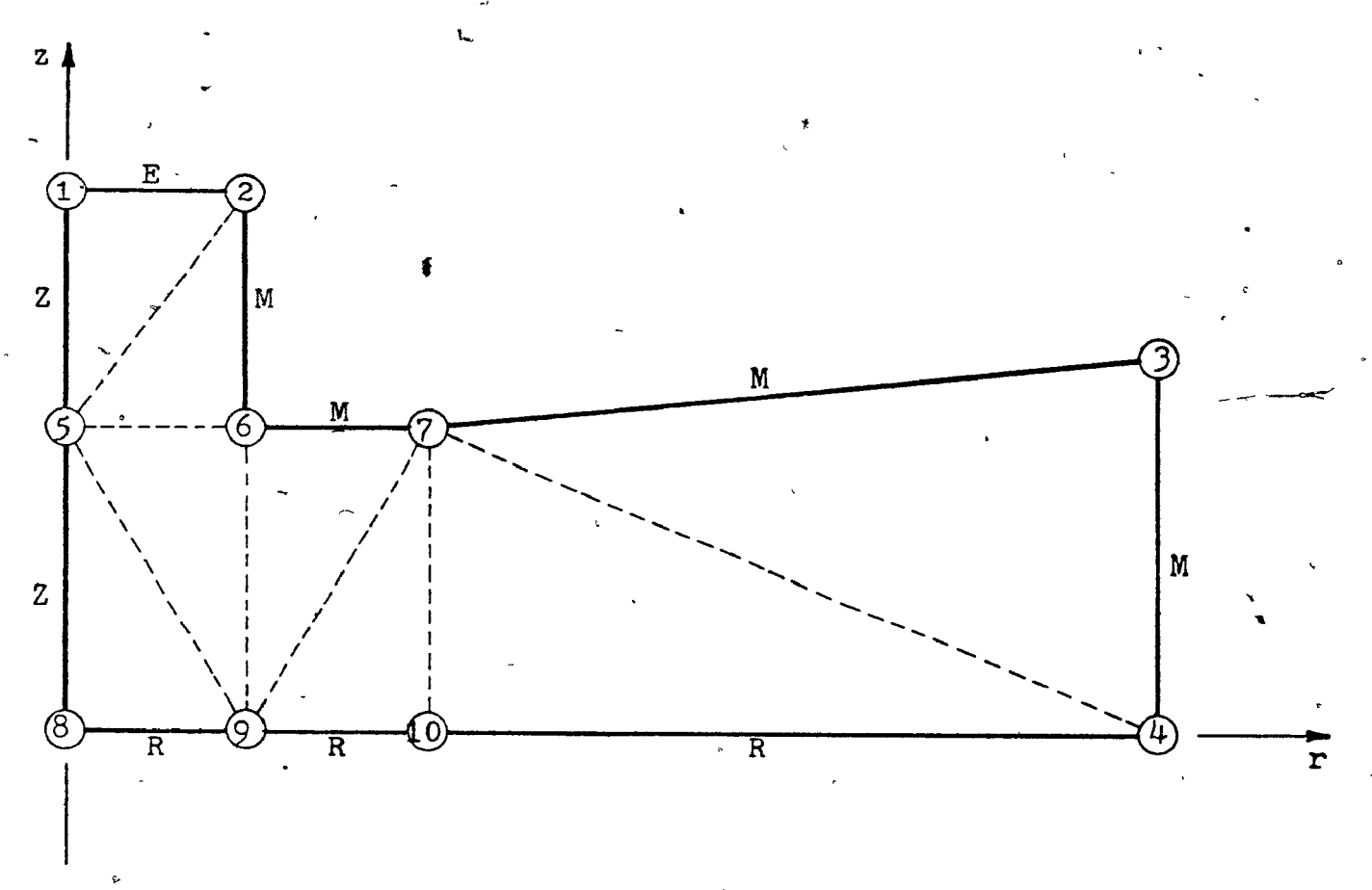


Figure 5.14a

The longitudinal cross-section and the triangulation of a cavity in which the drift-tube outer edge is not sharp.

#### \*\*\* INPUT POINT LIST \*\*\*

POINT	HORIZONTAL	VERTICAL
NO.	COORDINATE	COORDINATE
	(CENTIMETER)	(CENTIMETER)
1.	0.0	5.71500
2. ·	1.90000	<b>5.7</b> 1500
3.	11.43000	4.00000
4.	11.43000	0.0
5.	0.0	3.21500
6.	1.90000	3.21500
7. /	3.80000	3.21500
8	0.0	0.0
9.\	1.90000	0.0
. 10.	3.80000	0.0

#### \*\*\* INPUT ELEMENT LIST \*\*\*

TRIANGLE		VERTICES:			DIRICHLET CONSTRAINTS "			SEGMENT IDENTIFIERS		
	NO.	Δ	B	С		B_C	V_C	V_B	B_C	V_C
•	1.	1	2	5	l	0	1	Ę	×	Z
,	2.	6	2	5	0	0	0	M	*	*
	3.	6	9	5	0	0	0	*	*	*
	4.	8	9	5	0	0	1	R	*	Z
	5.	6	7	9	0	. 0	0	М	*	*
	6.	9 â	10	7	0	0	0	R	*	*
	7.	4	10	7	0	0 -	0	*	*	*
	8 •	7	3	4	0	0	0	M	M	*

# Figure 5.14b

Input point and input element lists for a cavity in which the drift-tube outer edge is not sharp (see Figure 5.14a).

N	1	2	3	4 .	5	6',
n	6	20	42	72	110	156
t(sec)	4.1	4.5	6.7.	13.4	33.0	80.0
f(MHz)	1001.39	067.025	964.923	964.689	964.415	964.301
V(MVolts)	139.874	135.409	139.915	138.563	137.962	138.076
P(Watts)	4137.51	4401.48	4672.15	4559.67	4558.65	4546.78
<u>T</u>	.817164	.844110	.816925	.824893	.828490	.827808
U(Joules)	.014367	.014754	.015602	.015255	.015252	.015215
Q	21847.4	20366.9	20246.2	20278.3	20274.0	20275.6
ZT²/L (MΩ/m)	27.6253	<b>25.</b> 9685	24.4641	25.0676	25.0732	25.1387

N: the degree of the interpolation polynomials used

n: the size of the eigenvalue problem t: computing time (CPU)

# Table 5.4

Results obtained for the cavity described in Figures 5.14a and 5.14b. The computing times required are indicated.

are not variationally stationary, but that frequency is variationally stationary, being related to the Rayleigh quotient. Indeed, the values computed are guaranteed to be an upper bound to the true frequency [37]. The Q-factor has has similar properties.

One additional comparison between the results obtained from LALA and LACC is possible. Hoyt has obtained the following results for the cavity of Figure 5.13a [83]

frequency: 838 MHz

Q-factor: 21830

Transit time factor T: 0.802

axiaf emf V:  $178 \text{ KV} \times 0.8 = 142.4 \text{ KV}$ 

ŹT<sup>2</sup>/L: 36.6 Mn/m

These values have roughly the same accuracy as the finite element results obtained with N=3 and N=4, as presented in Table 5.3, and are less accurate than the higher order results.

A general moral can be drawn from the above material:

it is insufficient to run a computer program only once and

to accept the results as definitive. One must be aware of the

limitations as well as the advantages of the method used.

All conclusions must be based on a comparison of the results

from different working programs based on several methods;

experimentation and analysis of every published computer /

program should be carried out in detail .

Of course, further improvements in LACC can be made, both with regard to speed and accuracy. LACC already incorporates

major improvements over the precedent program, AXISYMM-VECTOR-HELMHOLTZ-FINTEL6. The memory requirements of these programs are problem dependent and are essentially determined by the size of the global coefficient matrices [S] and [T]. As it stands, LACC requires 300K bytes of core.

(

The accuracy of LACC could be further improved by storing the constant finite element matrices [R], [Q<sub>111</sub>], [Q<sub>221</sub>], [Q<sub>121</sub>], [Q<sub>121</sub>], [U<sub>11</sub>], [U<sub>21</sub>], [Y<sub>11</sub>] and [Y<sub>21</sub>] (discussed in section 5.3) in double precision in the block data subprograms. This would require an extra 7551 words ( $\approx$ 30K bytes) of storage. The improvement in accuracy would probably appear in the 5-th or 6-th significant figures and would become noticeable when many high-order triangles are used. Accuracy improvements could also be brought about in some of the derived quantities by improving the procedures used to differentiate  $H_{\theta}$ .

Computing speed may well be improved by switching to an iterative method to solve the matrix eigenvalue problem. However, this would limit the program to the computation of only the fundamental mode, and rob the program of one of its nicest features.

# 5.8 Field Computation for Other Types of Cavities by the LACC Program

The LACC computer program has the capacity to compute all of the  $TM_{mn0}$  modes under the assumptions given in section 5.2. Toroidal resonators (i.e. resonators for which the z-axis is excluded from the solution region) may be treated as well

as cylindrical ones [52]. There are microwave power tubes that employ cavities with cylindrical symmetry (e.g. klystron buncher cavities, cvaxitrons) and operate in the TM<sub>010</sub> mode, the mode used by linear accelerator cavities, but with a frequency above 1 GHz. In previous applications, the LALA computer program has been used to design such cavities with success [90].

There are applications where it is desirable to operate in the neighbourhood of or above 10 GHz. Unfortunately, the size of a cavity that would operate at such frequencies in the  $TM_{010}$  mode is impractically small. Designers have tried to avoid this dilemma by operating some cavities in higher-order modes. For example, Hant and Seeger recently presented a modified conical cavity for millimeter and submillimeter wave applications [92] that would operate in the  $TM_{0n0}$  modes for n=5 to n=9. The maximum cavity radius used is 7.63543 centimeters while the wavelength ranges from about 1.5 centimeters to 3.73 centimeters.

Hant and Seeger performed an analysis of the cavity using analytical methods to obtain the fields and the frequency at resonance. The shape and dimensions of their cavity are reproduced in Figure 5.15. The diagram shows that the cavity is made of three distinct parts: a cylindrical waveguide (beam hole), a parallel-plate radial guide and a quasi-wedge radial waveguide. Each of these three components are tractable analytically although the analysis of Hant and Seeger is fairly long and tedious. In addition, even though difficult transcendental functions are employed, the analysis involves a

number of approximations. At the end of the analysis, the authors present design curves for a modified conical cavity without the beam hole, arguing that in many applications the beam hole diameter is small and may be neglected.

Using LACC, the solution of this problem can be obtained by an engineer in a matter of minutes. Only the input point and input element lists need to be calculated by hand (see Figures 5.16b and 5.16c); a representative triangulation is presented har Figure 5.16a. The drift-tube has been omitted here except for the region involving the parallel plate radial guide. The solution obtained is actually that of a davity without a beam hole (i.e. completely scaled) but the power loss and hence the Q-factor are computed as if a hole of radius 0.509 cm existed in the center of the cavity. Table 5.5 contains the resonant frequencies and the Q-factors computed by LACC together with the resonant frequencies estimated from the design curves of Hant and Seeger. The general behaviour of the Q values computed by LACC follows the design curves of Hant and Seeger.

Contour plots obtained for the  $TM_{050}$  mode are displayed in Figures 5.17a through 5.17d. The most illustrative among these plots is Figure 5.17b where lines of constant. If are shown and the five maxima and minima are clearly distinguishable. The electric field components which are obtained by differentiating  $H_{\theta}$  display remarkably smooth contours, keeping in mind that the  $TM_{050}$  mode is the 11-th eigenfunction returned by LACC.

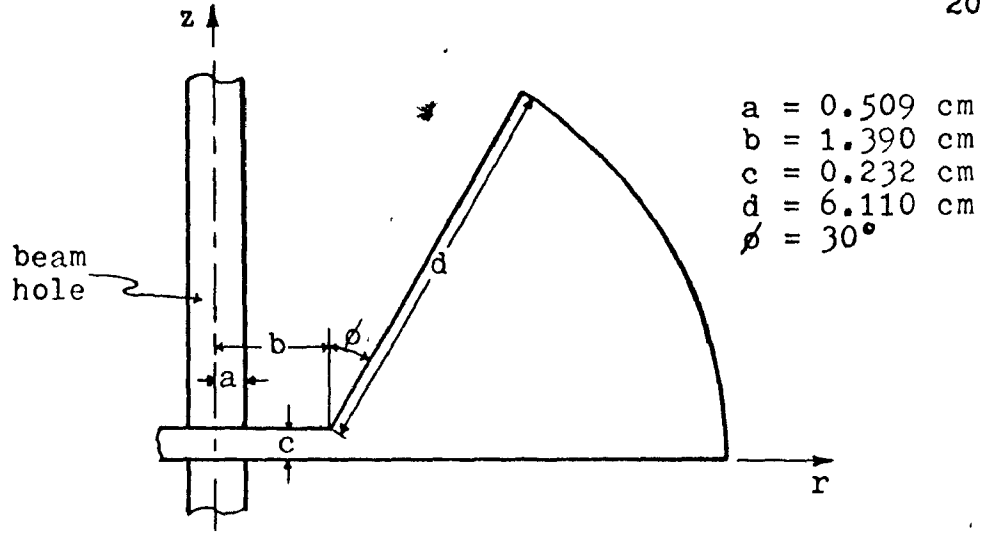


Figure 5.15

Shape and dimensions of the modified conical cavity of Hant and Seeger.

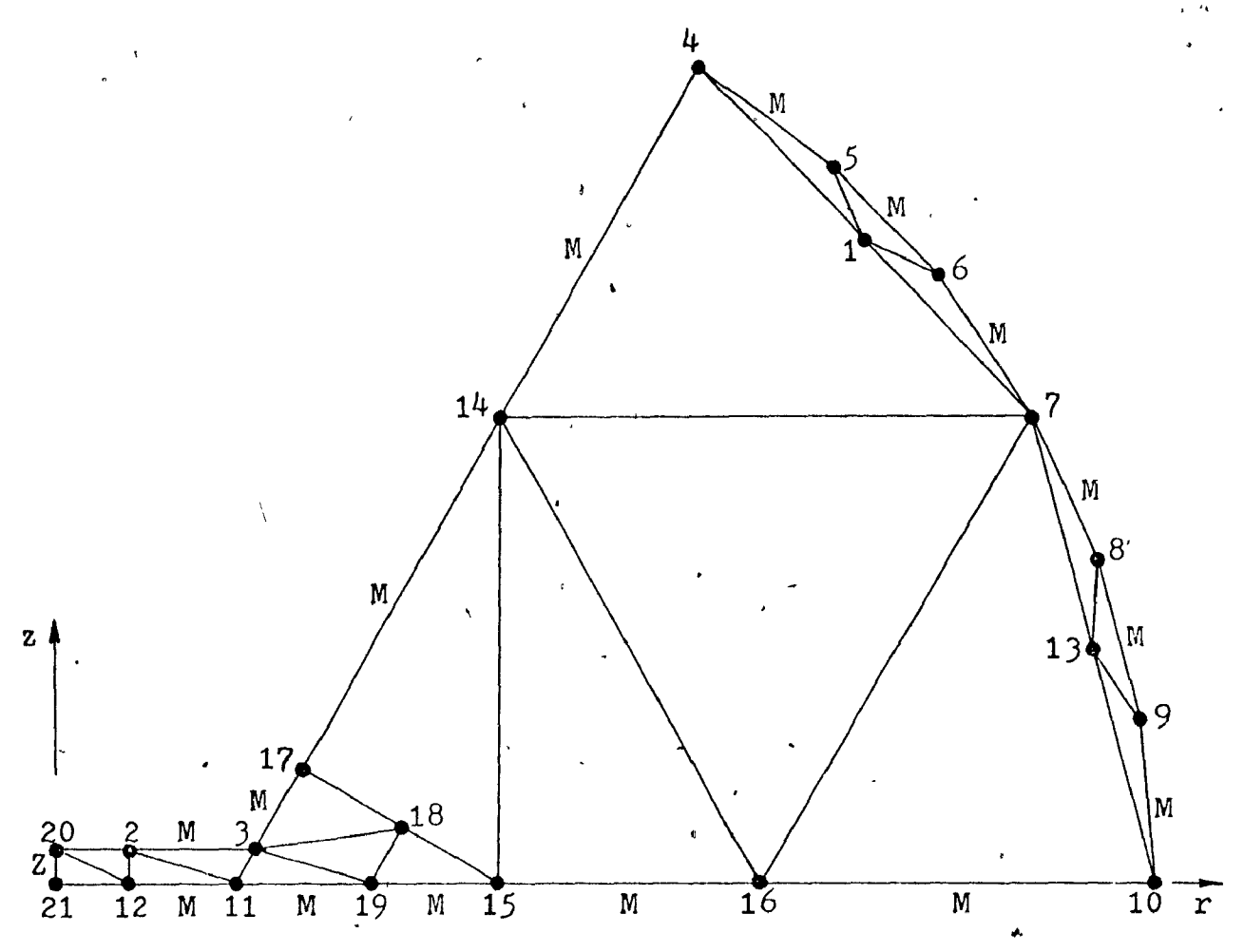


Figure 5.16a

Triangulation of the region of solution for the modified conical cavity of Hant and Seeger. The drift-tube has been omitted except in the region of the parallel plate radial waveguide.

### \*\*\*\* MCDIFIED CENICAL CAVITY FOR SUB-MM WAVES \*\*\*\*

SCALE = 1.00 MORIZONTAL	SCALE =	1.00	HOR I ZONT AL
-------------------------	---------	------	---------------

SCALE = 1.00 VERTICAL

#### \*\*\* INPUT POINT LIST \*\*\*

POINT	HORIZONTAL /	VERT ICAL
NO.	COORDINATE	COORDINATE
	(CENTIMETER)	CENTIMETER)
•		
1.	5.61418	4.35518
2.	0.50900	0.23200
3.	1.39000	0.23200
4.	4.44722 '	5.52215
5.	5.35769	4.88463
6.	6.14363	4.09869
7.	6.78115	3.18821
8.	7.25088	2.18087
9.	7.53856	1.10725
10.	7.63543	0.0
11.	1.25900	0.0
12.	0.50900	0.0
13.	7.20829	1.59410
14.	3.09971	3.18821
15.	3.09971	0.0
16.	4.94042	0.0
17.	1.67059	0.71294
18.	2.38515	0.35647
19.	2.17935	0.0
20.	0.0	0.23200
21.	. 0.0	0.0
<del>-</del> -		~ - ~

## Figure 5.16b

Input point list for the modified conical cavity of Hant and Seeger (see Figure 5.16a).

## \*\*\*\* MODIFIED CONICAL CAVITY FOR SUB-MM WAVES \*\*\*\*

\*\*\* INPUT ELEMENT LIST \*\*\*

									,	
TRIANGLE	ORDER		VERTICE	<b>S</b> :	DIR	ICHL	. E T	SE	EGME	NT
					CDNS	TRA	INTS	IDEN	NTIF	IERS
NO.	N	Δ	В	С	A_B.	B_C	4_C	<b>A_</b> B	8_C	<b>v</b> _c
1.	3	، 2	~ 11	12	0	0	0	*	М	*
2.	3	20	<sub>η</sub> 2	12	0	0.	0	*	*	*
3.	3	20	′′ 21	12	1	0	0	7	*	*
4.	3 3 3	2	3	11	0	0	0	М	, *	*
5.	<b>`</b> 3	19	3	11	0	0 -	0	**	*	м -
6.	3 * '	19	3	18	0	0	0	*	*	*
7.	3	17	3	18	0	0 🕹	0	М	*	*
8.	3	19	15	18	0	0	0	M	*	*
9.	6,	17	14	15	0	0	U	11	*	*
10.	6	16	] 4	15	0	0	O	*	*	М
1,1 •	6	16	14	7	0	0	O	*	*	*
12.	6	14	4	7	0	0	0	М	*	*
13.	6	16	10	7	0	0	0	M	*	*
14.	3	4	5	l	0	0	0	М	*	*
15.	3	5	6	1	0	0	0	M	*	*
16.	3	6	7	1	0	0	0	М	*	*
17.	3	7	. 8	13	0	0	Ō	М	*	×
18.	<b>`3</b>	8	9	13	Ô	0	ō	М	*	*
19.	3	9	10	13	Ö	0	, ŏ /	М	*	*

Figure 5.16c

Input element list for the modified conical cavity of Hant and Seeger (see Figure 5.16a).

LACC	7	N=1 and 2 n=27		N=2 and 4 n=88		N=3 and 6 n=183		Hant and Seeger design curves:	
Mode No.	Mode Type	f MHz	· Q	f MHz	Q	f MHz	Q	f MHz	
1.	TM010	750.019	9125.59	706.449	8738.83	700.823	8691.51	-	
2,	TM020	3067.89	11382.3	3019.49	11182.1	3013.90	11144.6	-	
4.	TM <sub>030</sub>	5588.34	12167.4	5361.93	12678.7	5356.39	12670.5	5091.0	
7.	TM <sub>040</sub>	8477.62	12359.4	7630.12	12153.9	7614.73	12220.7	7576.9	
11.	TM <sub>050</sub>	11180.8	11811.2	9718.95	9892.23	9670.06	9807.68	9523.6	
14.	TM060	14425.1	14184.8	11503.0	9807.12	11403.8	9327.10	11403.	
18.	<sup>TM</sup> 070	20490.6	15994.6	13715.2	14312.0	13219.6	13815.6	13321.	

N: order of approximation n: overall matrix size

Table 5.5 LACC results for the modified conical cavity.

- E

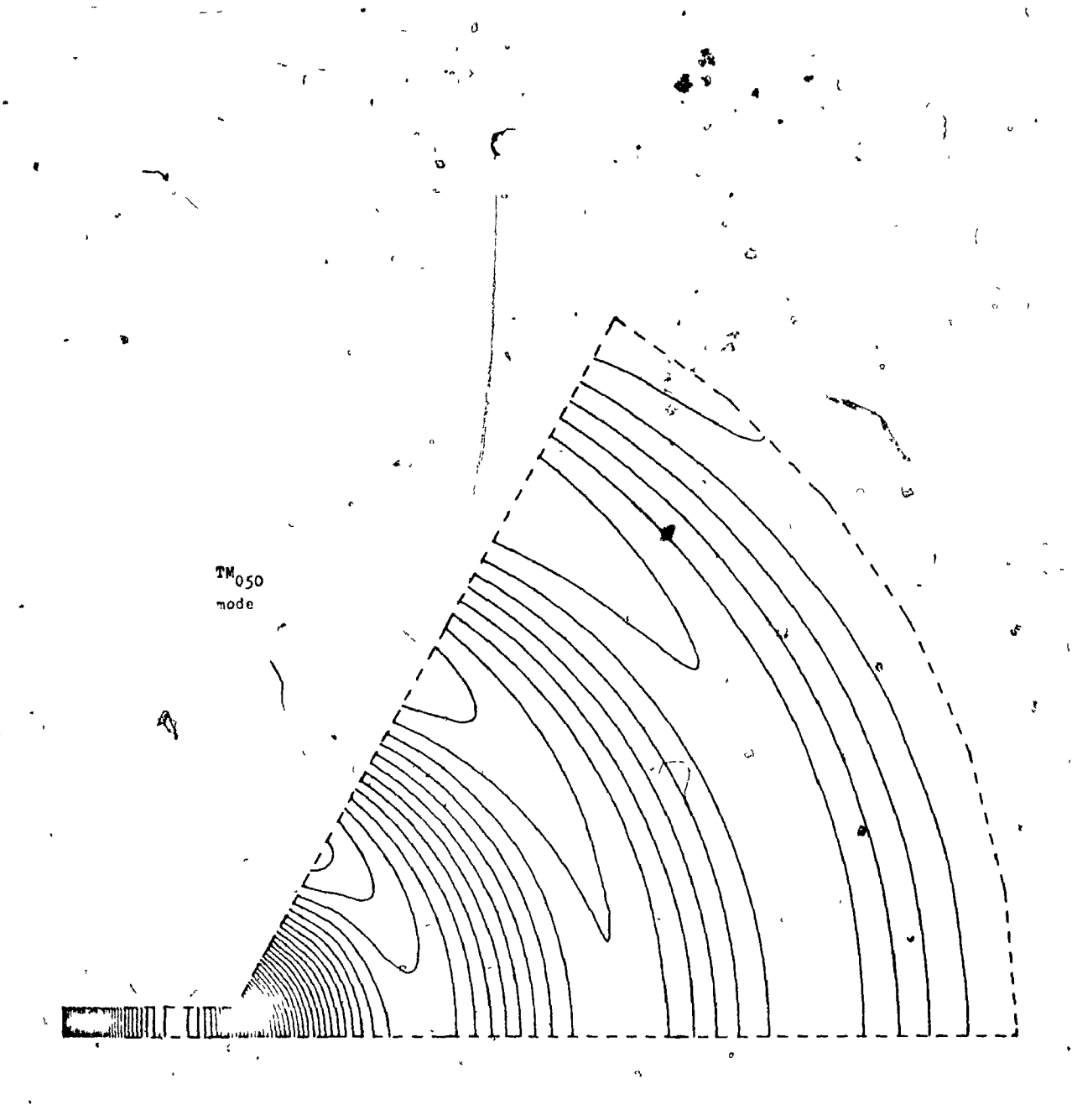


Figure 5.17a

Lines of constant  $H_{\theta}$  for the modified conical cavity.

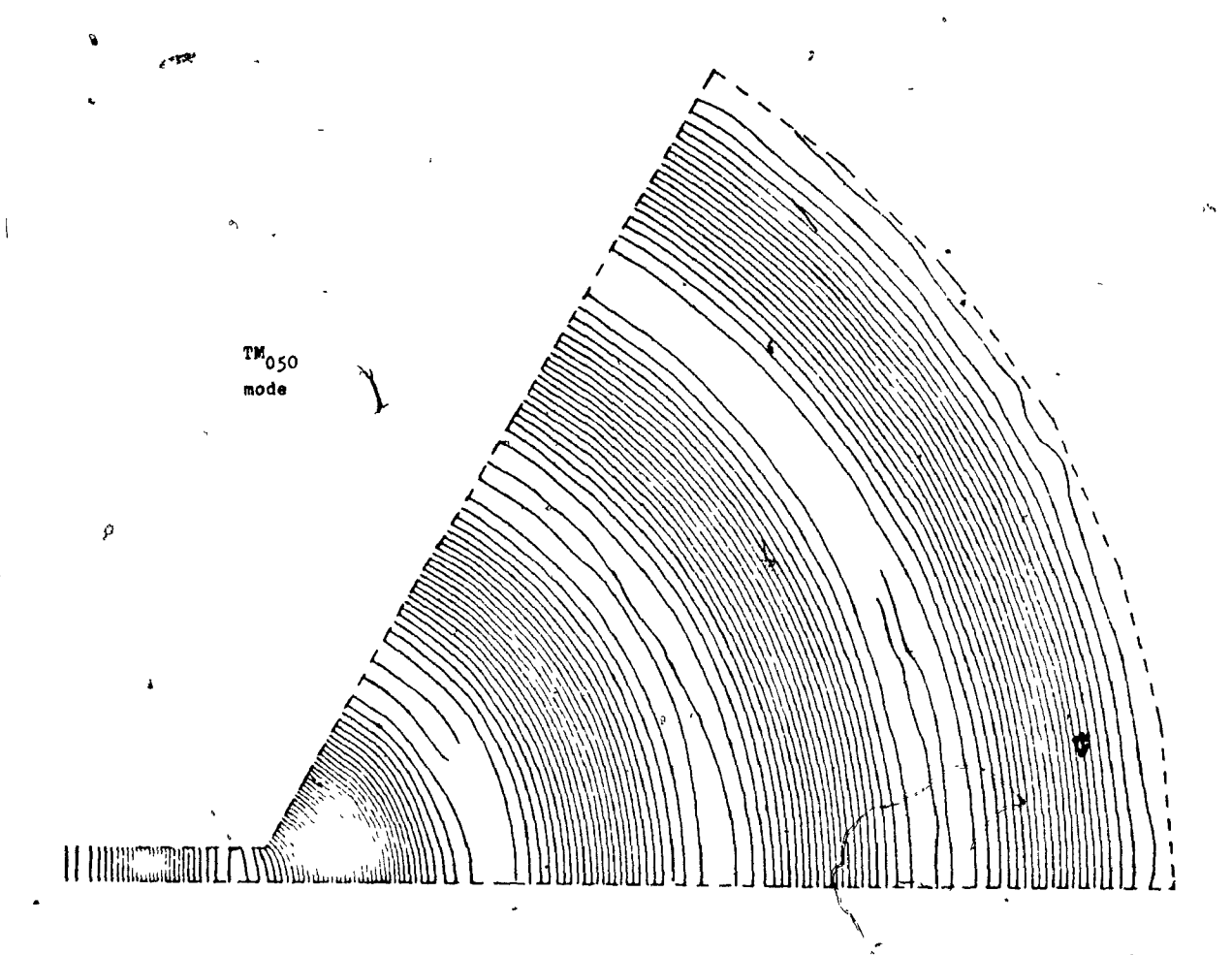


Figure 5.17b

Lines of constant  $\mathfrak{F}$  (= rH<sub>0</sub>) for the modified conical cavity. Maxima and minima are situated where the lines are sparse.

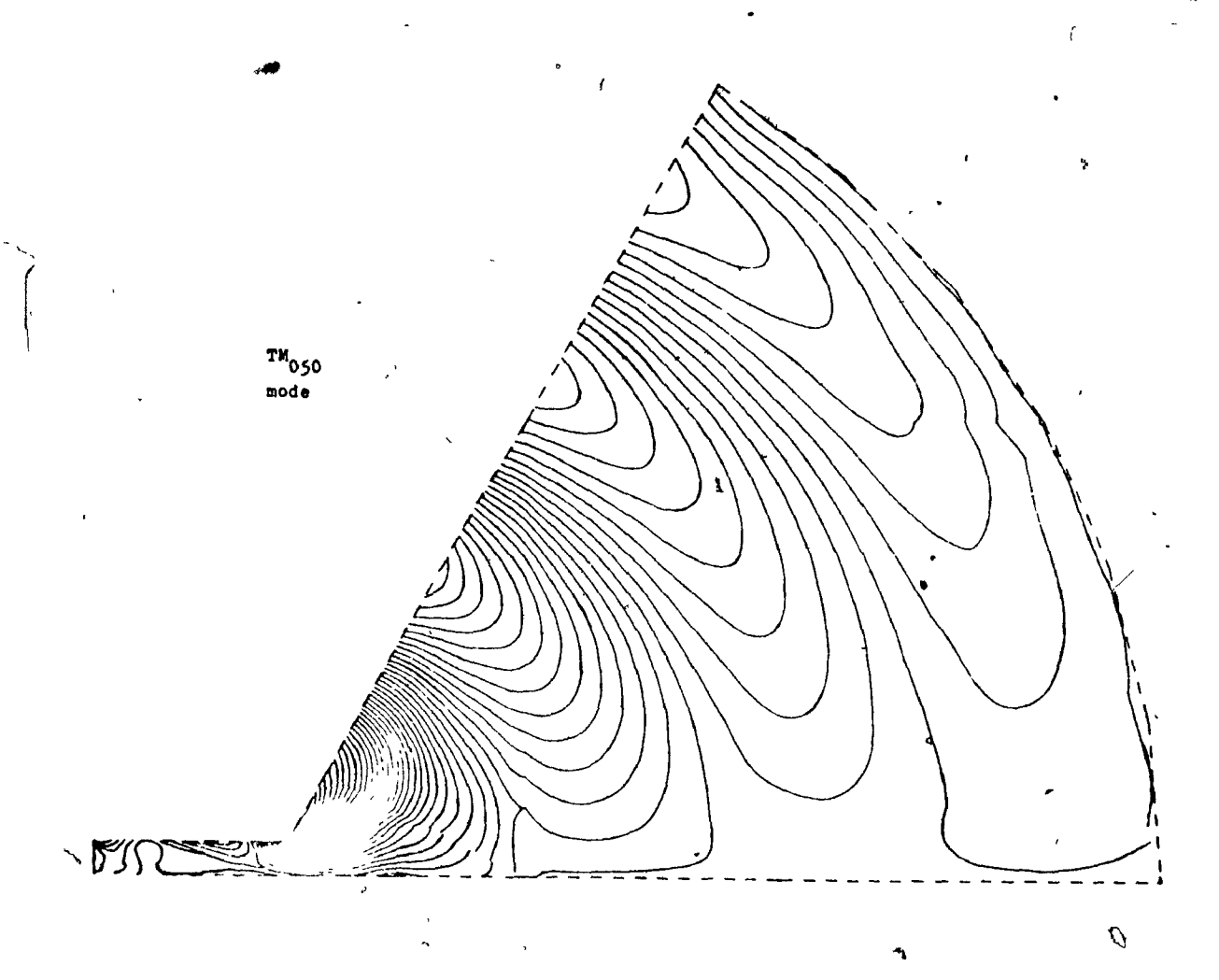


Figure 5.17c . Lines of constant  $\mathbf{E_r}$  for the modified conical cavity.

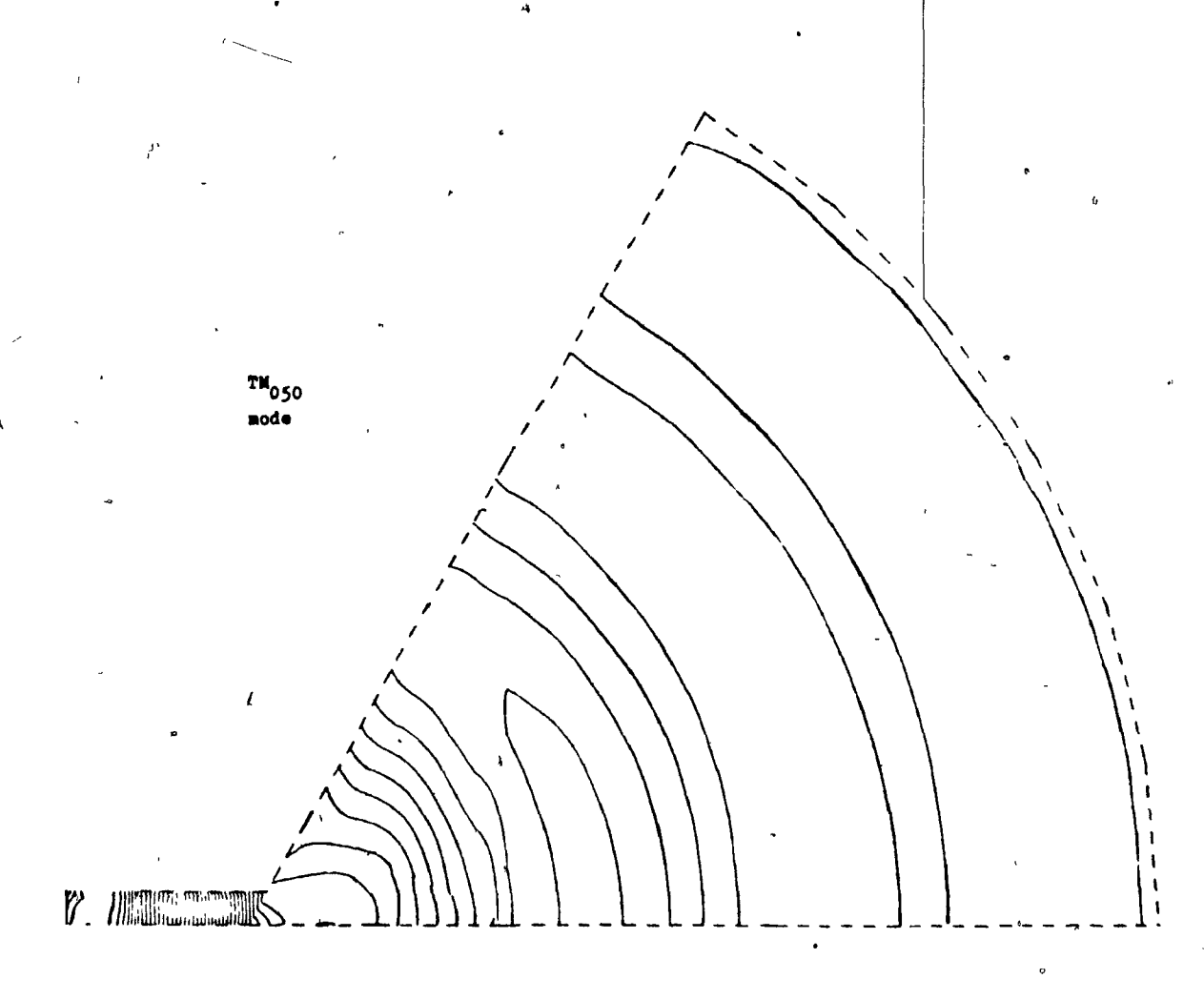


Figure 5.17d

Lines of constant  $\mathbf{E}_{\mathbf{Z}}$  for the modified conical cavity.

#### CHAPTER VI

#### CONCLUSIONS AND RECOMMENDATIONS

### 6.1 Summary

A finite element formulation of bounded electromagnetic field problems has been presented in which the medium may be anisotropic but must be linear and loss-free. This formulation has two main features:

- (1) the general description of electromagnetic fields presented in Chapters I and II and the adoption of the generalized curlcurl equation as the governing differential equation;
- (2) the choice of high-order polynomial triangular finite elements to solve the electromagnetic boundary value problem.

The generality and elegance of the method can be attributed mainly to the first aspect of the formulation mentioned above.

Maxwell' equations, though concise and clear from the mathematical point of view, do not easily lend themselves to a variational finite element approach. The curlcurl equation is an attractive alternative, especially since it is satisfied by both the electric and the magnetic field intensities. The vector Helmholtz equation, often used in its stead, is a special form applicable only to non-divergent electromagnetic fields and can in fact be derived from the curlcurl equation. Thus, a large variety of problems can be solved from the curlcurl equation including fields both in isotropic and anisotropic, homogeneous and in homogeneous media. The work presented in this thesis has been

restricted to source-free, non-conductive media, but the approach has a great potential for further development in the area of diffusion problems for conductive media, including anisotropic conductors, and also problems in which sources are involved.

Although primarily intended to demonstrate the new approach, it is hoped that the three-component magnetic field vector program of Appendix IV will be used to solve many more waveguide problems in addition to the ones given in Chapter IV. This is expected to be the case on the other hand with the linear accelerator cavity field analysis program LACC which rivals existing programs based on finite difference methods and demonstrates how far programming can be carried from a practical viewpoint.

### 6.2 Advantages and Disadvantages of the Method

An inherent advantage of the present three-component vector formulation is the absence of singularities at  $\beta=k'$  (air line) and  $\beta=\sqrt{\epsilon_r}\,k$  (dielectric line) on the dispersion diagram for inhomogeneous, isotropic problems. This advantage arises because the wave-number k and the propagation constant  $\beta$  (or the circulation constant m for axisymmetric problems) appear independently of the material property tensors. Another important positive factor in the present formulation is the possibility of choosing various types of waves, depending upon the choice of the material property tensors. The development in this thesis has pursued only linearly polarized travelling

waves and circulating waves; evanescent waves and circularly or elliptically polarized travelling waves can also be treated along similar lines.

The advantages of choosing the variational finite element method to solve the boundary value problem are many. For isotropic media, the curlcurl operator is positive self-adjoint and hence the minimum theorem applies. For lossless anisotropic media, the material property tensors are Hermitian and the self-adjoint property is preserved. Since the boundary conditions on the magnetic field intensity vector  $\overline{H}$  at perfect electric conductors are natural for the functionals derived in this thesis, physically meaningful solutions can be obtained even if no boundary conditions are explicitly enforced. Either the dielectric properties may be inhomogeneous or the magnetic properties may be, but not both because the interface conditions are satisfied automatically provided that the  $\overline{H}$  field vector is chosen for electric inhomogeneities and the  $\overline{E}$  field vector for magnetic inhomogeneities.

In addition to the advantages of the variational finite element method mentioned above, it should be noted that the eigenvalues returned are always upper bounds; therefore highly accurate solutions can be obtained by increasing the number of degrees of freedom for any particular problem. Even so, the matrix size remains relatively small compared to finite difference methods, permitting the use of direct methods to solve the eigenvalue problem.

The choice of triangular element shape has both advantages and disadvantages. Its chief advantage is that an arbitrary

polygon can be represented exactly by unions of triangles. Further, the integrations in the functional formulation can be carried out once and for all explicitly by separating shape, size and position describing factors from the integrations themselves. Thus the expensive computations required to obtain element matrices need not be repeated for every problem and solution times depend almost entirely on the matrix size, and on the 'equation solving' algorithms employed rather than the matrix assembly.

Although programming the finite element method using high-order interpolation polynomials is relatively complicated, it has the advantage that a general program may be written to solve a large category of problems. Data preparation for these general programs is relatively simple.

As for disadvantages, it must be pointed out that triangles with straight edges are not perfectly suited to model curved boundaries. Mixing triangular elements of various polynomial orders is a good way of handling such boundaries, but still leaves room for improvement.

Although the matrix size in a finite element formulation is usually very much smaller than in a finite difference method, in this case it is still quite large in view of the fact that three unknowns must be considered for every interpolation node. This creates difficulties with regard to computer memory requirements. The explicit enforcement of boundary conditions on the magnetic field vector  $\overline{H}$  would be useful in saving computer memory. The computer program LACC does not of course suffer from this shortcoming, but it would benefit from

exploitation of the sparsity of the coefficient matrices.

The presence of spurious, non-physical solutions in eigenvalue problems involving all three components of  $\overline{H}$  is a very annoying feature. Spurious modes can and should be filtered out by explicitly enforcing the boundary conditions at the metal walls and by reducing the coefficient matrix to full rank. As the program stands, analyzing results obtained by the three-component magnetic field vector program of Appendix IV can be a frustrating experience because of the presence of spurious modes.

A complete k-ß diagram can be obtained with the three-component magnetic field vector program for any bounded linear waveguide. However, the use of the program is restricted by the fact that a complete dispersion diagram is relatively expensive to produce. It is suggested that the modal approximation technique [8,12] be employed in the future in order to reduce costs.

The boundary condition  $\overline{n} \times \overline{E} = 0$  must be incorporated in the present program in order to make it capable of solving  $\overline{E}$  field problems. This addition is absolutely necessary for solving problems with inhomogeneities in the permeability tensor. There are abundant practical applications, for example phase shifters using ferrite slabs, which cannot be tackled with the present  $\overline{H}$  field program but could be treated with an  $\overline{E}$  field program. Also, in connection with the boundary condition  $\overline{n} \times \overline{H} = 0$ , it should be mentioned that this condition would make the three-component magnetic field vector program capable of exploiting symmetry; it is very desirable to employ

symmetry arguments since it reduces the matrix size.

Another restriction in the present formulation is that the material property tensors must be constant in every triangular element. For inhomogeneous media, the discontinuities in the material property tensors must therefore be step-like; smoothly varying permittivities or permeabilities could be handled, although they would complicate the formulation. Moreover, the method presented in this thesis has been restricted to frequency independent material property tensors. It is mainly a matter of numerical analysis and not of electromagnetic theory to extend the methodology to include the frequency dependence of the material property tensors.

Although the element matrices have been computed exactly, they are truncated to single precision word length (i.e. seven significant figures on the LBM 360/75 computer) in the block data subprograms. This introduces some error in the solutions, especially when many higher-order elements are used. Accuracy could be improved in these cases by storing the element matrices in double precision at the expense of using more computer memory. Ideally, one would like the computer program to perform the computations in integer arithmetic. Unfortunately, Fortran IV compilers on IBM computers restrict the use of integers to magnitudes less than  $2^{31}$ -1. The high-order element matrices in exact integer quotient form contain numbers which are close to or exceed this limit.

At present, double precision arithmetic is required in order to produce accurate solutions because round-off errors may accumulate in single precision computation for larger

matrix size. If the programs are ever rewritten or perfected, substantial savings in computer memory would result from using an iterative clean-up procedure instead of double precision arithmetic.

# 6.3 Recommendations for Further Research

Some recommendations for further work are implicit in the discussion given in the previous section. These recommendations are of a type which could be performed immediately and would perfect and extend the present computer programs in useful ways. For example, the formulation of the three-component axisymmetric vector problem has been given in general in the thesis and the required element matrices have all been computed. However, only a special case has been programmed in the LACC program. Another example is the three-component magnetic field vector program which could be modified in such a way that the propagation constant \$\begin{align\*} \text{could} \text{ be computed for any given value} \text{ of the wave-number } \text{ k. Further, the three-component magnetic field vector program could easily be modified to accept complex values in order to solve for waves which have complex propagation constant.

A logical extension of the method would be to the lossy case since losses are important in most practical anisotropic waveguide problems [48.93-95]. Since the material property tensors are not Hermitian for lossy media, the differential operator is not self-adjoint in this case. Consequently, the functionals derived for the loss-free case do not apply and new, bivariate functionals would need to be derived.

Finally, it should be noted that in addition to anisotropic media there exist media which are bianisotropic [96]. For such media the magnetic and electric flux densities depend upon both the electric and the magnetic field intensities. Consequently, the curlcurl operator needs to be extended for this case. The finite element formulation of the corresponding bianisotropic electromagnetic field problem is a logical possibility.

#### REFERENCES

- [1] A. Wexler, "Computation of electromagnetic fields",

  IEEE Trans. Microwave Theory Tech., Vol.MTT-17, No.8,

  Aug. 1969, pp.416-439.
- [2] R. F. Harrington, <u>Field Computation by Moment Methods</u>,
  New York: Macmillan, 1968.
- [3] R. R. Gupta, "A study of cavities and waveguides containing anisotropic media", Ph.D. Thesis, Syracuse Univ., July 1965.
- [4] C. D. Hannaford, "The finite difference/variational method for inhomogeneous isotropic or aniostropic waveguides", Ph.D. Thesis, University of Leeds, Febr. 1967.
- [5] D. G. Corr and J. B. Davies, "Computer analysis of the fundamental and higher ord r modes in single and coupled microstrip", IEEE Trans. Microwave Theory Tech.,

  Vol.MTT-20, No.10, Oct. 1972, pp.669-678.
- [6] J. S. Hornsby and A. Gopinath, "Numerical analysis of a dielectric-loaded waveguide with a microstrip line finite-difference methods", IEEE Trans. Microwave Theory Tech., Vol.MTT-17, No.9, Sept. 1969, pp.684-690.
- [7] Z. J. Csendes and P. Silvester, "Numerical solution of dielectric loaded waveguides: I finite-element analysis", IEEE Trans. Microwave Theory Tech., Vol.MTT-18, No.12, Dec. 1970, pp.1124-1131.

- [8] Z. J. Csendes and P. Silvester, "Numerical solution of dielectric loaded waveguides: II modal approximation technique", IEEE Trans. Microwave Theory Tech., Vol.MTT-19, No.6, June 1971, pp.504-509.
- [9] P. Daly, "Hybrid-mode analysis of microstrip by finiteelement methods", IEEE Trans. Microwave Theory Tech., Vol.MTT-19, No.1, Jan. 1971, pp.19-25.
- [10] M. K. Krage and G. I. Haddad. "Frequency-dependent characteristics of microstrip transmission lines", IEEE Trans. Microwave Theory Tech., Vol.MTT-20, No.10, Oct. 1972, pp.678-688.
- [11] D. G. Corr, J. B. Davies and C. A. Muilwyk, "Finite-difference solution of arbitrary-shaped dielectric loaded waveguides, including microstrip and coaxial structures", U.R.S.I. Symposium on Electromagnetic Waves, Stresa, Italy, 24th June, 1968.
- [12] Z. J. Csendes, "Solution of dielectric loaded waveguides by finite element methods", M.Eng. Thesis, McGill Univ.,
  March 1970.
- [13] A. D. Berk, "Variational principles for electromagnetic resonators and waveguides", IRE Trans. Antennas and Propagation, Vol.AP-4, April 1956, pp.104-111.
- [14] D. T. Thomas, "The role of boundary conditions in variational techniques", Technical Memorandum, Bell Telephone Laboratories Inc., Whippany, N.J., July 3, 1969.

- [15] D. T. Thomas, "Functional approximations for solving boundary value problems by computer", IEEE Trans.

  Microwave Theory Tech., Vol.MTT-17, No.8, August 1969, pp.447-454.
- [16] P. Silvester and Z. J. Csendes, "Numerical modeling of passive microwave devices", IEEE Trans. Microwave Theory Tech., Vol.MTT-22, No.3, March 1974, pp;190-201.
- [17] J. B. Davies, "Review of methods for numerical solution of the hollow-waveguide problem", Proc. IEE, Vol.119, No.1, Jan. 1972, pp. 33-37.
- [18] F. L. Ng, "Tabulation of methods for the numerical solution of the hollow waveguide problem", IEEE Trans.

  Microwave Theory Tech., Vol.MTT-22, No.3, March 1974, pp.322-329.
- [19] W. J. English and F. J. Young, "An E vector variational formulation of the Maxwell equations for cylindrical waveguide problems", IEEE Trans. Microwave Theory Tech., Vol.MTT-19, No.1, Jan. 1971, pp.40-46.
- [20] W. J. English, "Variational solutions of the Maxwell equations with applications to wave propagation in inhomogeneously filled waveguides", Ph.D. Thesis, Carnegie Institute of Technology, Aug. 1969.
- [21] W. J. English, "Vector variational solutions of the inhomogeneously loaded cylindrical waveguide structures", IEEE Trans. Microwave Theory Tech., Vol.MTT-19, No.1, Jan. 1971, pp.9-18.

- [22] Y. Satomura, M. Matsuhara and N. Kumagai, "Analysis of electromagnetic-wave modes in anisotropic slab waveguide", IEEE Trans. Microwave Theory Tech., Vol.MTT-22, No.2, Febr. 1974, pp.86-92.
- [23] G. O. Stone, "High-order finite elements for inhomogeneous accustic guiding structures", IEEE Trans. Microwave Theory Tech., Vol.MTT-21, No.8, Aug. 1973, pp.538-542.
- [24] P. Silvester, "High-order polynomial triangular finite elements for potential problems", Int. J. Eng. Sci., Vol.7, 1969, pp.849-861.
- [25] P. Daly, "Finite-element coupling matrices", Electronics Letters, Vol.5, No.24, 27-th Nov. 1969, pp.613-615.
- [26] G. O. Stone, "Coupling matrices for high-order finite-element analysis of acoustic-wave propagation",

  Electronics Letters, Vol.8, No.18, 7-th Sept. 1972,

  pp.466-468.
- [27] P. E. Lagasse, "Higher-order finite-element analysis of topographic guides supporting elastic surface waves",

  J. Acoustical Soc. Amer., Vol.53, No.4, April 1973,

  pp.1116-1122.
- [28] R. Burridge and F. J. Sabina, "The propagation of elastic surface waves guided by ridges", Proc. R. Soc. Lond., A.330, 1972, pp.417-441.
- [29] O. C. Zienkiewicz and Y. K. Cheung, <u>The Finite Element</u>

  <u>Method in Structural and Continuum Mechanics</u>, New York:

  <u>McGraw-Hill</u>, 1967.

- [30] D. H. Norrie and G. de Vries, <u>The Finite Element Method</u>, New York: Academic Press, 1973.
- [31] J. T. Oden, Fixite Elements of Nonlinear Continua, New York: McGraw-Hill, 1972.
- [32] G. Strang and G. J. Fix, An Analysis of the Finite Element Method, Englewood Cliffs, N.J.: Prentice-Hall, 1973.
- [33] C. S. Desai and J. F. Abel, <u>Introduction to the Finite</u>

  <u>Element Method A Numerical Method for Engineering</u>

  <u>Analysis</u>, London, England: Van Nostrand Reinhold, 1972.
- [34] O. C. Zienkiewicz, <u>The Finite Element Method in Engineering Science</u>, New York: McGraw-Hill, 1971.
- [35] G. N. Smith, An Introduction to Matrix and Finite Element

  Methods in Civil Engineering, London, England: Applied

  Science Publishers, 1971.
- [36] A. Konrad and P. Silvester, "A finite element program package for axisymmetric vector field problems", submitted for publication to Computer Physics Communications.
- [37] R. F. Harrington, <u>Time-Harmonic Electromagnetic Fields</u>,

  New York: McGraw-Hill, 1961.
- [38] S. Ramo, J. R. Whinnery and T. Van Duzer, <u>Fields and Waves in Communication Electronics</u>, New York: John Wiley & Sons, 1967.
- [39] P. Silvester and C. R. S. Haslam, "Magnetotelluric modelling by the finite element method", Geophysical Prospecting, Vol.XX, No.4, 1972, pp.872-891.

- [40] I. Stakgold, <u>Boundary Value Problems of Mathematical</u>

  <u>Physics</u>, Vol.II, New York: Macmillan, 1968.
- [41] R. Collin, <u>Foundations for Microwave Engineering</u>,

  New York: McGraw-Hill, 1966, pp. 344-362.
- [42] D. M. Bolle, "On the solution of the circularly cylindrical coordinate wave equation in homogeneous isotropic regions containing the coordinate axis", IEEE Trans. Microwave Theory Tech., Vol.MTT-21, No.3, March 1973, pp.158-159.
- [43] G. R. Fowles, <u>Analytical Mechanics</u>, New York: Holt, Rinehart and Winston, Inc., 1964.
  - [44] A. Wexler, "Finite-element field analysis of an inhomogeneous, anisotropic, reluctance machine rotor",

    IEEE Trans. Power, Apparatus Syst., Vol. PAS-92, No.1,

    Jan./Febr. 1973, pp.145-149.
  - [45] B. Lax and K. J. Button, <u>Microwave Ferrites and</u>
    Ferrimagnetics, New York: McGraw-Hill, 1962.
  - [46] R. F. Soohoo, <u>Theory and Application of Ferrites</u>, Englewood Cliffs, N.J.: Prentice-Hall, 1960.
  - [47] P. Clarricoats, <u>Microwave Ferrites</u>, New York: John Wiley, 1961.
  - [48] F. E. Gardiol, "Computer analysis of latching phase shifters in rectangular waveguide", IEEE Trans. Microwave Theory Tech., Vol.MTT-21, No.1, Jan. 1973, pp.57-61.

- [49] P. Chorney, "Power and energy relations in bidirectional waveguides", Technical Report 396, Massachusetts Institute of Technology, Research Laboratory of Electronics, Cambridge, Mass., Sept. 1961, (ASTIA: AD No.277030).
- [50] F. E. Gardiol, "Circularly polarized electric field in rectangular waveguide", IEEE Trans. Microwave Theory
  Tech., Vol.MTT-22, No.5, May 1974, pp.563-565.
- [51] S. F. Borg. Matrix-Tensor Methods in Continuum Mechanics, Princeton, N.J.: D. Van Nostrand, 1963.
- [52] A. Konrad and P. Silvester, "Triangular finite elements for the generalized Bessel equation of order m", Int. J. num. Meth. Engng., Vol.7, No.1, 1973; pp.43-55.
- [53] G. C. Best, "Helpful formulas for integrating polynomials in three dimensions", Math. Comp., Vol.18, 1964, pp.310-312.
- [54] M. A. Eisenberg and L. E. Malvern, "On finite element integration in natural co-ordinates", Int. J. num. Meth. Engng., Vol.7, No.4, 1974, pp.574-575.
- [55] A. Konrad, "Finite element solution of axisymmetric scalar fields", M.Eng. Thesis, McGill Univ., 1971.
- [56] P. Silvester and A. Konrad, "Axisymmetric triangular finite elements for the scalar Helmholtz equation", Int. J. num. Meth. Engng., Vol.5, 1973, pp.481-497.

- [57] A. Konrad and P. Silvester, "A finite element program package for axisymmetric scalar field problems", Comp. Phys. Comm., Vol.5, 1973, pp.437-455.
- [58] P. Silvester, "A general high-order finite element wave-guide analysis program", IEEE Trans. Microwave Theory
  Tech., Vol.MTT-17, April 1969, pp.204-210.
- [59] R. A. Waldron, Theory of Guided Electromagnetic Waves,
  London, England: Van Nostrand Reinhold Co., 1970, pp.
  357-359.
- [60] N. Marcuvitz\*(editor), <u>Waveguide Handbook</u>, New York:

  McGraw-Hill, 1351, Radiation Laboratory Series No.10,

  Chapter 8, pp.387-397.
- [61] C. Q. Lee and R. Christia, "High-order modes in a square coaxial waveguide", Proc. IEEE, Vol.61, No.12, 1973, pp. 1754-1755.
- [62] P. Silvester, "TEM wave properties of microstrip transmission lines", Prec. IEE, Vol.115, Jan. 1968, pp.43-48.
- [63] R. Mittra and T. Itoh, "A new technique for the analysis of the dispersion characteristics of microstrip lines", IEEE Trans. Microwave Theory Tech., Vol.MTT-19, No.1, Jan. 1971, pp.47-56.
- [64] E. J. Denlinger, "Dynamic solutions for single and coupled microstrip lines", Ph.D. Thesis, University of Pennsylvania, 1969.

- [65] T. S. Bird, "Dispersion and loss in microstrip", Proc. 14-th National Radio and Electronics Engng. Convention, Australia, 20-24th Aug. 1973, pp.30-31.
- [66] P. Daly, "Singularities in transmission lines", in
  J. R. Whiteman (editor), The Mathematics of Finite

  Elements and Applications, New York: Academic Press,

  1973, pp.337-350.
- [67] H. C. Martin and G. F. Carey, <u>Introduction to Finite</u>

  <u>Element Analysis Theory and Application</u>, New York:

  McGraw-Hill, 1973.
- [68] W. P. Allis, S. J. Buchsbaum and A. Bers, <u>Waves in</u>

  <u>Anisotropic Plasmas</u>, Cambridge, Mass.: M.I.T. Press,

  1963.
- [69] C. T. M. Chang, "Circular waveguide lined with artificial anisotropic dielectrics", IEEE Trans. Microwave Theory Tech., Vol.MTT-20, No.8, Aug. 1972, pp.517-523.
- [70] H. C. Hoyt, D. D. Simmonds and W. F. Rich, "Computer designed 805 MHz proton linac cavities", The Review of Scientific Instruments, Vol.37, No.6, June 1966, pp.755-762.
- [71] T. W. Edwards, "Proton linear accelerator cavity calculations", Report Number 622, Midwestern Universities Research Association (MURA), Madison, Wisconsin, June 15, 1961.

- [72] P. M. Lapostolle and A. L. Septier (editors), <u>Linear</u>

  <u>Accelerators</u>, Amsterdam: North-Holland Publishing Co.,
  1970.
- [73] A. Konrad, "Linear accelerator cavity field calculation by the finite element method", IEEE Trans. Nucl. Sci., Vol.NS-20, No.1, Febr. 1973, pp. 802-808.
- [74] P. Silvester, "High-order finite element waveguide analysis", IEEE Trans. Microwave Theory Tech., Vol.MTT-17, No.8, Aug. 1969, p.651.
- [75] A. Konrad and P. Silvester, "Scalar finite-element program package for two-dimensional field problems",

  / IEEE Trans. Microwave Theory Tech., Vol.MTT-19, No.12,
  Dec. 1971, pp.952-954.
- [76] A. Ralston, <u>A First Course in Numerical Analysis</u>, New York: McGraw-Hill, 1965.
- [77] P. Silvester, "Symmetric quadrature formulae for simplexes", Math. Comp., Vol.24, No.109, Jan. 1970, pp.95-100.
- [78] P. Silvester and A. Konrad, "Analysis of transformer leakage phenomena by high-order finite elements", IEEE Trans. Power Apparatus Syst., Vol.PAS-92, No.6, Nov./Dec. 1973, pp.1843-1855.
- [79] E. Kicak, "Directional derivatives of interpolation polynomials in two-dimensional finite element problems using triangular elements", Internal Report, Dept. Elec. Engng., McGill Univ., April 1973.

- [80] W. F. Rich and M. D. J. MacRoberts, "Numeric solution of the fundamental mode of cylindrically symmetrical resonant cavities", Los Alamos Scientific Laboratory of the Univ. of California, Los Alamos, New Mexico, Report No. LA-4219 (UC-32, TID-4500).
- [81] Z. J. Csendes, "Projective solution of differential equations", Ph.D. Thesis, McGill Univ., 1972.
- [82] Z. J. Csendes and P. Silvester, "Finplt: a finite-element field plotting program", IEEE Trans. Microwave Theory Tech., Vol.MTT-20, No.4, April 1972, pp.294-295.
- [83] H. C. Hoyt, "Numerical studies of the shapes of drift tubes and linac cavities", IEEE Trans. Nucl. Sci., Vol.NS-12, No.3, June 1965.
- [84] K. Mittag, private communication (letter dated Jan. 31st, 1974)
- [85] G. Parzen, "A mesh iteration program for calculation in linac cavities", Proc. 1968 Proton Linear Accelerator Conf., Part 2, May 1968, Upton, N.Y., pp.537-542.
- [86] M. Martini and D. J. Warner, "Numerical calculations of linear accelerator cavities", European Organization for Nuclear Research, Geneva (Switzerland), Proton Synchrotron Machine Division, 1968, CERN 68-11.
- [87] D. E. Young, R. S. Christian, C. D. Curtis, T. W. Edwards, F. J. Kriegler, F. E. Mills, P. L. Morton, D. A. Swenson and J. van Bladel, "Design studies of proton linear

- accelerators", Proc. Int. Conf. on High Energy
  Accelerators, Dubna, U.S.S.R., Aug. 21-27, 1963, p.454.
- [88] M. Sedlacek, "Computer program for calculation of electrical parameters in cavity resonators with cylindrical symmetry", Royal Inst. of Tech., Stockholm (Sweden), Div. of Electron Physics, Sept. 1971, TRITA-epp-71-06.
- [89], H. G. Kaper, G. K. Leaf and A. J. Lindeman, "A timing comparison study for some high order finite element approximation procedures and a low order finite difference approximation procedure for the numerical solution of the multigroup neutron diffusion equation", Nucl. Sci. and Engng., Vol.49. 1972, pp.27-48.
- [90] D. J. Liska, "Computer design of UHF power amplifier tubes", IEEE Trans. Nucl. Sci., Vol.NS-14, No.3, June 1967, pp.266-272.
- [91] E. A. Knapp, B. C. Knapp and J. M. Potter, "Standing wave high energy linear accelerator structures", The Review of Scientific Instruments, Vol.39, No.7, July 1968, pp.979-991.
- [92] W. Hant and J. A. Seeger, "A modified conical cavity for submillimeter wave applications", IEEE Trans. Electron Devices, Vol.ED-19, No.1, Jan. 1972, pp.80-85.
- [93] A. A. Laloux, R. J. M. Govaerts and A. S. Vander Vorst,
  "Application of a variation-iteration method to waveguides
  with inhomogeneous lossy loads", IEEE Trans. Microwave

Theory Tech., Vol.MTT-22, No.3, March 1974, pp.229-236.

- [94] F. E. Gardiol, "Anisotropic slabs in rectangular wave-guides", IEEE Trans. Microwave Theory Tech., Vol.MTT-18, No.8, Aug. 1970, pp.461-467.
- [95] F. E. Gardiol and A. S. Vander Vorst, "Computer analysis of E-plane resonance isolators", IEEE Trans. Microwave Theory Tech., Vol.MTT-19, No.3, March 1971, pp.315-322.
- [96] J. A. Kong, "Theorems of bianisotropic media", Proc. IEEE, Vol.60, No.9, Sept. 1972, pp.1036-1046.

Leaves 238, 239, 240 on microfiche.

For information pertaining to Appendixes I - VI please contact University.